CHAPTER 1

GENERAL ASPECTS OF NQR SPECTROSCOPY

Nuclear quadrupole resonance (NQR) is a branch of radiospectroscopy which measures weak interactions between nuclei having nonzero quadrupole moments (Q) and their local electric environment in the ground state of the solid systems. This interaction is characterized by the electric field gradient EFG $= \partial E_i/\partial x_i = \partial^2 V/\partial x_i^2$, where E_i is the strength of the electrostatic field at the nuclear site and V is the electrostatic potential. The set of NQR spectroscopic parameters includes the quadrupole coupling constant ($QCC = e^2 Q q_{zz}/h$), the electric field gradient asymmetry parameter ($\eta = (q_{xx} - q_{yy})/q_{zz}$), the resonance line width, and the longitudinal (T_1) and transverse (T_2) relaxation rates. These parameters can be measured over a wide temperature range and under various pressures so that their values provide an important and increasingly recognized data set which is concerned with various aspects of structure and chemical bonding. As the QCC and η values depend directly on the electron density distribution in the vicinity of the nucleus, the NQR results are important for a number of problems arising in theoretical chemistry. It is however to be noted that current theories used to convert the NQR parameters to conventional characteristics of chemical bonding, such as orbital occupancies, ionic- and covalent σ-character, π-bond effects are subject to certain assumptions such that the subsequent quantitative results are rather ambiguous. At the same time the method is highly sensitive towards very weak changes in electronic state of the substances and towards subtle structural changes. Conclusions based upon empirical relationships between NQR parameters and other characteristics in a series of related compounds usually appear very plausible and improve the understanding of many phenomena.

During the period of time since the first NQR experiments (Dehmelt and Kruger first observed signals of pure quadrupole resonance in 1950 [1, 2]), the method has found diverse chemical applications, and the range of its applicability is still expanding rapidly. Problems in the structural chemistry of organic and organoelement compounds in molecular crystals with relatively narrow spectroscopic lines have historically become the traditional domain of NQR investigations.

The recent advantages of pulse methods which removed the limitations imposed on the line width by continuous wave and super-regenerative techniques have stimulated intensive use of NQR in inorganic chemistry. Here NQR is especially effective in the study of chemical bonding and electron density distribution in coordination complexes. The increased sensitivity of methods with greater automation made NQR applicable to the study of practically all types of inorganic compounds including polymers with highly imperfect or disordered crystal lattices and amorphous compounds.

The detailed theoretical basis of NQR spectroscopy is available in several reviews and books [3—9]. The review series "Advances in Nuclear Quadrupole Resonance" started in 1974 (edited by J. A. S. Smith, Heyden & Son, London) also includes theoretical and methodological aspects of NQR. No attempt will therefore be made to give a detailed description of these questions, and in the following section we limit ourselves to a brief consideration of the nature of the phenomenon.

A. PHYSICAL PRINCIPLES OF NQR

A nucleus with a nonspherical charge distribution (and hence with a nuclear spin $I \geq 1$) possesses an electric quadrupole moment eQ which can interact with the electric field gradient (EFG) tensor $eq_{ij} = e\partial^2 V/\partial x_{ij}^2$ (V is the potential of electrostatic field) produced by neighbouring charges. The energy of interaction depends upon the orientation of the nucleus with respect to the axes of the EFG tensor. The change in nucleus orientation is accompanied by the absorption (dispersion) of radiofrequency energy corresponding to the separation of neighbouring quadrupole levels. The external radiofrequency energy stimulates quadrupole transitions, the phenomenon thus being of resonance nature.

Quite a number of elements (nearly two-thirds of the elements in the periodic table) have isotopes with nonspherical (ellipsoidal) charge distribution of their nuclei and can thus be studied by NQR spectroscopy. These are:

$(I = 3/2)$: ^{7}Li, ^{9}Be, ^{11}B, ^{23}Na, ^{37}Cl, ^{35}Cl, ^{63}Cu, ^{65}Cu, ^{69}Ga, ^{71}Ga, ^{75}As, ^{79}Br, ^{81}Br, ^{87}Rb, ^{135}Ba, ^{137}Ba, ^{197}Au, ^{189}Os, ^{201}Hg;

$(I = 5/2)$: ^{17}O, ^{27}Al, ^{55}Mn, ^{67}Zn, ^{85}Rb, ^{121}Sb, ^{127}I, ^{185}Re, ^{187}Re;

$(I = 7/2)$: ^{45}Sc, ^{51}V, ^{59}Co, ^{123}Sb, ^{133}Cs, ^{139}La, ^{175}Lu, ^{181}Ta;

$(I = 9/2)$: ^{93}Nb, ^{115}In, ^{209}Bi;

$(I = 1)$: ^{2}D, ^{6}Li, ^{14}N.

The nuclear quadrupole moment being a measure of the extent to which charge distribution departs from the spherical, the appropriate relation is given as

$$eQ = \int \varrho_n(3z_n^2 - r_n^2)\,\mathrm{d}v_n \qquad (1)$$

where ϱ_n is the charge density on a nucleus; z_n is the direction of the nuclear spin I, dv_n is the nuclear volume element, r_n is the distance between the volume element and the origin which is the centre of gravity of the nucleus (Fig. 1.1).

It is evident that integration over a sphere (i.e. for a nucleus with spin $I = 1/2$) yields $eQ = 0$ because $z_n^2 = r^2/3$.
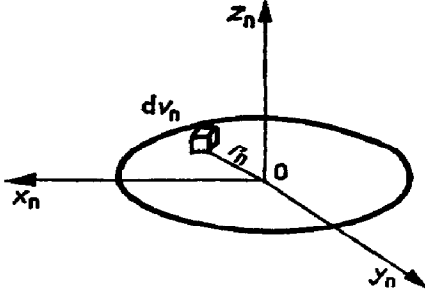

Figure 1.1 Cartesian coordinate system fixed at the quadrupole nucleus (index n).

In a crystal, quadrupole nuclei are sited in a non-uniform electrostatic field. Let the EFG at the site of nucleus be axially symmetric about its largest component which is conventionally labelled eq_{zz} ($eq_{xx} = eq_{yy}$). The nucleus will then precess about the 0_z direction under the action of the rotational moment proportional to $|eq_{zz}|$ and eQ, i.e. $|e^2 Qq_{zz}|$, at a frequency of $|e^2 Qq_{zz} \cdot h^{-1}|$ (h is Plank's constant). It is important that, as seen from Figure 1.1, both eq_{zz} and eQ quantities are defined in different coordinate systems. The frequency therefore depends on the orientation of the nucleus with respect to the components of the EFG. This is a fundamental difference between the NQR and NMR phenomena [8], in NMR the precession frequency being independent of orientation.

Because of its internal position, the nucleus is subject to the effects of electron charge distribution which create the electrostatic potential $V(r_n)$ at the nucleus elementary volume dv_n. The potential energy of the nucleus charge contained in that volume is then equal to $-\varrho_n\, dv_n V$. For the nucleus as a whole we have

$$W = -\int \varrho_n V(r_n)\, dv_n \tag{2}$$

Taking into consideration that $V(r_n)$ does not rapidly vary over the nucleus volume and expanding $V(r_n)$ in the Taylor series about the origin, we may rewrite equation (2) in the form

$$W = -\left\{ V(0) \int \varrho_n\, dv_n + \Sigma \left(\frac{\partial V}{\partial x_i}\right)_0 \int \varrho_n x_{in}\, dv_n + \frac{1}{2} \sum_{ij} \left(\frac{\partial^2 V}{\partial x_i\, \partial x_j}\right)_0 \int x_{in} x_{jn}\, dv_n + \cdots \right.$$

$$\tag{3}$$

The first term in equation (3) may be omitted as it does not depend on the nucleus orientation. It represents the Coulomb "monopole" energy and consequently gives no contribution to the quadrupole coupling.

The second term describes the interaction of the nuclear electrostatic dipole moment with the external electric field ($E_i = -\partial V/\partial x_i$). This term is equal to zero because nuclei possess no dipole moments [10].

The third term in which we are interested is the electric quadrupole term, ignoring for now, higher terms. It represents the potential energy of a quadrupole nucleus in a non-uniform external electrostatic field with the gradient $\partial^2 V/\partial x_i \partial x_j$ and may be written in the Cartesian coordinates as

$$W_q = -\int \varrho_n \frac{1}{2} \left\{ x_n^2 \left(\frac{\partial^2 V}{\partial x^2}\right)_0 + y_n^2 \left(\frac{\partial^2 V}{\partial y^2}\right)_0 + z_n^2 \left(\frac{\partial^2 V}{\partial z^2}\right)_0 + 2x_n y_n \left(\frac{\partial^2 V}{\partial x\,\partial y}\right)_0 \right.$$
$$\left. + 2z_n x_n \left(\frac{\partial^2 V}{\partial x\,\partial z}\right)_0 + 2y_n z_n \left(\frac{\partial^2 V}{\partial y\,\partial z}\right)_0 \right\} dv_n \tag{4}$$

One can see that equation (4) contains the components of the nuclear quadrupole moment tensor (9 terms involving the nuclear coordinates) and those of the electrostatic field gradient tensor (9 terms involving second derivatives of the electrostatic potential). As is known, a new coordinate system, the system of the principal axes, can always be used such that all off-diagonal terms are zero. The potential energy of a quadrupole nucleus in a non-uniform field thus becomes

$$W_q = -\int \frac{1}{2} \left\{ \varrho_n x_n^2 \left(\frac{\partial^2 V}{\partial x^2}\right)_0 + \varrho_n y_n^2 \left(\frac{\partial^2 V}{\partial y^2}\right)_0 + \varrho_n z_n^2 \left(\frac{\partial^2 V}{\partial z^2}\right)_0 \right\} dv_n \tag{5}$$

In the quantum mechanical approach, eQ entering equation (1) is conventionally redefined in such a way that the integration includes the state with the maximum component of the nuclear magnetic moment parallel to the z axis ($I_z = 1$). The parenthesized terms in equation (5) are then the expectation or mean values of the principal components of the EFG over the wave function of the molecule in the ground state. They are conventionally chosen in the order $|q_{zz}| > |q_{xx}| > |q_{yy}|$.

Neglecting small electrostatic charge distributions within the nucleus, we have according to the Laplace equation

$$\partial^2 V/\partial x^2 + \partial^2 V/\partial y^2 + \partial^2 V/\partial z^2 = 0 \tag{6}$$

Hence there are only two independent EFG components which describe the spatial electron distribution around the nucleus. They are chosen to be the maximum component of the EFG

$$eq_{zz} = \partial^2 V/\partial z^2 \tag{7}$$

and the EFG asymmetry parameter

$$\eta = (\partial^2 V/\partial x^2 - \partial^2 V/\partial y^2)/(\partial^2 V/\partial z^2) = (q_{xx} - q_{yy})/q_{zz} \tag{8}$$

The quantum mechanical expression for the Hamiltonian can be obtained from the classical potential energy equation (5) by replacing ϱ_n by its quantum-mechanical operator and by taking into account equations (6 −8):

$$\mathscr{H}_Q = \frac{e^2 Qq}{4I(2I-1)}\,[(3\hat{I}_z^2 - \hat{I}^2) - (\hat{I}_+^2 - \hat{I}_-^2)]$$

$$\hat{I}_+ = \hat{I}_x + i\hat{I}_y;\ \hat{I}_- = \hat{I}_x - i\hat{I}_y \tag{9}$$

where $\hat{I}$ is the operator of the total angular momentum or spin of the nucleus. The quadrupole interaction mixes the spin states since the operators $\hat{I}_+$ and $\hat{I}_-$ are present in equation (9).

In order to calculate the energy one has to evaluate the matrix elements of $\mathscr{H}_Q$ between nuclear states $|Im\rangle$:

$$\langle Im|\,\mathscr{H}_Q\,|Im'\rangle = \frac{e^2 Qq}{4I(2I-1)}\Big\{[3m^2 - I(I+1)]\,\delta_{mm'}$$

$$+ \frac{1}{2}\eta[(I \mp m)(I \mp m - 1)(I \pm m + 1)(I \pm m + 2)]^{1/2}$$

$$\times\ \delta_{m\pm2,m'} \tag{10}$$

where m is the z component of the total angular momentum which has $(2I+1)$ values. The quantity $e^2 Qq \cdot h^{-1}$ is known as the quadrupole coupling constant (QCC).

The solution of secular equations to obtain the energy eigenvalues is, in general, difficult, especially for half-integer spins, due to the mixing of states which differ by $\Delta m = 2$ [2]. For the case of $I = 1$ and $I = 3/2$ they can be solved exactly (Table 1.1). For other half-integral spins closed solutions do not exist, and the equations can be solved numerically for different values of η. The calculated frequency ratios can then be tabulated for various values of η as shown by Cohen [11].

The most simple situation is realized when the EFG is axially symmetric ($\eta = 0$). In this case the expression for the quadrupole energy levels is equation (11)

$$E_m = e^2 Qq\,\frac{3m^2 - I(I+1)}{4I(2I-1)} \tag{11}$$

which shows that the levels $\pm m$ are degenerate.

The probability for spontaneous transitions between neighbouring levels is exceedingly small. An external radiofrequency field according to equation

TABLE 1.1

Secular equations, transition frequencies and some energy eigenvalues for various nuclear spins I $\left(A = \dfrac{e^2Qq}{4I(2I-1)}\right)$

I	Secular equations	Units of E	Transition frequencies	Energy levels
3/2	$E^2 - 3\eta - 9 = 0$	A	$\nu_{\pm 3/2 \to \pm 1/2} = \dfrac{e^2Qq}{2h}\left(1 + \dfrac{\eta^2}{3}\right)^{1/2}$	$E_{\pm 3/2} = \dfrac{e^2Qq}{4}\left(1 + \dfrac{\eta^2}{3}\right)^{1/2}$ $E_{\pm 1/2} = \dfrac{e^2Qq}{4}\left(1 + \dfrac{\eta^2}{3}\right)^{1/2}$
5/2	$E^3 - (7\eta^2 - 21)E - 20(1 - \eta^2) = 0$	$2A$	$\nu_{\pm 5/2 \to \pm 3/2}$ $= \dfrac{3e^2Qq}{10h}(1 - 0.2037\eta^2 + 0.1622\eta^4)$ $\nu_{\pm 3/2 \to \pm 1/2}$ $= \dfrac{3e^2Qq}{20h}(1 + 1.0926\eta^2 - 0.6340\eta^4)$	$E_{\pm 5/2} = \dfrac{e^2Qq}{40}\left(10 + \dfrac{5}{9}\eta^2 + \dfrac{85}{2916}\eta^4 + \cdots\right)$ $E_{\pm 3/2} = \dfrac{e^2Qq}{4}\left(-2 + 3\eta^2 - \dfrac{23}{12}\eta^4 + \cdots\right)$ $E_{\pm 1/2} = \dfrac{e^2Qq}{4}\left(-8 - \dfrac{32}{9}\eta^2 + \dfrac{1376}{729}\eta^4 + \cdots\right)$
7/2	$E^4 - 42\left(1 - \dfrac{\eta^2}{3}\right)E^2 - 64(1 - \eta^2)E$ $\quad + 105\left(1 - \dfrac{\eta^2}{3}\right)^2 = 0$	$3A$	$\nu_{\pm 7/2 \to \pm 5/2}$ $= \dfrac{3e^2Qq}{14h}(1 - 0.1001\eta^2 - 0.0180\eta^4)$	

$$\nu_{\pm 5/2 \to \pm 3/2}$$
$$= \frac{2e^2Qq}{14h}(1 - 0.5667\eta^2 + 1.8595\eta^4)$$

$$\nu_{\pm 3/2 \to \pm 1/2}$$
$$= \frac{1e^2Qq}{14h}(1 + 3.6333\eta^2 - 7.2607\eta^4)$$

9/2

$$E^5 - 11(3 + \eta^2)E^3 - 44(1 - \eta^2)E^2$$
$$+ \frac{44}{3}(3 + \eta^2)^2E + 48(3 + \eta^2)$$
$$\times (1 - \eta^2) = 0$$

6A

$$\nu_{\pm 9/2 \to \pm 7/2}$$
$$= \frac{4e^2Qq}{24h}(1 - 0.0809\eta^2 - 0.0043\eta^4)$$

$$\nu_{\pm 7/2 \to \pm 5/2}$$
$$= \frac{3e^2Qq}{24h}(1 - 0.1875\eta^2 - 0.1233\eta^4)$$

$$\nu_{\pm 5/2 \to \pm 3/2}$$
$$= \frac{2e^2Qq}{24h}(1 - 1.3381\eta^2 + 11.7224\eta^4)$$

$$\nu_{\pm 3/2 \to \pm 1/2}$$
$$= \frac{1e^2Qq}{24h}(1 + 9.0333\eta^2 - 45.6910\eta^4)$$

$$E_\pm = \frac{e^2Qq}{4}(1 \pm \eta)$$

$$E_0 = -\frac{e^2Qq}{4}(-2\eta)$$

$$\nu_\pm = \frac{3e^2Qq}{4h}\left(1 \pm \frac{\eta}{3}\right)$$

$$\nu_{\Delta m=} = \frac{1e^2Qq}{2h}\eta$$

1

$$(-2A - E)[(A - E)^2 - A]^2 = 0$$

A

(12) of the frequency

$$\nu = \frac{3e^2Qq}{4hI(2I-1)} \left(2\,|m| - 1\right) \tag{12}$$

corresponding to the energy difference separating the levels stimulates both upward and downward transitions to the same extent. Nevertheless, the net result will be absorption of external field energy because, in accordance with the Boltzmann law, the lower level population should exceed that of the upper one under thermal equilibrium conditions where upon upward transitions will prevail. The NQR experiment consists of measurement of resonance absorption frequencies. These may be related to the QCC and η values by solving the secular equations listed in Table 1.1 [12], using the tabulated frequency ratios [11] or applying equation (10) if $\eta = 0$.

The determination of QCC and η-values at the nuclei sites with $I = 3/2$ requires additional experiments, for instance the Zeeman experiments in weak static magnetic fields, since the resonance frequency which is observed depends on both these quantities. In practice, however, finite η-values are often ignored because one can see from the relationship (Table 1.1) that an error of less than 0.2% is introduced into the QCC value when one ignores values of η up to 0.3. So when η is, on chemical grounds supposed to be small, the QCC value is usually set at twice the resonance frequency value.

In cases where a separate determination of QCC and η is still necessary, various versions of the Zeeman experiment are performed using single crystals or powders and the super-regenerative or pulse technique.

In Zeeman experiments with single crystals the orientation dependence of the NQR spectroscopic splitting is studied. A perturbing static magnetic field H_0 removes the double degeneracy $\pm m$ of the quadrupole levels since the energy of interaction of the nuclear magnetic moment with this field becomes different for the orientations of nuclear spin projection 'along' and 'opposite' the H_0 direction. The total interaction energy then becomes ($|m| > 1/2$) [13]

$$E_{\pm m} = \frac{e^2Qq}{4I(2I-1)} \left[3m^2 - I(I+1)\right] \mp mh\gamma H_0 \cos\theta \tag{13}$$

where γ is the gyromagnetic ratio for the quadrupole nucleus, θ is the angle between H_0 and z-axis of EFG (q_{zz} direction). Each $\pm m \rightarrow \pm m(m+1)$ transition is thus split by the applied field into a doublet ($\pm m\hbar\gamma H_0 \cos\theta$), both components having half intensity of the initial non-split line. Their relative intensities are independent of the Zeeman field orientation while the separation inside such a pair is evidently maximal at $\theta = 0°$ and zero at $\theta = 90°$.

When $m = \pm1/2$ mixing of the $\psi_{+1/2}$ and $\psi_{-1/2}$ states occurs in zero order of degenerate perturbation theory so that new states, ψ_+ and ψ_-, are produced. This leads to the appearance of four lines in the Zeeman spectrum (α, α', β, β',

Fig. 1.2), corresponding to the selection rule $\Delta m = \pm 1$. The quadruplet is symmetrical about the zero field NQR frequency.

The relative intensities of the doublets $\alpha(\alpha')$ and $\beta(\beta')$ depend on the orientation of the Zeeman field but the inner pair is always stronger [2].

The Zeeman NQR spectra for nuclei of any half-integer spins are characterized by several specific features [13]: when $\theta = 0°$, i.e. the Zeeman field is parallel to the z-axis of EFG, the splitting between α-components is maximal, while the β doublet is of zero intensity

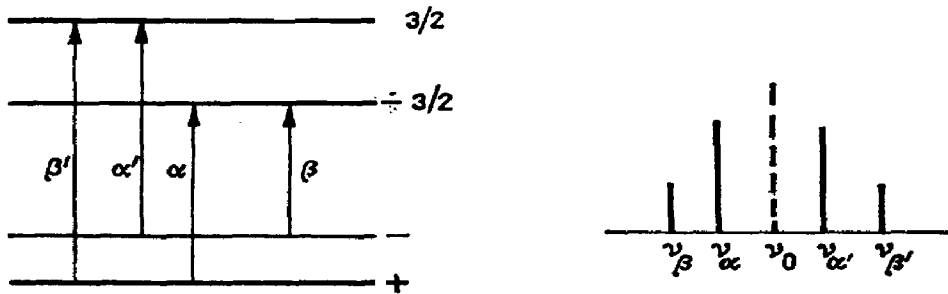$$\theta = 0°; \quad \Delta\nu_{\alpha\alpha'} = (2/h)\,\gamma H_0 \tag{14}$$

Figure 1.2 Zeeman splittings of the $m = \pm 3/2$ and $m = \pm 1/2$ energy levels; ν_0 is the NQR frequency when a magnetic field is absent.

If $\theta = 90°$, a single pair of lines is observed

$$\Delta\nu_{\alpha\alpha'} = \Delta\nu_{\beta\beta'} = (1/h)\,(I + 1/2)\,\gamma H_0 \tag{15}$$

For $\theta_0 = \dfrac{1}{\left(\tan\dfrac{2\sqrt{2}}{I + 1/2}\right)}$ the splitting is

$$\Delta\alpha\alpha' = 0; \quad \Delta\beta\beta' = 6/(h\gamma H_0) \tag{16}$$

In the latter case the $\alpha\alpha'$ lines coalesce producing a signal of double intensity at the zero-field NQR frequency. For nuclei with $I = 3/2$, $\theta = 54° \ 44'$. The locus of such zero-splitting of the $\alpha\alpha'$ components is determined by the directions of H_0 lying on a right circular cone with semivertical angle θ_0 around the z-axis of the EFG. Looking for this locus of H_0 orientation which retains unsplit components at the frequency of the unperturbed NQR transition is an essential part of one of the earliest way of determining η, namely the method of zero-splitting locus [14]. This uses single crystals and relatively weak (up to 100 gauss) magnetic fields. The following relationship (eqn. (17)) describes the zero-splitting elliptical cross-section around the z-axis with the ratio of semi-axes deter-

mining the η-value

$$\sin^2 \theta_0 = 1/(3 - \eta \cos 2\varphi) \tag{17}$$

here φ is the azimuthal angle with respect to the x-axis of the EFG tensor. The geometry of the locus thus determines the orientation of the EFG principal axes with respect to the crystal axes.

If θ_0 are known in two planes, for instance for $\varphi = 0°$ and $\varphi = 90°$, one can avoid a detailed orientation study, calculating the equation [14]

$$\eta = \frac{3[\sin^2 \theta_0(0°) - \sin^2 \theta_0(90°)]}{\sin^2 \theta_0(0°) + \sin^2 \theta_0 (90°)} \tag{18}$$

These θ_0 values can easily be found by taking into account that $\sin^2 \theta_0$ and thus θ_0 are maximal for $\varphi = 0°$ and minimal at $\varphi = 90°$. In general the method provides accurate values of η except when these are small. In this case the ellipticity of the cone also becomes small, presenting difficulties for measurement (it is less than $3°$ for $\eta \sim 0.1$). The field-frequency method is then preferred [15]. This consists in application of H_0 perpendicular to the z-axis of the EFG, the splitting of the spectrum then becoming equation (19).

$$\Delta \nu_{\alpha\beta} = \frac{\gamma H_0 \eta}{2\pi \hbar} \left[1 + \frac{\eta}{6} (\cos 2\varphi - \eta) \right]^{(\eta < 0.25)} \approx \nu_L \eta / \hbar \tag{19}$$

The dependence on φ is negligible for $\eta < 0.25$ so that η is calculated from the measured splitting $\Delta \nu_{\alpha\beta}$, if the direction of the z-axis is known. Magnetic fields of up to 500 gauss are used in this method.

Historically both methods suggested the observation of NQR using a super-regenerative technique. The first experiments with the use of NQR pulse spectrometers (later we shall discuss the recording technique in more detail) have, however, shown that it could also successfully be used for the study of Zeeman effects [16]. The determination of η according to the procedures described above appeared to be even less tedious when the pulse (spin-echo) technique was used [17]. The zero-splitting locus is identified more easily and to a higher degree of accuracy than with the c.w. technique, by observing the beats of the spin-echo signal. The pulse spectrometer in this case operates at zero-field frequency, and the frequency of the beats is defined by the differences between the $\alpha\alpha'$ Zeeman components since the radio-frequency pulses excite the Zeeman spectrum lines within $50 - 150$ kHz from the central frequency of pulses. When the frequencies of both α, α' components coincide, the period of beats increases. The width of the spin-echo signal serves as a control for observing the points of the zero-splitting locus [17]. If the field-frequency method is used, the H_0 field is located in the xy-plane of EFG, and the spectrometer operates at the frequency $\nu_{NQR} \pm \nu_L$ ($\nu_L = \gamma H_0 / 2\pi$ is the Larmor precession frequency of the quadrupolar nucleus in a magnetic field H_0). The

spin-echo signal shows, in this case, beats at the frequency difference between the α and β Zeeman components. There can not however be any zero-beats if η is of finite value. Measuring of a minimal value for a period of beats, on rotation of a sample, gives the separation $\Delta\nu_{\alpha\beta}$, and thus according to equation (19) the value of η for a certain Larmor frequency.

Although the pulse technique can simplify the orientation procedures of the Zeeman experiments, the problem of growing large single crystals (up to 1 cm^3 is often needed) still remains a serious limiting factor for the widespread use of these methods. Hence considerable attention has been paid to a report by Morino and Toyama [20] on the results of the Zeeman analysis of NQR spectra taken with crystalline powders. Using a super-regenerative spectrometer, they analyzed the shape of the first derivative (this form of the signal is recorded when using super-regenerative technique) of the NQR signal when applying a weak magnetic field parallel to a radio-frequency field, i.e. to an axis of the coil with the sample. According to the theory a pair of 'kinks' separated by $\Delta\nu = 2\eta\nu_L$ from each other, appears on the envelope of the NQR
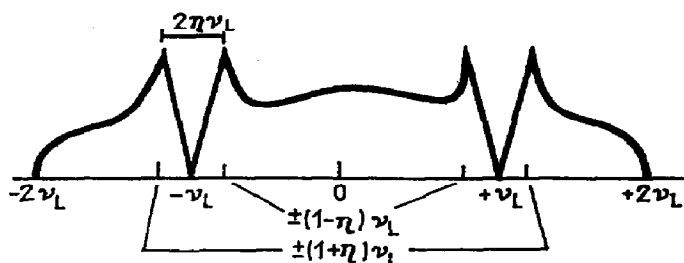

Figure 1.3   Theoretically predicted envelope shape ($I = 3/2$) in the magnetic field $H_0 \parallel H_{r.f.}$ for $\eta \neq 0$ [20].

signal, when a static magnetic field H_0 is applied to a sample containing crystallites of random orientation. The authors[20] introduce the parameter $\delta_1 = \Delta\nu/2\nu_L$ equal to the frequency difference between the maximum and minimum of the recorded signal (Fig. 1.3) which converges on η as $H_0 \to \infty$. In practice, however, measurements are only possible in weak magnetic fields since they require careful analysis of the line shape and hence also a high signal-to-noise (S/N) ratio. A number of reports devoted to the improvement of the original method are available, for instance, by comparing computer-simulated powder Zeeman spectra with experimental Zeeman NQR spectra [21 − 25].

Although many provide η values not markedly different from those measured on single crystals there are some results yielding asymmetry parameter values unexpectedly too high on pure chemical grounds, and much higher than values obtained for the same compounds using single crystal samples (Table 1.2).

The authors [26] suppose that one of the reasons for this discrepancy is that the polycrystalline samples used were not truly isotropic. The authors [27] constructed a super-regenerative spectrometer with optimized para-

2*

TABLE 1.2

Selected results of the measurements of η by single crystal and powder methods ([24] and references therein)

Compound	Iso-tope	T (K)	Frequencies ν (MHz)	Asymmetry parameter η (%)		Ref.
				Crystal	Powder	
HgCl$_2$	^{35}Cl	296	22.251	3.7		[26a]
			22.064	1.2		
		300	22.240		30 ± 1	
			22.058		28 ± 1	
GaCl$_3$	^{35}Cl	305	20.23	3.4 ± 0.8		
			19.08	8.9 ± 0.8		
		300	20.302		63	
			19.204		59	
GeCl$_4$	^{35}Cl	77	24.449	3.5 (average)		[26b]
			25.451		35 ± 8	

meters including modulation depth and capable of signal averaging, in order answer this question. They estimated values of η in several compounds by comparing the experimental and computer-simulated Zeeman NQR spectra. It was concluded that modulation depth, which is sometimes increased to improve the S/N ratio when using ordinary single-scan spectrometers, leads to a modulation broadening, which masks the structure of the line recorded. But even with the use of low modulation amplitudes and a signal averaging system the location of 'kinks' due to $\eta' \neq 0$ ('η-kinks') on the signal envelope is difficult. Since the Zeeman fields are weak (those under 10 gauss were used in [27]) the S/N ratio of the $\eta = 0$ background is very strong while the 'η-kinks' are barely discernible. An incorrect identification of the strong deflections in the signal background in the first-derivative representation as the 'η-kinks' is, in opinion of the authors [27], the main reason for the overestimated values of η reported. They confess that when looking for the 'η-kinks' they often guided themselves by the theory which states that the 'η-kinks' should be sited symmetrically with respect to the frequency $\nu_{NQR} \pm \nu_L$.

The application of stronger magnetic fields to improve discernibility of the structure of the signal recorded, leads to a further decrease of spectroscopic intensity. Apart from all these disadvantages, there is one more very serious limiting factor which reduces greatly the number of compounds that could be studied by stationary methods. If the line width originates from a distribution of the local EFG values over the sample due to imperfections of crystal lattice (the broadening due to crystalline inhomogeneity as distinct from much

less broadening due to relaxation processes), the stationary technique becomes ineffective. The vast majority of inorganic compounds, probably suffer this problem.

Hence NQR spectroscopysts now prefer pulsed methods which are free of the limitations imposed by the quality of the samples. They consider them to be equally suited for Zeeman studies of both single crystals and powders.

Thus to determine η in crystalline powders a method was developed [28] based upon the results of a quantum mechanical analysis [29, 30] of spin-echo envelope (See), influenced by η in a magnetic field. The mixing of the states $|+1/2\rangle$ and $|-1/2\rangle$ in pulse experiments leads to the appearance of 'slow' beats on the echo envelope. Their frequency $\Delta\omega_{1/2}$ is determined by the splitting of the lower level of the quadrupole system. Since this frequency depends on the θ and φ angles between the EFG components and magnetic field H_0, the full set of them, $\Delta\omega_{1/2}(\theta, \varphi)$, is contained in the oscillations of the See [25]:

$$\Delta\omega_{1/2}(\theta, \varphi) = \gamma H_0/(\varrho) \left[(\varrho + 1 - \eta)^2 \sin^2\theta \cos^2\theta + (\varrho + 1 + \eta)^2 \sin^2\theta \sin^2\varphi \right.$$
$$\left. + \cos^2\theta(2 - \varrho)^2)\right]^{1/2} \tag{20}$$

where $\varrho = (1 + \eta^2/3)^{1/2}$. Experiment [31] confirms that the asymmetry parameter η does not affect the position of the first minimum of See but influences the function modulating the beats of See. The spectrum of modulation is derived [28] using the standard program of fast Fourier transform of See in a magnetic field (30 − 100 gauss). To obtain η, the spectrum is further compared with the function $S(\nu, \eta)$ simulated with the help of histography. A theoretical analysis of the See in a magnetic field has been performed for powders containing nuclei with $I = 3/2$ in order to determine the value of η from the position of the first modulation minimum of the echo envelope [32, 33]. In agreement with the results [28, 31], the calculations showed that the position of the first minimum of the echo beat envelope is independent of η, while the positions of the modulation minima on the echo beat envelope are considerably affected by η. This enabled the authors [32, 33] to find η from the experimentally measured position of the first modulation minimum on the See. Comparison of the results of both methods [28, 32, 33] showed that they provide values of η in agreement with the published data available for single crystals and not differing from each other within experimental error, which appeared nearly the same over the entire range of η values studied by both methods.

One could determine [34] η-values in powder samples by performing the FFT of the Zeeman split NQR spectra, similar to that carried out in [24].

The NQR spectra in magnetic fields are recorded over the interval $\nu_{NQR} \pm 4\nu_L/\varrho$; $(\varrho = (1 + \eta^2/3)^{1/2})$. Their Fourier transform shows 4 maxima located at $\nu_{1,2} = \nu_{NQR} \pm (1 + \eta) \nu_L/\varrho$ and $\nu_{3,4} = \nu_{NQR} \pm (1 - \eta) \nu_L/\varrho$. The value of η is then found from the equation $\eta = (\Delta_1 - \Delta_2)/(\Delta_1 + \Delta_2)$, where $\Delta_1 = \nu_1 - \nu_2$ and $\Delta_2 = \nu_3 - \nu_4$.

The method developed in [28] was used to measure η in powder samples of previously unstudied compounds of tetra- and penta-coordinated phosphorus [35].

Thus there is a wealth of reasons for considering the pulse methods as most suitable for the Zeeman NQR studies of any type of compound. They provide reliable values of η, simplify the tedious experimental procedures and remove limitations imposed on the samples by stationary methods. In addition there is considerable room for a further increase in sensitivity of the pulsed methods and thus the accuracy of determining η which we shall discuss in the next section.

B. RECORDING NQR SPECTRA

Large line widths and low intensities are generally observed in NQR spectra imposing severe requirements on the equipment. An NQR spectrometer should provide a combination of high sensitivity, and stable radiofrequency power output over the whole scan range. The spectroscopic range of the quadrupole interactions is exceedingly wide, from below 1 to above 1000 MHz. Quadrupole transitions for a particular compound may cover several hundred MHz.

Instruments that satisfy the above requirements may be based on a number of different principles. A survey of experimental NQR techniques up to 1963 was reported by Grechishkin and Soifer [36]. We shall not provide instrumentation detail but give only a brief view of their advantages and shortcomings. Spectrometers using the continuous wave (c.w.) technique were the first NQR instruments, and this principle is still used in NQR instrumentation. The choice of the generator-detector is determined by the compound to be studied.

Regenerative spectrometers (marginal oscillators) are most efficient in the low frequency region. Practically, they cannot be used at frequencies exceeding 100 MHz and can best of all be applied to the study of compounds containing ^{14}N nuclei which are generally characterized by long relaxation times. In this case, the danger of saturating the resonance transitions is minimized because of the low radiofrequency power output. Marginal oscillators provide rather accurate reproduction of the resonance line shape. However they require much adjustment and monitoring of null stability in order to maintain the required sensitivity over the whole spectroscopic range. The theory of marginal oscillators-detectors has been described [3, 13, 37] and will not be discussed further here.

The first instruments which found practical application were spectrometers of the Pound and co-workers [38, 39] or Robinson type [40].

Super-regenerative spectrometers with internal or external quench have achieved a high reputation as instruments providing high radiofrequency power outputs in the range 20—300 MHz. Unlike marginal oscillators, they do not

require fine tuning during scanning. The necessary tuning is performed by internal automatic control systems. The physical processes responsible for the NQR signal rise in the super-regenerator-detector systems are exceedingly complex and line shapes suffer considerable distortion [41]. Super-regenerative oscillators are however believed to possess higher sensitivity than marginal oscillators because coherent nuclear precession gives rise to development of radiofrequency oscillations to a far greater extent than does noise [2; 13].

Sidebands appear at integral multiples of the quench frequency. These excite resonance transitions during scanning of the carrier frequency and are one of the disadvantages of super-regenerative systems. Spectra obtained with such systems represent series of closely spaced lines. This hinders determination of the correct resonance frequency and may mask multiplet structure of the NQR spectra. Ordinary super-regenerative spectrometers are thus unsuitable for the study of signal shapes and for determination of relaxation times. Another limitation is high radiofrequency output which makes spectrometers of this type inapplicable in the case of easily saturating resonance lines. In order to overcome some of these disadvantages a number of modified super-regenerative oscillators have been suggested: with frequency locking [42]; with suppression of sidebands accomplished in the super-regenerative circuit itself [43]; with frequency and phase locking and equipment for S/N ratio enhancement [44]. These instruments operate between $30-230$ MHz, combine high sensitivity and good frequency stability, and allow the stabilized line shape response through the use of an appropriate feedback circuit.

At frequencies above 150 MHz, super-regenerative oscillators with distributed circuit elements and push-pull oscillators are used. At still higher frequencies, cavity-type oscillators may be employed. A super-regenerative oscillator with a coaxial transmission line, automatic coherent gain control, sideband suppression and frequency calibration operating from 100 to 380 MHz has been reported [45]. This is a partly modified version of a standard commercially available Decca Radar NQR system. A wide range spectrometer with an oscillator of the microstrip type and suppression of sidebands has been designed to cover $250-1100$ MHz [46a]. A coaxial-cavity super-regenerative oscillator with cylindrical trimmer condenser for tuning, has also been reported to cover $300-1000$ MHz [46b].

Other disadvantages of c.w. spectrometers are the difficulty in determining the resonance transitions frequencies ν of the sideband series $\nu \pm n\nu_q$ (where ν_q is the quenching frequency and n is 1, 2, 3 ...), the impossibility of analyzing split signals, and poor line shape reproduction with super-regenerative oscillators. Recall also the limitations inherent in the stationary technique which impose severe requirements on the quality of the sample crystal lattice because of the strong dependence of the sensitivity on equivalent line quality, $Q_{equ} = \nu/\Delta\nu$, where ν is the resonance transition frequency and $\Delta\nu$ is the NQR line width.

The preparation of samples of high purity producing spectral lines of minimal width (broadening due only to relaxation contributions would be ideal) and hence of the highest Q_{equ} is most important in obtaining good NQR signals using stationary instrumentation [47]. For example deuterated p-dibrombenzene was used by Read in his experiments [44] to reduce dipolar broadening of the bromine resonance by substitution of hydrogen for deuterium. The resulting decrease of line width from 14.1 kHz to 5.3 kHz gave at resonant frequency $\nu = 223.781$ MHz, a value of $Q_{equ} = 42\,221$. The probability of detection of a NQR signal, using stationary methods, decreases rapidly at Q_{equ} below 5000 MHz, and the signal becomes practically indetectable with c.w. instruments when Q_{equ} does not exceed 10^3 MHz [48]. Most compounds, especially inorganic compounds and coordination polymers, show broad lines originating from the scatter of local EFG values, over far from ideal crystalline lattices containing impurities, dislocations, vacancies and other defects. NQR resonance signals from such compounds have line widths from about 30 to 50 kHz in the best crystals; typically, NQR line widths are of the order of 50—150 kHz. At a resonance frequency of say 60 MHz nuclei of [79,81]Br, [185,187]Re, [75]As, [121,123]Sb, [209]Bi in a number of compounds give resonances close to this frequency value, this gives Q_{equ} values of ca. 700.

For this reason in particular, comparatively little work has been done on the NQR spectra of inorganic compounds using the stationary technique.

The pulsed methods (quadrupole spin-echo) offer an effective approach to overcoming all the limitations of marginal and super-regenerative instruments. According to this technique, a sample experiences pulsed radiofrequency power, while spin-echo signals are detected in the intervals between pulses. The suggestion that a spin-echo technique, similar to that used in NMR spectroscopy, can be applied to detect NQR signals was put forward and experimentally realized in 1954 [16, 49—51].

Since those first experiments and theoretical considerations [50, 52, 53], systematic investigation of the potential of the pulsed method in NQR spectroscopy [54—62] revealed many attractive advantages of spin-echo spectrometers over the marginal and super-regenerative instruments. The amplitude of the spin-echo signal depends insignificantly on the value of Q_{equ} which provides superior sensitivity in searching for new resonances in compounds with broad lines ($Q_{equ} < 5000$).

The spin-echo technique has also proved effective in measurements of low-frequency weak resonances characterized by long relaxation times. The construction of the pulsed NQR spectrometer with coherent mode operation and phase detection (1—5 MHz) enabled the authors [63—66] to use the ^{14}N NQR method for the successful study of a large number of nitrogen-containing compounds. Peterson and Oja [67] also reported the construction of a pulsed coherent NQR spectrometer covering 0.5—30 MHz together with comments on the advantages of pulsed techniques over marginal and super-regenerative

oscillators. They underline the considerably higher sensitivity of the pulsed method than that of any stationary technique, the much wider variety of information supplied by the former method (i.e. ability to obtain data quickly and to conveniently measure relaxation times and line shape), and much faster scan rates without suffering from saturation problems. Subsequently a panoramic NQR spectrometer covering $2-20$ MHz (ISP-1) was constructed in the SKB IRE of the USSR Academy of Sciences [68]. The pulsed method also offers much promise in the high frequency range. Pulsed spectrometers have been described in [69, 70], one of which [70] covers the interval $2-1000$ MHz. Pulsed methods have become preferred by most researchers. Several types of pulsed NQR systems are now commercially available (Matec Inc. of Warwick, Bruker SXP). The laboratory-made or modified commercial pulsed systems often possess advanced spectroscopic equipment with signal averaging systems and computer units, providing for automation of the measurements [18, 71, 72].

With a view to further enhance the sensitivity of pulsed instruments, attempts have been made to reduce the effective line width. The width of an NQR line, $\Delta\nu$, is determined by several factors

$$\Delta\nu = (T_2^*)^{-1} \simeq (T_1)^{-1} + (T_2)^{-1} + \Delta B \qquad (21)$$

The statistical distribution of local EFG components over the sample, due to crystal inhomogeneity, is reflected by the term ΔB; magnetic dipole interactions which determine mainly spin—spin relaxation time or spin-phase memory T_2 and are measured from the decay of the echo envelope (this is supposed to occur according to the law $\exp[-(\tau/T_2)^2]$ [73]); molecular motions, such as torsional oscillations or reorientations, determining mostly the spin-lattice relaxation time $T_1 \cdot T_2^*$ is the inverse of the line width parameter. This determines the time necessary for the free induction decay (FID) amplitude to decrease to $(e)^{-1}$ of its initial value [73]. The Fourier transform of the FID signal restores the real undistorted line shape.

The vast majority of inorganic compounds possess line widths mainly determined by the third term in equation (21) reflecting inhomogeneous broadening due to lattice imperfections, while the contribution of the relaxation terms is much smaller. The pulsed NQR technique however eliminates the contribution due to inhomogeneous broadening since the decay time of the echo envelope is characterized by the homogeneous contribution to the line width. Typical values for T_2 lie normally in the interval from several tens to several hundreds of microseconds. The T_1 values are often orders of magnitude longer than T_2, and therefore the contribution to the line width of the first term in equation (21) is much less than that of the second.

The main purpose for experiments on pulsed line narrowing thus consists in searching for the conditions which would provide for slower decay of the

spin-echo envelope. According to equation (21) this leads to a decrease of the term $1/T_2$ which is effectively equivalent to line narrowing. Physically these conditions favour removal of the contribution to the line width from magnetic dipole interactions.

Having modified the Lee—Goldberg technique ([74] and refs. cited therein) the authors used a sequence of radiofrequency pulses which enabled them to observe the FID in the rotating frame which appeared 25 times slower than it was in the laboratory frame due to the suppression of both inhomogeneous and dipole—dipole sources of line broadening.

The possibility of suppressing the inhomogeneous line width and to considerably reduce the contributions to the line broadening of heteronuclear dipole—dipole interactions in powders through the action of a strong alternating magnetic field in quasi-stationary states, has been theoretically analyzed [75].

The line narrowing of ^{35}Cl NQR in $p\text{-}C_6H_6Cl_2$ (lengthening of ^{35}Cl NQR spin-echo envelope decay time T_2) can also be caused [76] by a nonresonant circularly or elliptically polarized radiofrequency field at a frequency much higher than the line width of ^{35}Cl and ^1H. This line narrowing arises from averaging the local field due to protons having thus suppressed the contribution of the heteronuclear dipole—dipole interactions. The Larmor frequency of the protons around the effective field is so high that the fluctuating local field at this frequency (although it is still much lower than the NQR frequency) does not contribute to the ^{35}Cl echo decay. Therefore, the local field from the protons responsible for the echo decay is reduced and the line narrows. The contribution of this field to the ^{35}Cl echo decay is found to be reduced by a factor of almost 10^{-2}.

Attempts to narrow the NQR line by eliminating heteronuclear dipole—dipole contributions through the use of multipulse sequencies similar to those by Carr—Purcell in NMR, have also been made [71, 77—79] and theoretical calculations reported [80]. The authors [71, 79] report conditions which enable them to observe ^{14}N echo trains persisting for times of the order of the spin-lattice relaxation times T_1 which is orders of magnitude longer than is determined by the value of T_2.

Parallels to efforts for enhancing the sensitivity of NQR detection, by further improvement of the experimental technique, methods alternative to direct NQR detection are rapidly developing; for example, a double resonance spectroscopy which greatly increases the sensitivity of NQR observation. In this technique, the quadrupole transitions on the nuclei with low abundance or small quadrupole coupling constant (Q spin system) are observed indirectly, i.e. by their influence on abundant species (P spin system) for example, protons which give strong signals easily detected by NMR. Under certain conditions the radio frequency excitation of the Q spin system is transferred to the P spin system due to dipole—dipole interactions and is recorded as a change of the NMR signal on the P nuclei. The energy exchange between the two nuclear

spin systems is facilitated in a considerable number of ways. Thus, double resonance experiments have been realized successfully in high, zero and weak external magnetic fields. In all kinds of experiments, three important steps include the polarization of the P spin system, the heating of the Q system and the partial heat transfer to the P system due to the thermal contact between the two systems. The latter monitors the amplitude of the resultant free induction decay of the P system, which is recorded.

Various experimental techniques have been developed for the study of particular spin systems, e.g., with large PQ dipole−dipole interaction, with PP dipole−dipole interaction much larger than PQ (or QQ); with large QQ dipole−dipole interaction. These have been extensively reviewed and their relative advantages discussed [81−88]. Among them there are techniques which are referred to as double resonance in the rotating frame (DRRF), double resonance between the rotating and laboratory frame (DRLF), double resonance via level crossing (DRLC), double resonance with coupled multiplets (DRCM), spin-echo quadrupole−quadrupole double resonance (SEDOR), triple resonances.

This field of NQR spectroscopy is now at its initial and ascending stage, but the results obtained with the help of double resonance demonstrate a highly successful approach to a great diversity of problems which could not be solved using a single frequency technique. They are concerned with a study of rare nuclei (for instance, ^{17}O in its natural abundance, 0.037%) or nuclei near impurity sites; the determination of QCC and η of the nuclei $^{39,41}K$, ^{23}Na, ^{133}Cs, $^{85,87}Rb$, $^{35}Cl^-$ in ionic compounds; the analysis of chemical effects, especially H-bonding, in ice and many biochemically interesting compounds containing ^2H, ^{17}O, ^{14}N; the investigation of phase transition mechanisms in ferroelectric ionic compounds. Many of the observed spectra showed fine structure yielding information on dipolar coupling, for example, D−D in groups such as −ND_2, =CD_2, OD_2; D−Mn in $DMn(CO)_5$; D−Cl in DCl, etc. ([84] and refs. cited therein).

Using DRCM, Popplett resolved $^{17}O-^1H$ dipolar fine structure for the ^{17}O sites of the oxonium ion $H_2SO_4 \cdot H_2O$ [89] and for the hydroxide ion in several hydroxide compounds [90], all at natural abundance.

Appropriate space cannot however be given here to discuss in detail the many unusual aspects of this new field of spectroscopy. The interested reader is referred to the reviews mentioned above [81−88] which give a complete bibliography together with essential comment as well as reference to more recent original papers [89−94].

C. INTERPRETING NQR SPECTRA

Existing methods of interpreting NQR data differ in the approximations introduced to relate the NQR spectral parameters ($QCC = (e^2Qq_{zz})/h$, $\eta = (|q_{xx}| - |q_{yy}|)/|q_{zz}|$) to those associated with electron density distribution.
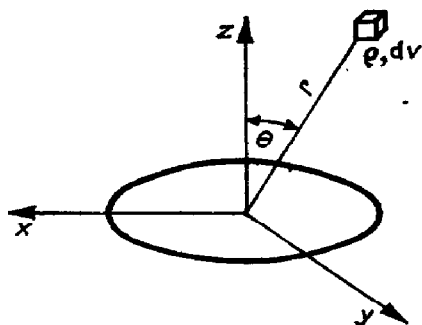

Figure 1.4   Cartesian coordinate system of molecular charge distribution.

The volume element dv of the molecular charge density distribution ϱ (Fig. 1.4) produces the electrostatic potential

$$V = \varrho \, dv/r \tag{22}$$

at the origin. Clearly

$$\frac{\partial^2 V}{\partial z^2} = \varrho(3\cos^2\theta - 1)/r^3 \, dv \tag{23}$$

since

$$\frac{\partial V}{\partial z} = -\varrho(z/r^3) \, dv = -\varrho(\cos\theta/r^2) \, dv \tag{24}$$

and

$$\frac{\partial r}{\partial z} = \frac{z}{r} = \cos\theta$$

Similarly

$$\frac{\partial^2 V}{\partial x^2} = \varrho(3\sin^2\theta\cos^2\varphi - 1)/r^3 \, dv \tag{25}$$

and

$$\frac{\partial^2 V}{\partial y^2} = \varrho(3\sin^2\theta\sin^2\varphi - 1)/r^3 \, dv \tag{26}$$

The expression for EFG at the origin may be obtained by integration of equation (23) over the molecular charge volume (eqn. (27)).

$$V_{zz} = \int \varrho (3\cos^2\theta - 1)/r^3 \, dv \tag{27}$$

In terms of quantum mechanical notations $\varrho \, dv$ should be replaced with the Bohr probability criterion $\Psi^* \Psi \, dv$. Further, we may separate from the right hand side of equation (27), the terms describing the contribution of adjacent nuclei which to a good approximation behave as point charges [8]

$$eq_{zz} = -e \int \Psi^* \left(\frac{3\cos^2\theta - 1}{r^3} \right) \psi \, dv + \sum_i z_i e \left(\frac{3\cos^2\theta_i - 1}{R_i^3} \right) \tag{28}$$

Here z_i is the full charge localized on the nuclei lying at a distance of R_i from that under consideration. The corresponding term depends only on the molecular geometry and may be calculated directly. The first term in equation (28) describes the contribution to QCC from the molecular electronic structure. Hence if wave functions are known, the QCC parameter gives the mean $(3\cos^2\theta - 1)/r^3$ value over the molecular charge distribution at a fixed point of an atom in the ground state, providing the nuclear quadrupole moment value Q is available. The experimental QCC value may, in its turn, serve as a criterion for the choice of the wave function [8].

Within the MO LCAO approximation, a molecule is described by a set K of doubly occupied orthogonal molecular orbitals. Each of the MOs is given as a linear combination of K orthogonal atomic orbitals (AO) φ_i

$$\Psi_j = C_{1j}\varphi_1 + C_{2j}\varphi_2 + C_{3j}\varphi_3 + \cdots C_{Kj}\varphi_K = \sum_i^K C_{ij}\varphi_i \tag{29}$$

Substitution of equation (29) into (28) yields equation (30).

$$eq_{zz} = -e \sum_j K_j \sum_i \sum_K C_{ij}C_{Kj} \int \varphi_i^* \left(\frac{3\cos^2\theta - 1}{r^3} \right) \varphi_K \, dv + eq_{zz}^{\text{nucl.}} \tag{30}$$

where K_j is the number of electrons in Ψ_j. The summation over all occupied orbitals in the first term leads to basic integrals of three different types. Let us analyze the QCC on the nucleus 1. The first type of integral then has the form (31).

$$C_{2j}C_{3j} \int \varphi_2^* \left(\frac{3\cos^2\theta - 1}{r^3} \right)_1 \varphi_3 \tag{31}$$

These are three-centre integrals since they include contributions from three atoms (having indices 1, 2 and 3).

The integrals of the second type are two-centre integrals

$$C_{1j}C_{2j} \int \varphi_1^* \left(\frac{3\cos^2\theta - 1}{r^3} \right) \varphi_2 \, dv \tag{32}$$

Lastly, we have one-centre integrals (33).

$$C_{1j}^2 \int \varphi_1^* \left(\frac{3\cos^2\theta - 1}{r^3}\right)_1 \varphi_1 \, dv \qquad (33)$$

The current NQR theories differ in how they treat these three types of integral. Let the EFG values measured in a molecular crystal be fully determined by contributions from the isolated molecule under consideration, so that the effects by neighbour molecules may be neglected (the second term in eqn. (30)).

The theory of Townes and Dailey [95] provides a rather simple means of determining information about the nature of chemical bonds in covalent compounds. This theory, based on the approximation of localized orbitals, was the first applied to NQR spectra and it still remains the one most widely used today. The approximations proposed by Townes and Dailey follow:

a) The neighbouring atoms give negligibly small contributions to EFG at the atom under study. In molecular crystals, this gives a contribution of less than 40 kHz to QCC [13].

b) Two-centre integrals of the type (32), which describe contributions to EFG from the overlap of electron density distribution between the atom under consideration and other atoms, are also neglected. According to Townes and Dailey [95] the neglect of the overlap density on the bonds formed by the atom under study leads to errors of about 5% in case of halogens.

c) Three-centre integrals of the type (31) give contributions to QCC from the overlap of electrons on bonds other than those for medby the atom considered. These are far less important than those preceding, and may certainly be neglected.

d) With the assumptions specified above (30) becomes equation (34):

$$eq_{zz} = -e \sum_j K_j \sum_i C_{ij}^2 \int \varphi_i^* \frac{3\cos^2\theta - 1}{r^3} \varphi_i \, dv \qquad (34)$$

Expression (34) describes contributions to QCC from electrons localized on the atom studied.

In the absence of polarization effects, internal orbitals possess spherical symmetry and consequently give no contribution to QCC. The summation in equation (34) is therefore taken only over valence orbitals. However polarization of internal orbitals often occurs (the Sternheimer effect [96]) and cannot be neglected. Still as we are mainly concerned with the ratio of QCC in a molecule to its value in a free atom, the corrections for the Sternheimer factor may cancel out on the assumption that their magnitudes vary only insignificantly on going from one molecule to another. This justifies consideration of only valence orbitals in all cases. The Townes and Dailey theory [95] proceeds by assuming that the cross-terms in equation (34) may be neglected. Separating

them out from equation (34) we have

$$(eq_{zz})_j = -eK_j \left(\sum_i C_{ij}^2 \int \varphi_i^* \frac{3\cos^2\theta - 1}{r^3} \varphi_1 \, dv \right.$$

$$\left. + \sum_i \sum_{i'} C_{ij}C_{i'j} \int \varphi_1^* \frac{3\cos^2\theta - 1}{r^3} \varphi_{i'} \, dv \right) \tag{35}$$

where the second term is formally nonzero if the orbital quantum numbers of φ_i and $\varphi_{i'}$ differ by 2. If only p and s orbitals contribute to chemical bonding, the second integral is zero. With d orbitals, the neglect of small but nonzero contributions to QCC from the s-d integral leads to some errors in calculated QCC values. The contributions from the s orbitals are also neglected, within the Townes and Dailey theory [95], because of their spherical symmetry.

Using equation (28) and hydrogen-like wave functions, Townes and Shawlow [97] have shown that the contributions to QCC from the p, d, and f orbitals are related to each other as $21:3:1$. The expression (35) may thus be reduced to consideration of only valence p orbitals to within a 15% uncertainty, and we obtain

$$(q_{zz})_j = C_x^2 q_{zz}^x + C_y^2 q_{zz}^y + C_z^2 q_{zz}^z \tag{36}$$

where $q_{zz}^x = \int p_x \frac{3\cos^2\theta - 1}{r^3} p_x \, dx, \ldots$, etc.

Following from equations (6) and (7), in axial symmetry $\left(\dfrac{\partial^2 V}{\partial x^2} = \dfrac{\partial^2 V}{\partial y^2} \right)$ the expression (37) is true.

$$q_{yy}^x = q_{xx}^y = q_{zz}^y = q_{yy}^z = q_{zz}^x = q_{xx}^z = -\frac{1}{2} q_{zz}^z \tag{37}$$

It is also true that

$$q_{xx}^x = q_{yy}^y = q_{zz}^z = q_p \tag{38}$$

where the parameter q_p characterizes the EFG produced by one unbalanced p electron; its value can be determined empirically from microwave or optical spectra. The quantity e^2Qq_p/h is usually referred to as atomic QCC.

From equations $(36 - 38)$, the principal relationship of the Townes and Dailey theory [95] which determines the EFG produced by valence p-electrons in a single MO, may be written in the form

$$(q_{zz})_j = \left[C_z^2 - \frac{1}{2} (C_x^2 + C_y^2) \right] q_p \tag{39}$$

Cyclic permutation gives

$$(q_{yy})_j = \left[C_y^2 - \frac{1}{2} (C_x^2 + C_z^2) \right] q_p \tag{40}$$

$$(q_{xx})_j = \left[C_x^2 - \frac{1}{2} (C_y^2 + C_z^2) \right] q_p \tag{41}$$

Clearly, the coefficients C_i^2 describe the weights of the respective p-orbitals used in the MO approach, so that we can write $C_i^2 = N_i$. The components of total EFG can be obtained by summing equations (39—41) over all the MOs in accordance with equation (34). Then the two experimentally measured quantities can be expressed in terms of the occupancies N_i of valence p-orbitals as

$$e^2Qq/h = \sum_j K_j \left[N_{zj} - \frac{1}{2} (N_{xj} + N_{yj}) \right] e^2Qq_p/h \tag{42}$$

$$U_p \eta = 3/2 \sum K_j (N_{xj} - N_{yj}) \tag{43}$$

where

$$U_p = e^2Qq/e^2Qq_p$$

Using the Townes and Dailey approach [95] which is based on the approximation of localized orbitals, it is necessary to locate the EFG principal axes with respect to the bond directions. In a general case, this may be done on the basis of NQR and X-ray studies of single crystals. For a large number of simple molecules, symmetry considerations may prove sufficient. With terminal atoms, the z-axis of the EFG coincides with the direction of the chemical bond. If a lone pair is present, the latter usually determines the z direction though its own orientation cannot always be determined unambiguously if there are sterically strained fragments or if charged particles are present in its vicinity. The results of numerous investigations of single crystals show that the EFG reflects the local symmetry of the crystal lattice. With molecular crystals, the EFG is determined by molecular symmetry.

We now consider the Townes and Dailey theory [95] applied to the most simple case of a halogen atom, e.g. chlorine, linked with only one atom R. The localized orbital approximation takes into consideration only valence orbitals on both halogen and R atoms. The EFG axis should naturally coincide or almost coincide with the R—Cl direction. Let the chlorine bonding orbital Ψ_1 be a $3s3p$ hybrid

$$\Psi_1 = s\varphi_s + (1 - s^2)^{1/2} \varphi_{pz} \tag{44}$$

and have occupancy b. The antibonding Ψ_2 orbital with occupancy a has the form

$$\Psi_2 = (1 - s^2)^{1/2} \varphi_s - s\varphi_{pz} \tag{45}$$

Lastly, the two π-orbitals having occupancies N_x and N_y, respectively, may be written as

$$\Psi_3 = \varphi_{px} \tag{46}$$

$$\Psi_4 = \varphi_{py} \tag{47}$$

TABLE 1.3

One-centre contributions to EFG at the chlorine nucleus
in the molecule RCl [8]

Orbital	EFG along the z-axis	Orbital occupancy	Total contribution to EFG
Ψ_1	$(1 - s^2) q_p$	b	$b(1 - s^2) q_p$
Ψ_2	$s^2 q_p$	a	$as^2 q_p$
Ψ_3	$-q_p/2$	N_x	$-N_x q_p/2$
Ψ_4	$-q_p/2$	N_y	$-N_y q_p/2$

The one-centre contributions are listed in Table 1.3, overlap terms being neglected.

Hence the expression for the total EFG has the form

$$q = -q_p(-b + bs^2 - as^2 + N_x/2 + N_y/2) \tag{48}$$

Multiplication of both parts of (48) by e^2Q yields

$$e^2Qq/e^2Qq_p = U_p = \left\{ b(s^2 - 1) - as^2 + \frac{1}{2}(N_x + N_y) \right\}$$

$$= \{b(1 - s^2) + as^2\} + \frac{1}{2}(N_x + N_y) \tag{49}$$

Let us apply equation (49) to the Cl_2 molecule. Neglecting overlap of orbitals and assuming $b = 1$, $a = 2$, $N_x = N_y = 2$ we obtain $U_p = (1 - s^2)$. As the experimental values are $e^2Qq \cdot h^{-1} = 108.9$ and $e^2Qq_p \cdot h^{-1} = 109.7$ MHz, s^2 should be nearly zero. There are other indications of a low degree of hybridization in the bonding orbitals formed by one-coordinate chlorine [98] and the conclusion drawn from the NQR data agrees with the generally accepted point of view.

On the assumption that d-orbital contributions may be neglected, in the absence of π bonding ($N_x = N_y = 2$) and with a set equal to 2, equation (49) becomes

$$U_p = e^2Qq/e^2Qq_p = (1 - s^2)(2 - b) \tag{50}$$

Within the framework of the valence bond scheme, valence orbital occupancies depend on bond ionicity, i, which in its turn correlates with the electronegativity difference of the bonded atoms. With chlorine having a higher electronegativity than R, its p_z orbital occupancy is given by $1 + i$ and the term $2 - b$ should be replaced with $1 - i$, where i is the fractional ionic character of σ-bonding.

If both $3p_x$ and $3p_y$ chlorine orbitals give equal contributions to π-bonding with R, their occupancies become $2 - \pi$, where π is the degree of double bonding. We have for U_p in that case

$$U_p = e^2Qq/e^2Qq_p = (1 - s^2)(1 - i) - \pi \tag{51}$$

If only one $3p_x$ orbital contributes to π-bonding, the asymmetry parameter becomes nonzero, the bond loses axial symmetry, and the following relationship becomes valid according to equation (43)

$$U_p\eta = \frac{3}{2}\pi \tag{52}$$

The asymmetry parameter η serves as a measure of double bonding in this case [95].

Even after excluding the d orbitals from consideration there remain three unknowns: i, π, and s, (equations (51), (52)) while only two quantities can be measured. The Townes and Dailey theory [95] is often criticized on these grounds. The number of unknown parameters can, however, often be reduced, especially for a series of related compounds, from independent considerations based on the data of other methods.

On the whole, the majority of workers express the opinion that the Townes and Dailey theory [95] furnishes a much better approach than might be expected, considering the many assumptions it includes. For that reason, the absolute occupancy values so obtained, can hardly be relied upon; if, however, relative changes in electron distribution are examined over series of related compounds, NQR spectroscopy provides quite reliable trends for such changes. As the one-centre terms increase with atomic number, the Townes and Dailey method [95] becomes more satisfactory for the heavier elements. Attempts to improve the theory, even on strict theoretical grounds, often lead to deterioration of the agreement between theory and experiment. Thus, the exceedingly simple theory by Townes and Dailey provides an adequate description of the observed trends, reveals subtle effects, and in favourable cases, gives quantitative estimates and correct predictions. No wonder therefore, that it achieved deserved success and is still being extensively used for the interpretation of a considerable body of experimental data.

Many authors attribute the success of the Townes and Dailey model [95] to the balancing of errors of opposite signs. Thus the neglect of the d-hybridization effects on QCC in halides may be cancelled out by the neglect of s-hybridization in certain cases [99]. Schempp and Bray [13] note that the representation of the LCAO is most adequate in the vicinity of the nucleus. The EFG is also determined mainly by the electron density distribution in the immediate vicinity of the nucleus where the approximations are best [100]. The particular form of the Townes and Dailey expression is, of course, determined by the structural environment of the resonance atom. Later we shall consider several

bonding situations in order to give corresponding general Townes and Dailey formulae for the EFG at the resonance nucleus.

The model suggested by Cotton and Harris [101] is based on the LCAO approach. The bond parameters i, π, σ which are empirical parameters in the Townes and Dailey theory [95], are now implicitly included in the coefficients of the basis orbitals of occupied MOs. The three-centre integrals are again neglected, and some of the two-centre integrals cancel out together with the nuclear term in equation (28). The remaining two-centre contributions are approximated by a relationship including overlap integrals S_{ik}. The contributions from the Sternheimer polarization of inner shells [96] are again assumed to vary only insignificantly from one molecule to another. The principal equation of the Cotton and Harris theory [101] has the form

$$e^2Qq_{zz}/h = \sum f_i e^2 Q q_p/h \qquad (53)$$

where

$$f_i = \sum_j K_j(C_i^2 + C_i \sum_{k>i} C_k S_{ik}) \qquad (54)$$

is the occupancy of atomic orbital φ_i in terms of MO theory.

Clearly, equation (53) reduces to the Townes and Dailey [95] relationship (42) if $S_{ik} = 0$.

The QCC values for molecules such as Cl_2 and Br_2 coincide with the QCCs of the free atoms (e^2Qq_p/h) to within 1%. This shows that there is no significant charge concentration in the overlap regions. Otherwise, charge redistribution with withdrawal of electrons from the regions in the immediate vicinity of the nuclei, to the overlap regions would cause a decrease of the QCC values in molecules with respect to those in free atoms, which is not the case. Observations of this type lend support to the Townes and Dailey theory [95] neglecting overlap integrals. There are however cases in which consideration of the electron densities in the overlap regions may be of importance. The DCl molecule provides an example [13]. The theory by Townes and Dailey [95] fails to explain the experimental QCC values of the deuteron in these molecules. Casabella and Oja [102] have compared the calculated and experimental QCC and η values for boron trihalides. They conclude that overlap electrons and halogen atom electrons make considerable contributions to the [11]B QCC values in these molecules having short bond distances.

In cases like these, the approach suggested by Cotton and Harris [101], which expresses overlap integrals explicitly, should be preferred.

Several ab initio QCC calculations have been published [103—110]. In some cases, the calculated values show good agreement with experiment [103, 104, 109, 110]. The calculations show in particular that σ and π electrons give significantly different contributions to EFG, with contributions from σ

electrons prevailing. In other words, one electron e^2Qq/h values should differ depending on whether the electron occupies a σ or a π orbital. The most general conclusion drawn is that ab initio calculations are more effective for the computation of a series of large molecules when larger basis set is used.

On the whole, the calculated QCC values rarely show good agreement with experiment, even when the most elaborate wave functions are used. EFG values are very sensitive to the analytical form of the wave function in the vicinity of the nucleus thus imposing rigorous requirements on the choice of the latter. A wave function providing reasonably good approximations in many other respects, may prove unsuitable for calculating QCC (cf. Townes and Dailey in [13]).

A theoretical QCC and η calculation with wave functions known at present, cannot be performed with an accuracy comparable to that of the experiment. The latter may, in general, be very high, the error being determined by the line width ($\Delta\nu$) and signal-to-noise ratio (S/N): $\delta = 2\dfrac{\Delta\nu}{(S/N)}$. This means that for arsenic-containing compounds showing NQR spectra with moderately broad lines ($\Delta\nu \sim 50$ kHz) and quite typical signal-to-noise ratios (S/N ~ 10 to 20), the absolute accuracy of frequency measurements is $\delta \simeq 5-10$ kHz. At the resonance frequencies of $\nu \sim 50$ MHz which are lowest for the ^{75}As nucleus, this gives a relative error of $\delta/\nu \sim 10^{-4}$. The latter can be further increased by orders of magnitude, taking into account a wide frequency range, where quadrupole nuclei resonate ($1\,\text{MHz} \leq \nu \leq 1\,000\,\text{MHz}$) and small line widths in highly ordered and pure molecular crystals. In this case we have $\Delta\nu \leq 10$ kHz.

As to a semiempirical treatment of NQR parameters on a relative scale, this appears also to be, in general, more reliable than theoretical calculations, which again justifies the use of approximations based on the Townes and Dailey theory [95].

D. INFORMATION SUPPLIED BY NQR

The NQR, being highly sensitive to changes in electron density distribution, provides diverse information on structural and chemical properties of compounds.

(i) Structural aspects of NQR information

When applied to structural investigations, NQR spectra may prove an effective tool for preliminary study of crystal structure in the absence of detailed X-ray data. Such parameters as spectroscopic shifts, multiplicity, spectroscopic

splitting, resonance line widths, the temperature dependence of resonance frequencies and relaxation rates, afford useful structural information and provide insight into the factors determining the formation of certain structural types.

It is important to note that correspondence is usually observed between the number of resonances and the number of inequivalent positions occupied by the resonance atom of a certain element in a crystal lattice. Violations of this correspondence are very rare, resulting as a rule from secondary intramolecular interactions such as H—bonding. We can therefore classify frequency separations between components of spectroscopic multiplets in accordance with their origin.

As is evident from the definition, the electronic structure of "chemically equivalent" atoms [2, 4, 11] should be identical. The violation of chemical equivalence of resonance atoms due to a change in chemical bonding, such, as for example, polymerization of initially monomeric species, leads to a significant (often 40—50%) splitting of the spectroscopic multiplet caused by a difference in the electronic structure of bridging and terminal atoms.

If the spectroscopic splitting is caused by the location of the atoms at crystallographically different sites, they are called "crystallographically inequivalent". The corresponding components of the EFG at the respective sites differ from each other in magnitude and direction due to the "crystal field effect". This generally includes contribution to the EFG of electrostatic forces between molecules, dispersion forces, intermolecular bonding and short-range repulsion forces [111, 112]. The crystal field effect on NQR spectra is less important relatively than chemical bonding, and the corresponding frequency splittings rarely exceed 5% [3], although some exceptions occur when strong H-bonding or space interactions considerably increase the splitting observed.

"Physically inequivalent" sites differ from each other only in the direction of the EFG components, their magnitudes being identical. To distinguish between such sites, Zeeman analysis of the NQR spectrum is required.

The intensities of spectroscopic lines are also important characteristics. They reflect the relative concentration of resonance nuclei at certain sites although one also has to take into account transition probabilities and life times of the energy states of the system investigated [111].

The correspondence between the number and intensities of resonances and the number of inequivalent sites occupied by a resonant atom in a crystal lattice, is very helpful in a preliminary structure study made with the use of NQR. Such a study enables one to derive, from NQR spectra, valuable information on crystal symmetry [4, 111, 113]. Thus Table 1.4 [113] gives the number of sites which can be determined by NQR Zeeman analysis for an atom at the general point position. Determination of this number is in fact, identical to determination of the Laue group of the crystal, the positive and

TABLE 1.4

The correspondence between the number of orientations of the EFG components of atoms at the central point positions and Laue symmetry for different crystal classes [113]

Crystal class	Laue symmetry	Number of possible orientations of the EFG components
Triclinic	$\bar{1}$; C_i	1
Monoclinic	$2/m$; (C_{2h})	2
Orthorhombic	$m\,m\,m$; (D_{2h})	4
Tetragonal	$4/m$; (C_{4h})	4
Tetragonal	$4/m\,m\,m$; (D_{4h})	8
Rhombohedral	$\bar{3}$; (C_{3i})	3
Rhombohedral	$\bar{3}\,m$; (D_{3d})	6
Hexagonal	$6/m$; (C_{6h})	6
Hexagonal	$6/m\,m\,m$; (D_{6h})	12
Cubic	$m\,3$; (T_h)	12
Cubic	$m\,3\,m$; (O_h)	24

negative directions of the z-axes of the EFG, being indistinguishable in the Zeeman splitting patterns.

The NQR single-crystal Zeeman analysis can provide information about special point positions occupied by the quadrupole atoms. Their number is usually lowered by the symmetry operations of the Laue group.

In general, an NQR single-crystal Zeeman study determines the orientation of the EFG components with respect to the crystal axes, which essentially facilitates the most difficult and time-consuming stage of the X-ray analysis.

TABLE 1.5

The angles between the directions of C—Cl bonds and the crystal axes in 1,3,5-trichlorobenzene according to NQR [114] and X-ray [115] results

Chlorine position	Crystal axes					
	a		b		c	
	NQR	X-ray	NQR	X-ray	NQR	X-ray
Cl_1	119.1°	118.8°	149.5°	150°	81.7°	80.9°
Cl_2	64.1°	65.0°	31.3°	30.2°	73.7°	74.3°
Cl_3	24.8°	24.0°	90.4°	90.5°	114.8°	114.0°

Table 1.5 gives comparison of the angle values between the crystal axes and the EFG z-axis at the chlorine atoms (i.e. the directions of the C—Cl bonds) in 1,3,5-trichlorobenzene, determined by the two methods.

In order to illustrate more completely the aspects of structure information which can be obtained by NQR single-crystal Zeeman spectroscopy, we consider in more detail an NQR study of $BiCl_3$ [116] whose structure is known [117]. This consists of discrete distorted pyramidal molecules with Bi—Cl bonds according to the structure in Figure 1.5. The space group is orthorhombic $Pn2_1a$ according to [117] with four molecules in a unit cell: $a = 0.764$ nm;
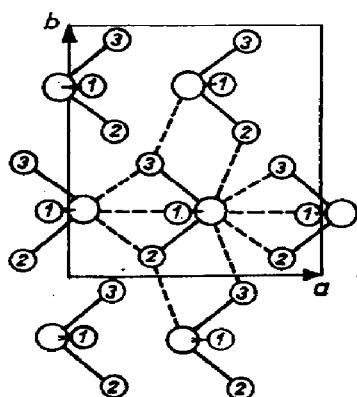

Figure 1.5   Projection of the structure of $BiCl_3$ on the ab plane showing the chlorine bridging between a single $BiCl_3$ molecule and its neighbours [117].

$b = 0.917$ nm; $c = 0.629$ nm. Cl(2) and Cl(3) atoms in Figure 1.5 are nearly equal. There are Bi⋯Cl intermolecular distances which are shorter than the sum of the van der Waals radii of the corresponding atoms, so that the bismuth atom is surrounded by five neighbouring chlorine atoms apart from the three nearest chlorine atoms (Fig. 1.5). The two chlorine atoms (Cl(2) and Cl(3)) are involved in bridging to two other Bi atoms while the Cl(1) atom is involved in bridging to only one other Bi atom. The ^{35}Cl and ^{209}Bi NQR parameters of $BiCl_3$ measured by means of the single-crystal Zeeman method are listed in Table 1.6. The assignment of ^{35}Cl resonances is unambiguous due to direct correspondence of the lower frequency line of double intensity to the two Cl atoms which are crystallographically nearly equivalent (Fig. 1.5). The asymmetry parameter η, for the chlorine atoms, has been determined, using the zero-splitting cone method described above. According to the results the $BiCl_3$ crystal belongs to the Laue symmetry of D_{2h} and therefore to the orthorhombic crystal class. The Cl(1) and Bi atoms occupy the special point positions in the lattice since only two non-equivalent directions of the corresponding EFG components have been detected for them, while four orientations have been found for the EFG components at the site of Cl(2, 3) atoms.

TABLE 1.6

^{35}Cl and ^{209}Bi NQR spectra of BiCl$_3$ [116]

Isotope	T(K)	Transition frequencies (MHz)				$\dfrac{e^2Qq}{h}$ (MHz)	$\eta(\%)$	Assignment
		1/2—3/2	3/2—5/2	5/2—7/2	7/2—9/2			
^{35}Cl	291	15.952(2)*)				30.960	43.1	Cl(1)
		19.173(1)				38.145	17.8	Cl(2)
^{209}Bi	294	31.865	25.132	37.362	51.776	318.9	55.5	

*) Relative intensities of the lines are shown in parentheses.

The $Pn2_1a$ space group [117] assumes three kinds of chlorine atoms in a unit cell which are expected to give three equally intense ^{35}Cl resonances. Moreover, each resonance must split into four zero-splitting components in an applied magnetic field. The number of observed ^{35}Cl resonances, as well as the Zeeman-splitting pattern, do not agree with these predictions, but suggest that the molecule possesses a mirror plane and therefore the centrosymmetric group $Pnma$. The lower frequency resonance of double intensity is then to be assigned to the chlorines out of the mirror plane while the higher frequency line corresponds to one lying in the mirror plane. The shorter (i.e. more covalent) bond length of the latter corresponds to the higher resonance frequency as expected in accordance with equation (51).

Table 1.7 lists the angles between the EFG z-axes and the crystal axes in BiCl$_3$ resulting from the NQR single-crystal analysis compared with their values calculated assuming the $Pn2_1a$ space group. The calculations were performed on the assumption that the z-axes lie on the relevant Bi—Cl bonds. As one can see from Table 1.7 the angle values compared show rather good numerical agreement even though determined within different space groups. This indicates that the z-axis on each Cl atom is directed along the intramolecular Bi—Cl bond despite from the large asymmetry parameter value (Table

TABLE 1.7

The interbond angles ⊰Cl—Bi—Cl in BiCl$_3$

	Cl(2)—Bi—Cl(3)	Cl(1)—Bi—Cl(2)	Cl(1)—Bi—Cl(3)
NQR [116]	85.5°	92.3°	92.3°
X-ray [117]	84.5°	93.2°	94.9°

1.6). The intermolecular secondary bonds between Cl and Bi atoms may partly be responsible for η being so large, although these bonds seem to be still considerably weaker than the intramolecular bonds since they do not affect the direction of the EFG z-axis.

One can see from this example that NQR spectroscopy provides a great deal of structural information which is of great value even if the results of the X-ray analysis are available. Thus, the NQR data enabled the author [116] to correct the space group of the compound determined by the X-ray study.

We shall later return again to this paper in order to discuss aspects of bonding obtained with the help of NQR.

The fact that the difference between chemically non-equivalent atomic positions is readily revealed in NQR spectroscopic splitting may be utilized to identify geometric isomers. Octahedral complexes of tin tetrachloride, $SnCl_4 \cdot 2D$, form either cis- or trans-isomers. In cis-isomers the axial and equatorial chlorine atoms have different electron density distributions [118]. The chemical inequivalence produces considerable splitting in the NQR spectra.
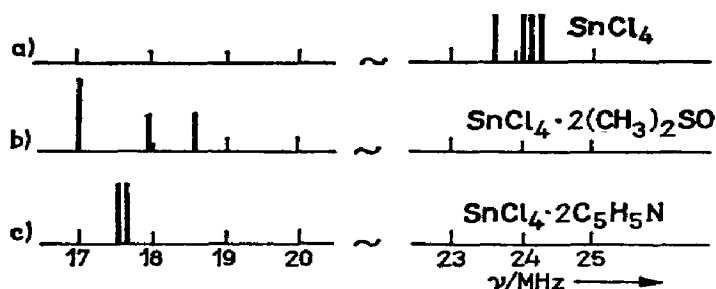

Figure 1.6 ^{35}Cl NQR patterns of the initial $SnCl_4$ (a) and octahedral complexes of composition $SnCl_4 \cdot 2L$ [119]; b) cis-$SnCl_4 \cdot 2(CH_3)_2SO$; c) trans-$SnCl_4 \cdot 2C_5H_5N$.

In trans-complexes, all four chlorine atoms are chemically equivalent with identical electron density distribution. Splitting in the NQR spectra of these isomers, arises therefore from crystallographic inequivalence of the chlorine positions. Indeed, the observed NQR splitting of two complexes (Fig. 1.6) provides evidence for the cis-configuration of $SnCl_4 \cdot 2(CH_3)_2SO$ and the trans-configuration of $SnCl_4 \cdot 2C_5H_5N$ [119] confirmed by X-ray data [120, 121].

The width of the NQR signal also incorporates important structural information. In molecular crystals of high order and purity, the line width is not much different from the value determined by the sum of the two first terms in equation (21). In the majority of inorganic compounds, the lines are however inhomogeneously broadened by lattice imperfections such as defects, vacancies, admixtures and dislocations, so that their widths are mainly determined by the third term of equation (21). Systematic study of spectroscopic shifts and broadening produced by a continuous change of the relevant sources of

broadening, makes an effective approach to the investigation of problems concerned with distribution of mixtures over a matrix, the nature of their interaction with matrix, the mechanisms of disorder, the local order in vitreous compounds, etc.

(ii) Aspects of bonding from NQR spectra

The Townes and Dailey approach [95] is the most widely used to provide a meaningful account of bonding trends within a series of related compounds. The precise form of the formulae depends on the environment of the resonant atom, and some of the most widespread in inorganic chemistry are collected in Table 1.8 (they are labelled as N^*). The example of a singly coordinated resonant atom bonded to another atom or group R, was considered in some detail earlier as an illustration of the Townes and Dailey method [95]. Recall that consideration is restricted to systems with only one-centre integrals arising from the valence p-orbitals, s-hybridization being ignored. No correction for the distortion of the valence p orbitals by the effective nuclear charge is introduced. In this case, we have according to equations $(39-41)$:

$$q_{zz}/q_p = U_p^z = |N_z - (N_x + N_y)/2|$$

$$q_{xx}/q_p = U_p^x = |N_x - (N_y + N_z)/2|$$

$$q_{yy}/q_p = U_p^y = |N_y - (N_x + N_z)/2| \tag{55}$$

and

$$\eta U_p^z = \frac{3}{2}(N_x - N_y) \tag{56}$$

where N_x, N_y and N_z are the occupancies of the p_x, p_y and p_z orbitals respectively, and q_p is the EFG along the axis of the valence p orbital produced by a single electron in that p-orbital. The symbols σ and i in Table 1.8 denote the covalent and ionic character of $R-Cl$ bonding, respectively; X is the electronegativity of the atom. The formulae $(1^*)-(3^*)$ of Table 1.8 for a singly or multiply one-coordinate resonant atom bonded are evident from equations (55) and (56).

Our next model is the two-coordinated resonant atom in the symmetric and asymmetric bonding environment AR_2. A molecular orbital (MO) population analysis is again performed here. The MO system is given in Table 1.8 for the general case of a symmetric AR_2 system assuming that the σ-bonds of the system are represented by sp^2 hybrid orbitals, the interbond angle is 2γ, and the π-electrons occupy an MO which is a pure p_f orbital. Several particular situations have been analyzed using this general model.

One is the population analysis of the ^{14}N atom in pyridine enabling one to evaluate the nitrogen $\sigma(a)$ and π-bond (b) orbital populations (eqns. 10^*, 11^*

TABLE 1.8

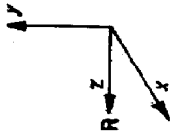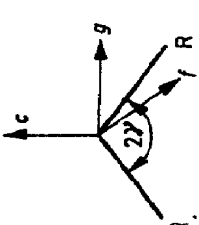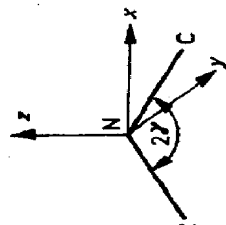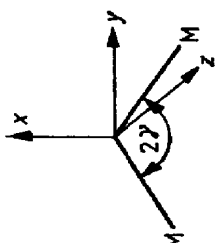Several bonding models and their description in terms of the Townes and Dailey approach (see text)
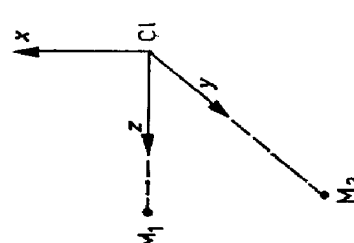
Model	Formulae	(N*)
1. AR	Orbital occupancies:	
$s = 0$	a) $N_{p_z} = b$; N_{p_x}; $N_{p_z} = 2$; b) $N_{p_z} = b$; $N_{p_x} = 2$; $N_{p_y} = 2 - \pi$	
	a) $U_p^z = \dfrac{e^2 Q q_{zz}}{e^2 Q q_p} = 2 - b \quad \begin{aligned} &= 2 - (1+i) = 1 - i\,(x_A > x_R) \\ &= 2 - (1+i) = 1 + i\,(x_A < x_R) \end{aligned}$	(1*)
	b) $U_p^z = -(2 - \pi/2 - b)$	(2*)
	$\eta U_p^z = \dfrac{3}{2}\pi$	(3*)
	x = electronegativity	
2. AR$_z$	Orbital occupancies:	
$\Psi_1 = \cot\gamma\,\varphi_s + \sqrt{1 - \cot^2\gamma}\,\varphi_e$ $\Psi_2 = \varphi_f$ $\Psi_3 = 1/\sqrt{2}\{\sqrt{1 - \cot^2\gamma}\,\varphi_s - \cot\gamma\varphi_e + \varphi_g\}$ $\Psi_4 = 1/\sqrt{2}\{\sqrt{1 - \cot^2\gamma}\,\varphi_s - \cot\gamma\varphi_e - \varphi_g\}$	c b a a	
	$U_p^s = \dfrac{e^2 Q q_{ss}}{e^2 Q q_p} = (1 - \cot^2\gamma)(c - a) + (a - b)/2$	(4*)
	$U_p^g = (1 - \cot^2\gamma)(a - c)/2 + (a - b)/2$	(5*)
	$U_p^f = (1 - \cot^2\gamma)(a - c)/2 + (b - a)$	(6*)
a) ^{14}N NQR in C$_5$H$_5$N	Orbital occupancies:	
	$c = 2$	
	$U_p^z = (1 - \cot^2\gamma)(2 - a) + (a - b)/2$	(7*)
	$U_p^z = (1 - \cot^2\gamma)(a - 2)/2 + (a - b)/2$	(8*)
	$U_p^y = (1 - \cot^2\gamma)(a - 2)/2 + (b - a)$	(9*)
	$\dfrac{2}{3} U_p^z \eta = a - b$	(10*)
	$2 - a = \dfrac{3}{2} U_p^z (1 - \eta/3)$	(11*)

TABLE 1.8 (continued)

Model	Formulae	(N*)
b) ^{35}Cl NQR in symmetrically bridged compounds	Orbital occupancies:	(12*)
	$c = 2; b = 2$	(13*)
	$U_p^x = (1 + \cot^2 \gamma)(1 - a/2)$	(14*)
	$U_p^z = (1/2 - \cot^2 \gamma)(2 - a)$	(15*)
	$U_p^y = (2 - \cot^2 \gamma)(a/2 - 1)$	(16*)
	$U_p^z = (2 - a)/(1 + \eta/3)$	
	$\eta = -3 \cos 2\gamma$	

c) ^{35}Cl NQR in asymmetrically bridged compounds	HgI$_2$ · dioxane	
σ_T is partial covalent character of the terminal bond; σ_{B_1} is partial covalent character of primary (short) bridge bond; σ_{B_2} is partial covalent character of secondary (long) bridge bond.	Orbital occupancies:	(17*)
	$N_z = 2 - \sigma_{B_1}$	
	$N_x = 2; N_y = 2 - \sigma_{B_2}$	
	a) $U_p^z = \sigma_{B_1} - \sigma_{B_2}/2$	(18*)
	$\eta = 3/2 \dfrac{\sigma_{B_2}}{\sigma_{B_1} - \sigma_{B_2}}$	
	$\sigma_{B_1} = U_p^z \left(\dfrac{\eta}{3} + 1\right)$	(19*)
	$\sigma_{B_2} = \dfrac{2}{3} U_p^z \eta$	(20*)
	b) when a terminal bond is also available; ν is NQR frequency	
	$2(\nu_T - \nu_{B_1})/e^2 Q q_p \cdot h^{-1} = (\sigma_T - \sigma_{B_1}) + \sigma_{B_2}/2$	(21*)
	$\sigma_{B_2} \approx 2.4 (\nu_T - \nu_B)/e^2 Q q_p \cdot h^{-1}$	(22*)
	$\eta \approx 1.8 (\nu_T/\nu_B - 1)$	(23*)

3. AR₃ or XAR₃

a) for AR₃:

$$U_p^z = -3(2 - a) \cos \alpha / (1 - \cos \alpha) \tag{24*}$$

$$\eta = 0$$

b) for XAR₃:

$$U_p^z = -3(b - a) \cos \alpha / (1 - \cos \alpha) \tag{25*}$$

$$\eta = 0$$

Orbital occupancies:

$$\Psi_1 = s \varphi_s + \sqrt{1 - s^2} \, \varphi_{p_z} \qquad b$$

$$\Psi_2 = s_1 \varphi_s + \sqrt{1 - s_1^2} \left(\varphi_{p_z} \cos \theta - \varphi_{p_x} \sin \theta \right) \qquad a$$

$$\Psi_3 = s_1 \varphi_s + \sqrt{1 - s_1^2} \left(\varphi_{p_z} \cos \theta + \varphi_{p_x} \frac{\sin \theta}{2} - \sqrt{3} \, \varphi_{p_y} \frac{\sin \theta}{2} \right) \qquad a$$

$$\Psi_4 = s_1 \varphi_s + \sqrt{1 - s_1^2} \left(\varphi_{p_z} \cos \theta + \varphi_{p_x} \frac{\sin \theta}{2} + \sqrt{3} \, \varphi_{p_y} \frac{\sin \theta}{2} \right) \qquad a$$

$$s^2 + 3 s_1^2 = 1; \quad s_1^2 = \cos \alpha / (1 - \cos \alpha)$$

of Table 1.8) if the values of $U^z_p = e^2Qq/e^2Qq_p$ and η are measured experimentally. Table 1.8 shows the orientation of the EFG axes at the ^{14}N atom site.

Another example presents the situation where the quadrupole atom A (halogen) makes a symmetrical bridge between two metal atoms, often the case in polymeric metal halides of composition MX_n ($n = 3-5$). The metal atoms do not form π-bonds with the bridging halogens, therefore b and c (the occupancies of π and lone pair orbitals, respectively) must be set equal to 2. The z-axis of the EFG lies, in this case, along the axis perpendicular to the molecular plane (Table 1.8), and the asymmetry parameter η is, according to equation (15*), completely determined by the angle between hybrid σ-orbitals [123]. The bridging halogen σ-bond orbital population (a) can be estimated according to equation (16*).

A situation which is frequently realized in inorganic coordination compounds, involves formation of so-called "secondary bridging" when the halogen atom bridges two metal atoms by means of two considerably different bond lengths. The Townes and Dailey approach has been modified for the analysis of such systems (antimony and mercuric halide adducts) [124]. It was shown that the asymmetrically bridging halogen uses pure p orbitals for the secondary bonding, denoting the covalent bond characters of primary (short) and secondary (long) metal—halogen bond as σ_1 and σ_2, respectively. Each of these may easily be estimated, according to equations (19*) and (20*) of Table 1.8, from the experimental QCC (U^z_p) and η values. Equation (20*) appears useful in yielding a contribution to the EFG at the site of the terminal halogen atom, from electron distribution in the crystal lattice outside the molecule studied. This contribution is σ_{CF}, which is a falsely deduced element of covalency. Its value was found to be within $\pm 1\%$ of σ_T. It arises mainly from asymmetry of the crystal field, leading to a non-zero η value at the terminal halogen while it should ideally be zero. Having substituted the measured η value into equation (20*) Wulfsberg and Weiss [124] found error of ± 0.02 in the estimation of the covalent bond order, due to asymmetry in the crystal field (mercury complexes and some other compounds having both terminal and asymmetrically bridging halogen atoms). Some of their results are listed in Table 1.9 which provides estimates of secondary bonding effects. The Table 1.9 also lists the difference $\sigma_T - \sigma_B$ between the covalent character of the terminal halogen and that of primary (short) bonding of the asymmetrically bridging halogen. This gives an estimate of the polarization of the primary metal—halogen bond as a result of the secondary bonding. The mean value of the ratio $\sigma_{B_2}/(\sigma_T - \sigma_{B_1})$, the highest and lowest values being deleted, lead the authors to an approximate relationship

$$\sigma_{B_2} \approx 3(\sigma_T - \sigma_{B_1}) \tag{57}$$

providing evidence that about one third of the electronic effect of the secondary bonding is transmitted through the chlorine to the primary bond, in-

TABLE 1.9

Fractional covalent bond orders σ of metal—halogen bonds calculated from NQR data [124]: σ_T covalent bond order for terminal halogen atom; σ_{CF} fictitious "secondary bond order" of terminal halogen atoms arising from asymmetry of the crystal field; σ_{B_1} primary bond order and σ_{B_2} secondary bond order for the bridging halogen atom (RT room temperature)

Compound	T (K)	Terminal halogens		Bridging halogens			
		σ_T	σ_{CF}	σ_{B_1}	σ_{B_2}	$\sigma_T - \sigma_{B_1}$	$\sigma_{B_2}/(\sigma_T - \sigma_{B_1})$
$HgI_2 \cdot$ diglyme	77	0.518	0.022				
		0.512	0.008				
$HgI_2 \cdot$ triglyme	77	0.516	0.015	0.508	0.021	0.008	2.6
$HgI_2 \cdot$ tetraglyme	77	0.511	0				
	RT	0.504	0.013				
$HgI_2 \cdot$ dioxane				0.515	0.055		
$HgI_2 \cdot$ py-N-oxide[a])	RT	0.501	0.012	0.491	0.041	0.020	2.0
HgI_2-γ-pic-N-oxide[a])	RT	0.508	0				
$2SbCl_3 \cdot C_6H_6$	RT	0.365	0.021	0.354	0.036	0.008[b])	4.5
		0.365	0.013	0.352	0.013	0.010[b])	2.5
		0.363	0.028				
		0.356	0.028				
$2SbCl_3 \cdot C_{10}H_8$	RT	0.373	0.018	0.368	0.021	0.005	4.2
				0.361	0.029	0.012	2.4

[a]) py pyridine; pic picoline;
[b]) average of σ_T values are used for all terminal halogens.

creasing the polarization (ionic character) of the latter. In other words, Wulfsberg and Weiss [124] offer the following picture of the formation of a "typical" secondary bond: 0.03 electrons are polarized or transferred towards the metal atom from the halogen p_s orbital, and the halogen acquires an additional 0.01 electron in the primary (shorter) bond with the metal.

When studying chlorine or bromine-containing compounds, η is usually not available unless the Zeeman experiments are performed. In this case the relationships given in Table 1.8 may be replaced by approximate ones dealing with [35,37]Cl and [79,81]Br NQR frequencies instead of U_p^z (QCC) values. Since the neglect of the square root term in the expression

$$\nu = e^2Qq(2h)^{-1} \cdot (1 + \eta^2/3)^{1/2} \tag{58}$$

leads to a negligible error, especially when η is not too high (for $\eta \leq 0.17$ which is typical for secondary bonding in compounds discussed in [124], the

error is less than 0.5%), we have for the terminal halogen

$$2\nu_T/e^2Qq_p h^{-1} = \sigma_T \tag{59}$$

instead of $U_p^z = \sigma_T$, and for the bridging halogen one obtains

$$2\nu_B/e^2Qq_p \cdot (h^{-1}) = (\sigma_{B_1} - \sigma_{B_2})/2 \tag{60}$$

instead of equation (17*). One easily comes now to equation (21*). After substitution of equation (60) into the latter we have equation (22*) which permits us to estimate the covalent character of the secondary bond from frequency splitting between terminal and bridging halogen atoms. Combining equations (20*) and (22*) one obtains equation (23*) to predict from the frequency splitting the η value at the site of secondary-bonded chlorine (or bromine).

Wulfsberg and Weiss [124] believe the self-consistency of the estimation justifies the use of the covalent-bonding language of the Townes and Dailey theory although they admit that the mechanism for the influence of secondary bonding on the EFG could be different. For instance, the electrons may be polarized electrostatically from the halogen p_y orbitals into some other halogen orbitals.

One more bonding model included in Table 1.8 is concerned with pyramidal molecules AR_3 or XAR_3. The idealized model has a 3-fold axis of symmetry, so that the EFG at the site of resonance atom A is axially symmetric, therefore $\eta = 0$. The populations of the σ-bonds A—R are labelled a, that of the fourth orbital is b. The corresponding relation between the quadrupole parameter U_p^z, the RAR interbond angle α and the orbital populations are given by equation (25*). The latter is very sensitive to the angular term. Often in certain compounds, the fourth atom X is absent, the appropriate orbital being occupied by a lone pair of electrons. In this case b is set equal to 2 and equation (24*) is valid.

We now return to the discussion of the NQR results for $BiCl_3$ [116] with respect to chemical bonding. As shown in Figure 1.5 there are two Cl atom positions in the structure, one being three coordinated to Bi atoms ($Cl_{2,3}$) and the other making an asymmetrical bridge between the two neighbouring Bi atoms (Cl_1). Furukawa [116] uses the Townes and Dailey approach to derive chemical information from the NQR results. The nearest atom environments of both the chlorine atoms are, however, different from those considered in Table 1.8. Around $Cl_{2,3}$ there is a non-regular trigonal pyramid with different bond lengths and interbond angles, while a regular pyramid has been analyzed in Table 1.8. The other (Cl_1) although forming an asymmetric bridge, gives no evidence for retaining the direction of the EFG along the short Cl—Bi bond which was the case in the example considered in Table 1.8.

Furukawa [116] simplifies the situation with $Cl_{2,3}$, assuming the two intermolecular bonds to be equivalent. Three bismuth atoms around the $Cl_{2,3}$ positions are nearly co-planar, and the angles between intramolecular Bi—$Cl_{2,3}$

and both the intermolecular $Bi\cdots Cl_{2,3}$ bonds are practically the same. The z-axis of the EFG is then placed along the intramolecular $Bi-Cl_{2,3}$ bond, and the x- and y-axes lie parallel and perpendicular to the plane of the bridge. The intramolecular bond which is suggested to have a small amount of s-character ($s = 0.15$) is represented by σ. The intermolecular bonds are supposed [116] to be formed by the transference of p_π electrons from chlorine into bismuth vacant orbitals leading to a decrease in the e^2Qq/h value at the $Cl_{2,3}$ atom and to increase in the η value at the $Cl_{2,3}$ site due to imbalance between the p_x and p_y populations. The fractional contribution of intermolecular bonds to the total EFG is denoted by π as the sum of two.

Thus, the components of the EFG are given as follows:

$$eq_{xx} = \{-1/2\sigma + 1/2\pi(3\sin^2\theta - 1)\}\,eq_p$$

$$eq_{yy} = -1/2(\sigma + \pi)\,eq_p$$

$$eq_{zz} = \{\sigma + 1/2\pi(3\cos^2\theta - 1)\}\,eq_p \tag{61}$$

Here θ is the angle between the intra- and intermolecular bonds. The ionic character of the $Bi-Cl$ bond is, in this case, given as $\sigma = (1 - \sigma)(1 - i_\sigma)$. Substituting the experimental values of U_p^z and η from equation(8) into equation (61) one obtains the bonding characteristics listed in Table 1.10. The intramolecular $Bi-Cl_{2,3}$ bonds have a covalency of 0.37 while the formation of two intermolecular bonds occurs, due to transfer of 0.09 e$^-$ from p_π electrons to the two neighbouring Bi atoms. This is reflected by the difference in the two interatomic distances. The total charge on the Cl atoms is represented by δ.

In reality the contributions of the two intermolecular bonds are different from each other, and the z-axis may not be directed along the $Bi-Cl_1$ bond. The extent of the deviation depends on the gap between the two contributions. The assumption of C_2 symmetry around the $Cl_{2,3}$ atom is not far from the truth considering the interatomic distances, and the z-axis retains the direction along the bond in spite of the large η value (0.431) [116].

TABLE 1.10

Chemical bonding characteristics of chlorine atoms in $BiCl_3$ from NQR data [116] (i_σ ionic character of $Cl-Bi$ σ-bond; π double bond character; δ the net charge on Cl atom)

Atom[a])	$\dfrac{e^2Qq}{h}$ (MHz)	$\dfrac{e^2Qq}{h}p$ (MHz)	$\eta(\%)$	i_σ(e)	π(e)	$-\delta = i_\sigma - \pi$(e)
Cl_1	30.960	109.75	43.1	0.63	0.09	−0.542
Cl_2	38.145	109.75	17.8	0.60	0.07	−0.531

[a]) See text for definition.

When considering the Cl_2 position with only one intermolecular bond and a lack of C_2 symmetry, one must take into account the non-vanishing off-diagonal xz component of the EFG:

$$eq_{xz} = -\frac{3}{2}\,\pi \sin\theta \cos\theta \qquad (62)$$

This makes the direction of the z-axis ambiguous, and one must rotate the coordinates about the y-axis to diagonalize the components. These are:

$$eq_{xx'} = \left[\frac{1}{4}(\sigma + \pi) - \frac{3}{4}\{(\sigma + \pi)^2 - 4\pi\sigma \sin^2\theta\}^{1/2}\right]eq_p$$

$$eq_{zz'} = \left[\frac{1}{4}(\sigma + \pi) + \frac{3}{4}\{(\sigma + \pi)^2 - 4\pi\sigma \sin^2\theta\}^{1/2}\right]eq_p$$

$$eq_{yy'} = -\frac{1}{2}(\sigma + \pi)\,eq_p, \qquad (63)$$

eq_{yy} evidently remaining unchanged from equation (61). Substituting the experimentally measured NQR parameters into equation (63) one obtains the bonding characteristics shown in Table 1.10. The angle of rotation α is deduced from the expression

$$\tan 2\alpha = 2eq_{xz}/(eq_{xx} - eq_{zz}) \qquad (64)$$

This yields $5°$ meaning that the direction of the z'-axis lies within $5°$ of the $Bi-Cl_1$ bond direction, according to the model used.

The i_σ values listed in Table 1.10 are, on the whole, reasonable and consistent with the corresponding bond lengths as well as with the estimations according to Gordy's electronegativity difference (0.58). It is interesting that the results show nearly the same total electronic charge at both Cl positions in spite of the large difference of the corresponding NQR parameters.

The examples discussed do not of course exhaust the potential of NQR as a tool for structure and chemical bonding. These are only simple illustrations to the applied aspects of NQR spectroscopy. We shall extend consideration of the latter in later Chapters.

Now it seems to the point to say a few words about the rank NQR holds among other methods. The study of nuclear quadrupole interactions in solids can be made using other than NQR methods, such as Mössbauer spectroscopy, perturbed angular correlations of γ-rays, electron paramagnetic resonance (EPR), quadrupole effects in broadline NMR spectroscopy. The hyperfine structure of molecular rotation spectra can also give the EFG values but they refer to gaseous molecules.

The Mössbauer spectroscopy is a rather expensive tool using γ-rays of high energy, while the NQR is the lowest energy spectroscopy providing the least

perturbation to the substance under study. The accuracy of the QCC values determined by the former method is however low compared to NQR. The hyperfine structure of the quadrupole splitting in Mössbauer spectra is often difficult to resolve so that the information about crystallographically non-equivalent atoms remains uncertain [537].

The other advantage of NQR is that it gives an information about the ground state charge distribution while the most techniques (for instance, electronic absorption spectra) measure the parameters dependent on the properties of electronic excited states.

Like NMR and EPR, NQR provides a microscopic probe and enables therefore to study local aspects of various phenomena. It means that the information yielded by these techniques is complementary to that provided by light scattering and neutron scattering which are sensitive to the collective excitation in crystals. It is meanwhile interesting to note that NQR is more sensitive than neutron scattering when the effects due to atomic displacements are concerned. The displacements of $\sim 0.01\%$ can easily be detected by NQR [152].

Although NQR has the field of applications different from that of NMR, the Zeeman splitting of NQR spectra has much in common with the well-known shifts in NMR. The NQR spectroscopysts however restrict themselves to the case when the magnetic interaction can be considered as a perturbation $(e^2Qq/4I(2I-1) \gg \mu H$, where μ is the maximum projection of the magnetic dipole moment vector into the direction of magnetic field, H is the strength of the field).

Magnetic dipole—dipole interactions and electron-coupled spin—spin interactions measured in NMR were in the past years not usually observed in NQR, except for very favourable cases [111]. The recent progress in double resonance technique facilitated however both, detection of well-resolved dipolar structure of NQR resonance lines and their interpreting. The results are now available in the double resonance literature and reviewed in [556].

NQR is nevertheless not as extensively useful at present as NMR. The best results on light nuclei, such for example as those on ^{27}Al QCC in mineral samples, have been made using NMR ([537] and refs. therein). The changes in NMR spectra were considered as a function of the orientation of a single crystal in external magnetic field. The NQR could however directly measure the same QCC data using neither single crystals nor an external magnetic field. NQR measurements possess high spectral resolution, precision, specificity and speed of measurements. The reason for relatively limited practical application of NQR seems to lie in the lack of sufficiently sophisticated equipment [537].

CHAPTER 2

COMPOUNDS WITH DISCRETE STRUCTURAL UNITS

This chapter is devoted to consideration of compounds which contain nominally isolated species in their crystalline lattices. Very often these species form electrically charged or neutral complex groups of considerable size, such as heteroatomic ions, dimeric molecules or units of molecular adducts. Understanding of the origin of the EFG can assist in the solution of many problems concerning structural, electronic and other crystallochemical properties.

We shall discuss the geometric configuration of ions, the nature of intra-ionic chemical bonding, the probable mechanism of cation influence on the spectroscopic parameters of anions, the factors which determine the sensitivity of anionic octahedra to cationic effects, etc.

A. CHEMICAL BONDING AND STRUCTURE OF HEXAHALOMETALLATES OF THE TYPE $R_2M^{IV}X_6$; CATION INFLUENCE ON THE EFG AT THE SITE OF THE HALOGEN ATOM

The most extensive NQR and X-ray data are available for hexahalometallates(IV). They provide a good deal of material clarifying trends and regularities observed in the experiment.

Kubo and Nakamura [125] summarized their NQR data on R_2MX_6 type compounds. They estimated the ionicities of metal−halogen bonds (i) and central atom effective charge values (δ_M) in heavier element hexa-anions, from the observed halogen resonances, using the Townes and Dailey theory [95] approximations. Their calculations are based on the assumption that the EFG at the halogen atom depends only on intra-anionic metal-halogen interactions. They assumed negligible d-character and 15% s-character in the $M-X$ bond.

In fact, differences in the σ-character are the dominant factors in variations of the EFG at the halogen sites over Main Group element ions. The changes in chlorine NQR frequencies in germanium(IV), tin(IV) and lead(IV) hexachloride ions have been shown [127] to correlate with the ionization potentials of the Ge, Sn, and Pb atoms, respectively. Data on bond ionicities [125] show

an almost linear dependence on the corresponding metal—halogen electro-negativity differences within the series of derivatives of the same Group elements.

Kubo and Nakamura neglected possible π-bonding contributions to the M—hal bonds due to delocalization of halogen p_π electrons over t_{1u} MOs in octahedral complexes.

There is however experimental evidence that weak but "non-negligible" π-bonding is present in $[GeCl_6]^{2-}$ and in $[SnCl_6]^{2-}$ anions [126, 127]. Thus a comparison [127] between the ^{35}Cl NQR frequencies in isostructural salts of $(NMe_4)_2MCl_6$ with the corresponding thermochemical bond energies of $[MCl_6]^{2-}$ leads to the conclusion that π-bonding decreases in the order Ge $>$ Sn $\lesssim$ Pb. With π-bonding taken into account variations of the chemical bond parameter values for tin halides estimated for the whole range of positive charges on the
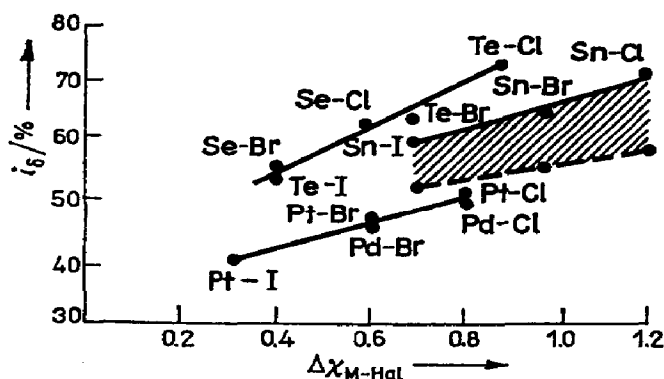

Figure 2.1 Metal—halogen bond ionicity i_σ (%) as a function of difference of electronegativity between the metal and halogen atoms ($\Delta\chi_{M-hal}$) in hexahalogen anions. Solid line correspond to the data [125] recalculated for $s = 0$. Shaded area covers possible i_σ values for tin hexahalides calculated for the effective charges on the central atom (δ_{Sn}) varying within the limits $0_{(\pi\,max)} < \delta_{Sn} < \delta_{(x=0)}$.

central atoms, fall within the limits shown in Figure 2.1. The i_σ values estimated in [125] correspond then to the upper limit of the variation range for positive δ_M values in tin hexahalides. π-Electron contributions to M—hal bonds clearly reduce the effective charge on the central atom. Neglect of the π-bonding contribution might possibly be the reason for the fact that an almost equal ionic character for the M—X bond is obtained [125] for both K_2SnCl_6 and Rb_2TeCl_6, while Sn(IV) is more electropositive than Te(IV).

In order to analyze the effect of external charges on the electron distribution within the complex anion $[MX_6]^{2-}$ one has evidently to measure the halogen resonance frequency shifts within families of complexes with the same central atom. Systematic analysis of the ^{35}Cl NQR frequency shifts due to cations, in the hexahalometallates $R_2M^{IV}Cl_6$ ($M^{IV} = Sn, Pt, Re, Te, Pb$; $R = K, NH_4, Rb$, Cs, $(CH_3)_4N$) has been carried out by Brill et al. [128] (Table 2.1).

TABLE 2.1

^{35}Cl and ^{81}Br NQR frequencies of octahedral anions at 298 K (MHz) [130, 131]

Cation	$[TeCl_6]^{2-}$	$[SnCl_6]^{2-}$	$[PbCl_6]^{2-}$	$[PtCl_6]^{2-}$	$[ReCl_6]^{2-}$
K^+	15.13	15.06		25.82	13.89
	14.99				
Rb^+	15.14	15.60		26.29	14.28
Cs^+	15.60	16.05	17.71	26.60	14.61
NH_4^+	14.98	15.45	17.05	26.07	14.09
$MeNH_3^+$	15.52	15.81	17.50		
Me_3NH^+		16.63			
Me_4N^+	16.29	16.67	18.54		
$Et_2NH_2^+$	15.91				
Et_3NH^+	15.48	14.94	15.39		
$(pyH)^{+a)}$	16.49	17.37	19.44		
			19.30		
$(2,6\text{-lutH})^{+a)}$	16.54	17.02	18.75		
$(4\text{-picH})^{+a)}$	16.68	17.81	19.87		
			19.63		
			18.58		
$(4\text{-ClpyH})^{+a)}$	16.66	17.52	19.71		
	16.37	17.32	15.53		
	15.56	14.97			
$Mg(H_2O)_6^{2+}$	15.55	15.83			

a) $(pyH)^+$ stands for pyridinium, $(lutH)^+$ for lutidinium, and $(picH)^+$ for picolinium.

Within a series of isostructural salts of the hexachlorostannate(IV) anion having a cubic antifluorite (F_{m3m}) structure[1]), no correlation existed between the frequency shifts and the Sn—Cl distances, while the former correlate well with the unit cell dimensions. Thus the ^{35}Cl frequency values, shifting upwards by 1.6 MHz along the series, are accounted for neither by Sn—Cl bond length changes, nor by the variation in orbital occupancies. They correlate, however, with changes in cation dimensions, or the anion—cation and anion—anion contact distances. These shifts correlate with the Born—Mayer potential which describes the repulsion between the chlorine atoms of adjacent octahedra. A plot of the Born repulsive potential $e^{-r/\varrho}$ (r is the separation between the Cl atoms in adjacent anions; $\varrho = 0.33 \times 10^{-8}$ is the "hardness parameter")

[1]) Among the compounds compared (K^+, Rb^+, Cs^+, NH_4^+, Me_4N^+ salts), the salt $(Me_4N_2)SnCl_6$ does not have [129] an antifluorite, but rather a cubic structure $Fd3c$ ($a_0 = 2.573$ nm) at room temperature. It becomes cubic antifluorite F_{m3m} ($a_0 = 1.297$ nm) above 365 K.

vs the ^{35}Cl resonance frequency was found [128] to be linear, indicating that the frequency increases with increase in size of the cation (Fig. 2.2). The cation influences the frequency [128] through the change of polarization of the chlorine inner shells (quenching of the chlorine Sternheimer antishielding). With increasing size of the cation the inter-ionic $Cl—Cl$ distances increase, the repulsion between them weakens, and the Sternheimer antishielding factor (γ_∞)[1] decreases. As a result, the part of the EFG produced by the external charge $(q_{ext.})$ decreases, and since it has the opposite sign to the contribution produced by the intra-anion charge distribution $(q_{int.})$, the NQR frequency must increase, which is observed experimentally.
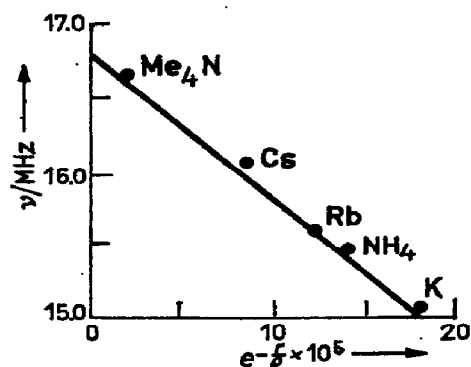

Figure 2.2   Plot of the Born-Mayer potential $(e^{-r/\varrho})$ vs ^{35}Cl resonance frequencies in R_2SnCl_6 [128] ($R = Me_4N$, Cs, Rb, NH_4, K; r is the separation between the Cl atoms in adjacent anions; $\varrho = 0.33 \cdot 10^{-8}$ is the "hardness parameter").

Ikeda et al. [131] also noticed that halogen NQR frequencies increased with the lattice parameter values in the complexes $R_2M^{IV}hal_6$ ($R = K, NH_4, Rb, Cs$; $M(IV) = Re, Pt$; hal = Cl, Br). All these compounds possess cubic antifluorite structures (F_{m3m}) at room temperature, except the platinum(IV) hexabromides whose structure were not determined. Calculations [131] using the point charge model led to the conclusion that the contribution to the EFG at the site of the halogen, associated with the direct electrostatic effect of the external ionic charges $(q_{dir.})$ is much smaller than the indirect effect $(q_{ind.})$ originating from polarization of the halogen core electron shells by external ions. The direct electrostatic effect is thus amplified by the Sternheimer antishielding factor (γ_∞), giving rise to a large indirect effect $\left(q_{ind.} = (1 - \gamma_\infty) q_{dir.}\right)$ responsible for the NQR frequency variations observed experimentally in these complexes:

$$\nu = q_{int.} + q_{ext.}; \qquad q_{ext.} = q_{dir.} + q_{ind.} \tag{65}$$

[1]) The Sternheimer factor relates, in general, to the difference in polarization of valence and core electrons; the latter gives an enormous contribution to the EFG (antishielding); the multiplicative factor of the value for chlorine is in the range 25—55 [128]. The empirical value is accepted usually to be much less.

In fact, a variation of the empirical Sternheimer factor within $10-15$ is sufficient to fit the observed frequency shifts [128]. The influence of the cations on halogen resonance frequency shifts, through the change of polarization of the halogen inner shells, is more or less common for the majority of hexahalosalts crystallizing in the cubic antifluorite lattices. Plots of the ^{35}Cl NQR frequencies in various hexachlorometallates(IV) against the ^{35}Cl NQR frequencies in $[SnCl_6]^{2-}$ are essentially linear (Fig. 2.3) with the slopes reflecting the sensitivity of the anions to the cation influence. The smaller and more compact
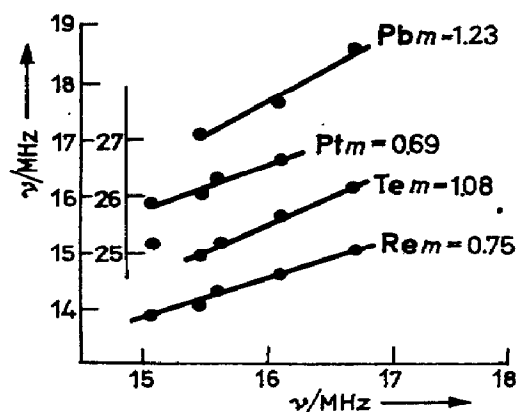

Figure 2.3 ^{35}Cl resonances in hexachlorometallates(IV) of type R_2MCl_6 (M = Pb, Pt, Te, Re) vs ^{35}Cl resonances in R_2SnCl_6 with the same cations (R) [128].

anions ($[PtCl_6]^{2-}$, $[ReCl_6]^{2-}$) are less easily perturbed and hence less sensitive to the cation influence than $[SnCl_6]^{2-}$, in contrast to the larger anions $[TeCl_6]^{2-}$ and $[PbCl_6]^{2-}$.

These observations lead to a conclusion [128] that the interaction including ion—ion repulsion and acting through the electron shell polarization of the Cl anions, is a dominant factor determining the "crystal field effect" in these salts. However it may not be completely responsible for the frequency shifts which occur. Among other non-zero contributions there may be changes in anion—cation covalency, changes in the electric dipole moments of the M—Cl bond, differences in torsional motions of the ions, electrostatic contributions, etc. Analysis of their relative importance is a major problem in interpreting the NQR data. These factors, however, do not provide a consistent explanation of the experimental data [128].

Brill and Welsh [130] pay attention to the behaviour of hexahalotellurates(IV) which demonstrate an exception to the valence shell electron-pair repulsion theory of Gillespie and Nyholm (VSEPR) [132]. The latter predicts distortion of octahedral species possessing the seventh electron pair. The NQR results (Table 2.1) readily reflect inequivalence in the chlorine positions and hence distortion of the octahedral species; however there is the strong tendency for the $[Te^{IV}Cl_6]^{2-}$ anions to form undistorted octahedra. Even the

preparation of compounds with cations of low symmetry which reduce the symmetry of the $(Te^{IV}Cl_6]^{2-}$ lattice sites did not noticeably affect this tendency. Hence the lone pair on the Te(IV) atom in the $[Te^{IV}Cl_6]^{2-}$ anion is stereochemically inactive and causes no angular distortion. The ion $[Pb^{IV}Cl_6]^{2-}$ having essentially the same dimensions (Pb $-$ Cl $= 0.250$ nm, Te $-$ Cl $= 0.250$ nm) but not lone pair, suffers, according to Table 2.1, stronger distortion due to influence of unsymmetrical cations. An extra pair of electrons does not distort the O_h structure [133] if it occupies the a_{1g} antibonding MO localized primarily on the tellurium atom. This is the case when the ns orbital of the central atom plays little part in bonding.

Another interesting aspect [128] is concerned with the low sensitivity of the hexachlorotellurate(IV) ion to cationic effects. As was mentioned above the relative measure of this effect was a NQR frequency shift suffered by halogen when cations run from K^+ to Cs^+ and $(Me_4N)^+$ over the series of isostructural salts. As was shown in Fig. 2.3, the appropriate frequency shifts depended linearly on the ionic radia of the cations (NQR data for K_2TeCl_6 were ignored because they deviated from the straight-line dependence). The slopes of the straight lines were associated with the sensitivity of various anions to the cationic effect. The latter appeared to depend mostly on the sizes of the anions, the larger ones being more easily perturbed and hence more sensitive. The exception made tellurium(IV) anions. Being of approximately the same size as $[PbCl_6]^{2-}$ they showed abnormally low sensitivity to the cationic effects. The inclination for the tellurium(IV) and lead(IV) anions measured with respect to the smaller tin(IV) anions (Sn $-$ Cl $= 0.241$ nm) appeared to be 0.106 for $[TeCl_6]^{2-}$ and 0.123 for $[PbCl_6]^{2-}$ anions. The more extended data of Table 2.1, including compounds of structures other than F_{m3m}, show that $[TeCl_6]^{2-}$ anions tend to be even less perturbed than $[SnCl_6]^{2-}$ if the whole ranges of frequency changes are compared [130].

Since the frequency shifts due to cationic effect were considered [130] to originate from polarization of halogen's inner electron shells by external cationic charges, one can suggest that the Cl^- anions are less polarizable in $[TeCl_6]^{2-}$ than in $[PbCl_6]^{2-}$. The reason for this seems to be the lone pair of electrons localized on the Te atom. Being subject to a short range influence of its negative charge, the inner electron shells of the Cl atoms reflect the superposed antishielding due to more distant cationic charges to a relatively weaker extent than those in anions with no extra electron pair. This gives rise to a smaller NQR frequency increase along the series of tellurium than of lead anions.

A strong tendency of $[TeCl_6]^{2-}$ octahedra to remain undistorted, regardless of the site symmetry, seems also to arise from the presence of the lone pair electron cloud localized on the tellurium atom.

Summarizing all the results of NQR investigations on various hexahalo-metallates(IV) we can state that the electron distribution within the anion is

mainly determined by the intra-anionic metal—halogen interactions. Weak but non-negligible π-bonding is present in the IVth Main Group element hexachlorides which decreases in the order Ge > Sn $\gtrsim$ Pb. The influence of the cations on the halogen NQR frequency mainly determining the "crystal field effect" in cubic $R_2M^{IV}X_6$ salts, seems to include ion—ion interactions (repulsions) acting through the electron shell polarization of the Cl anions. The electronic structure of the anions is also an important factor contributing to the mechanism of cation influence on the ^{35}Cl frequencies.

A number of papers are devoted to analysis of the contributions of other effects into the EFG, wich are non-zero but not of primary importance, such as lattice charge distribution, anion—cation covalency, polarization of the complex ion by the electrostatic field from neighbouring atoms, bending vibrations of M—X bonds, etc. The reader will find them reviewed in [134].

Transition metal hexahalides of the types $R_2M^{IV}X_6$ (M(IV) = Pt, Pd, Ir, Rh, Os, Ru, Re, Tc, W, Mo) have been thoroughly studied using NQR. NQR data on them have been reviewed [125, 134, 135]. Some of the compounds, namely those crystallizing in a cubic lattice, show crystallochemical properties much in common with the related compounds of the non-transition elements. In both types, the EFG at the halogen sites has mainly an intra-anion origin as well as a similar mechanism for the influence of the cation on NQR frequency shifts [128, 131]. A specific temperature behaviour was observed however in salts of the third transition hexachlorides(IV) series which did not occur with the Main Group metal complexes. The temperature coefficient of the halogen NQR frequencies increased linearly with the number of vacancies in the metal antibonding t_{2g}^* orbitals in the order $[PtCl_6]^{2-} < [IrCl_6]^{2-} < [OsCl_6]^{2-} < [ReCl_6]^{2-} < [WCl_6]^{2-}$ (Fig. 2.4, [125]). The authors [125] advocated the idea of an increasing role for the $p_\pi - d_\pi$ halogen-to-metal bonding in this series, in accordance with an increasing possibility of the t_{2g}^* orbitals participating in delocalization of the halogen atom p_π electrons (the central
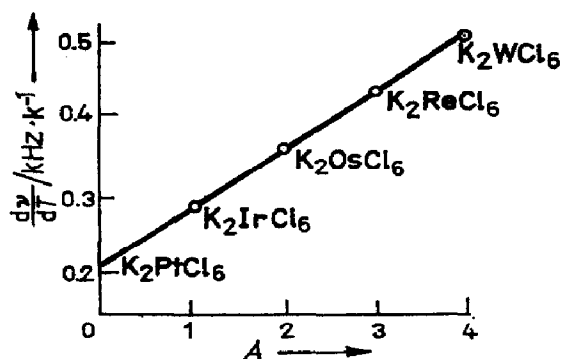

Figure 2.4 ^{35}Cl NQR frequency temperature coefficients $d\nu/dT$ (kHz · deg^{-1}) in transition metal hexahalides depending on the number of vacancies (A) in the t_{2g}^* orbitals [125].

metal valence shell configuration changing from d^6 to d^2 in the same direction). They suppose two mechanisms govern the temperature effect on the NQR frequency in these compounds. One is the usual Bayer—Kushida mechanism [136, 137] lowering the resonance frequency with temperature due to the averaging of the EFG by the growing amplitude of thermal motions according to

$$\nu_T = \nu_0 \left\{ 1 - \frac{3}{4} \sum_i (\hbar A_i/\omega_i) \coth (\hbar \omega_i/2KT) \right\} \tag{66}$$

where ν_0 is the resonance frequency in the static lattice, A_i gives the relative weight of the ith mode to the nuclear motion and has a dimension of moment of inertia and ω_i is the angular frequency of the ith mode.

The other mechanism superimposed on the first, is related to the π-bonding contribution in such a way that increase of the latter along the series, regularly enhances the temperature coefficients from negative to positive values. It was later shown [138, 139] that the second transition row metal hexahalides have temperature coefficients varying in a similar manner (Table 2.2).

Extensive attempts have been made to describe the particular vibration mechanism which reduces the π-character of the M—Cl bond and thus increases the resonance frequency in accordance with equation (42) leading to a positive temperature coefficient.

TABLE 2.2

^{35}Cl NQR frequencies ν (MHz) at 300 K and their temperature coefficients $d\nu/dT$ (kHz · deg^{-1}) for the second and third transition row metal hexahalides ([125, 134, 139] and references therein)

Cation	Anion		Δx [b])	ν (MHz)	$d\nu/dT$ (kHz · deg^{-1})
K$^+$	PdCl$_6^{2-}$	d^6 [a])	1.48	26.77 [c])	—0.89
	PtCl$_6^{2-}$		1.39	25.77	—0.93
Cs$^+$	RhCl$_6^{2-}$	d^5	1.38	21.86	—0.53
K$^+$	IrCl$_6^{2-}$		1.28	20.73	—0.54
K$^+$	RuCl$_6^{2-}$	d^4	1.41	17.34	—0.04
	OsCl$_6^{2-}$		1.31	16.82	—0.22
K$^+$	TcCl$_6^{2-}$	d^3	1.47	14.19	+0.15
	ReCl$_6^{2-}$		1.37	13.88	+0.13
Cs$^+$	MoCl$_6^{2-}$	d^2	1.53	10.74	+0.76
	WCl$_6^{2-}$		1.43	10.91	+0.35

[a]) Central metal electron configuration;
[b]) electronegativity difference values [148];
[c]) at 77 K.

Haas and Marram [140] conclude that $d_\pi - p_\pi$ metal—halogen overlap decreases with temperature because of an increase in the amplitudes of the bending vibrations. Accordingly, the degree of π-bonding also decreases.

Brown and Kent [141] reported, however, that anharmonic $M-X$ stretching vibrations rather than the $M-X$ bonding mode are responsible for reduction of π-overlap to a greater extent than for reduction of σ-overlap, producing a temperature shift of the NQR line to higher frequencies.

O'Leary and Wheeler [142, 143] concluded that the anomalous temperature dependence of the ^{35}Cl NQR frequency in K_2ReCl_6 above the phase transition point at 110.9 K (Fig. 2.5) is accounted for by a strong temperature dependence
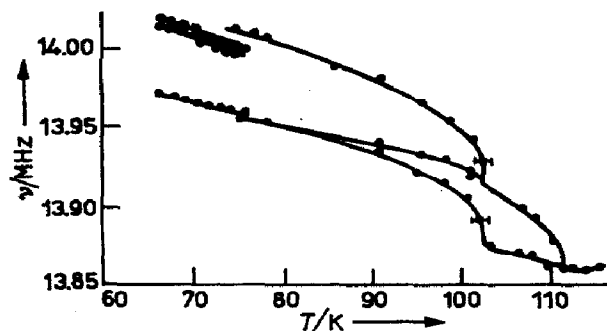

Figure 2.5   Temperature dependence of ^{35}Cl NQR frequencies in K_2ReCl_6 [142].

of the $K = 0$ torsional mode. This softens from 25 to 1 cm^{-1} in the range 300 to 112 K dominating the phase transition from cubic antifluorite to tetragonal structure. This would render unnecessary the suggestion concerning π-bonding as a factor determining the positive value for the temperature coefficient of NQR frequencies.

Following this Armstrong and co-workers [144 — 146] performed a multimode analysis of the ^{35}Cl NQR data on K_2IrCl_6 and K_2OsCl_6 to conclude that better results are obtained if one takes into account a weakening of the $M-Cl$ π-bonding with temperature.

Commenting on the role of a soft vibrational mode to produce a positive temperature dependence of the NQR frequency, note [137, 138] that $(NH_4)_2ReI_6$, K_2RuCl_6 and K_2TcCl_6 exhibit, like K_2ReCl_6, anomalous temperature dependence, but unlike K_2ReCl_6, have no phase transitions down to 77 K.

The correlation between the temperature coefficient of the ^{35}Cl NQR frequency, the absolute value of the frequencies and the number of vacancies in the central metal t_{2g}^* orbitals is particularly distinct along the series Rb_2WCl_6 (d^2), $RbWCl_6$ (d^1) and WCl_6 (d^0) [141]. Their corresponding temperature coefficients are all positive and grow in value as $+0.49$ kHz K^{-1}, $+0.54$ kHz K^{-1}, $+1.8$ kHz K^{-1}, which [141] is evidence for strong $d_\pi - p_\pi$ character in the $W-Cl$ bonds, still increasing along the series.

Summarizing, the majority of authors share the opinion that the positive temperature dependence of the halogen resonance frequencies originates from metal—halogen π-bonding although the mechanism relating π-bond weakening to the NQR temperature dependence remains unclear.

Lucken [147] however denies any irrefutable relationship between positive temperature coefficients and the presence of π-bonding. Having reviewed the origin of the vibrational dependence of gas-phase QCC in simple molecules, he proposes that intramolecular vibrations are likely to give rise to positive contributions to NQR temperature dependence with nearly the same probability as negative contributions. In fact, the temperature coefficients correlate with their resonance frequency values which themselves are linearly dependent on the extent of π-bonding (equation (51)). The temperature coefficients of K_2PtCl_6, Cs_2PtCl_6, $CsPbCl_6$, Cs_2SnCl_6, K_2SeCl_6 and Cs_2TeCl_6 are examples supporting this conclusion [147]. All of these compounds possess complete d-shells and therefore have no appreciable π-bonding. They have similar molecular and crystal structures, similar dimensions and are therefore expected to have similar temperature coefficients of resonance frequencies, if the latter are directly related to the extent of $d_\pi - p_\pi$ bonding. Contrary to this, their temperature coefficients, although all negative, show widely different magnitudes (-1.04; -0.83; -0.5; -0.48; -0.67; -0.21 kHz K^{-1} at 298 K, respectively). Therefore intramolecular vibrations increase the QCC with increasing temperature and provide a dominant contribution to the anomalous temperature dependence [147]. There is consequently no need to postulate unusual vibrational modes or bonding situations to explain the observed temperature coefficients.

These conclusions are of course not to be understood as denying the presence of any π-character in transition metal—halogen bonds in the complex hexahalides(IV). π-Bonding in transition metal hexahalides(IV) leads to considerable lowering of the halogen frequencies (Table 2.2) which can hardly be accounted by the change in electronegativity difference of the corresponding atom-partners. The situation is most impressive in bridging dimers of the transition elements ($NbHal_5$, $TaHal_5$ and others). The terminal halogen frequencies in these dimers are shifted lower than their bridging halogen frequencies, while in non-transition element dimers ($SbCl_5$, $Gahal_3$) the reverse is rue [149—151]. Later these compounds are discussed in more detail.

Many R_2MX_6 hexahalometallates(IV) undergo structural phase transformations from cubic to lower symmetry lattices when the temperature decreases. The NQR technique together with relaxation measurements have been widely and very fruitfully applied to the study of a vast field of problems related to the dynamic behaviour of these compounds. There are experiments clarifying the phase transition mechanisms and revealing local dynamic processes. They specify the order of transition and determine the phase transition points. Other studies analyze vibrational modes dominating motional averaging of

the EFG at the halogen sites and governing the phase transitions, etc. Discussion of the appropriate results is however beyond the scope of this account, and we refer the reader to several detailed reviews [152—154], devoted to the analysis of relationship between NQR parameters and various dynamic and static characteristics of crystal lattices.

We also set aside R_2MX_6 bromo- and iododerivatives, since most of the literature deals with an NQR study of lattice dynamics in these compounds. The $^{79,81}Br$ and ^{127}I NQR spectra can be found in books and reviews [4, 125, 135].

B. HEXAHALOMETALLATES OF THE TYPES RM^VX_6 AND $R_3M^{III}X_6$; STRUCTURAL TRENDS, MIXED-VALENCE HEXABROMOANTIMONATES

Octahedral hexahalogenoanions, bearing various charges and existing nominally as isolated units within a crystal, are formed by the Vth Main Group elements and some transition metals of higher groups (in lower oxidation states): Mo(III), W(V), W(III), Ir(III).

Table 2.3 lists ^{35}Cl NQR data on hexahalocomplexes of composition RM^VX_6. ^{35}Cl frequencies in Main Group metal(V) hexachlorides have been reported [155—157] to be fully determined by the nature of the intra-anion bonding which is essentially covalent. The calculated magnitudes of the direct and indirect ionic contributions to the EFG appeared not to exceed 0.5% of the total EFG for the majority of the compounds. As a matter of fact, the average values of the ^{35}Cl frequencies in $[Sb^VCl_6]^-$ anions are practically independent of the cations and are determined nearly completely by the internal electron distribution (Table 2.3). We have, however, seen above that the cation influence causes a frequency shift of 7% in cubic (F_{m3m}) hexachlorostannates(IV) and 8% in isostructural hexachloroplumbates(IV). The shifts were produced by variation of the inner shell polarization of the Cl anions when the separation between them increased with increasing size of the cations. It is however clear that the separation between the octahedra influences the NQR frequencies until a limiting value is reached. After that changes in the lattice dimensions do not produce any appreaciable shift in the NQR frequency. This is a probable explanation of the experimentally observed insensitivity to the cation influence of many phosphorus, arsenic and antimony hexachlorides normally crystallizing with large cations.

A uniform mean ^{35}Cl frequency value in $[M^VCl_6]^-$ anions is highly characteristic and may be used to identify anions in unkown compounds [157, 170].

Few data are available for uni-negative transition metal(V) hexahaloanions. The three hexachlorotungstates(V) crystallizing with alkali metal cations (Table 2.3) show regular, although small, (2.3% from K^+ to Cs^+) shifts in ^{35}Cl NQR frequencies with variation in cation [141, 158].

TABLE 2.3

^{35}Cl NQR spectra ν (MHz) of hexachlorometallate(V) anions

Cation Ref.	T (K)	[PCl$_6$]$^-$	[AsCl$_6$]$^-$	[SbCl$_6$]$^-$	[TaCl$_6$]$^-$	[NbCl$_6$]$^-$	[WCl$_6$]$^-$
[PCl$_4$]$^+$ 155, 156, 163—164	77	29.61; 30.07 30.45; 30.62		22.8; 23.02			
[Et$_4$N]$^+$ 156, 165	77	29.32; 30.06 30.34	28.37; 29.15 30.07	24.01; 24.21 24.67; 24.86			
[SCl$_3$]$^+$ 166—168	77			22.305; 22.390 23.270; 24.169 24.813; 25.828	7.684; 7.893 8.660; 9.050 9.163; 9.224	7.078; 7.373 7.510; 7.565 9.235	
[NO]$^+$ 156	77			22.35; 22.97 23.15; 25.03 25.48			
[N$_3$P$_3$Cl$_5$]$^+$ 170	77			24.62; 24.80			
[N$_4$P$_4$Cl$_7$]$^+$ 170	77			24.64; 24.74 24.88; 25.14			
[I$_2$Cl]$^+$ 159	RT*)			20.78; 24.83 21.03; 25.69			
[K]$^+$ 141, 158	RT						11.335; 11.455
[Rb]$^+$ 141, 158, 169	RT			23.609; 23.777 24.232			11.320; 11.546
[Cs]$^+$ 141, 158	RT				8.803; 9.172	8.589; 9.245	11.605; 11.748

*) RT room temperature.

The remarkable feature of the NQR spectra listed in Table 2.3 is their splitting. All anions without exception exhibit split spectra, the spread of the ^{35}Cl resonances in hexachloroantimonates(V) being extra-ordinarily large. Thus the chlorine atoms are crystallographically inequivalent in these anions, the latter suffering distortion from octahedral symmetry even in the presence of small (Rb$^+$) and highly symmetric [Et$_4$N]$^+$ cations. The spectra cited in Table 2.3 for 77 K are also split at room temperature.

Distortion of the [Sb^{V}Cl$_6$]$^-$ anions is common [159—163]. More than a 0.02 nm range in Sb—Cl distance and a 3° range in angle variation have been observed [131] in different hexachloroantimonates(V). In ICl$_2^+$ · SbCl$_6^-$ [161] the scatter of the Sb—Cl distances was found to be 0.015 nm and that of inter-

bond angles at the antimony atom was 13.6°. Merryman and Corbett [159] also measured both the ^{35}Cl NQR and ^{121,123}Sb NQR spectra in $I_2Cl^+ \cdot SbCl_6^-$. Although the anion in this salt is nominally octahedral, the antimony quadrupole coupling constant (QCC) value is fairly high (122.2 MHz for ^{121}Sb), the

TABLE 2.4

^{35}Cl and ^{79}Br NQR frequencies of hexahalometallates(III) and mixed-valence compounds of the type $R_4Sb^{III}Sb^VBr_{12}$ [174]

Compound	T (K)	Isotope	ν (MHz)		Ref.
$Cs_2LiSbCl_6$	77	^{35}Cl	13.500		4
$Cs_2NaSbCl_6$	77	^{35}Cl	13.544		4
Cs_2KSbCl_6	77	^{35}Cl	13.476		4
$Cs_2AgSbCl_6$	77	^{35}Cl	12.344		4
$Cs_2PbSbCl_6$	77	^{35}Cl	13.495		4
$[(C_2H_5)_2NH_2]_3SbBr_6$	77	^{79}Br	39.02;	123.68	171, 172
$[n(C_3H_7)_2NH_2]_3SbBr_6$	77	^{79}Br	78.26		172
$Cs_2NaBiCl_6$	77	^{35}Cl	12.432;	12.518	4
			12.734;	13.330	
Cs_2KBiCl_6	77	^{35}Cl	12.433;	12.526	4
			12.770;	13.314	
$[(C_2H_5)_2NH_2]_3BiCl_6$	300	^{35}Cl	12.601		173
$[C_2H_5NH_3]_3BiCl_6$	300	^{35}Cl	12.295;	10.064	173
$[(C_2H_5)_2NH_2]_3BiBr_6$	77	^{79}Br	45.85;	104.87	171, 172
$[n(C_3H_7)_2NH_2]_3BiBr_6$	77	^{79}Br	72.89		172
$[(CH_2CHCH_2NH_3]_3BiBr_6$	300	^{79}Br	54.080;	54.448	173
			80.512;	82.421	
K_3MoCl_6	300	^{35}Cl	9.54;	9.83	158
K_3IrCl_6	298	^{35}Cl	16.639;	17.690	139
			17.845;	18.435	

			$[Sb^{III}Br_6]^{3-}$ ν (MHz)	$[Sb^VBr_6]^-$ ν (MHz)
$(NH_4)_4Sb_2Br_{12}$	298	^{79}Br[a]	69.69 (ax)[b]	182.00 (ax)
			74.03 (eq)[b]	184.25 (eq)
$Rb_4Sb_2Br_{12}$	298	^{79}Br[a]	73.16 (ax)	183.00 (ax)
			77.66 (eq)	185.45 (eq)
$Cs_4Sb_2Br_{12}$	298	^{79}Br[a]	77.40 (ax)	186.60 (ax)
			77.62 (eq)	190.31 (eq)

[a]) Calculated from ^{81}Br frequencies in accordance with the quadrupole moment ratio $eQ(Br^{79})/eQ(Br^{81}) = 1.1971$;

[b]) (ax) and (eq) stand for axial and equatorial bromine atoms, respectively.

asymmetry parameter value (η) being 0.38. Such a value of η can be produced by as little as a 3% imbalance in the population of the antimony $p_{x,y}$ orbitals with respect to the axially symmetric state [162]. Angular distortions seem to be highly effective in this situation. The anionic distortions are in most cases attributed to packing effects [160].

The average ^{35}Cl NQR frequency corresponding to relatively unperturbed $[SbCl_6]^-$ ions is 23.7 $\pm$ 0.7 MHz at room temperature [156].

While we have no examples of undistorted octahedral configurations among the $[M^VX_6]^-$ anions considered here, hexahalometallates(III) of the same central elements do sometimes form regular octahedra (Table 2.4). Alkali metal salts of the composition $R_3M^{III}X_6$ appear [171] not to exist under normal conditions. Many $R_2R'MX_6$ hexahalometallates(III) crystallizing in face-centered cubic (f.c.c., F_{m3m}) lattice ([175] and refs. cited therein) are however known. This is also indicated by the ^{35}Cl NQR data (Table 2.4). Hexachlorobismuthates(III) need some comment. While the f.c.c. (F_{m3m}) lattice was reported [175] for $Cs_2NaBiCl_6$ at room temperature, the NQR spectra show a distorted anion geometry at 77 K. In addition, ^{35}Cl NQR data reported [4] for $Cs_2NaBiCl_6$ and Cs_2KBiCl_6 are identical within experimental error; this is rather surprizing in view of the high sensitivity of NQR in revealing distinct differences in ^{35}Cl frequencies of similar hexachloroantimonates(III) (Table 2.4).

Some of the alkylammonium hexahalometallates(III) also form regular octahedra according to their NQR spectra. This is in agreement with X-ray data [172] on the propylamine hexabromoantimonate(III).

A very interesting class of hexahaloantimonates has a formal composition R_2SbX_6 but contains not Sb(IV) atoms but a mixture of Sb(III) and Sb(V), being mixed-valence compounds $R_4Sb^{III}Sb^VX_{12}$. Antimony atoms form two types of octahedral anions $[Sb^VX_6]^-$ and $[Sb^{III}X_6]^{3-}$, differing from each other by the oxidation state of the central atom. Several bromides of this type ($R = NH_4$, Rb, Cs) have been studied by NQR [174]. The results together with the X-ray data [175 — 177], give a sensitive means for comparing crystallochemical features and elucidating the electronic state of both molecular moieties.

The crystals of the NH_4 and Rb salts form tetragonally distorted K_2PtCl_6 lattices ($14_1/amd$) with unit cell dimensions $a = 1.066$ nm, $c = 3.152$ nm (NH_4^+) [175] and $a = 1.070$ nm, $c = 2.169$ nm (Rb$^+$) [176], respectively. X-ray powder results [177] for the Cs salt ($a = 1.085$ nm, $c = 2.197$ nm) together with the NQR data (Table 2.4) give reasons for considering this salt to have a similar structure [174]. The bond lengths and angles of ammonium and Rb salts are given in Table 2.5.

As one can see from Table 2.5 X-ray analysis [175] (as well as the ^{121}Sb Mössbauer effect [178]) show no distortion of the $[Sb^{III}Br_6]^{3-}$ anion in $(NH_4)_2SbBr_6$. NQR spectra however show considerably different resonance frequencies assigned to equatorial and axial Br atoms in this polyhedrum sug-

TABLE 2.5

Bond lengths and angles in the mixed-valence hexabromoanti-
monates $R_2Sb^{III}Sb^VBr_{12}$. (The Br_a and Br_e stand for axial and
equatorial bromine atoms.)

Cation (R) Ref.	Polyhedrum	Bond lengths (nm)	Bond angles (°)
NH₄⁺ 175	$[Sb^VBr_6]^-$	0.256 Sb—Br_a	86.33 ∢ Br_e—Sb—Br_a
		0.257 Sb—Br_e	90.23 ∢ Br_e—Sb—Br_e
	$[Sb^{III}Br_6]^{3-}$	0.279 Sb—Br_a	89.68 ∢ Br_e—Sb—Br_a
		0.279 Sb—Br_e	90.00 ∢ Br_e—Sb—Br_e
Rb⁺ 176	$[Sb^VBr_6]^-$	0.264 Sb—Br_a	88.72 ∢ Br_e—Sb—Br_a
		0.253 Sb—Br_e	90.03 ∢ Br_e—Sb—Br_e
	$[Sb^{III}Br_6]^{3-}$	0.271 Sb—Br_a	88.80 ∢ Br_e—Sb—Br_a
		0.279 Sb—Br_e	90.03 ∢ Br_e—Sb—Br_e

gesting distortion of the latter to probably D_{2d} symmetry, similar to the distor-
tion of $[Sb^VBr_6]^-$ in this salt and both anions in the Rb salt (Table 2.4).

Differences in crystal chemistry of the two polyhedra in the mixed-valence
compounds are similar to those observed in the corresponding $[M^VX_6]^-$ and
$[M^{III}X_6]^{3-}$ anions with the central atom solely in oxidation state Sb(V) or
Sb(III). Thus the Sb(III)—Br bonds are longer and the Br NQR frequencies
are lower than those of the Sb(V)—Br bonds. This suggests a relatively higher
ionicity (i) of the Sb(III)—Br bonds. Within the Townes and Dailey approach
[95], Terao [174] calculated values of i from the measured $^{79,81}Br$ resonance
frequencies. He estimated the net charges δ on the Sb atoms from the equation

$$\delta = F - 6(1 - i) \tag{67}$$

where F denotes the formal charges on the Sb atoms ($F = 3$ for $[Sb^{III}Br_6]^{3-}$
and $F = 5$ for the $[Sb^VBr_6]^-$, respectively) and 6 is the coordination number of
the Sb atom. The calculated values of i and δ are listed in Table 2.6 together

with those of some other hexabromometallates(IV). As expected the Sb(III) —
Br bonds have a larger ionic character than Sb(V) — Br bonds. The ionic
character of the Sb(IV) — Br bond of a fictitious $[Sb^{IV}Br_6]^{2-}$ ion is the average
of those of the Sb(III) — Br and Sb(V) — Br bonds. It is interesting that accord-
ing to the NQR results (Table 2.6) the net charges on the Sb(III) and Sb(V)
atoms are almost equal in spite of the different formal charges, i.e., the number
of electrons on both atoms is almost the same. Terao [174] neglected delocali-
zation of the $5s^2$ electrons of the Sb(III) atom, a very small effect (less than
0.1% according to estimation [429] from the single crystal electronic spectra
of a series of similar hexachloroantimonates).

TABLE 2.6

Ionic character i of the M — Br bonds
and net charge δ on the central metal in
some octahedral anions according to NQR
data ([174] and refs. therein)

Complex ion	i	δ
$[Sb^{III}Br_6]^{3-}$	0.75 — 0.79	1.53 — 1.66
$[Sb^{V}Br_6]^{-}$	0.42 — 0.44	1.53 — 1.64
$[Sn^{IV}Br_6]^{2-}$	0.60	1.60
$[Te^{IV}Br_6]^{2-}$	0.58	1.48

Summarizing, among the octahedral complex antimonates (bismuthates)
considered here those containing the central atoms in a lower oxidation state
(14-electron complexes) commonly possess undistorted octahedral configu-
ration, making them exceptions to the valence shell electron pair repulsion
(VSEPR) model [132]. Qualitative MO arguments [179] account for the differ-
ences in bond lengths and strengths between 12- and 14-electron complexes
and rationalize trends in complex stabilities as related to ligand substitution
(distortion from octahedral symmetry). Typical bond distances (nm) in MX_6
pairs which differ only in the oxidation state of the central atom are [179]:
12-electron complexes: $[Pb^{IV}Cl_6]^{2-}$, 0.250; $[Sb^{V}Cl_6]^{-}$, 0.235; $[Sb^{V}Br_6]^{-}$, 0.255;
14-electron complexes: $[Pb^{II}Cl_6]^{4-}$, 0.296; $[Sb^{III}Cl_6]^{3-}$, 0.265; $[Sb^{III}Br_6]^{3-}$,
0.280.

The relative trend of 12- and 14-electron complexes to retain an undistorted
octahedral geometry is clarified through comparison of the MX_6 complex MO
energies octahedral (O_h) and trigonal prismatic (D_{3h}) configurations.

In 14-electron complexes the highest occupied orbital is the antibonding $2a_{1g}$
MO which accounts for longer M — X bonds in these complexes, when compared
with the corresponding 12-electron complexes. The distortion of the 14-electron

complexes from octahedral symmetry is related to the relative values of central atom and ligand AO coefficients in the $2a_{1g}(O_h)$ orbital, determined by differences in central atom and ligand AO energies. The $2a_{1g}$ MO in the 14-electron complexes is stabilized by large ligands through in-phase ligand—ligand overlaps.

The highest occupied orbital in 12-electron complexes is e_g. It is stabilized by large central atoms and small ligands (F) through ligand—ligand out-of-phase overlaps. All the 12-electron complexes considered here possess rather large volume ligands which perhaps account for their distortion from regular octahedral configuration.

C. CRYSTAL CHEMISTRY OF SQUARE-PLANAR AND TETRAHEDRAL HALOMETALLATES

(i) Complexes with square-planar tetrahaloanions

The NQR spectra of nominally isolated square-planar complex anions are presented in Table 2.7. Tetrachloro- and tetrabromoaurates(III) were systematically studied by Sasane et al. [180, 185, 186] using ^{35}Cl and ^{79,81}Br NQR. The number of resonances evidently indicates the number of inequivalent halogen atoms. As indicated by X-ray powder patterns, tetrahaloaurates(III) form crystals of lower than tetragonal symmetry with no isostructural relationships between chlorides and bromides of similar composition. The majority of compounds form crystals containing various mole fractions of water. Such hydrated compounds are not included in Table 2.7, since their anions are not generally isolated, while a wide enough NQR data set is available for anhydrous tetrahaloaurates(III).

Anhydrous $CsAuBr_4$ gives nearly as large a splitting in its NQR spectrum, as hydrated compounds with H-bonds usually do. The $[AuBr_4]^-$ anion has rhombic symmetry and is twisted through a small angle, so that the two axial Br atoms undergo torsional oscillations of much smaller amplitudes than the other two [180]. With such oscillation the principal axis direction and EFG value will change. This leads to an abrupt frequency drop in the corresponding (lower frequency) resonances when the temperature increases from 77 K, accounting for the large splitting in the NQR spectra at 193 K (Table 2.7).

Having studied the resonance frequencies, temperature dependence, it is concluded [180] that the tetrachloroaurate(III) anions have rotational freedom in the crystals. All tetrachloroaurates(III) except for the rubidium salt exhibit broadening of resonance lines at low temperature, indicative of a random orientation of tetrachloroaurate(III) ions.

On the whole, the splitting is the distinguishing feature of tetrahaloaurate(III) NQR spectra [180, 181, 185, 186]. Cations seem to have a markedly stronger

TABLE 2.7

^{35}Cl, ^{79}Br and ^{127}I NQR spectra of square-planar tetrahalometallates
(*RT* room temperature)

Compound	T (K)	ν (MHz)	Ref.	Compound	T (K)	ν (MHz)	Ref.
KAuCl$_4$	193	27.205; 27.415 27.724; 27.881	180	(Me$_4$N)$_2$PtCl$_4$	273	18.38; 19.16	181
NH$_4$AuCl$_4$	193	27.180; 27.980	180	K$_2$PtBr$_4$	300	138.70	183
RbAuCl$_4$	193	27.056; 27.435	180	KICl$_4$	298	22.369	190, 191
CsAuCl$_4$	193	27.330; 28.151	180	KICl$_4$·H$_2$O	298	16.84; 20.14 24.86; 28.17	189— 191
KAuBr$_4$	193	213.69; 214.33 216.48; 217.08	180	NaICl$_4$·2 H$_2$O	77	20.010; 22.656 23.251; 23.827	186, 190
RbAuBr$_4$	193	214.02; 218.60	180	(NH$_4$)ICl$_4$	295	22.23	191
CsAuBr$_4$	193	213.98; 220.44	180	(NH$_4$)ICl$_4$·H$_2$O	296	19.98 24.68; 27.96	191
(PrNH$_3$)$_2$CuCl$_4$	77	11.290; 11.781	188	RbICl$_4$(I)^c) (II)^c)	77	22.576 22.116; 22.628	190 4
KPdCl$_4$	77	16.795		CsICl$_4$	77	22.612; 22.892 22.975; 22.705	190, 202
(PyH)$_2$PdCl$_4$	273	16.61; 17.08	181	(PyH)ICl$_4$(I)^c) (II)^c)	RT 77	22.375 19.924; 25.664	191 189
(Et$_4$N)$_2$PdCl$_4$	273	17.97	181				
K$_2$PdBr$_4$	300	129.34	183				
K$_2$PtCl$_4$	273	17.925	182				
(PyH)$_2$PtCl$_4$	273	18.41; 18.60	181				

Compound	T (K)	ν (MHz) 1/2—3/2	ν (MHz) 3/2—5/2	$\frac{e^2Qq}{h}$ (MHz)	η (%)	Ref.
KTlI$_4$	291	154.94		1033^a)		184
KTlI$_4$·2 H$_2$O	291	157.45		1050^a)		184
NH$_4$TlI$_4$	291	155.88^b)		1039^a) (av.)		184
NH$_4$TlI$_4$·2H$_2$O	291	157.19	312.50	1043	6.8	184
RbTlI$_4$·2H$_2$O	291	157.78	313.7	1056	6.8	184
CsTlI$_4$·2H$_2$O	291	157.85		1052^a)		184

^{a}) Calculated assuming $\eta = 0$; ^{b}) doublet; ^{c}) polymorph modifications.

effect on the configuration of the [Auhal$_4$]$^-$ anions than on complex hexahalo-metallates. In most cases, tetrahaloaurates(III) show different Au—hal bond lengths within the same anion, and planar [Auhal$_4$]$^-$ anions have low symmetry.

The average frequency of the [AuCl₄]⁻ groups is determined [189] to be about 27.3 MHz at room temperature. The spread is unexpectedly rather small (e.s.d. 0.26 MHz) in spite of the high multiplicity of the ³⁵Cl NQR spectra. This means that the crystal structure and the type of cation (as well as the presence of crystallization water) have only minor contributions into the average NQR frequency [180]. In agreement with these experimental observations calculations [187] show that the external ion contributions to the EFG at the halogen site are responsible only for the spectroscopic splitting, while the average NQR frequency is determined by the electronic distribution within the anion.

Tetrachloroiodates(III) also have square-planar anions, and distortions from D_{4h} symmetry cause very pronounced effects on their ³⁵Cl NQR frequencies [189], (Table 2.7). Some, however, are not distorted. There is remarkable constancy in the average ³⁵Cl NQR frequency which is 22.634 MHz at
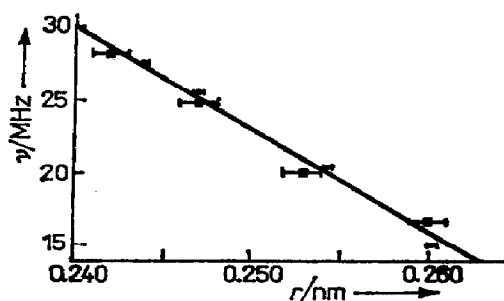

Figure 2.6   Relationship between ν ³⁵Cl and bond distances r in some tetrachloro-iodates(III) at room temperature [189].

■ KICl₄ · H₂O; ● SCl₃ · ICl₄ (I)

77 K for 16 sets of data (e.s.d. = 0.13 MHz) [189]. There is a distinct correlation between the iodine—chlorine bond lengths and the corresponding ³⁵Cl frequencies (Fig. 2.6). This correlation is considered to be helpful for predicting "missing" NQR frequencies as well as for the prediction of bond lengths from measured NQR frequencies in structurally unknown compounds. Thus the I—Cl distance is predicted to be 0.251 nm in KICl₄ from NQR results [189]. Evidently the high mean value of the ³⁵Cl frequency in NH₄ICl₄ [191] implies that the resonance frequency at 16.7 MHz was not detected in this complex.

Data for the hydrated compound KICl₄ · H₂O in Figure 2.6 serves to support the inclusion in Table 2.7 of several hydrated chloroiodates which contain relatively discrete anionic units. X-ray results [203] on KICl₄ · H₂O show only slight pyramidal distortion of the anions with the I—Cl bond distances varying within 0.242 —0.260 nm. Weak hydrogen bonding is reflected in a very moderate splitting of the spectrum of NaICl₄ · 2H₂O [186] on the basis of ³⁵Cl NQR temperature dependence study and analysis of the X-ray powder pattern.

Unlike tetrahaloaurates(III), many anhydrous and hydrated tetrahalo-thallates(III) including those listed in Table 2.7, crystallize in cubic lattices $F_{m3c}(O_h^6)$. They have square-planar $[Tl^{III}hal_4]^-$ units of D_{4h} symmetry, located on a cube face [184]. Accordingly, the ^{127}I NQR $[TlI_4]^-$ anion spectra show that all iodine atoms are crystallographically equivalent (Table 2.7). The ^{127}I QCC values seem to be independent with a few percent of the cation as well as of the presence of water molecules. According to X-ray analysis [184] all the tetraiodothallates(III) studied are isostructural with $CsTlI_4$. The latter is cubic F_{m3c} (O_h^6), with lattice constant $a_0 = 1.994$ nm and the distance $Tl-I = 0.294$ nm. Each $[TlI_4]^-$ square anion is situated on a cube face. The $Tl-I$ bonds make a small angle $(2.4°)$ with the face diagonal. It is presumed that in dihydrates the water molecules are located about the Tl atom, above and below the plane of the square coordination. The finite though small η values are suggested [184] to originate from electrostatic effect of external charges rather than from the nature of $Tl-I$ bonds involving π-character. They can hardly be accounted for by p_x-d_π bonding, since the Tl(III) atom has no vacant d orbitals. In order to analyse if p_x-Tlp_x interaction contributes to the ^{127}I NQR parameters, one can compare them with the corresponding parameters of octahedral K_2PtI_6, where any π interactions are usually ignored [125]:

	T (K)	ν_1 (MHz)	ν_2 (MHz)	$\dfrac{e^2Qq}{h}$ (MHz)	U_p	η
$KTlI_4$	291	154.94				
	77	157.86		1046[a])	0.46[a])	0.068[a])
$RbTlI_4 \cdot 2H_2O$	291	157.78	313.7	1046	0.46	0.068
K_2PtI_6	77			1356.4 (av.)	0.59 (av.)	0.028 (av.)

[a]) Assumed basing on similar ν_1 values in $KTlI_4$ (77 K) and in $RbTlI_4 \cdot 2H_2O$ (291 K).

Applying further Eqns. (42) and (43) of the Townes and Dailey approach one has

$$U_p = \frac{e^2Qq(^{127}I)}{e^2Qq_p(^{127}I)} = \frac{N_{p_x} + N_{p_y}}{2} - N_{p_z} = (1-s)(1-i-\pi) - \pi/2$$

and

$$\frac{2}{3} U_p \cdot \eta = N_{p_x} - N_{p_y}$$

where $s = 0.15$ [184]; $i + \sigma + \pi = 1$; $N_{p_z} = 2 - \pi_z$; $N_{p_y} = 2 - \pi_y$; $\pi_x + \pi_y = \pi$; $e^2Qq_p/h(^{127}I) = 2292.8$ MHz.

Since the electronegativities of both Pt and Tl are equal to each other (χ_{Pt} $= \chi_{Tl} = 1.44$ [148]), one can suggest that the Pt—I and Tl—I bonds have identical ionic character hence obtaining the relationship

$$U_p^{K_2PtI_4} - U_p^{KTlI_4} = 1.35\pi_{Tl-I}$$

This gives $\pi_{Tl-I} = 0.096e$*), the occupancies of the iodine p_π orbitals being $N_{p_x} = 1.962e$ and $N_{p_y} = 1.942e$. This amount of π bonding could be attributed to the p_π—Tlp_π interaction were it not for some dubious points.

First, the square-planar $[MX_4]^-$ ions are expected to have a finite η because of the two-fold symmetry about the Tl—I bond. If the η were produced by the estimated amount of π bonding it would have the magnitude $\eta = 31.3\%$. The observed η in $[TlI_4]^-$ is however not much different from the $\eta = 2.0 - 4.5\%$ of iodine in octahedral $[PtI_6]^{2-}$ [125], where the symmetry does not require the η to be non-zero, and finite values of η are accounted for the influence of external ions.

Second, fairly large negative temperature coefficients observed for ν_1 in $[TlI_4]^-$ ions have been considered [184] as an evidence for a negligible contribution of π character to Tl—I bonding.

Third, the components of the EFG tensor at the iodine due to the direct electrostatic effect of external ions have been computed [184] in $RbTlI_4 \cdot 2H_2O$ to conclude that the origination of η can easily be accounted for this effect, considering that q_{xx}^{ext} and q_{yy}^{ext} can be amplified by the Sternheimer factor $(1 - \gamma_\infty)$ which is about 46 in value. The detailed calculations [184] show the η can come mostly from the two nearest Rb ions separated from the iodine atoms by 0.345 and 0.370 nm.

As these findings show, too much emphasis should not be laid on the p_π—Tlp_π bonding in $[TlI_4]^-$ ions.

The halogen NQR frequencies of square-planar tetrahalopalladates(II) and tetrahaloplatinates(II) (Table 2.7) appear to be lower than those in the corresponding hexahaloanions of Pd(IV) and Pt(IV) [182, 183]. This was interpreted [183] by an increase of the M—hal bond covalency in the hexahalometallates(IV) compared to that in the tetrahalometallates(II) of the same metal atom. One can see from the frequencies in Table 2.7, that the covalency of the M—hal bond shows a tendency to increase in the order of increasing electronegativity (Pd(II) < Pt(II)). Fryer and Smith [181] have pointed out however, that deviations from the expected order of frequencies take place when the cations are varied. (See, for instance, the NQR spectra of $(Et_4N)PdCl_4$ and K_2PtCl_4, Table 2.7.) This may give evidence for the importance of solid-state effects in these compounds.

A number of chloro complexes of copper(II) with square-planar $[CuCl_4]^{2-}$ units have been studied by Scaife [188] using ^{35}Cl NQR, but nearly all of them,

*) $\pi_{Tl-I} = 0.087e$, if one assumes $s = 0$.

except $(PrNH_3)_2CuCl_4$ listed in Table 2.7, gave two resonances with large spectral splitting interpreted to suggest no isolated complex anions in these compounds: $(MeNH_3)_2CuCl_4$, -10.780 and $12.157\ MHz$; $(EtNH_3)_2CuCl_4$, -10.817 and $12.074\ MHz$; $(enH_2)CuCl_4$ -10.27 and $11.907\ MHz$; (all measurements were made at 77 K). A long-bond interaction between square-planar units, involving chlorine bridging completing the tetragonally distorted sixfold coordination of the Cu(II) atoms has been proposed [188].

The ionic character of the Au—hal bond is compared [180] with that of Pt—hal and Pd—hal bonds and the net charge values on the central atoms in the corresponding tetracoordinated square-planar complex ions are also compared. The results obtained within the Townes and Dailey [95] theory approximations are listed in Table 2.8. As with tetrahaloplatinates(II), the Au—Cl bonds appear more ionic than Au—Br bonds. The data also show the Au—hal bonds to be less ionict han those of Pt—hal, in agreement with expection from the electronegativity values and anionic charges.

TABLE 2.8

The nature of M—hal bonds in square-planar complex ions ([180] and refs, therein)

Complex ion	Bond ionicity i	Net metal charge δ
$[PdBr_4]^{2-}$	0.60	0.40
$[PtCl_4]^{2-}$	0.61	0.44
$[PtBr_4]^{2-}$	0.57	0.28
$[AuCl_4]^-$	0.41	0.64
$[AuBr_4]^-$	0.34	0.36
$[TlI_4]^-$	0.46	0.84

(ii) Complexes with tetrahedral anions

Tetrahedral anions, similar to square-planar units, also show distortion of their geometry from regular configuration in most cases (Table 2.9).

Compounds containing chloroaluminate(III) groups were studied systematically by Merryman et al. [196, 197]. $NaAlCl_4$ was studied by Scheinert and Weiss [193] using single-crystal Zeeman ^{35}Cl NQR as well as ^{23}Na and ^{27}Al NMR. They also redetermined the crystal structure of the complex. The ^{35}Cl QCC values lie within $21.6-23.0\ MHz$ and the corresponding η values varied within $0.18-0.32$. The small scatter in the QCC values is in agreement with small variations in the Al—Cl bond lengths about the mean value of $0.213\ nm$. The wide range of η values was accounted for by the combined contributions of external charges into the EFG at the chlorine nuclei, of the interactions between the Cl atoms inside the anion, and of the anisotropic thermal vibrations

TABLE 2.9

^{35}Cl, ^{79}Br and ^{127}I NQR spectra of complexes with tetrahedral anions

Compound	T (K)	ν (MHz)	Ref.	Compound	T (K)	ν (MHz)	Ref.
$NaAlCl_4$	RT	11.009; 11.272	192,	$(Bu_4N)GaCl_4$	77	16.204; 16.418	201
		11.385; 11.583	193			10.484; 10.593	
$CuAlCl_4$	302	11.739	194	Cs_2CuCl_4	77	10.856	205 b
$GaAlCl_4$	RT	10.296; 10.382	195	$(Ph_4P)TlCl_4$	77	19.86	198
		10.460; 11.312					
Ph_4PAlCl_4	77	11.23	198	$(Ph_4As)TlCl_4$	77	20.00	198
$Bi_5(AlCl_4)_3$	RT	10.479; 10.779	196	$(Me_4N)_2NiCl_4$	273	8.85; 9.05	181
$\beta\text{-}I_3\cdot AlCl_4$	RT	9.960; 10.874	197	$(Et_4N)_2NiCl_4$	220	8.96; 9.45	181
		11.046; 11.091					
$I_5\cdot AlCl_4$	RT	10.988; 11.086	197	$LiAlBr_4$	77	85.505; 94.443c)	208
		11.124; 11.440				98.113	
$I_2Cl\cdot AlCl_4$	RT	10.297; 10.474	197	$NaAlBr_4$(I)a)	77	89.925; 93.021c)	208
		11.265; 11.283				99.031	
				(II)a)	77	89.809; 90.993c)	208
						93.472; 95.336	
$ICl_2\cdot AlCl_4$	RT	10.802; 10.843	196	$(Me_4N)AlBr_4$	77	90.641; 92.653c)	208
		11.297; 11.413				94.674	
$NaGaCl_4$	77	16.118; 16.370	199	$CsAlBr_4$	77	89.042; 90.079c)	208
		16.825; 16.961				90.213; 90.862	
						91.017; 91.721	
						91.780; 91.875	
						92.458; 96.044	
						97.315; 98.208	
						99.333; 100.907	
$KGaCl_4$(I)a)	77	16.483; 16.553	199	$CuAlBr_4$	297	98.62	194
(II)a)	242	15.795; 15.846					
		16.003; 16.486					
$RbGaCl_4$	77	15.182; 16.001	199	$NaGaBr_4$	304	138.01; 124.34	194
		16.349; 16.587				123.43	
$CsGaCl_4$	77	15.456; 15.468	199	$KGaBr_4$	298	125.53; 128.02	194
		15.485; 15.524				131.39; 132.43	
		16.325; 16.604					
		16.755; 16.958					
$GaGaCl_4$ (I)a)	77	16.072; 16.250	199	NH_4GaBr_4(I)a)	298	124.94; 125.38	194
(II)a)	316	15.104; 15.231	232			131.42	
		15.457; 16.337		(II)a)	298	123.25; 127.12	
						127.97; 128.06	
						128.83; 128.58	
						129.42; 131.80	
						132.03	

TABLE 2.9 (continued)

Compound	T (K)	ν (MHz)	Ref.	Compound	T (K)	ν (MHz)	Ref.
CuGaCl$_4$	303	16.258	194	RbGaBr$_4$	77	125.68; 127.29	194
						128.30; 130.09	
						132.65; 135.05	
						136.30; 137.54	
CsGaBr$_4$ (I)[a])	297	121.88; 127.22	194				
		130.61					
(II)[a])	77	121.87; 124.63					
		124.89; 126.17					
		127.27; 127.63					
		127.98; 128.20					
		129.49; 134.27					
		135.17; 135.66					
		136.76; 136.95					
		139.05; 140.55					
GaGaBr$_4$	293	128.94; 128.87	194				
(Bu$_4$N)GaBr$_4$	77	131.7; 133.6[c])	201				

Compound	T (K)	ν (MHz)		e^2Qq/h (MHz)	η (%)	Ref.
		1/2—3/2	3/2—5/2			
(Bu$_4$N)GaI$_4$	77	8 sets of freqs.		960.12 average	6.0	201
CuGaI$_4$	299	169.68	253.38	887.5	53.73	194
CsGaI$_4$	296	150.09	288.18	966.8	18.0(18.5)[b])	194
		145.05	287.6	960.0	8.2(7.2)[b])	
		134.93	269.73	899.2	1.9	
		130.50	257.48	860.1	10.3	

[a]) Polymorphic modifications;
[b]) η values due to alternative combination of resonance frequencies;
[c]) calculated from ^{81}Br frequencies according to $eQ(^{79}\text{Br})/eQ(^{81}\text{Br}) = 1.1971$.

of chlorine anions. The ^{27}Al QCC value was 1.4895 MHz due to distortion of [AlCl$_4$]$^-$ anions from T_d symmetry.

Comparison of the chloroaluminate(III) NQR data with IR spectra and X-ray data, whenever available, enabled Merryman et al. [196, 197] to show that the average ^{35}Cl NQR frequency and the range of spectral splitting may serve as a criterion in structural diagnosis of such compounds. The resonances of relatively free [AlCl$_4$]$^-$ groups in ionic compounds were found to average 10.6 —11.3 MHz with a splitting range of $\leq$ 1 MHz. Strong coordination of [AlCl$_4$]$^-$ to cations as well as the formation of bridging anionic groups such as

$[Al_2Cl_7]^-$ is reflected in the shift of the whole family of resonances and/or in an increase in the range of spectral splitting.

Some chloroaluminate(III) complexes with polyhalogen cations behaving like relatively unperturbed ions are also included in Table 2.9.

Table 2.9 lists the NQR data for tetrahalogallates(III). Several [194, 199] exist in two polymorphic modifications (I and II).

The average ^{35}Cl frequency of the tetrahedral gallium anion, seems to be independent on the cation. Although the number of halogen resonances (Z) and thus the symmetry of the $[Gahal_4]^-$ anion changes with the change of cation, no simple correlation between Z and the ionic radius of the cation or its electric dipole polarizability was found [194, 199]. This is demonstrated in Table 2.10 [194] where the proposed symmetry of $[GaBr_4]^-$ is shown, based on the multiplicity of their $^{79,81}Br$ NQR spectrum. NH_4GaBr_4 (phase II) shows 9 resonances at 298 K (Table 2.9) accounted [194] for by an accidental coincidence of a larger number of lines (possibly twelve).

Covalency in the $Ga-X$ bonds increases in the series $[GaCl_4]^- < [GaBr_4]^- < [GaI_4]^-$ in the complexes $(Bu_4N)GaX_4$ [201].

Calculations of the ionic bond character (i) within the two series of tetra-

TABLE 2.10

Average ^{79}Br and ^{35}Cl NQR frequencies $\bar{\nu}$ (MHz), and number of observed resonances Z, in tetrahalogallates(III) at 77 K and RT (room temperature) ([194], [199] and refs. therein)

Compound	$\bar{\nu}$ (MHz)	Z_{77}	Proposed symmetry of GaX_4^- at 77 K	Z_{RT}	Proposed symmetry of GaX_4^- at RT
$GaGaBr_4$	130.88	2	C_2 or mm	2	C_2 or mm
$NaGaBr_4$	131.83	3	m	3	m
$KGaBr_4$	132.37	4	asymmetric	4	asymmetric
NH_4GaBr_4 (phase I)	131.70	3	m	3	m
$RbGaBr_4$	131.61	8	asymmetric (two inequivalent tetrahedra)	—	—
$CsGaBr_4$	131.03	16	asymmetric (four inequivalent tetrahedra)	3	m
$GaGaCl_4$	16.161	2			
$NaGaCl_4$	16.569	4			
$KGaCl_4$	16.520	2			
$RbGaCl_4$	16.021	4			
$CsGaCl_4$	16.072	8			

halogallates(III), $CsGaX_4$ and $CuGaX_4$, according to the Townes and Dailey theory gave a linear relationship between the values of i and the corresponding Ga—X electronegativity differences [194]. This also confirmed that the Ga—halogen bond character is not influenced much by the cation. The wide range of η in $CsGaI_4$ is accounted [194] for by different polarizations within the complex ion, due to external charges as well as intra-ionic interactions between the large iodine atoms.

The Cu—I interaction in $CuGaI_4$ is supposed to be stronger than in the corresponding alkali and alkylammonium salts, and is considered [194] as a possible reason for a large value of η in $CuGaI_4$ (Table 2.9).

Thallium(III) tetrachlorides appear to have anions of high symmetry. If the resonances reported in [198] are the complete set of NQR spectra for the $[TlCl_4]^-$ groups, their symmetry is not lower than S_4.

NQR data available for both tetrahedral and square-planar Ni(II) complexes [181, 204] make a good basis to demonstrate the difference in chemical bonding between these two types of configuration. Data for tetrahedral $[NiCl_4]^{2-}$ anions are included in Table 2.9. Further NQR frequencies (^{35}Cl, ^{79}Br, ^{127}I) have been reported [204] for uncharged tetrahedral complexes (at 298 K): $(Ph_3P)_2NiCl_2$, 9.471 MHz; $(Ph_3P)_2NiBr_2$, 71.07; 75.15 MHz; $(Ph_3P)_2NiI_2$, 71.04 MHz ($1/2-3/2$), 138.0 MHz ($3/2-5/2$). Complexes of similar composition, but having square-planar anion configuration, gave quite different NQR frequencies (^{35}Cl, ^{79}Br): $(Pr_3^nP)_2NiCl_2$, 15.852 MHz (298 K, [204]); $(Bu_3^nP)_2NiCl_2$, 15.99 MHz (273 K, [181]); $(Pr_3^nP)_2NiBr_2$, 126.26 MHz (308 K, [204]); $(Bu_3P)_2NiBr_2$, 126.53 MHz (308 K, [204]). Comparison of the NQR frequencies for both types of compound, reveals those of the tetrahedral species to be half those of the square-planar complexes. These differences are [204] attributed to the presence of partially filled nickel orbitals, available for metal—halogen π-bonding in the tetrahedral complexes, while no such orbitals are present in the square-planar units. An estimate of π-bonding in the tetrahedral compounds, within the Townes-Dailey approximation, gives values of about 10% [204].

Zinc(II), cadmium(II) and mercury(II) form many complex halides containing isolated tetrahedral $[MX_4]^{2-}$ ions. Tetrahedrally coordinated Zn(II), Cd(II) and Hg(II) all have a d^{10} electron configuration and present a simple σ-bonding situation such that comparison of the NQR data over the appropriate series of compounds is useful in both structure and bonding aspects.

In recent years, tetrahedral halides of the type R_2MX_4 have gained much attention, due to their structural phase transitions into incommensurate phases, with ferroelectric properties occurring in some cases. Representative compounds which have been studied by NQR (review [213] and refs. cited therein) include Rb_2ZnCl_4, Rb_2ZnBr_4, K_2ZnCl_4, $(NH_4)_2ZnCl_4$, Cs_2CdBr_4 and Cs_2HgBr_4. Their NQR spectra with some other complexes of the same type are listed in Table 2.11. The number and relative intensities of the NQR lines

TABLE 2.11

^{35}Cl, ^{81}Br and ^{127}I NQR spectra (MHz) of tetrahedral $[MX_4]^{2-}$ species in metal(II) complex halides (*RT* room temperature)

Compound	T (K)	ν (MHz)	Ref.
Cs_2ZnCl_4	77	8.893 9.175 9.628	205b
Cs_2ZnBr_4	77	59.008 61.266 63.240	205b
	293	57.620 59.780 62.730	207
Rb_2ZnCl_4	320	8.37 8.69 9.64	214, 215
Rb_2ZnBr_4	350	55.4 57.5 64.0	216
$(pyH)_2ZnCl_4$	298	8.890 9.477	205b 206
$(pyH)_2ZnBr_4$	RT	57.551 59.826 62.750	206

Compound	T (K)	ν (MHz)		$\dfrac{e^2Qq}{h}$ (MHz)	η (%)	Ref.
		1/2–3/2	3/2–5/2			
Cs_2ZnI_4	77	79.037				205a
	298	72.560 75.726 79.172	144.40 150.78 157.60			205b
Rb_2ZnI_4	298	70.416 77.399 83.727				205a
Tl_2ZnI_4	298	78.650 80.863				205a
K_2HgI_4	292	123.46 129.30 148.49				211
Ag_2HgI_4	160	142.1				212
Cs_2HgI_4	77	97.82 104.36 120.12	195.44 208.25 234.55	651.6 694.4 784.8	2.8 4.2 13.7	210
Cu_2HgI_4	160	126.2				212
Cs_3HgI_5	77	99.62 103.47	198.78 206.42	662.84 688.34	4.2 4.4	210

Compound	T (K)	Values	Ref.		Compound	T (K)	Values	Ref.
(NH₄)₂ZnCl₄	150	8.11; 8.32	217				108.34	
		8.50; 8.62	205b				121.51	
		8.80; 8.95					214.65	
		9.05; 9.25					241.49	
		9.40; 9.70					716.56	
		9.85; 10.00					805.77	
							8.6	
							7.0	
Tl₂ZnBr₄	298	62.525	205a		Cs₃HgBr₄	293	78.35	207
							80.95	
							91.30	
K₂ZnBr₄	298	52.84	205b		(pyH)₂HgCl₄	RT	11.99	209
							14.25	
							15.72	
Cs₃ZnCl₅	298	9.065	205a		Cs₃CdBr₄	293	57.36	207
Rb₃ZnCl₅	298	8.964	205a				59.80	
							65.90	
(NH₄)₃ZnCl₅	298	8.190	205b		(pyH)₂CdBr₄	77	64.102	206
		9.121					64.778	
		9.137				RT	65.227	
							66.867	
							61.675	
							63.097	
Rb₃ZnBr₅	298	56.064	205a				63.962	
		61.475						
		67.200						
(NH₄)₃ZnBr₅	298	55.117	205a					
		60.508						
		61.196						

serve as a reliable and convenient indicator of the site symmetry of the anionic groups in these complexes.

Table 2.12 gives the cell dimensions of the compounds calculated from single crystal and powder X-ray diffraction data. The site symmetry of the $[MX_4]^{2-}$ anions, determined from their NQR spectra is also indicated. Table 2.12 shows

TABLE 2.12

Structural data and relative intensities of halogen NQR signals in complex zinc(II) halides

Compound	Lattice symmetry	Unit cell dimensions (nm)				Site symmetry of $[MX_4]^{2-}$ (Relative intensities of NQR signals in order of increasing frequency)	Ref.
		a	b	c	$\beta^{(0)}$		
(1) Cs_2ZnCl_4	Ortho-rhomb. P_{nma}	0.974	0.741	1.296		C_s (2:1:1)	205 b, 220
(2) Cs_2ZnBr_4	P_{nma}	1.018	0.777	1.352		C_s (2:1:1)	207, 205 b, 220
(3) Cs_2CdBr_4	P_{nma}					C_s (2:1:1)	207
(4) Cs_2HgBr_4	P_{nma}					C_s (2:1:1)	207
(5) Cs_2ZnI_4	P_{nma}	1.084	0.829	1.445		C_s (2:1:1)	205 b
(6) Rb_2ZnCl_4	P_{nma}	0.927	0.731	1.274		C_s (2:1:1 (at 320 K))	205 b, 214, 215
(7) Rb_2ZnBr_4	P_{nma}	$3 \times$ 0.980	0.771	1.325		C_s (2:1:1 (at 350 K))	205 a, 205 b 216
(8) $(pyH)_2ZnCl_4$						C_{2v} (1:1)	206, 205 b
(9) $(pyH)_2ZnBr_4$						C_s (2:1:1)	206
(10) Rb_2ZnI_4	Monocl.	1.050	0.801	0.758	109.6	(2:1:1)	205 a
(11) Tl_2ZnI_4	Monocl.	0.986	0.761	1.389	110	(incomplete)	205 a

TABLE 2.12 (continued)

Compound	Lattice symmetry	Unit cell dimensions (nm)				Site symmetry of $[MX_4]^{2-}$ (Relative intensities of NQR signals in order of increasing frequency)	Ref.
		a	b	c	$\beta^{(0)}$		
(12) Rb_3ZnCl_5	Tetragon. $I4/mcm$	0.881	0.881	1.415		S_4 (a singlet)	205a
(13) Cs_3ZnCl_5	$I4/mcm$	0.923	0.923	1.448		S_4 (a singlet)	205a, 222
(14) Cs_3ZnBr_5	$I4/mcm$	0.964	0.964	1.513		S_4 (a singlet)	205a, 222
(15) $(NH_4)_3ZnCl_5$	P_{nma}					C_s (1:1:2)	205b, 221
(16) $(NH_4)_3ZnBr_5$	P_{nma}	0.905	1.035	1.324		C_s (1:2:1)	205a
(17) Rb_3ZnBr_5	P_{nma}	0.908	1.032	1.342		C_s (1:2:1)	205a
(18) Cs_3ZnI_5	P_{nma}	1.016	1.159	1.433		C_s (incomplete)	205a

a close correspondence between the structural information obtained from X-ray data and NQR spectroscopic patterns. Compounds (1)—(7) of Table 2.12 are isomorphous [207, 208, 220] based on results of X-ray analysis. The NQR spectroscopic patterns of these compounds also show a close resemblance to each other in multiplicity and relative intensities supporting their isomorphism.

Tripling of the a-dimension was reported [205b] in Rb_2ZnBr_4 which was later [205a] interpreted to be a consequence of a stacking fault. This complex, as well as Rb_2ZnCl_4 and K_2ZnCl_4, are known to belong to a family undergoing a sequence of phase transitions ([213, 216, 218, 219, 430] and refs. cited therein): para-electric phase P_{nma} ($Z = 4$) ↔ incommensurate phase $Pn2_1a$ ↔ ferro-electric phase $Pn2_1a$ ($Z = 12$) with a tripling of the unit cell volume ↔ polar monoclinic ($Z = 24$). (In Table 2.11, NQR spectra are in the para-electric high-temperature phase.)

Similar temperature behaviour but with a different phase sequence and without a ferroelectric phase, has been observed [207] for $Cs_2M^{II}Br_4$ (M = Cd, Hg): P_{nma} ($Z = 4$) ↔ incommensurate phase ↔ $P2_1n$ ($Z = 4$) ↔ unknown low-temperature phase. Table 2.11 lists the NQR spectra of these compounds in the high-temperature orthorhombic phase P_{nma}.

The phase transition from an incommensurate to a ferroelectric phase ($P2_1cn$) accompanied by a tripling of the c-dimension of the unit cell was detected [217] in $(NH_4)_2ZnCl_4$ at 266 ± 0.5 K. The NQR spectrum of the compound is given (Table 2.11) in the low-temperature ferroelectric phase.

Compounds (8) and (9) in Table 2.12 differ from each other both in their halogen NQR spectra and in their X-ray diffraction patterns [205b].

Complexes (12)—(14) R_3ZnX_5, have the tetragonal structure [205a, 222] of Cs_3CoCl_5. They therefore contain $[ZnX_4]^{2-}$ units of S_4 site symmetry and Cs^+ and X^- ions, the latter giving too low a frequency to be detected with the technique used [205a]. The NQR singlets from the four equivalent X atoms in the $[ZnX_4]^{2-}$ units are in agreement with structural conclusions.

Complex (15) has a structure [221] very closely related to those of compounds (16) and (17) (Table 2.12) but with small, although significant, shifts in atomic positions [205a]. The NQR spectroscopic pattern of (15) however shows a quite pronounced difference from the NQR spectra of the other two, demonstrating a high structural sensitivity for the NQR technique.

A remarkable constancy [205a] is noted in the mean frequency values in tetrahedral zinc(II) halides. They fall near 8.97 MHz for chloride complexes and near 60.05 MHz (^{81}Br) for the related bromides in spite of differences in the symmetry of the anion sites. Thus contributions from external lattice charges to the EFG at the halogen sites do not exceed the spread of frequencies about the mean estimated [205a] as 9.1% over the complexes listed in Table 2.11.

Few data are available for tetrahalomercurates(II) and tetrahalocadmiates(II) (Table 2.11). Some have unknown structures and incomplete NQR spectra. The species $(pyH)_2HgCl_4$ can hardly contain discrete anionic groups considering its largely split ^{35}Cl spectrum [209]. Cs_2HgI_4 and Cs_3HgI_5 are reported [210] to form isolated tetrahedral anions $[HgI_4]^{2-}$ with highly ionic Hg—I bonds. The single ^{127}I resonances observed in Ag_2HgI_4 and Cu_2HgI_4 [212] confirm the presence of regular tetrahedral anionic groups in both complexes.

The M(II)—Br σ-covalent bond character was estimated in some Zn(II), Cd(II) and Hg(II) bromide complexes using the Townes and Dailey approximations [206] with the reasonable assumption of negligible π-bonding and s-hybridization of the appropriate bonds. σ-values of the order of 0.19—0.20 were obtained requiring that the effective charges (δ) on the Br atoms in these compounds to be of the order of $-0.8e$.

D. INTERACTIONS BETWEEN HETEROATOMIC ION PAIRS

Interionic interactions in ionic compounds with quadrupole atoms contained in cation and anion species are studied using NQR. As shown above the isolated complex ions are charaterized by a small scatter in the average frequency

values. They vary typically within 15.8 ± 0.8 MHz for $GaCl_4^-$, 23.7 ± 0.7 MHz for $SbCl_6^-$, 22.6 ± 0.13 MHz for ICl_4^-, 27.8 ± 0.5 MHz for $AuCl^-$ and 10.9 ± 0.4 MHz for $AlCl_4^-$. Frequency values outside the appropriate limits, as well as increased splitting, point either to formation of bridging anion groups or to strong interionic coordination [196]. Most of the anions indicated above show considerable variations in intra-anion bond distance as found by X-ray analysis. This naturally leads to splitting of the NQR spectra even for the isolated groups.

Interionic interactions nevertheless can be recognized from (i) shifts to lower frequency by halogens bridging ions, or (ii) upwards shifts of the whole resonance family, due to a partial removal of the negative charge by an electrophilic partner, or vice versa if the ion bears an opposite charge.

TABLE 2.13

^{35}Cl NQR spectra of compounds of the type $[SCl_3]^+ \cdot [M^xCl_{x+1}]^-$ at 77 K. (Relative intensities in parentheses.)

Compound	Cation		Anion		Ref.
	ν (MHz)[a]	$\Delta\gamma$[c] (%)	ν (MHz)[a]	$\Delta\gamma$[c] (%)	
$[SCl_3]^+ \cdot [ICl_4]^-$ (I)[b]	41.726 42.091 42.637 [42.12]	2.8	14.85 20.95 28.12 [22.46]	59.0	227
$[SCl_3]^+ \cdot [ICl_4]^-$ (II)[b]	41.80 42.45 42.90 [42.38]	2.1	20.07 21.58 23.53 25.25 [22.61]	22.9	227
$[SCl_3]^+ \cdot [SbCl_6]^-$	42.946(2) 42.192 [42.69]	1.8	22.305 22.390 23.370 24.169 24.813 25.828 [23.8]	14.8	166—168
$[SCl_3]^+ \cdot [FeCl_4]^-$	42.62				168
$[SCl_3]^+ \cdot [AlCl_4]^-$	42.00 42.10 43.40 [42.50]	3.3	10.178 10.378 10.787 11.285 [10.632]	11.3	167, 168, 421

TABLE 2.13 (continued)

Compound	Cation		Anion		Ref.
	ν (MHz)[a]	$\Delta\gamma$[c] (%)	ν (MHz)[a]	$\Delta\gamma$[c] (%)	
$[SCl_3]^+ \cdot [TaCl_6]^-$	42.072 42.684 42.806 [42.52]	1.7	7.684; 7.893 8.660; 9.050 9.163; 9.224 [8.61]	17.9	167, 168
$[SCl_3]^+ \cdot [NbCl_6]^-$	41.793 42.477 [42.37]	2.5	7.078; 7.373 7.510; 7.565(2) 9.325; [7.72]	29.1	167, 168
$[SCl_3]^+ \cdot [AsF_6]^-$ above 77°K	42.26 42.44 42.58 [42.43]	0.73			168
$[SCl_3]^+ \cdot [AuCl_4]^-$	41.295 42.321 42.743 [42.12]	3.4	25.247 27.917 27.956 30.613 [27.93]	20.0	167
$[SCl_3]^+ \cdot [UCl_6]^-$	41.883 42.135 42.318 [42.11]	1.0			168
$[SCl_3]^+ \cdot [MoOCl_4]^-$	41.832				168
$[SCl_3]^+ \cdot [HfCl_5]^-$	41.709 42.466 43.289 [42.49]	3.7			226
$[SCl_3]^+ \cdot [ZrCl_5]^-$	41.880 41.943 42.063 [41.96]	0.4	4.552(1) 4.762(1) 5.094(3) [4.92]	11.0	226
$[SCl_3]^+ \cdot [GaCl_4]^-$	41.960 42.080 43.404 [42.48]	3.4	15.150 15.519 15.748 16.793 [15.80]	10.3	167

[a]) Average frequency values are given in square brackets;
[b]) crystal modifications;
[c]) spectroscopic splitting.

Consider complexes of the type nSCl$_4 \cdot$ Mhal$_x$, known to form [SCl$_3$]$^+$ $\cdot$ [MCl$_{x+1}$]$^-$ ion pairs for the majority of metals. Those studied by NQR spectroscopy are listed in Table 2.13. The available X-ray data are scanty [223—225], but the ^{35}Cl NQR spectra give clear proof of the ionic nature of these compounds. That the average ^{35}Cl frequencies for both the anion and cation groups fall within a limited range, that for the cation group being 42.3 $\pm$ 1.1 MHz. The anion average frequencies lie in the typical ranges listed above for the
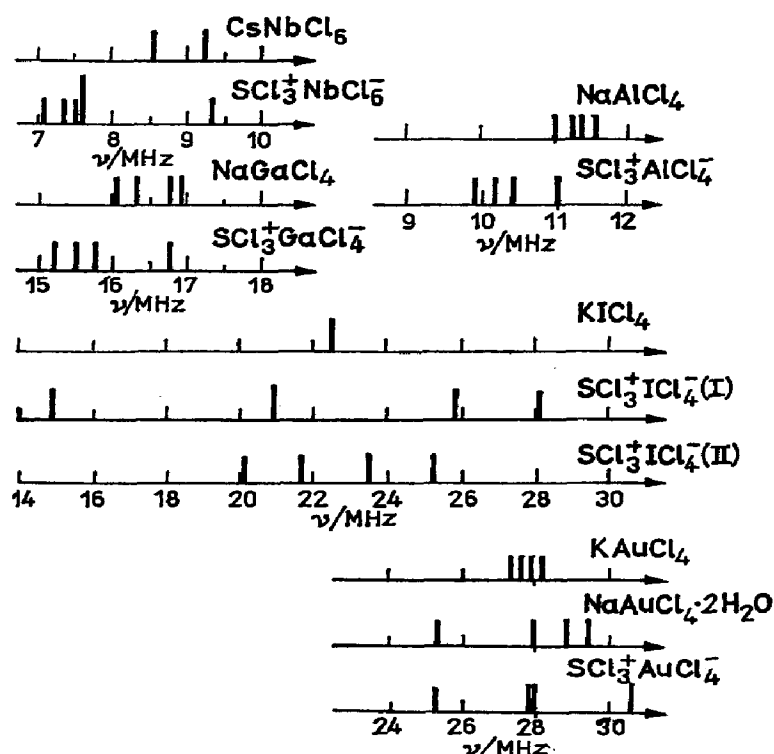
Figure 2.7 ^{35}Cl NQR patterns of anions in several ionic compounds demonstrating increased spectroscopic splitting in compounds with cations [SCl$_3$]$^+$ [168 b].

ionic compounds. Several of them show considerably increased splitting. In Figure 2.7 we compare the ^{35}Cl spectra of such compounds with the spectra of compounds having the same ions but forming no secondary interionic bonds.

X-ray data available for crystal modification (I) of [SCl$_3$]$^+$ $\cdot$ [ICl$_4$]$^-$ [223] established considerable secondary interactions I—Cl$\cdots$S between the ionic groups of the compound, which is consistent with the highly split anionic spectrum (Fig. 2.8).

The structure of SCl$_3^+$ $\cdot$ AlCl$_4^-$ has also been studied [224]. According to X-ray data three chlorine atoms of the AlCl$_4^-$ tetrahedra make asymmetrical bridges with the sulphur atoms of three adjacent cation units. As a result,

the environment of the sulphur atom is completed to a distorted octahedral configuration. The primary S—Cl bonds comprise two longer distances (0.199 and 0.198 nm) and one shorter distance (0.196 nm) which is in agreement with the ^{35}Cl NQR spectrum of the cation species. The tetrahedra $[AlCl_4]^-$ are distorted, three bridging bonds being longer than the terminal Al—Cl bond. The ^{35}Cl NQR spectra of the two related compounds $[SCl_3]^+$ · $[AlCl_4]^-$ and $[SCl_3]^+$ · $[GaCl_4]^-$ (Fig. 2.7) correspond closely to a description of the structure . There is considerable splitting in their anion spectra between

S—Cl₁ = 0.200
S···Cl₄ = 0.312
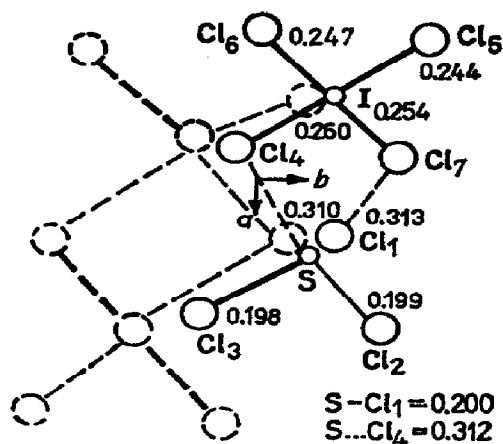
Figure 2.8   Projection of the $[SCl_3]^+$ · $[ICl_4]^-$ structure unit and that related by the center of symmetry (shown dashed) down 001 (after [223]).

the high frequency line and lower frequency triplet. The spectroscopic patterns of the cations of these compounds are also very similar enabling one to suggest that the structures of the tetrachloroaluminate(III) and tetrachlorogallate(III) salts share very similar. In Figure 2.7, the anions in $NaAlCl_4$ and $NaGaCl_4$ show spectroscopic splitting produced apparently by the crystallographic inequivalence of the chlorine positions, which are much less significant.

The spectroscopic splitting of the $[AuCl_4]^-$ group in $[SCl_3]^+$ · $[AuCl_4]^-$ is nearly 20%, which is higher than the corresponding splitting in $NaAuCl_4$ · $2H_2O$ (Fig. 2.7), where formation of O—H···Cl bonds is suggested [180]. Thus strong Au···Cl···S interionic coordination in the former compound [167] is very probable.

The complex $[SCl_3]^+$ · $[NbCl_6]^-$ shows a split anion spectrum, the splitting considerably exceeding that of $[SCl_3]^+$ · $[TaCl_6]^-$. It is also considerably higher than the anion splitting in $CsNbCl_6$ (Fig. 2.7).

The ^{35}Cl spectra of the SCl_3^+ groups, in all these compounds, also show increased splitting, and their average frequency values are shifted slightly downwards with respect to those of the remaining compounds in Table 2.13. This is consistent with the formation of secondary interionic bonding according to (i) and (ii).

It is interesting that a distinct correlation has been observed between the

cation average ^{35}Cl frequency and the difference in metal and halogen electronegativity in the anions of Table 2.13 (Fig. 2.9). The correlation is essentially linear for complexes whose ion pairs, according to NQR spectra, interact most weakly. This is understood to reflect the pure electrostatic nature of the interactions between the ions in such complexes. The more covalent and short are the M —hal bonds in the anion, the longer and weaker are the interionic distances M —hal···S, the less perturbed is the [SCl$_3$]$^+$ cation and relatively higher are the corresponding ^{35}Cl NQR frequencies. Interacting ions are expected to show low frequency shifts in the [SCl$_3$]$^+$ groups due to charge transfer from the anions
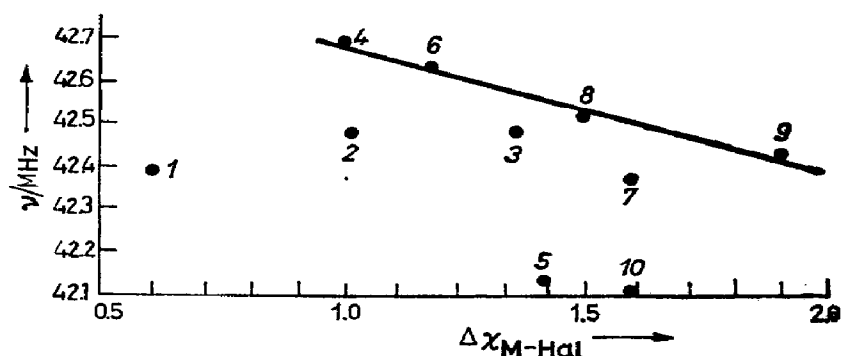
Figure 2.9   Relationship between the cation average $\bar{\nu}$ ^{35}Cl frequency and metal —halogen electronegativity difference of anions in compounds of type [SCl$_3$]$^+$ · [M^{x}hal^{1+x}]$^-$; 1 SCl$_3$ · ICl$_4$(II); 2 SCl$_3$ · GaCl$_4$; 3 SCl$_3$ · AlCl$_4$; 4 SCl$_3$ · SbCl$_6$; 5 SCl$_3$ · AuCl$_4$; 6 SCl$_3$ · FeCl$_4$; 7 SCl$_3$ · NbCl$_6$; 8 SCl$_3$ · TaCl$_6$; 9 SCl$_3$ · AsF$_6$; 10 SCl$_3$ · UCl$_6$.

through the secondary bonds Cl$_{anion}$···S —Cl$_{cation}$. Compounds 1, 2, 3, 5, 7, 10 are examples presented in Figure 2.9.[1]) The remaining compounds in the diagram seem to possess ionic pairs which do not interact with each other.

The NQR spectra of other compounds of similar type such as nRCl$_4$ · Mhal$_x$, where R = Se, Te, show that most part of them also form ionic pairs n[RCl$_3$]$^+$ · [Mhal$_{x+n}$]$^{n-}$, although ZrCl$_4$ and HfCl$_4$ [226] give molecular adducts ZrCl$_4$ · 2RCl$_4$ (R = Se, Te) and HfCl$_4$ · 2TeCl$_4$.

Table 2.14 lists compounds whose ionic nature is indicated by the NQR spectra of the anion species. For some compounds, this is known from X-ray data [161]. According to the latter and also from bond theory ([197] and refs. cited therein) and Zeeman analysis of NQR spectra [228] a V-shaped geometry has been suggested for the heteroatomic cation in all these compounds. For the first two substances in Table 2.14, the single crystal ^{27}Al NMR rotation pattern of the central lines ($-1/2 \leftrightarrow +1/2$) have also been

---

[1]) The compound 10 contains, according to the x-ray data at room temperature [225] only weakly interacting ions. Its NQR spectrum, inconsistent with [225] at 77 K, was however inobservable at room temperature.

TABLE 2.14

NQR spectra of ionic compounds with V-shaped cations (*RT* room temperature)

Compound	T (K)	Cation species					Anion species					Ref.
		Isotope	ν (MHz) 1/2→3/2	ν (MHz) 3/2→5/2	$\frac{e^2Qq}{h}$ (MHz)	η (%)	Isotope	ν (MHz) 1/2→3/2	ν (MHz) 3/2→5/2	$\frac{e^2Qq}{h}$ (MHz)	η (%)	
[SbBr₂]⁺[AlBr₄]⁻	296	¹²¹Sb	97.406	113.3	415.9	82.1	²⁷Al	(at 295 K)		7.2	56 ± 3	228
		⁸¹Br	143.63	287.2	2.4		⁸¹Br	76.637	146.6	54.3	
			149.99	300.0	1.1			79.088	152.5	47.7	
								81.930	161.3	30.7	
								82.689	164.8	14.1	
[SbI₂]⁺[AlI₄]⁻	296	¹²¹Sb	75.681	94.832	343.2	73.6	²⁷Al	(at 285 K)		5.7	55 ± 3	228
		¹²⁷I	186.88	373.79	1246.0	0.0	¹²⁷I	118.18	200.48	686.6	38.2	
			207.39	414.40	1382.6	2.7		118.86	232.68	778.2	13.0	
								123.04	201.73	694.9	42.6	
								123.19	214.40	731.1	34.7	
α-[I₃]⁺[AlCl₄]⁻	RT	¹²⁷I	308.6 (c)ᵃ				³⁵Cl	10.129				197
			415 (t)ᵃ	527		37.3		10.590				
			428 (t)ᵃ					11.090				
								11.450				
[I₂Cl]⁺[SbCl₆]⁻	RT	¹²⁷I	429.1 (c)ᵃ				³⁵Cl	20.78				159
			517.1 (t)ᵃ					21.00				
		³⁵Cl	38.28					24.83 (2)ᵇ				
								25.69 (2)ᵇ				
							¹²¹Sb	21.03	35.70	122.2	37.9	

Compound	T	Nuclide	Frequency (MHz)	Nuclide					Ref
$[ICl_2]^+[AlCl_4]^-$	RT	^{127}I	458 (c)[a]; 518 (t)[b]		2650.7 (c)		35.0		197
		^{35}Cl	38.690; 39.086	^{35}Cl	10.802; 10.843; 11.297; 11.413				192
$[ClF_2]^+[SbF_6]^-$	77	^{35}Cl	79.375	^{121}Sb	23.93	47.67	159.00	5.6	229
$[ClF_2]^+[AsF_6]^-$	77	^{35}Cl	78.952	^{75}As	26.472				230
$[ClF_2]^+[BiF_6]^-$	77	^{35}Cl	79.336	^{209}Bi	13.281	25.523	307.85	6.3	231
					13.502	24.805	300.94	9.4	
$[ClF_2]^+[NbF_6]^-$	77	^{35}Cl	80.066						230
$[ClF_2]^+[TaF_6]^-$	77	^{35}Cl	80.172	^{181}Ta	59.936	117.415	824.20	7.1	230
					57.913	114.209	800.97	5.8	
$[ClF_2]^+[Sb_2F_{11}]^-$	77	^{35}Cl	78.253	^{121}Sb	42.531	58.375	207.67	63.3	229
					33.150	48.143	169.49	56.9	
$[ClF_2]^+[Sb_4F_{21}]^-$	77	^{35}Cl	77.08	^{121}Sb	47.315	56.996	207.83	78.1	229
					39.981	58.728	206.33	55.65	

a) (c) = central atom; (t) = terminal atom; b) relative intensity of signal in parentheses.

studied [228]. The [27]Al QCC and η-values, thus obtained supported the existence of distorted tetrahedral [Alhal$_4$]$^-$ ions in the compounds. NQR Zeeman analysis for the same compounds enabled determination of the η-values on [81]Br atoms in the [SbBr$_2$]$^+$ and [AlBr$_4$]$^-$ species [228]. Those in the cation appear negligibly small indicating unperturbed terminal halogen atoms. In the [AlBr$_4$]$^-$ ions the η-values are much higher. The angles between the z-axes of the EFG at the Br sites vary from 103.9 to 118.1°. This is consistent with the existence of a distorted tetrahedral [AlBr$_4$]$^-$ ion, the bromine EFG z-axes deviating from the Al−Br bond axes because of the large η-values. The
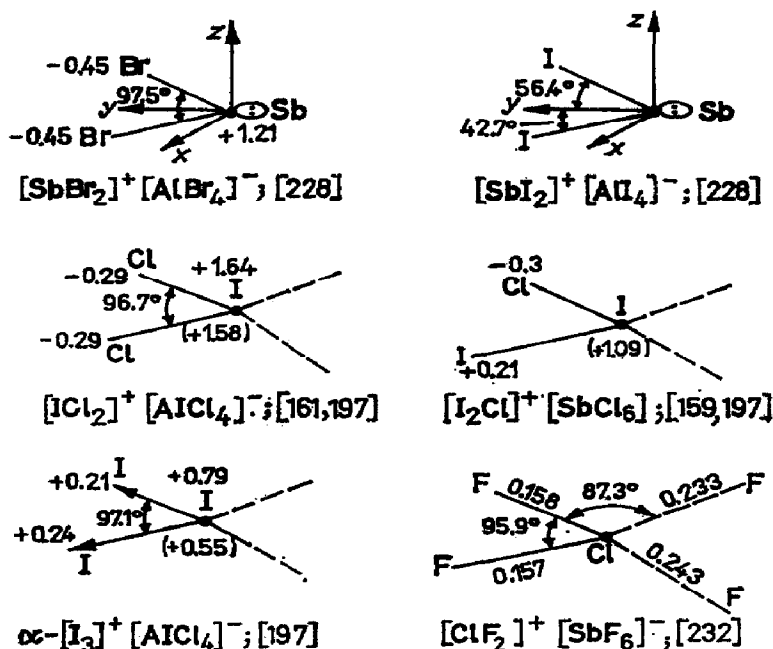
Figure 2.10 Geometry of V-shaped cations and electron distribution according to NQR data.

variation of the [81]Br frequency values in the anion is also large, approaching 12% (Table 2.14). Both these factors provide evidence for the interaction of the Br atoms in the anion species with other neighbouring atoms. The NQR spectroscopic pattern of the related iodide complex is very similar.

Thus, the [Sbhal$_2$]$^+$ and [Alhal$_4$]$^-$ ions are linked together by weak secondary bonds between the Sb atoms in the cation and the halogen atom in the anion [Alhal$_4$]$^-$ [228]. The spatial arrangement of the cationic species in these complexes with respect to the antimony EFG axes, as determined from NQR Zeeman analysis, is shown in Figure 2.10, which also gives the electron charge distribution in the [SbBr$_2$]$^+$ cation calculated [228] using sp^2 hybridized antimony orbitals with C_{2v} symmetry, within the Townes and Dailey approximations.

The NQR data for the remaining species in Table 2.14 are less complete although X-ray results [161] are available for $[ICl_2]^+ \cdot [AlCl_4]^-$ and $[ICl_2]^+ \cdot [SbCl_6]^-$. There is a weak interaction between ionic pairs which occurs through the Cl atoms of the anions and the I atom of cations. The $Cl_2I\cdots Cl-M$ interaction completes a plane tetrafold environment for the iodine atom. Such coordination is considered [197] to be responsible for the shifts in the average cation ^{35}Cl frequencies in $[I_2Cl]^+$ and $[ICl_2]^+$ salts, with variation in anion, assuming an approximately constant geometry at the central iodine atom. Thus slightly stronger coordination of $[I_2Cl]^+$ with $[AlCl_4]^-$ than with $[SbCl_6]^-$ (38.02 MHz vs. 38.28 MHz) and a relatively stronger coordination to $[ICl_2]^+$ with $[SO_3F]^-$ than with $[AlCl_4]^-$ (38.12 MHz vs. 38.894 MHz) was suggested.

Using the X-ray data [161] on the value of $Cl-I-Cl$ angle ($\theta = 96.7°$) in $[ICl_2]^+ \cdot [AlCl_4]^-$ the η at the iodine site was estimated [197] from the relationship $\eta = -3\cos\theta$ to complete the ^{127}I NQR spectra. The use of the observed ^{127}I lower transition ($\Delta m = 1/2 - 3/2$) frequency together with the estimated η value and the atomic QCC (2292.8 MHz) gives the σ-bond populations on the central iodine atom. The terminal atom σ-bond populations were calculated separately using the observed ^{35}Cl resonances and the atomic QCC value with the assumption of axial symmetry for the chlorine EFG ($\eta = 0$) and no s-contribution to bonding by that atom. The σ-bond population sum in $[ICl_2]^+$ thus obtained averaged about 1.97 electrons very close to the expected value of 2.

Charge distributions calculated as above in the cation of this, and two other complexes, are shown in Figure 2.10. The additional values in parentheses, for the central iodine are calculated by difference from the terminal charge and the total ionic charge of $+1$.

Differences found for the central atom by the two approaches are attributed [197] both to the limitation of the model, including the presumed absence of any s-character in the bonding of the terminal atoms and to real effects of anion coordination to the central atom, ignored during the calculation.

Table 2.14 also lists NQR data for the fluoride ionic pairs. X-ray investigations on $[ClF_2]^+ \cdot [SbF_6]^-$ [232] and $[ClF_2]^+ \cdot [AsF_6]^-$ [233] show the structural similarity of the cation fragments in these compounds and in $[ICl_2]^+ \cdot [SbCl_6]^-$ [161] (Fig. 2.10). The $[ClF_2]^+$ cation like $[ICl_2]^+$, possesses a V-shaped configuration with angles close in value. Secondary interionic bonds $Sb-F\cdots ClF_2|$ in $[ClF_2]^+ \cdot [SbF_6]^-$ complete coordination of the central Cl atom to the distorted square plane. The F atoms of $[SbF_6]^-$ octahedra participate in interionic coordination and are located $trans$ with respect to each other. This agrees with the small η-values at the Sb sites of the ^{121}Sb NQR spectrum [229] (Table 2.14). The latter seems to be incomplete since two crystallographically independent $[SbF_6]^-$ polyhedra are present in the crystalline lattice of the compound, according to X-ray results [232]. In this respect the description of the structure agrees better with the NQR spectra of

$[ClF_2]^+ \cdot [BiF_6]^-$ and $[ClF_2]^+ \cdot [TaF_6]^-$ providing reasons for suggesting the structural similarity of these compounds including the *trans*-location of bridging fluorine ligands in the anion groups.

In compounds of $[ClF_2]^+$ with the polyanions $[Sb_2F_{11}]^-$ and $[Sb_4F_{21}]^-$, the η-values at the Sb sites are much higher (Table 2.14) interpreted [229] as evidence for the *cis*-location of the bridging fluorine atoms in the polyanions, similar to that established [234] for $[BrF_4]^+ \cdot [Sb_2F_{11}]^-$.

An IR study of XeF_2 complexes with various Lewis acids [236] shows the electron-acceptor ability of the anions decreases in the order:

$$[Sb_4F_{21}]^- > [Sb_2F_{11}]^- > [SbF_6]^- > [TaF_6]^- \tag{68}$$

In compounds with $[ClF_2]^+$ cations (Table 2.14) the ^{35}Cl NQR frequency increases in the same order. Considering this increase as a criterion for anion electron-acceptor ability [230] the series may be extended as follows:

$$[Sb_4F_{21}]^- > [Sb_2F_{11}]^- > [AsF_6]^- > [BiF_6]^- > [SbF_6]^- > [NbF_6]^- > [TaF_6]^- \tag{69}$$

This succession evidently shows increasing order of interionic interaction. Using the frequency increase as a measure of the acceptor ability of the anions, it was assumed, of course, that the ^{35}Cl QCC values increased in the same order [230]. This is reasonable firstly because determination of the QCC value as simply twice the corresponding ^{35}Cl frequency is less than 0.5% erroneous until η reaches 0.3. Secondly, the available spectroscopic and structural data suggest similarity in atomic arrangement and electron distribution in the $[ClF_2^+]$ cations. Therefore the asymmetry parameter at the chlorine site does not vary considerably over the compounds discussed although it can be non-negligible in absolute value. This evidently contradicts the assumption [230] of zero asymmetry parameter at the chlorine site in $[ClF_2]^+$ cations. Indeed, one can see from Table 2.14 that the η values at the ^{127}I sites in $[ICl_2]^+ \cdot A^-$ are of the order of 35% and Figure 2.10 shows that the $Cl-I-Cl$ angles in $[ICl_2]^+$ and $F-Cl-F$ in $[ClF_2]^+$ which determine the η-values, are similar to one another.

Another type of fluoroionic compound with a heteroatomic cation arises due to the interaction of chlorine(V) pentafluoride with various mole amounts of metal halides. The ionic pairs so produced are listed in Table 2.15 together with their NQR spectra. X-ray data are available only for $[BrF_4]^+ \cdot [Sb_2F_{11}]^-$ [234]. The geometry of the $[BrF_4]^+$ is a trigonal ψ-bipyramid. The two secondary bonds which the central Br atoms form with the fluorine atoms of adjacent anions (0.224 and 0.249 nm) complete a distorted octahedron. A similar arrangement in the cations $[IF_4]^+$ and $[ClF_4]^+$ is suggested [235] in compounds with antimony pentafluoride, the latter being taken in various mole ratios.

The anions are characterized by relatively high asymmetry parameters at the Sb atoms. The η value in $[ClF_4]^+ \cdot [SbF_6]^-$ is nearly the same as in the structurally studied [237] $[BrF_2]^+ \cdot [SbF_6]^-$ (Table 2.15) where the *cis*-position of

TABLE 2.15

NQR spectra of the central atoms in heteroatomic fluoroions at 77 K [235]

Compound	Cation	Anion ^{121}Sb			
	ν (MHz)	ν (MHz)		$\dfrac{e^2Qq}{h}$ (MHz)	η (%)
		1/2 — 3/2	3/2 — 5/2		
$^{35}ClF_4^+ \cdot SbF_6^-$	27.200	11.207	21.036	70.84	22.7
$^{35}ClF_4^+ \cdot TaF_6^-$	26.651				
$^{81}BrF_4^+ \cdot SbF_6^-$	124.320				
	104.460				
$IF_4^+ \cdot SbF_6^-$		17.03	33.69	112.5	9.2
$^{35}ClF_4^+ \cdot Sb_2F_{11}^-$	27.291	38.542	56.410	198.32	56.0
		35.728	52.285	183.79	56.1
$^{35}ClF_4^+ \cdot Sb_4F_{21}^-$	27.430	48.546	60.195	218.31	74.7
		38.710	63.012	217.36	43.4
$^{81}BrF_4^+ \cdot Sb_2F_{11}^-$	128.153	40.917	51.448	186.01	73.2
		37.660	44.560	163.04	80.1
$^{81}BrF_4^+ \cdot Sb_3F_{16}^-$	127.039	40.923	60.025	210.96	55.7
		40.923	58.456	246.12	58.8
		40.224	55.556	197.40	62.6
$BrF_2^+ \cdot SbF_6^-$		16.197	33.306	102.10	23.3
		16.039	30.202	101.65	22.1

the bridging fluorine atoms is established. This suggests a similar arrangement of bridging fluorine atoms in the former compound.

The polyanions $[Sb_xF_{5x+1}]^-$ in compounds with the known structures $([BrF_4]^+ \cdot [Sb_2F_{11}]^-, [IF_4]^+ \cdot [Sb_2F_{11}]^-, [Br_2]^+ \cdot [Sb_3F_{16}]^-$ and $[ClO_2]^+ \cdot [Sb_2F_{11}]^-$, [235] and refs. cited therein) form chains of $[SbF_6]^-$ octahedra joined to each other by bridging fluorine atoms at *cis*-positions. This agrees with the high η values at the Sb atoms in $[BrF_4]^+ \cdot [Sb_2F_{11}]^-$ and in other ionic compounds listed in Table 2.15.

The ^{121}Sb QCC value will decrease with an increase in the strength of the Sb — F bridging bond [235]. At the same time this increase reflects as an increase in the donor ability of the cations. Thus the order of variation in the average anion ^{121}Sb QCC value provides the following order of cation donor ability:

$$BrF_3 < ClF_5 < ClF_3 < BrF_5 < IF_5 \qquad (70)$$

E. THE ORIGIN OF THE EFG AT THE COMPLEX ION CENTRAL ATOM

Clearly valuable crystallochemical information can be obtained from the NQR spectra of both central and ligated atoms in ionic complexes. While ligand NQR spectra yield information on the geometry of the ions and the chemical interactions between them, mainly from shifts and splitting of resonances, the central atom spectra contain such information in their QCC value and the asymmetry parameter of the EFG.

Now let us consider some NQR data pertaining to the central atom in these complex ions, in order to analyze the sources contributing to the EFG.

Table 2.16 lists NQR data for a number of cobalt(III) ionic complexes in which the central atom is located in cations of roughly octahedral configuration. The sites with cubic point group symmetry are known to have zero EFG, so that these ^{59}Co QCC values serve partially as a measure of the distortion of these cations from octahedral symmetry.

In the first row transition elements, the principal contribution to the EFG derives from electrons on the $4s$, $4p$ and $3d$ orbitals. Though the contribution from the $3d$ electrons prevails and the $4p$ orbitals have far lower occupancies, the contributions of the latter should also be taken into account. The review by Brown [238] devoted to an NQR study of various types of cobalt compound contains data on EFG values due to the unpaired $3d_{z^2}$ (q_{320}) electrons for three isoelectronic metals (Table 2.17). Table 2.17 also includes EFG values arising from $4p_z$ electrons (q_{410}) for Fe(0) having the configuration $4s^1 3d^6 4p^1$. These are not much smaller than q_{320}. The contribution to the EFG, from valence orbital populations, can be written as

$$q_{zz} = q_{320} \left[N_{d_{z^2}} + \frac{1}{2} \left(N_{d_{xy}} + N_{d_{yz}} \right) - \left(N_{d_{xy}} + N_{d_{x^2-y^2}} \right) \right]$$
$$+ q_{410} \left[N_{p_z} - \frac{1}{2} \left(N_{p_x} + N_{p_y} \right) \right] \tag{71}$$

In addition, in coordination compounds of Co(III) where the charges on the cobalt and ligand atoms are non-zero some contribution to the EFG is made at the central atom by the external charge distribution. The electrons on valence orbitals as well as the external charges can polarize the inner core electrons, generating a Sternheimer shielding or antishielding contribution to the EFG.

Three possible factors which determine the EFG at the cobalt atoms have been discussed by Watanabe et al. [239] who interpreted the ^{59}Co NQR data for octahedral cobalt complexes: metal valence electrons, ionic charges on the ligand atoms bonded to the metal, and outer ion charges (lattice charges). The ionicities of the Co—Cl bonds in the [Co(NH$_3$)$_5$Cl]$^{2+}$ cation were estimated from ^{35}Cl NQR data via the Townes and Dailey [95] theory approximations, and appeared to be about 70%. Ligand charge contributions have been deter-

TABLE 2.16

NQR spectra of some cobalt(III) octahedral complexes and related compounds at room temperature

Compound[a]	Iso-tope	Transition frequencies (MHz)			$\dfrac{e^2Qq}{h}$ (MHz)	η (%)	Ref.
		1/2 — 3/2	3/2 — 5/2	5/2 — 7/2			
[Co(NH₃)₅Cl]Cl₂	⁵⁹Co	2.733	4.399	6.758	31.74	25.1	239
Co[(NH₃)₅Cl]SO₄·H₂SO₄	⁵⁹Co	2.405	4.773	7.161	33.43	4.2	239
		2.526	4.892	7.364	34.39	8.9	
cis-[Co(en)₂Cl₂]Cl·H₂O	⁵⁹Co	3.168	4.980	7.668	36.05	26.8	241
cis-[Co(en)₂Cl₂]NO₃	⁵⁹Co	2.654	4.741	7.201	33.71	17.3	241
(II)tr.-[Co(en)₂Cl₂]NO₃	⁵⁹Co	4.777	8.877	13.426	62.78	13.2	242
(at 270 K) innersphere	³⁵Cl	16.426					246
tr.-[Co(en)₂Cl₂]Cl	⁵⁹Co	5.367	8.368	12.892	60.63	27.2	242
(III)tr.-[Co(en)₂Cl₂]ClO₄	⁵⁹Co	4.614	8.404	12.859	60.14	14.6	243
		4.601	8.452	12.708	59.86	14.8	244
innersphere	³⁵Cl	16.515					
		16.828					
tr.-[C(en)₂Br₂]Br	⁵⁹Co		8.392	12.860	60.36	23.5	242
tr.-[Co(NH₃)₄Cl₂]Cl	⁵⁹Co		8.370	12.665	59.23	13.6	245
(I)tr.-[Co(en)₂Cl₂]Cl	⁵⁹Co	5.979	10.001	15.296	71.73	22.2	240
·HCl·xH₂O innersphere	³⁵Cl	16.058			31.91	22.4	247
outersphere	³⁵Cl	2.858			5.04	90.4	
(V)tr.-[Co(tn)₂Cl₂]Cl	⁵⁹Co		8.690	13.143	61.45		246
·HCl·2H₂O[b])							
innersphere	³⁵Cl	16.331					246
(VI)tr.-[Rh(en)₂Cl₂]Cl							
·HCl·xH₂O innersphere	³⁵Cl	17.089					248
tr.-[Cr(en)₂Cl₂]Cl							
·HCl·xH₂O innersphere	³⁵Cl	10.300			20.55	7.3	247
outersphere	³⁵Cl				5.26	90.2	
tr.-[Co(en)₂Cl₂]Br	⁵⁹Co	4.890	8.405	12.821	60.08	20.4	243
tr.-[Co(en)₂Cl₂]I	⁵⁹Co	4.528	8.237	12.485	58.41	15.6	243
tr.-[Co(en)₂Cl₂]SCN	⁵⁹Co		8.395	12.870	60.43	24.5	239
tr.-[Co(en)₂Cl₂]BrO₃	⁵⁹Co		9.057	13.880	65.15	23.8	244
tr.-[Co(en)₂Br₂]ClO₄	⁵⁹Co		8.096	12.264	57.38	14.9	244
(IV)tr.-[Co(en)₂Br₂]Br	⁵⁹Co	6.212	10.104	15.503	72.80	24.4	240
·HBr·2H₂O							
innersphere	⁷⁹Br	127.34					

a) tr. trans; b) tn trimethylenediamine.

TABLE 2.17

$3d$ and $4p$ unpaired electron contributions to the EFG at some metals in specific states [238]

Atom	Configuration	State	q_{320}*) 10^{-15}	q_{410}*) 10^{-15}
			Electrostatic cgs units cm^{-3}	
Mn	$4s^2 3d^6$	^5D	−6.70	•
Fe	$4s^2 3d^6$	^5D	−9.23	
Co$^+$	$4s^2 3d^6$	^5D	−12.16	
Fe	$4s^1 3d^6 4p^1$	^7P	−8.79	−4.79

*) q_{nlm}.

mined with the assumption that the point charges are located at the sites of the ligated atoms (nitrogen and chlorine) with the use of the Sternheimer factor of $1 - \gamma = 8$. Outer charge contributions have been calculated from the structure data ([239] and refs. cited therein) with the assumption of $1 - \gamma_\infty = 8$. These contributions appeared to be negligibly small. The estimates, thus obtained, led to the following atomic charge values for $[Co(NH_3)_5Cl]^{2+}$ cation: Co -0.48; N $+0.63$; Cl -0.67, if one assumes that $q > 0$ in accordance with [238] and refs. cited therein. The unreasonable charges on the cobalt and nitrogen atoms are, according to Brown [238], due mainly to the assumptions made in evaluating contributions of the ionic charges on the ligand atoms bonded to the central atoms.

There is at present no adequate theoretical model for the choice of the $1 - \gamma$ value in calculations of ligand charge contributions and of the $1 - \gamma_\infty$ value in calculations of lattice charge contributions.

For that reason, Brown [238] suggests use of the model of additive partial field gradient (p.f.g.). This model is often used in interpreting the data for ^{57}Fe and ^{119}Sn Mössbauer quadrupole splitting. The contribution from a certain ligand, to the EFG at the central atom, is regarded as a parameter characteristic of that ligand, and the EFG components are determined by summation of effective contributions over individual ligands.

The NQR data for complexes of Co(III), listed in Table 2.16, reflect the effect of the outer ions on the central atom QCC values. As seen from these data, changing the anion shows no strong effect upon the EFG at the Co atom, if no specific interactions such as hydrogen bonding, are suspected to occur between the ligands and external ions. At the same time, lattice effects on the η-value can be quite pronounced as it is seen from the non-zero asymmetry parameter in the trans-$[Co(NH_3)_4Cl_2]^+$ cation (Table 2.16). Calculations [239, 244] show, however, that the outer charge contributions to the EFG are too small

to significantly affect either the QCC or η values. In Brown's opinion [238], the most probable reason for non-zero η values in the compounds in question is distortion of the coordination polyhedron with displacement of the ligands from positions having four-fold axial symmetry.

The study of contributions to the EFG at the ^{59}Co and hal (X) sites in several compounds containing the $tr.$-[Co(en)$_2$X$_2$]$^+$ ions (X = Cl, Br) (I—VI in Table 2.16) have required measurement of the temperature dependences of ^{59}Co and ligand halogen NQR frequencies [246]. Using thermal parameters from a neutron diffraction study of (I), a rigid-body analysis of the effects of librational motion led to the conclusion that the latter accounts for less than 15% of the change in the ^{59}Co EFG with temperature. Point charge model calculations indicated small direct contributions to the EFG at ^{59}Co and ^{35}Cl from lattice charges. On the basis of extended Hückel MO calculations, it was concluded that hydrogen bonds involving the complex ions appear to offer an explanation of some of the temperature effects, in terms of changes in orbital populations, although the explanation is incomplete. The authors [246] concluded that study of the NQR temperature dependences in the deuterated analogues as well as precision diffraction studies of more of the compounds would be necessary to provide more definitive information about hydrogen bonding, the rigid-body motion and the bond lengths in order to continue efforts to sort out contributions to the NQR parameters in these compounds.

In general, if no specific interaction exists between ligands and outer charges, and the configuration of the cation is determined, then both QCC and η values at the central atom provide information about the electron distribution within the ion. Table 2.16 contains ^{35}Cl NQR data [247, 248] on the related cations $trans$-[M(en)$_2$Cl$_2$]$^+$ where M is Rh and Cr. There are strong reasons to suggest that these compounds are isostructural to the corresponding Co(III) complexes [248]. Thus lattice contributions to the EFG at the chlorine atom should remain approximately the same along the series, and resonance frequency variations from one compound to another should be due to changes in the electronic distribution within the ions. Lowering of the ^{35}Cl NQR frequencies from Rh to Co to Cr is consistent with a decrease of the electronegativity difference between the M and Cl atoms in the same direction. The rapid ^{35}Cl resonance frequency decrease on passing to the chromium cation may be explained [248] by the presence of half-filled d_π orbitals on that metal which may participate in p_π (Cl) $-d_\pi$(Cr) interactions. These should result in halogen atom resonance frequency lowering. The corresponding Co and Rh orbitals are filled, and the extent of Co —Cl π-bonding is small compared to σ-bonding ($\sim$ 3%).

Hartmann et al. [247] studied single crystals of $trans$-[Co(en)$_2$Cl$_2$]Cl · HCl · xH$_2$O and $trans$-[Cr(en)$_2$Cl$_2$]Cl · HCl · xH$_2$O by the NMR technique, to obtain halogen atom QCC values for the complex cation and outer sphere anions. They made an approximate estimate of the M —Cl bond ionicities (i) in terms of the Townes and Dailey theory, for the cases of $\pi = 0$, 0.05 and 0.1. For the

TABLE 2.18

185Re and 127I NQR spectra of perrhenates and periodates (*RT* room temperature)

Compound	T (K)	ν (MHz)		$\frac{e^2Qq}{h}$ (MHz)	η (%)	Ref.
		1/2—3/2	3/2—5/2			
HReO₄	296	30.05	60.15	200.4	0.0	260
LiReO₄	77	32.056	53.550	183.9	40.0	255
		44.483	52.902	193.20	80.0	
		51.403	61.883	225.7	78.0	
NaReO₄	RT	45.007	89.996	300.02	2.6	256
KReO₄	RT	28.312	56.00	178.75	1.8	251
AgReO₄	RT	39.79	79.51	250.9	0.0	256
NH₄ReO₄	297	17.603	35.203	117.35	1.7	261
NDReO₄	297	17.825	35.665	118.85	0.0	261
RbReO₄	298	21.35	42.69	142.3	0.0	257
TlReO₄	285	23.33	41.48	141.4	0.31	422

Compound	T (K)	ν (MHz)		$\frac{e^2Qq}{h}$ (MHz)	η (%)	Ref.
		1/2—3/2	3/2—5/2			
NaIO₄	296	6.362	12.723	42.4	0.0	256
KIO₄	296	3.114	6.227	20.76	0.0	256
AgIO₄	RT	4.45	8.90	29.7	0.0	252
NH₄IO₄	RT	(1.50)*)	3.01	(10.0)*)	(0.0)*)	252
RbIO₄	RT	2.36	4.72	15.7	0.0	252
CsIO₄				1.0	0.3	252
(Me₄N)IO₄	RT	(2.31)*)	4.63	(15.4)*)	(0.0)*)	252

*) Assumed magnitudes are given parenthetically.

Co—Cl bonds, i values were of the order of 0.8, 0.7 and 0.6, respectively, while for the Cr—Cl bonds these values were of the order of 0.9, 0.8 and 0.7.

Perrhenates and periodates ($AM^{VII}O_4$) make the class of ionic compounds which numerous representatives have been studied by NQR at the central atom (Table 2.18). Most of them crystallize in a tetragonal scheelite (space group $14_1/a$) or rhombic pseudoscheelite lattice ([252, 261] and refs. cited therein). The isolated ions $[ReO_4]^-$ and $[IO_4]^-$ in the scheelite structure suffer small distortions from tetrahedral symmetry being compressed, like $NaIO_4$ [249], or elongated, like $KReO_4$ [250], along the c-axis. They form a tetragonal bisphenoid (D_{2d}) arrangement of atoms. Their distortion in solids is proposed [251] presumably to arise from interactions with the lattice. The site symmetry of the anion species S_4, requires a zero asymmetry parameter (η) at the rhenium (iodine) atom, which is the case in compounds with the scheelite structure (Table 2.18). In the complexes with the pseudoscheelite structure the anions form rhombic bisphenoids of lower symmetry (D_2) [252] accompanied by an increase in the η value at the site of the central atom ($CsIO_4$, $TlReO_4$ in Table 2.18). Table 2.18 also includes the NQR spectrum [252] of the compound $N(CH_3)_4IO_4$ which belongs to neither scheelite nor to the pseudoscheelite family, but is isotypic with tetragonal perrhenates and perchlorates [253, 254], which enables the authors [252] to suggest $\eta = 0$ in this compound. The structure of $LiReO_4$ seems to be unknown. From the ^{187}Re NQR spectrum of $LiReO_4$ there is evidences for at least three crystallographically independent $[ReO_4]^-$ groups in the crystal lattice, all having large asymmetry parameters. Hydrogen-like bonds of the type $Li\cdots O-Li$ are probably present in the compound [255].

The relatively large magnitudes of the QCC at the central atoms in the compounds discussed here, result from (i) a contribution to the EFG from outer point charges in the tetragonal lattice $q(e)$ $[1 - \gamma_\infty]$, (ii) partial covalent bonding inside the anion $q(p)$ and (iii) polarization of the central metal atomic core by the external charges. Relative values of these contributions have been estimated [256] in $KReO_4$ and $NaIO_4$ using X-ray results [249, 250] and a valence bond formalism. Magnitudes of the Sternheimer factor γ_∞ were obtained and fitted as adjustable parameters, to get agreement between the total value of the calculated EFG $q = q(e)$ $[1 - \gamma_\infty] + q(p)$ and the experimentally measured value $|q_{obs}|$. Their results are given below [256]:

Compound	Isotope	Quadrupole moment $Q \times 10^{-24}$ (cm²)	$\|q_{obs}\|$ $\times 10^{14}$ (esu)	$q(p)_{calc}$ $\times 10^{14}$ (esu)	$q(e)_{calc}$ $\times 10^{14}$ (esu)	γ_∞
$NaIO_4$	^{127}I	—0.88	7.8	—12.3	+1	—19.1
$KReO_4$	^{185}Re	2.6	11.2	—3.54	—0.456	—15.8

The relative importance of these contributions is naturally different for particular compounds, but in general, contributions (i) and (iii) prove rather significant. The large value of the quadrupole moment of the Re isotopes as well as the more ionic $M-O$ bonds in the rhenium compounds, seem to account for the greater QCC values in perrhenates than in related periodates.

Burkert et al. [252, 257, 258] note a good linear correlation of the ^{185,187}Re and ^{127}I QCC magnitudes in scheelite structures to c^{-3} (c is the length of the unit cell) and to V_0^{-1} (V_0 is the unit cell volume). This agrees with the conclusion [259] that the temperature expansion of the lattice makes an important contribution to the EFG at the central metal, and the magnitude of this contribution varies with cation even in a series of compounds with the same type of structure (scheelite).

Another type of tetrahedral ionic compound which has been extensively investigated by NQR, is represented by mono- and dihydrogen arsenates R_2HAsO_4 (PbHAsO$_4$) and RH_2AsO_4 (KDA). They belong to the highly important hydrogen bonded ferroelectric and antiferroelectric group.

KDA crystals consist of tetrahedral $[AsO_4]^{3-}$ groups connected by $O-H\cdots O$ bonds. The dynamics in the hydrogen bonds play an important role in the ferroelectric properties of these crystals. In the ferroelectric phase, their structure is orthorhombic, C_{2v}, and spontaneous polarization occurs along the c-axis [262]. The EFG on the ^{75}As nucleus is strongly dependent on the mutual disposition of the four protons contributing to the $O-H\cdots O$ bonding of the $[AsO_4]^{3-}$ group. The EFG is, in addition, enhanced by the displacement of the As atom from the centre of the tetrahedron [263]. The NQR frequency provides therefore, a measure of the distortion of the $[AsO_4]^{3-}$ tetrahedron. In the paraelectric phase the crystals exhibit a structure of tetragonal symmetry D_{2d} [262].

Some of the monoclinic monohydrogen and dihydrogen arsenates of the PbHAsO$_4$ and TlH$_2$AsO$_4$ families, also undergo ferroelectric phase transitions [264].

An ^{75}As NQR study of ferroelectric and antiferroelectric arsenates (Table 2.19) is of great interest, due to the considerable contribution of the $[AsO_4]^{3-}$ tetrahedron, to spontaneous polarization in the crystal. A remarkable isotope effect ($6-7$ MHz) was observed [265] on deuteration of the KDA type compounds (Table 2.19) indicating an important role for hydrogen bonding in the $[AsO_4]^{3-}$ distortion.

Most papers devoted to the NQR study of these substances, report the results of pressure and temperature effects on the ^{75}As NQR frequencies. The latter incorporate information about various microscopic parameters, characterizing the dynamic properties of the compounds, such as the tunnelling energy, dipole—dipole interactions [262], type of proton ordering in the hydrogen bonds $O-H\cdots O$ connecting the tetrahedral $[AsO_4]^{3-}$ groups [266]. They also provide valuable information concerning molecular mechanisms

TABLE 2.19

^{75}As NQR frequencies in monohydrogen and dihydrogen arsenates at 77 K (ferroelectric phase)

Compound	ν (MHz)	Ref.
$PbHAsO_4$	25.491	267
$Na_2HAsO_4 \cdot 7\,H_2O$	42.110	264
$Na_2HAsO_4 \cdot 5\,H_2O$	40.80	264
Na_2HAsO_4	47.400	264
$(NH_4)_2HAsO_4$	32.740	264
$(ND_4)_2DAsO_4$	33.770	264
TlH_2AsO_4	37.760	264
	38.475	264
KH_2AsO_4	35.07	265
KD_2AsO_4	42.62	265
RbH_2AsO_4	35.70	265
RbD_2AsO_4	42.68	265
CsH_2AsO_4	37.23	265
CsD_2AsO_4	42.98	265
$NH_4H_2AsO_4$	35.18	265
$ND_4D_2AsO_4$	38.78	265
	39.45	265

responsible for the temperature and pressure effects (rotation of $(NH_4)^+$ groups, vibrations contributing to intermolecular gradients, geometrical effects, thermal expansion of crystal lattice, etc. [266]) as well as the mechanisms of phase transitions.

These problems are however beyond the limits of this paper, and we shall not dwell on them here.

F. DONOR—ACCEPTOR BONDING AND CHARGE DISTRIBUTION
IN $GaCl_3 \cdot L$, $SnCl_4 \cdot 2L$, AND $SbCl_5 \cdot L$ MOLECULAR ADDUCTS

Reports on the use of NQR to study molecular adducts or electron donor—acceptor (EDA) complexes have become available along with the first papers dealing with chemical applications of the method [274]. Thereafter, interest in this problem has been increasing due, on the one hand, to the wide use of these complexes in extraction, catalytic and preparative chemistry and, from the other, because of the diverse potential of the NQR technique which provides subtle information on various aspects of complexation phenomena.

The EDA complexes are formed by means of electron charge transfer from the highest occupied donor MO to the lowest vacant MO of the acceptor moiety. They are conventionally classified according to the nature of orbitals which take part in the donor—acceptor interactions: $\pi-\pi$, $\pi-\sigma$, $n-\sigma$ and $\sigma-\sigma$ complexes. Donor—acceptor interactions of this type, as a rule involve molecules containing atoms with lone pairs of electrons (donor molecules) and those possessing low-lying vacant orbitals (acceptor molecules). In this section we consider the discrete molecular complexes of the $n-\sigma$ class where constituent moieties (donor and acceptor) can clearly be identified.

The important problems which arise in the study of EDA complexes concern the determination of the amount of charge transferred from donor to acceptor and the analysis of the distribution of charge over the system of interacting components. These features are the principal characteristics of the complexation process. The application of NQR requires us therefore to establish the relationship of these characteristics to the NQR spectroscopic parameters.

The most extensive data are now available for complexes of the type $GaCl_3 \cdot L$, $SnCl_4 \cdot 2L$ and $SbCl_5 \cdot L$ [134, 270, 271], the most extended data being reviewed in [274].

The complexes appear attractive because their acceptor molecules contain none but quadrupole atoms (the [119]Sn QCC values in $SnCl_4 \cdot 2L$ complexes being measured by Mössbauer spectroscopy).

NQR studies of these complexes became available already in early papers [118, 200, 268, 269]. They compared the [35]Cl frequency shifts due to complexation, with respect to their frequencies in free components. The decrease of electron density in a donor system and its increase in the acceptor system which accompanies the formation of the complex was assumed to shift the [35]Cl frequency upwards in a donor fragment and downwards in an acceptor fragment. This was observed in experiment, and the relative values of the shifts were treated as a measure of the strength of the complexes studied.

The variation in NQR frequencies as a consequence of complexation is caused by the combined action of a number of contributions. These include reorganization of the electron structure of the constituents, the change in the environment of the quadrupole atom in the adduct compared to that in the starting component, as well as the influence of spatial interactions.

The effect of the change in the environment on the NQR spectroscopic parameters is associated with a solid-state effect. Shifts are due to intermolecular interactions in the solid, molecular motions in crystals and electric charges on atoms [269]. The steric interactions may also play an important role in complex formation [270]. They can hinder approach of molecules to each other thus limiting charge transfer. Although the donating power of a donor may be high, the amount of charge transfer will be small in this case. Steric interactions may lead to distortion of the constituent molecules and

polarization of their atomic shells. All the factors mentioned above require us to use caution in interpreting NQR spectra [271—273] since their relative importance may vary widely from one compound to another. Clearly, to have reliable information on the electronic processes occuring upon complex formation one must be sure that the spectroscopic changes observed originate from the reorganization of electron structure rather than from steric interactions or solid-state effects.
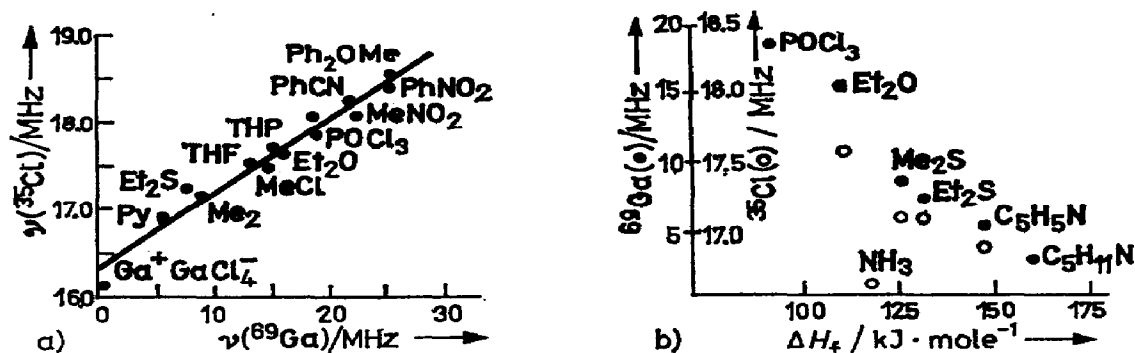

Figure 2.11 a) ^{35}Cl NQR frequencies vs ^{69}Ga NQR frequencies in complexes of type $GaCl_3 \cdot D$; b) correlation of ^{35}Cl and ^{69}Ga NQR frequencies with heats of formation in the gaseous phase (ΔH_f) for complexes of type $GaCl_3 \cdot L$ [200].

In this respect the paper by Tong [200] is instructive. This presents the results of an NQR investigation of $GaCl_3 \cdot L$ complexes in the form of correlations between the ^{35}Cl and ^{69}Ga NQR frequencies, and between these frequencies and the enthalpies of formation of the complexes in gaseous phase ΔH_f (Fig. 2.11). The energy of formation of the donor—acceptor bond in complexes $MCl_n \cdot L$ (ΔH_{DA}) is related to the enthalpy of complex formation in the gaseous phase (ΔH_f) as follows [119]:

$$\Delta H_f = \Delta H(MCl_n) + \Delta H_L + \Delta H_{DA}. \tag{72}$$

Here $\Delta H(MCl_n)$ is the energy of rearrangement of the acceptor molecule due to complexation (in the first approximation it is the energy of transformation of the acceptor molecule from the configuration it has in a free molecule to the configuration it has in the molecule of complex), ΔH_L is the energy of rearrangement of the donor molecule. The magnitudes of $\Delta H(MCl_n)$ and ΔH_L have signs opposite to that of ΔH_{DA}. The value of $\Delta H(MCl_n)$ may, as a rule, be considered constant; values of ΔH_L are generally less than ΔH_{DA}. The value of ΔH_f may therefore be considered as a measure of the strength of the donor—acceptor bond in the complexes $MCl_n \cdot xL$. If the energy of formation of the donor—acceptor bond due to the interaction of components MCl_n and L, does not exceed the sum of the energies necessary for the rearrangement of molecules $\{\Delta H(MCl_n) + \Delta H_L\}$, i.e. $-\Delta H_f < 0$, the formation of the donor—acceptor bond and thus of molecular complex is not profitable energetically.

The correlations established undoubtedly show that, in these compounds, the NQR frequency shifts are dominated by the electronic charge transfer effects rather than solid-state or steric interactions, and the frequency shifts can therefore be considered as a measure of the strength of the donor—acceptor interactions. Since the number of complexes studied by NQR is so great and their spectroscopic parameters are available in the reviews mentioned above, we shall not cite them here repeatedly but discuss the results in terms of general regularities in spectroscopic changes which relate to the basic structure and bonding characteristics of these types of complex.

Most of the authors applying NQR to the study of molecular adducts have interpreted their results within the Townes and Dailey-approximation theory. Detailed MO calculations of $n - \sigma$ complexes are rather complicated since their formation is accompanied by a significant electron reorganization, which involves the donor lone pair orbitals and the acceptor vacant orbitals. The most widely used approach consists therefore in setting up hybrid orbitals of definite symmetry which are centered at the quadrupole atom. With the help of the Townes and Dailey relationships (eqns. (42, 43)) one can obtain from NQR data, basic chemical characteristics of the complexes such as the amount of charge transfer as well as the net electron charges located at various atoms in the complexes.

We shall repeat this procedure [276] for complexes of the type $GaCl_3 \cdot L$ which, according to Tong [200], are usually monomeric and possess a distorted tetrahedral configuration. The four orthonormal hybrid orbitals of symmetry C_{3v} were supposed [276] to be centered at the Ga atom. The z-axis of the EFG at the Ga atom is chosen along the C_{3v} axis

$$\Psi_1 = s\varphi_s + \sqrt{1 - s^2}\,\varphi_{p_z}$$

$$\Psi_2 = s_1\varphi_s + \sqrt{1 - s_1^2}\,(\varphi_{p_z}\cos\theta - \varphi_{p_x}\sin\theta)$$

$$\Psi_3 = s_1\varphi_s + \sqrt{1 - s_1^2}\left(\varphi_{p_z}\cos\theta - \frac{\varphi_{p_x}}{2}\sin\theta - \frac{\sqrt{3}}{2}\varphi_{p_y}\sin\theta\right)$$

$$\Psi_4 = s_1\varphi_s + \sqrt{1 - s_1^2}\left(\varphi_{p_z}\cos\theta + \frac{\varphi_{p_x}}{2}\sin\theta + \frac{\sqrt{3}}{2}\varphi_{p_y}\sin\theta\right) \tag{73}$$

where s^2 and s_1^2 are, respectively, the partial s-characters of the Ga—L and Ga—Cl bonds. The angles L—Ga—Cl are denoted by θ. The occupation number of the Ψ_1 orbital directed to L is a_{Ga} which evidently determines the amount of charge transfer from the ligand L. The occupations of Ψ_2, Ψ_3 and Ψ_4 are labelled by b_{Ga}. Then we have

$$\sum_{i=1}^{4} (N_z)_i = (1 - s^2)\,a_{Ga} + 3(1 - s_1^2)\cos^2\theta b_{Ga}$$

$$\sum_{i=1}^{4} (N_x)_i = (1 - s_1^2) \sin^2 \theta b_{Ga} + (1 - s_1^2) \sin^2 \theta \frac{b_{Ga}}{2} = \frac{3}{2}(1 - s_1^2) \sin^2 \theta b_{Ga}$$

$$\sum_{i=1}^{4} (N_y)_i = (1 - s_1^2) \frac{3}{2} \sin^2 \theta b_{Ga} \tag{74}$$

In accordance with equation (42) we obtain

$$e^2Qq_{zz} \cdot h^{-1} = \left[(s^2 - 1) a_{Ga} + b_{Ga}(s_1^2 - 1)\left(3\cos^2\theta - \frac{3}{2}\sin^2\theta\right)\right] e^2Qq_p \cdot h^{-1}$$

$$\tag{75}$$

Orthogonality of the wave functions (73) requires

$$s^2 = 2\cos^2\theta/\sin^2\theta; \quad s_1^2 = 1 - \frac{2}{3}\sin^2\theta \tag{76}$$

which leads to the relationship

$$e^2Qq_{zz} \cdot h^{-1} = (b_{Ga} - a_{Ga})(3 - 2/\sin^2\theta) e^2Qq_p \cdot h^{-1} \tag{77}$$

It can be easily found from equations (73) and (74) that $q_{xx} = q_{yy}$ which means that $\eta = 0$ and the EFG at the Ga site is axially symmetrical, consistent with C_{3v} symmetry. The QCC at Ga is then obtained by simple doubling of the NQR frequency

$$2\nu_{Ga} = e^2Qq \cdot h^{-1}(1 + \eta^2/3)^{1/2} = e^2Qq \cdot h^{-1} \tag{78}$$

Combining (77) and (78) we have

$$\nu_{Ga} = e^2Qq_p \cdot (2h)^{-1}\left[(b_{Ga} - a_{Ga})(3 - 2/\sin^2\theta)(1 + \delta_{Ga}\varepsilon)\right] \tag{79}$$

Here δ_{Ga} is the positive charge at the Ga atom and $\varepsilon(Ga)$ is a parameter which takes into account the increase in q_{Ga} due to a positive charge at the Ga atom. According to [97] $\varepsilon = 0.25$.

By analogy we have for the ^{35}Cl NQR frequency, provided that $N_z = b_{Cl}$, $N_x = N_y = 2$

$$\nu_{Cl} = \left[(1 - s^2)(2 - b_{Cl})/(1 + \delta\varepsilon)\right] e^2Qq_p \cdot (2h)^{-1} \tag{80}$$

In this case $\varepsilon(Cl) = 0.25$ takes into account the decrease in q at the Cl atom due to the negative charge at the latter atom.

The net charges δ on the Cl and Ga atoms relate to the occupation numbers as follows

$$\delta_{Cl} = b_{Cl} - 1 \tag{81}$$

$$\delta_{Ga} = 3 - (3b_{Ga} + a_{Ga}) \tag{82}$$

Assuming the self-consistency of this approach we must obtain

$$b_{Ga} + b_{Cl} = 2 \tag{83}$$

Deeg and Weiss [276] used the same values of s^2 and ε as those ($s^2 = 0.15$ and $\varepsilon = 0.25$) which caused self-consistency in a similar approach when the charge distribution in Me_2X_6 [123] and $[Ga_2Cl_7]^-$ [199] was calculated.

One can now estimate the characteristics of two particular $GaCl_3 \cdot L$ complexes, with $L = Cl^-$ and $L = 4\text{-}ClC_6H_5OH$ [276]. The ligand Cl^- is assumed to possess a greater donating power than all other ligands which means that the $[GaCl_4]^-$ anions can in some respects, be considered the most strong complexes of the type $GaCl_3 \cdot L$. According to Tong [200] the $\nu(^{69}Ga)$ is lowered with increasing gas phase enthalpy of formation of the complexes $(-\Delta H_f)$. The higher the value of $\nu(^{69}Ga)$, the weaker is the complex produced. The complex of $GaCl_3$ with 4-chlorophenol therefore presents an example of the weakest complex among those estimated in [276][1]). All the necessary spectroscopic and structural parameters taken from [276] and the results obtained with equations (77 − 80) are listed in Table 2.20. It was also estimated that nearly half of the total charge transfer from the ligand to the acceptor resides at the 3 chlorine atoms of the latter [276]. This is evident from the results of Table 2.20. One can easily find that the increase in the occupation number of the three orbitals directed from Cl to Ga ($3\Delta b_{Cl}$) represents the fraction of the charge gained by the chlorine atoms when the charge transfer increases by Δa_{Ga}, due to the change of donor from the relatively weak (4-chlorophenol) to the strongest (Cl^-). The sum ($\Delta a_{Ga} + 3\Delta b_{Ga}$) evidently represents the fraction of charge gained by the Ga atom (or $\Delta \delta_{Ga}$) under the same conditions. Their ratio, $3\Delta b_{Cl}/(\Delta a_{Ga} + 3b_{Ga}) \approx 1$ reflects therefore the tendency to redistribute the charge transfered from the ligand to the acceptor molecule so that nearly half of the density received from the ligand is accumulated on the Ga atom.

From the correlation by Tong [200] the following ligands order reflecting the increase of their donating power is suggested according to the lower frequency shifts measured at the chlorine and gallium sites in the acceptor moieties.

$$PhNO_2 < PhOMe < POCl_3 < Et_2O < THF < Et_2S \tag{84}$$
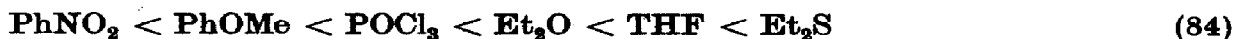
Kuz'min et al. [119, 169] attempted to analyze in a similar manner, NQR data available for the $SbCl_5 \cdot L$ complexes. They obtained a linear correlation

---

[1]) The amount of charge transfer (a_{Ga}) calculated [276] for several complexes including those we are discussing here showed a linear dependence on $\nu(^{69}Ga)$. As follows from the correlation $\nu(^{69}Ga) = f(-\Delta H_f)$ found by Tong [200] and interpreted by Deeg and Weiss [276] in terms of the Townes and Dailey analysis, only an electrostatic interaction between the ligand and acceptor is taken into account by this approach. This suggests that $\Delta H_f \sim f(a_{Ga}^2)$. This however also means that one would expect $\nu(^{69}Ga) \sim f(a_{Ga}^2)$ which is not confirmed by the results [276]. The discrepancy may be accounted for by the inadequacy of a simple ionic model for the EDA complexes as well as for the various simplifications inherent in the Townes and Dailey theory [95].

TABLE 2.20

NQR data and estimated characteristics of the chemical bonds in complexes $GaCl_3 \cdot L$ [276], the hypothetical complexes $SbCl_5 \cdot L$, the strongest ($-\Delta H^0_{max} = 46$ kcal $\cdot$ mole^{-1}) and the weakest ($-\Delta H^0 = 0$) [119, 169].
$\delta(Cl)$ the net electron charge on the Cl atom in the acceptor moiety; a_M the amount of charge transfer; $\delta(M)$ the net electron charge on the central atom; b_M the electron occupancy of the central atom bonding orbital directed to the Cl atom.

Complex	ν (MHz)		$\dfrac{e^2Qq}{h}$ (^{121}Sb) (MHz)	$\delta(Cl)$ (e)	$a_M(e)$	$\delta(M)$ (e)	$b_M(e)$
	(^{35}Cl)	(^{69}Ga)					
NaGaCl$_4$ ($\sphericalangle$ Cl—Ga—Cl = 109.5°)	16.569	2.500^a)		—0.59	0.37	+1.41	0.41
GaCl$_3$ · 4ClC$_6$H$_4$OH ($\sphericalangle$ L—Ga—Cl = 104.5°)	18.480	22.514		—0.55	0.15	+1.50	0.45
SbCl$_6^-$ ($-\Delta H^0 = 46$ kcal ×mole^{-1})	24.00		0.0	—0.51^b)	0.49	+2.04	0.49
SbCl$_5$·L ($-\Delta H^0 = 0$)	26.741		240.0	—0.46^b)	0.17	+2.11	0.54

^{a}) Calculated [276] from ^{27}Al NMR data on NaAlCl$_4$;
^{b}) zero s-hybridization of the chlorine bonding orbitals was assumed [119, 169].

between the average ^{35}Cl NQR frequency of the acceptor moiety $\bar{\nu}(^{35}$Cl) and the enthalpy of formation of the complexes in the gaseous phase ($-\Delta H_f$) (Fig. 2.12):

$$\bar{\nu}(^{35}\text{Cl}) = -0.059(-\Delta H_f) + 26.741 \tag{85}$$
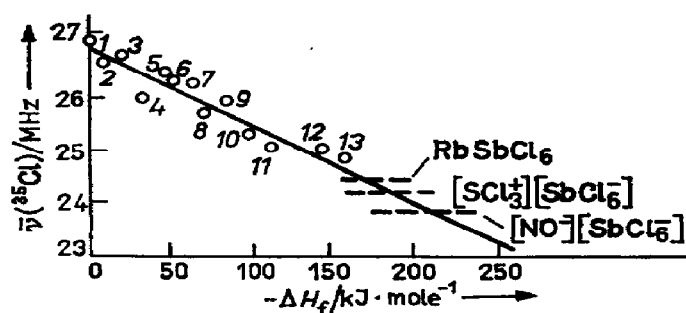
Figure 2.12   Correlation of ^{35}Cl NQR average frequencies of acceptor moiety with heats of formation in the gaseous phase for complexes of the SbCl$_5$ · L type [169], L: *1* SOCl$_2$; *2* PhCOCl; *3* PhNO$_2$; *4* PhCOCH$_3$; *5* POCl$_3$; *6* PhCN; *7* MeCN; *8* EtOH; *9* O(CH$_2$)$_4$; *10* (CH$_3$O)$_3$PO; *11* Me$_2$NCOH; *12* Py; *13* (Me$_2$N)$_3$PO.

The correlation shows that the ionicity of the Sb—Cl σ-bonds in these complexes is also enhanced with the strengthening of the donor-acceptor interactions. The authors [169] report that a linear correlation exists between $(-\Delta H_f)$ and the ^{35}Cl average frequencies of individual axial and equatorial atoms whenever the NQR spectra distinguish between these kinds of atoms. This leads them to the conclusion that both kinds of chlorine atom in SbCl$_5$ are identical with respect to accepting the electron density transfered from the ligand.

There is a tendency [169] for the ^{121}Sb QCC to decrease in value with decreasing $\bar{\nu}(^{35}$Cl), the correlation not being too distinct because of the susceptibility of the antimony coupling constants to deformations of the local C_{4v} symmetry [273] and to an insufficient number of experimental points. More extensive experimental data with complexes of similar ligands might improve the correlation.

The correlation (85) may be used [119, 169] to estimate extreme values of the ^{35}Cl NQR frequencies in complexes within the limits of complexation from $-\Delta H_f = 0$ to $-\Delta H_f = -\Delta H_f(\text{max})$. These NQR parameters are ascribed to the two hypothetical complexes, with the strongest and the weakest ligand. The former is evidently the complex with the ligand of the greatest donor ability, i.e. Cl$^-$. This means that the lower limit of the ^{35}Cl frequency is that of the [SbCl$_6$]$^-$ ion. The EFG at the antimony site of the ion is zero or very small if the latter is not highly distorted. According to the correlation (85) the value of ν_{min} (^{35}Cl) is 24.0 MHz which is really very close to $\bar{\nu}(^{35}$Cl) of RbSbCl$_6$ (24.08 MHz [119]). The spectroscopic parameters of the weakest hypothetical complex are not very different from those of the complex SbCl$_5\cdot$SOCl$_2$ [169]. They are listed in Table 2.20 together with estimates of the chemical parameters (the amount of charge transfer and the net charge located at the Cl atoms and central metal) which were also estimated for GaCl$_3\cdot$L complexes.

Estimation of the electron distribution around the Sb atom was based [169] on the simplified approach of the sp^3d^2 hybrid orbitals of ideal C_{4v} symmetry:

$$\Psi_1^\pm = \frac{1}{\sqrt{6}}\,\varphi_s \pm \frac{1}{\sqrt{2}}\,\varphi_{p_z} + \frac{1}{\sqrt{3}}\,\varphi_{d_{z^2}}$$

$$\Psi_{2,3}^\pm = \frac{1}{\sqrt{6}}\,\varphi_s \pm \frac{1}{\sqrt{2}}\,\varphi_{p_y} - \frac{1}{2}\,\varphi_{d_{x^2-y^2}} - \frac{1}{\sqrt{12}}\,\varphi_{d_{z^2}}$$

$$\Psi_{4,5}^\pm = \frac{1}{\sqrt{6}}\,\varphi_s \pm \frac{1}{\sqrt{2}}\,\varphi_{p_x} + \frac{1}{2}\,\varphi_{d_{x^2-y^2}} - \frac{1}{\sqrt{12}}\,\varphi_{d_{z^2}} \tag{86}$$

The occupation number of the Ψ_1 orbital directed to the ligand is again denoted by a_{Sb} and those of the $\Psi_2 - \Psi_5$ orbitals are denoted by b_{Sb}.

The Townes-Dailey relationship was then applied in the form

$$e^2Qq \cdot h^{-1}(\text{Sb}) = e^2Qq_p \cdot h^{-1}(\text{Sb}) \left[N_z - \frac{N_x + N_y}{2} \right] \qquad (87)$$
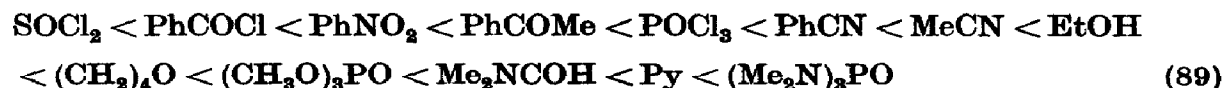
the contribution of d-orbitals into the EFG at the antimony atom being ignored. With the use of equation (86) this transforms into

$$e^2Qq \cdot h^{-1}(\text{Sb})/e^2Qq_p \cdot h^{-1}(\text{Sb}) \left[1 + \varepsilon\delta_{\text{Sb}} \right] = (b_{\text{Sb}} - a_{\text{Sb}})/2 \qquad (88)$$

Here $(\text{Sb}) = 0.15$ and $\dfrac{e^2Qq_p^{(121\text{Sb})}}{h} = 980 \text{ MHz}$

Comparison of the electronic characteristics estimated for $GaCl_3 \cdot L$ and $SbCl_5 \cdot L$ could lead to the conclusion that the antimony atom is a better conductor of electron density than gallium in the sense that it transfers a larger fraction of the electron density gained from the ligand to the chlorine atoms. One can see from Table 2.20 that nearly half of the density received from the ligand is accumulated on the Ga atom $(3\Delta b_{\text{Cl}}/(\Delta a_{\text{Ga}} + 3\Delta b_{\text{Ga}}) \approx 1)$, while in the $SbCl_5 \cdot L$ complexes $0.25e$ of the total amount of $0.32e$ gained by the $SbCl_5$ moiety $(\Delta\delta_{\text{Sb}})$ goes to the chlorines $(5\Delta b_{\text{Cl}} = 0.25)$ when the ligands are changed from the weakest to the strongest ones. This conclusion should however be treated with considerable caution because of the approximate level of interpreting the ^{121}Sb NQR data [119, 169].

Figure 2.12 shows the following order of increasing in the ligand donating power in the complexes $SbCl_5 \cdot L$:

$$\text{SOCl}_2 < \text{PhCOCl} < \text{PhNO}_2 < \text{PhCOMe} < \text{POCl}_3 < \text{PhCN} < \text{MeCN} < \text{EtOH}$$

$$< (\text{CH}_2)_4\text{O} < (\text{CH}_3\text{O})_3\text{PO} < \text{Me}_2\text{NCOH} < \text{Py} < (\text{Me}_2\text{N})_3\text{PO} \qquad (89)$$

This order is consistent with the NQR results reported by others [272, 424], as well as from thermochemical studies and IR spectroscopy [424].

The results (Table 2.20) show that in both types of complex, the increase in donor-acceptor interaction going from the weaker ($-\Delta H_f = 0$) to the strongest complexes ($-\Delta H_f$ max) is accompanied by an increase in both the amount of charge transfer and the net negative charges on the Cl atoms of acceptor moieties.

Complexes of the type $SnCl_4 \cdot 2L$ have also been extensively studied by NQR. The studies are however complicated by *cis-trans*-isomerism in these complexes. In this connection the spectroscopic splitting becomes important because it is related directly to the configuration of the complex.

In *trans*-complexes all four halogen atoms are chemically equivalent. Spectroscopic splitting in these isomers should therefore arise from crystallographic nonequivalence of halogen atom positions in the absence of steric or other specific interactions. In the *cis*-isomers, the axial and equatorial halogen atoms have different electron densities [118] and hence are chemically inequivalent

which gives rise to considerable splitting in the NQR spectra. The equatorial chlorine atoms show the higher frequencies as a rule (i.e., they are more covalently bonded to Sn) than the axial chlorines [279] which is in agreement with the X-ray data where available [280 — 282].

The NQR experiments undoubtedly reflect isomerism in the complexes, the extent of splitting distinguishing between the *cis*- and *trans*-isomers. Thus, the NQR ^{35}Cl spectra of structurally studied *cis*-isomers [120, 280 — 282] show considerably larger splittings than the spectra of complexes possessing a *trans*-configuration according to X-ray and vibrational data ([118, 121] and refs. cited therein; Table 2.21).

TABLE 2.21

^{35}Cl NQR frequencies ν (MHz) of several $SnCl_4 \cdot 2L$ isomers at 77 K

Complex	ν (MHz)	Assignment	Ref.
cis-$SnCl_4 \cdot 2CH_3CN$	19.192; 19.580 19.825; 20.625	axial equatorial	278
cis-$SnCl_4 \cdot 2SeOCl_2$	16.917 19.678	axial equatorial	424
cis-$SnCl_4 \cdot 2(CH_3)_2SO$	16.93; 17.17 17.98; 18.74	axial equatorial	119, 278
cis-$SnCl_4 \cdot 2POCl_3$	21.146 (2) 19.035; 19.807	axial equatorial	118, 268 269
trans-$SnCl_4 \cdot 2C_5H_5N$	17.644; 17.760		119
trans-$SnCl_4 \cdot 2(C_2H_5)_2O$	19.438; 19.473		118, 268
trans-$SnCl_4 \cdot 2CH_3O(CH_2)_2OCH_3$	19.620		118

The splittings in *trans*-isomers however may be enhanced by specific inter- or intramolecular interactions. If such interactions affect the NQR spectra of *trans*-isomers, the increased splittings will mask their spectroscopic difference from the *cis*-isomers [270]. This often happens with bulky ligands and additional analysis or employment of other methods are necessary to obtain unambiguous information on the configuration of complexes. Sometimes the study of the temperature dependences of the resonance frequencies appear to be useful for the assignment of lines to equatorial or axial atoms, i.e. for the correct determination of the configuration of the complex [277, 278]. Temperature coefficients of NQR frequencies are determined by the amplitude of thermal motion of fragments containing quadrupole atoms and should therefore be different for axial and equatorial chlorines (Fig. 2.13).

Specific interactions may however also interfere here. The difference in temperature behaviour due to positioning of the atoms may then be indistinguishable from that induced by specific interactions [273]. In general, caution is necessary on interpreting NQR spectra of isomers [5, 272] since the relative importance of specific interactions may vary widely from complex to complex.

Halogen average frequency shifts due to complexation and spectroscopic splittings in *cis*-isomers are not independent of each other. The magnitude of the latter decreases as the ligand donating power increases [279]. It vanishes in the limiting case of $L = Cl^-$. This means that the splitting may serve as a supporting criterion for the donor basicity of the ligands.
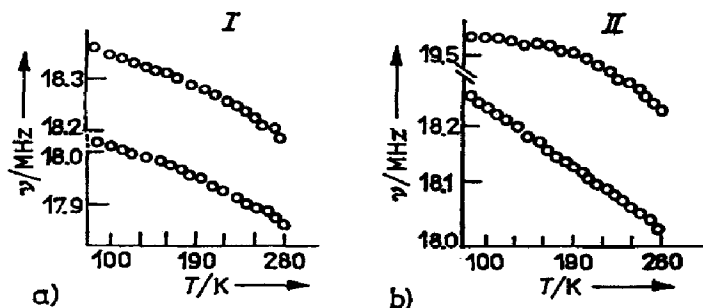
Figure 2.13 Temperature dependence of the ^{35}Cl NQR frequencies in two complexes of the $SnCl_4 \cdot 2L$ type:

I *trans*-$SnCl_4 \cdot [(C_2H_5)_2P(O)(SC_2H_5)]_2$;
II *cis*-$SnCl_4 \cdot [(n\text{-}C_4H_9O)_2P(O)SCH_3]_2$.

In the complexes $GaCl_3 \cdot L$, $SbCl_5 \cdot L$ and $SnCl_4 \cdot 2L$, the shift in the lower frequency halogen resonance increases with increased strength of the donor-acceptor interaction. The order of ligands in *cis*-$SnCl_4 \cdot 2L$ is [118, 270]:

$$EtOH > POCl_3 > MeOCH_2Cl > PhNO_2 > PhOCH_2Cl \tag{90}$$

The use of the reciprocal of the splitting, $(1/\overline{\delta\nu})$ gives nearly the same order of ligands [279]

$$POCl_3 \sim MeOCH_2Cl > PhNO_2 > EtOH > PhOCH_2Cl \tag{91}$$

the change of the position of EtOH perhaps being due to hydrogen bonds OH···Cl wich enhance the spectroscopic splitting. On the whole the average frequency shift of the chlorine atoms is more reliable than the splitting for distinguishing the ligand positions and comparing their donating power since it is relatively less sensitive towards steric and other specific effects [270]. On the contrary the splitting is very sensitive to distortion of valence angles and bond lengths requiring special consideration in each particular case.

The ^{35}Cl NQR and ^{119}Sn Mössbauer spectroscopy data for $SnCl_4 \cdot 2L$ were analyzed to compare their chemical characteristics with $GaCl_3 \cdot L$ complexes

[119]. The similar nature of donor-acceptor interaction in all three types of complexes, namely $GaCl_3 \cdot L$, $SbCl_5 \cdot L$ and $SnCl_4 \cdot 2L$, enables one to expect a linear correlation between the average ^{35}Cl NQR frequency in the $SnCl_4 \cdot 2L$ complexes and the enthalpy of their formation in the gaseous phase ($-\Delta H_f$). Such a correlation has indeed been established for the *trans*-isomers

$$\bar{\nu} = -0.0592(-\Delta H_f) + 20.290 \quad (15 \text{ points}; r = 0.975) \tag{92}$$

This provides evidence that the ionicity of the Sn—Cl bonds increases when the donor-acceptor interactions become stronger.

In *cis*-isomers, with the enthalpy values available the average ^{35}Cl frequencies of the atoms trans to each other (i.e. making a linear Cl—Sn—Cl fragment) also appeared to follow the correlation (92). Thus the general correlation valid for the linear Cl—Sn—Cl fragments in both *cis*- and *trans*-isomers of $SnCl_4 \cdot 2L$ is given [119] as follows

$$\bar{\nu}(Cl-Sn-Cl) = -0.06(-\Delta H_f) + 20.304 \quad (20 \text{ points}; r = 0.969) \tag{93}$$

The dependence of the average frequencies of the chlorines at *trans*-position to the ligands (making a Cl—Sn—L fragment) on the values of $-\Delta H_f$ is found [119] to be

$$\bar{\nu}(Cl-Sn-L) = -0.081(-\Delta H_f) + 21.95 \tag{94}$$

Both correlations (93) and (94) are given in Figure 2.14. The diagram corresponding to Eqn. (94) includes the frequencies of the eight complexes *cis*-$SnCl_4 \cdot 2L$ with unknown values of $-\Delta H_f$, the ^{35}Cl frequencies assigned to the Cl—Sn—Cl fragments being suggested to follow the dependence (93).

Given that the donor strength of ligands in both *cis*- and *trans*-$SnCl_4 \cdot 2L$ complexes does not exceed that of Cl^- ion, the average ^{35}Cl frequency in the anion $[SnCl_6]^{2-}$ of Rb_2SnCl_6 ($\bar{\nu} = 15.63$ MHz) was taken as the lower limit of both, $\bar{\nu}(Cl-Sn-Cl)$ and $\bar{\nu}(Cl-Sn-L)$. This gave a value of $-\Delta H_f = 78$ kcal/mole (Fig. 2.14) for the complex Rb_2SnCl_6. The diagram shows that the separation between the axial and equatorial Cl atoms in the *cis*-isomers increases with a decrease in the ligand donor ability, consistent with expectation [279]. Splitting in the *cis*-isomers of complexes with relatively strong ligands becomes less significant, which complicates the assignment of complexes to *cis*- and *trans*-isomers. The unsplit NQR spectrum, like in $SnCl_4 \cdot 2py$, provides however an unambigous evidence for a *trans*-configuration.

An attempt was also made to estimate [119] the chemical characteristics of hypothetical *cis*- and *trans*-$SnCl_4 \cdot 2L$ complexes, corresponding to the extreme values of $-\Delta H_f$ ($-\Delta H_f = 0$ and $-\Delta H_f(\text{max})$). ^{119}Sn quadrupole splitting values ($\Delta = 1/2e^2Qq \cdot h^{-1}$) measured by Mössbauer spectroscopy were used together with the sp^3d^2 hybrid orbitals at the Sn atom, again ignoring contribution of the d-orbitals to the EFG at the tin site. The results do not

however look very reasonable (the isomers are not electrically neutral), so they are not cited here.

From these results, one can conclude the following: as the donating power of the ligands grows, the negative charge on the Cl atoms in the acceptor moieties increases, while the positive charge on the tin atom decreases slightly.
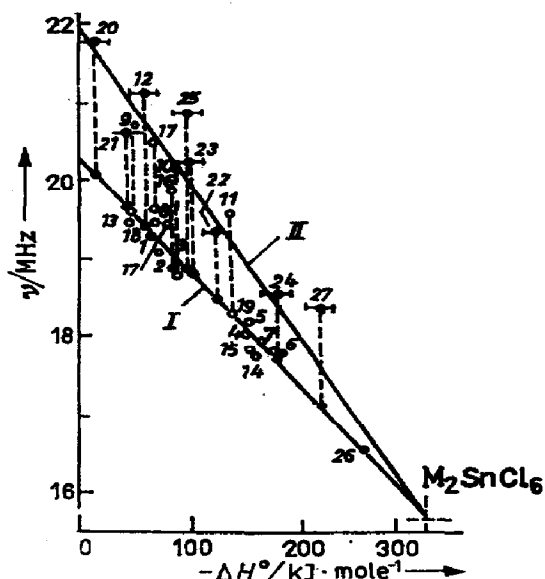

Figure 2.14 Correlation of ^{35}Cl NQR average frequencies of linear fragments Cl—Sn—Cl (*I*) and Cl—Sn—L (*II*) in the complexes *trans*-SnCl$_4$ · 2L (1—8, 13—15, 17, 18, 19, 26) and *cis*-SnCl$_4$ · 2L (9—12, 16, 17, 20—25, 27) with heats of formation in the gaseous phase [119]. L: *1* PhPOCl$_2$; *2* MePOCl$_2$; *3* (CH$_2$)$_4$O; *4* Ph$_2$OMe; *5* (Me$_2$N)$_3$PO; *6* (Me$_2$N)$_2$MePO; *7* HCONMe$_2$; *8* (Me$_2$N)POCl$_2$; *9* MeCN; *10* Me$_2$CO; *11* (C$_4$H$_9$O)$_2$(SMe)PO; *12* POCl$_3$; *13* Et$_2$O; *14* C$_5$H$_5$N; *15* Ph$_2$(NMe$_2$)PO; *16* MeCOOEt; *17* (CH$_2$)$_4$O$_2$; *18* PhCOMe; *19* Ph$_3$PO; *20* MeOCH$_2$Cl; *21* CH$_2$(OMe)$_2$; *22* (EtO)PO(SMe); *23* EtPOCl$_2$; *24* Me$_2$PO(OMe); *25* (MeO)POCl$_2$; *26* (Me$_2$N)$_3$P; *27* Me$_2$SO.
Black circles indicate the complexes *cis*-SnCl$_4$ · 2L with unknown values of —ΔH°.

A large number of octahedral tin tetrachloride complexes with bulky organophosphorus ligands has been studied [277, 283—286] by NQR, IR and γ-ray spectroscopy and the factors favouring the formation of *cis*- or *trans*-isomers were discussed. The assignment of the complexes to *cis*- or *trans*-isomers was made by analysis of the ^{35}Cl frequency temperature dependence in acceptor fragments. The *cis*-isomers are formed by ligands of relatively smaller size, causing no steric hindrance [277, 283]. If the ligands are of similar size, those of higher donor ability prefer to be located at *trans*-positions with respect to each other. However the same ligands may form different isomers in solids and in solution as reported for SnCl$_4$·2(C$_2$H$_5$O) [118]. The observation was

also made [119] that freshly prepared $SnCl_4 \cdot 2(CH_2)_4O_2$ has a *cis*-configuration which spontaneously changes into a *trans*-form. This is consistent with the conclusions [119, 277, 283] that relatively weaker donors preferably form *cis*-complexes. The latter might, however, be sterically hindered which favours rearrangement of the complex a *trans*-form.

In complexes with quadrupole atoms in the ligand moiety, the NQR registers a shift of its frequency consistent with the transmission of electron density in the direction of the donor centre. In the complex $SbCl_5 \cdot C_6H_5COCl$ an increase in the ^{35}Cl frequency of the coordinated benzoyl chloride was observed with respect to the frequency in the free molecule [169]. This corresponded to the transfer of $0.077e$ from this Cl atom to the carbon atom. The electron density is probably shifted back to the oxygen atom to partly compensate the loss due to the charge transfer to the acceptor molecule.

Ligand chlorine atoms in tin tetrachloride complexes with phosphorus derivatives [277, 284] also showed considerably higher frequency shifts indicative of the P—Cl bond ionicity decreasing on complexation. In *trans*-isomers the ionicity appeared to fall almost linearly with the ionicity of the Sn—Cl bond in the acceptor fragment. The strengths of the complexes with various ligands were found [277, 284] to decrease in the order:

$$\rangle P: \; > \; \rangle P{=}S \; \approx \; \rangle P{=}O$$
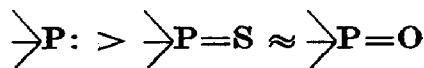
The change due to complex formation of the electron distribution in the ligands $(Me_2N)_nR_{3-n}P(O)$, $(Me_2N)_nR_{3-n}P(S)$ (R = OMe, Ph, EtCl) and $Me_2NRC(O)$ (R = H, Me, Ph, Cl, CH_2, NMe_2) has also been studied using ^{14}N, ^{35}Cl NQR, IR and γ-ray spectroscopy [277, 286]. According to the conclusions made the complexation influences mostly the N—P (N—C) σ-bonds, the occupancy of the corresponding nitrogen orbitals being decreased. The occupancy of the nitrogen orbital of lone electron pair also decreases as a result of complexation. It points out that in the ligands the N—P (N—C) multiple bond character increases due to complex formation.

Summarizing one can conclude that the NQR gives a useful information concerning these "classical" EDA complexes:

(i) Evidence is provided for complex formation, also yielding supporting data on the composition of the product. The NQR spectrum of each complex differs distinctly from the spectra of the interacting components. If one studies a mixture of the components, taken in an arbitrary mole ratio (for example, 1:1 when the complex has a stoichiometry 1:2) the NQR spectrum will contain, in addition to the lines of the complex, the lines of pure starting components;

(ii) NQR gives structural information including that concerning isomerism of the complex molecules;

(iii) the charge distribution, as well as the amount of charge transfer, can also be estimated from NQR spectra. The results are reliable in elucidating relative trends in redistribution of the electron density over the interacting components (donor and/or acceptor fragments) in series of similar complexes;

(iv) NQR spectra permit comparison of the donating power of ligands and of the strengths of the complexes produced.

One must however keep in mind that NQR, like any other method, is not free of limitations. Most of the conclusions based on NQR are nevertheless consistent with those made on the basis of other spectroscopic or structural methods.

G. MOLECULAR ADDUCTS OF METAL HALIDES OTHER THAN $GaCl_3$, $SnCl_4$ AND $SbCl_5$

We shall now discuss NQR data on complexes of similar composition to those discussed in the preceding section but with different metal halides. They have much in common with adducts of $GaCl_3$, $SnCl_4$ and $SbCl_5$, as far as crystallochemistry and donor—acceptor interactions are concerned.One can however expect that some individual features may appear in their NQR spectra as a consequence of the substitution of the central atom.

(i) Complexes of the type $M^{III}X_3 \cdot L$ ($M^{III} = B, Al, In, As, Sb, Bi$)

Metal(III) halides behave as acceptors in a large number of complexes, due to the presence of low-lying vacant orbitals in their electronic structure.

We start with a short characterization of boron trihalide complexes. Considerable ^{35}Cl NQR data are available for BCl_3 complexes with nitriles, ethers, thioethers, arsines, amines, phosphines, pyridines and phosphorus oxychloride ([274] and refs. cited therein). In more recent papers, halogen NQR data on boron trihalide complexes with phosphorus trihalides [287] and trimethylamine (TMA) [288] can be found. The ^{11}B NQR spectra are much less extensive, although they are available for uncomplexed boron trihalides (QCC ≈ 2.5 MHz [288, 292, 294]).

Free BX_3 molecules are known to have a triangular planar geometry and do not show any tendency for polymerization. The ^{11}B QCC values decrease in the series [13; 102]

$$BF_3 > BCl_3 > BBr_3 > BI_3 \tag{95}$$

and the B—X ionic bond character decreases in the same order. This is accounted for by the parallel increase in double bonding between the halogen p_π electrons and boron vacant p_z orbitals [13, 102]. The planar configuration of the molecules favours formation of the B=X double bond which is reflected in large asymmetry parameters η at the halogen site (Table 2.22). According

TABLE 2.22

^{35}Cl, ^{81}Br and ^{127}I NQR spectra of several boron trihalide complexes at 77 K (relative intensities of lines are parenthesized; tma = trimethylamine)

Compound	Isotope	ν (MHz)		$\frac{e^2Qq}{h}$ (MHz)	η (%)	Ref.
		1/2 — 3/2	3/2 — 5/2			
BCl$_3$	^{35}Cl	21.582		41.208	54.0	292
BCl$_3$·tma	^{35}Cl	21.532		43.064	0^b)	293
		21.779(2)		43.556		
BBr$_3$	^{81}Br	146.43		283.45	45.0	294
BBr$_3$·tma	^{81}Br	144.28		288.56	0^b)	288
		147.20(2)		294.40		
PBr$_3$	^{81}Br	184.257				423
(at 83K)		182.636				
BBr$_3$·PBr$_3$	^{81}Br^a)	151.90		306.5(BBr$_3$)	0^b)	
		153.92(2)		(average)		
	^{81}Br^a)	216.64		432.6(PBr$_3$)	0^b)	287
		216.24(2)		(average)		
PI$_3$	^{127}I	230.46	457.9	1527.9	7.1	287
		231.63	460.00	1535.1	7.4	
		233.80	463.81	1548.2	7.9	
BBr$_3$·PI$_3$	^{81}Br^a)	147.31(1)		298.98	0^b)	287
		150.59(2)		(average)		
	^{127}I	289.91(1)		1931	0^b)	
		289.61(2)		(average)		
BI$_3$	^{127}I	214.00	342.95	1186.3	45.3	288
BI$_3$·tma	^{127}I	186.65(2)	371.19(2)	1238.4	6.6	288
		190.48(1)	378.84(1)	1263.9	6.6	
BI$_3$·PBr$_3$	^{127}I	203.41(2)	401.22(2)	1340	12.7	287
		207.58(1)	399.80(1)			
	^{81}Br	216.12(2)		432.6	0^b)	
		216.80(1)		(average)		

^{a}) Recalculated from the data on ^{79}Br according to $\dfrac{Q(^{79}\text{Br})}{Q(^{81}\text{Br})} = 1.1971$;

^{b}) is assumed to be zero.

to the Townes and Dailey relationship (eqn. (42)), the increase in π-electron donation from the halogen p_x orbital [295] to the vacant p_z orbital of boron, decreases QCC at the halogen site. However use of the halogen NQR spectra to calculate ^{11}B QCC in terms of the Townes and Dailey theory [102] appeared to be unsuccessful due to neglect of overlap terms by this theory. The latter can hardly be negligible because of the short bond distances in boron compounds [13, 102].

Several specific features have been noted [274, 287, 288, 290, 291] in the NQR spectra of BX_3 complexes. Complexation of the BX_3 molecules is accompanied by unusually high frequencies for the halogen resonances (acceptor) with respect to those in parent BX_3 molecules. The other peculiarity in the $BCl_3 \cdot L$ complexes, is concerned with a relatively low sensitivity of the ^{35}Cl frequencies to the nature of donor, and hence to the amount of charge transfer (the ^{35}Cl resonances lie mostly within $21-22$ MHz in the complexes considered [274]). The acceptor properties of the BCl_3 groups are nevertheless significant as is evident from the shift of the donor ^{35}Cl to higher frequency, within the series of complexes with the same donor molecule ($POCl_3$) [292]

$$BCl_3 > SbCl_5 > FeCl_3 > SnCl_4 \tag{96}$$

The NQR experimental results and theoretical calculations show that the complexation enhances the $B-Cl$ ionic character in the BCl_3 compounds but also reduces the π-bonding character [289]. Since these effects give contributions of opposite sign to the ^{35}Cl frequency shift, this apparently explains the low sensitivity of the ^{35}Cl spectra to the nature of donor [274].

Further illustration of the characteristic features of these complexes is presented in more recent NQR data [287, 288] on several boron trihalide complexes, listed in Table 2.22 together with the spectra of parent molecules. As is seen from Table 2.22, the halogen QCC values of uncomplexed BX_3 molecules are lower than those in the complexes. The asymmetry parameters (η) which are rather high in uncomplexed BX_3 molecules, are reduced considerably in the complexes. When the triangular planar BX_3 molecule, having considerable $B-X$ double bond character and hence showing a large η value, forms a complex, it rearranges to a pyramidal configuration which is accompanied by a donation of halogen π-electrons, participating in the boron-halogen π-bonding, back to the halogen atom. As a consequence the asymmetry parameter at the halogen atom is considerably reduced in the complexes.

It is assumed [287, 288] that the $B-X$ bond is represented by resonance between $B-X$, $B^- = X^+$ and B^+X^-. This leads one to the relationship

$$v_p = e^2Qq/e^2Qq_p = (1-s)(1-i) - \frac{f}{2}\{1 - (1-2s)\varepsilon\} \tag{97}$$

where s is the partial s character of the $B-X$ bond (assumed to be 0.15), ε is the correction for the increase in EFG due to the positive charge at the halogen atom (is set 0.14, 0.13 and 0.12 for Cl, Br and I, respectively), i is the ionic character.

Relating the $B-X$ double bond character f to the η value as

$$\eta = 3f(1 + \varepsilon)/2v_p \tag{98}$$

gives chemical parameters for the $B-X$ bonds which are listed in Table 2.23.

One can see from this estimation that complexation generally increases the halogen QCC values, the change being composed of two contributions of opposite sign: the increase in σ-bond ionic character and the decrease in π-bond character. The latter factor is evidently responsible for the net increase in the QCC values upon complex formation.

TABLE 2.23

The nature of the B—X bond in BX_3 molecules and their complexes with trimethylamine (tma) ([288] and refs. therein)

Compound	$U_p(X) = \dfrac{e^2Qq}{e^2Qq_p}$	Ionic character i (%)	Double bond character f (%)
BCl_3	0.376	50	12
$BCl_3 \cdot tma$	0.395	54	0
BBr_3	0.441	42	12
$BBr_3 \cdot tma$	0.455	47	0
BI_3	0.517	32	14
$BI_3 \cdot tma$	0.544	35	2

The ionic character of the B—X bonds in the complexes, although it does not change very significantly with respect to the parent molecules, decreases consistent with the electronegativity values (chlorine > bromine > iodine). The net change in QCC due to complexation is evidently dominated by back donation of π-electron density, highly characteristic for BX_3 complexes [274, 289, 290].

The $^{10,11}B$ NQR data in the complexes are much less extensive since they are too low for study in zero fields [13]. Using NMR, the ^{11}B QCC in BX_3 complexes with tma is estimated [288] to be less than 500 kHz in each complex.

NQR data on $n\sigma$-complexes of other metal(III) halides, AlX_3 and InX_3, provide evidence for the similarity of the latter to complexes of the type $GaCl_3 \cdot L$ discussed above. NQR studies of the majority of the compounds were carried out in the frame of a general study to learn about the geometry, chemical bonding and relative strength of donors, assuming the mechanism of donor—acceptor interaction is similar in all these complexes. NQR data on indium trihalide molecular complexes are much less extensive than those on aluminium trihalide adducts, although some reports are available on the complexes of trimethyl derivatives of indium ([274] and refs. cited therein).

The starting AlX_3 and InX_3 compounds show a strong tendency to dimerize [302—304]. On complexation they act as acceptors of n- or π-donors. Depend-

ing on the nature of the latter they either remain dimeric in complexes or become monomeric.

Most of the NQR data are available for molecular adducts of $AlBr_3$. It forms $n\sigma$-complexes with ethers, thioethers, sulphones, ketones and amines extensively studied by NQR and reviewed in [274].

The $AlBr_3$ complexes with sulphones can be formed in two composition ratios, $AlBr_3 \cdot R_2SO_2$ and $2AlBr_3 \cdot R_2SO_2$ depending on whether one or two oxygen atoms in the sulphone group participate in the donor—acceptor interaction. A correlation was reported [296] to exist between the shift of the average ^{79}Br resonance frequency in complexes and the enthalpy of complex formation in the gaseous phase, indicating that charge transfer is responsible for the shifts to lower frequency of the $^{81,79}Br$ resonance in the complexes.

TABLE 2.24

^{81}Br NQR spectra of $AlBr_3$ complexes at room temperature (relative intensities of lines in parentheses)

Compound	ν (MHz)	$\dfrac{e^2Qq}{h}$ (MHz)	η (%)	Ref.
Al_2Br_6	79.85 br.[a])	158.1	24.8	344
(at 301 K)	92.36 t.[a])	184.6	7.3	
	93.47 t.[a])	186.6	10.6	
$AlBr_3 \cdot tma^{b})$	79.108			297
	80.47 (2)			
$AlBr_3 \cdot 2tma^{b})$	83.168 (2)			297
	84.290			
$AlBr_3 \cdot py$	79.575			
	80.565			297
	81.424			
$AlBr_3 \cdot 2py$	69.875	139.71	4.0	297
	69.955	139.69	9.8	
	79.589	159.14	3.7	
	79.667	159.17	7.8	
	81.328	162.40	9.7	
	81.331	162.57	5.9	
$AlBr_3 \cdot PhNH_2$	79.194	158.11	10.3	297
	79.899	159.58	9.0	
	84.853	169.68	3.2	
$AlBr_3 \cdot Ph_2NH$	78.497			297
	85.380			
	85.511			

[a]) br. bridging; t. terminal; [b]) tma trimethylamine.

A more recent NQR study [297] was devoted to the investigation of several AlBr$_3$ molecular complexes with amines (Table 2.24). The first NQR results have been reported on complexes of the type AlBr$_3 \cdot 2$L. The ^{81}Br NQR spectrum of AlBr$_3 \cdot$tma was interpreted as evidence for an ethane-like structure for the complex with an Al$-$N bond, similar to the AlCl$_3 \cdot$tma structure studied by X-ray diffraction ([297] and refs. cited therein). Based on NQR and Raman spectra, the authors concluded that AlBr$_3 \cdot 2$tma forms a complex of trigonal-bipyramidal configuration with three bromine atoms at equatorial sites. Complexes of two compositions, 1:1 and 1:2, have also been prepared with pyridine. Single crystals of the latter compound were studied using NQR Zeeman zero-splitting patterns [297]. The compound appeared to be ionic with the cationic species [AlBr$_2$(py)$_4$]$^+$ of roughly octahedral configuration and the anionic species [AlBr$_4$]$^-$ of distorted tetrahedral configuration.

Fairly large η values at the Br sites were measured using the Zeeman zero-splitting patterns of the AlBr$_3 \cdot$PhNH$_2$ complex (Table 2.24) and were interpreted to show that some Br atoms participated in intermolecular interactions. In general, contributions of solid-state effects to the ^{79,81}Br frequency shifts, are important in AlBr$_3$ complexes.

The ^{75}As NQR study of AlCl$_3$, GaCl$_3$ and BCl$_3$ complexes with Me$_3$As and Et$_3$As as donors [298] lead to the conclusion that AlCl$_3$ is a weaker acceptor than BCl$_3$ and GaCl$_3$ with respect to Me$_3$As. Aluminium trihalides also form $\pi\sigma$-complexes with various π-donors, and in this way they differ from the other metal halides discussed above. AlBr$_3$ forms complexes with benzene, o- and p-xylene, acting as weak π-donors [299, 300] towards dimeric Al$_2$Br$_6$ molecules. In these complexes, the frequency shift due to complex formation is usually small, so that from NQR spectra it is difficult to distinguish between the effect of charge transfer and the solid-state and/or spatial effects. Aluminium bromide retains its dimeric form on complexation, the two widely separated groups of lines observed in the NQR spectra being assigned to the bridging and terminal Br atoms of Al$_2$Br$_6$.

In stronger complexes the dimers are broken, and the lines in these complexes are distributed over a frequency interval which is less than the separation between the bridging and terminal resonances in dimeric molecules.

The strength of an aromatic donor is related to the number of methyl group substituents on the ring [274]. Durene and mesitylene are hence stronger π-donors, breaking the dimeric structure of AlBr$_3$ and forming 1:1 complexes with AlBr$_3$, while benzene, ortho- and para-xylene form dimeric AlBr$_3$ complexes [299, 300]. Consistent with this the decrease in frequency of the bromine NQR signals is more than 7% in complexes of AlBr$_3$ with durene and mesitylene and less than 1% in those with each xylene. The increase in donor ability was reported [300, 301] to follow a decrease in the ionization potential of the aromatic ligands.

If the aromatic ligand contains a heteroatom (such as oxygen or nitrogen) it

can form the complexes of $n\sigma$ and $\pi\sigma$ types. This was observed for the 2:1 AlBr$_3$ complex with benzophenone [300]. One AlBr$_3$ molecule in this complex was supposed attached to the ketonic oxygen atom via an $n\sigma$ interaction between the lone pair of this oxygen and the vacant valence orbital of the Al atom, while the other AlBr$_3$ molecule was bound to the benzene ring via an $\pi\sigma$ interaction, such that π-donation took place towards the Br atom.

The $\pi\sigma$ complexes of the type MX$_3$·Ar or MX$_3$·2Ar, where M = As, Sb, Bi; X = Br, Cl; Ar = aromatic molecule, belong to the well known class of Menshutkin complexes. Many NQR results are available for these complexes which are reviewed in [274]. Although all the atoms in the acceptor moieties of these systems are quadrupole, their NQR spectra are not simple to interpret due to varying the QCC value at the central atoms over a wide frequency range. In several AsX$_3$·Ar complexes the ^{75}As NQR frequency is decreased [305, 306] considerably with respect to pure AsX$_3$, the ^{75}As frequency shifts showing a linear correlation with the ionization potential of the aromatic molecule [307, 301].

In Menshutkin complexes of the SbX$_3$·Ar type a weak donor—acceptor interaction takes place between the SbX$_3$ and the π-electron system of the aromatic ring. The change of EFG at the antimony atom, due to complexation, is determined by a contribution of both electronic and steric effects. The former is related to the strength of the donor—acceptor interaction and involves the change in the antimony hybridization state, the variation in the Sb—X bonding parameters and the charge transfer from donor to acceptor. The steric effect considers various nonvalence interactions between the constituent parts of the molecules and depends on the spatial arrangement of the interacting components. The combined contribution of these effects, of comparable importance in weak complexes, gives, in general, rather complicated NQR spectra.

Some regularities concerning complexation have nevertheless been reported ([310, 274, 5] and refs. therein) in the systems nSbCl$_3$·Ar, where Ar is an aromatic molecule such as benzene, substituted benzene or polycyclic aromatic hydrocarbons. Although a distinct linear correlation was not observed between the antimony QCC and the ionization potential of the donor molecule in such complexes, there is a linear trend in the variation of antimony QCC and ionization potentials of chemically related aromatic donors [5, 310]: $e^2Qq/h = 350$ to $383I$ ($r = 0.61$). The antimony QCC values in the complexes were often found in a higher frequency range than in the pure SbCl$_3$. The shifts were explained by a change in the antimony hybridization state, becoming sp^3d in the complexes from sp^3 in the starting SbCl$_3$, so that the higher d-hybridization on the Sb atom was related to the greater high frequency shift of its QCC value. The p_z character of a lone pair of antimony electrons was assumed to remain nearly unaffected by the increase in the antimony d-hybridization while the occupancies of the p_x and p_y orbitals reduced considerably, [270], thus raising the ^{121,123}Sb e^2Qq/h value. The contribution of the hybridization

change to the shift in EFG at the antimony site is almost constant through complexes of the same acceptor. It means that the increase in donor ability of the aromatic molecule must be reflected in a decrease in the QCC value at the Sb atom. This trend was clearly observed as donor ionization potential decreased in a number of complexes of composition $SbCl_3 \cdot Ar$, where Ar is benzene and its derivatives ([5] and refs. therein). In the complexes of composition $2SbX_3 \cdot Ar$, the antimony QCC values were found always to exceed those in related 1:1 complexes since the amount of charge transfer per one acceptor molecule was evidently less in the former case.

As to the NQR frequencies at the halogen sites, they appeared only slightly shifted to lower frequencies upon complexation, thus confirming the small extent of charge transfer [5, 310, 274]. Based on NQR data, the aromatic donors with heteroatoms such as benzophenone were classified [310] as π-donors when interacting with $SbCl_3$. The chlorine NQR spectra of the 1:1 and 1:2 complexes with benzophenone showed no marked difference from each other, that was accounted by the interaction of $SbCl_3$ molecules with π-electrons of the ring only.

More recently [311] an attempt has been made to compute the parameters of the $SbCl_3$ molecule and its complexes with benzene and aniline on an sp-basis using the CNDO/2 approach. It was suggested that the antimony d-orbitals do not participate in chemical bonding, so that any change in the antimony QCC value upon complexation is due to charge transfer effects. The QCC values on the Sb and Cl atoms were calculated within the Townes and Dailey approximations and compared with experiment. The amount of charge transfer in $SbCl_3 \cdot C_6H_6$ was found to be $0.01e$, while $0.26e$ appeared to be in $SbCl_3 \cdot C_6H_5NH_2$, not much different from the results [312] based upon NQR measurements.

In the $SbCl_3 \cdot$ aniline complex the greatest increase in negative charge, due to complexation, occurred at the axial Cl atom trans- the ligand [311]. This observation was interpreted in terms of the formation of three-centre four-electron $N-Sb-Cl$ bonds. The $Cl_{axial}-Sb-N$ angle being close to 180°, the electrons are transmitted along this linear fragment in the direction of more electronegative atoms such as axial chlorines.

Okuda et al. [313, 314] observed a similar tendency in the electron density distribution in the naphtalene $\cdot 2SbCl_3$ and ethylbenzene $\cdot SbCl_3$ complexes.

The change in the $^{121, 123}Sb$ e^2Qq/h values in complexes of $SbCl_3$ with benzene and aniline, appeared to be in opposite directions with respect to the antimony e^2Qq/h value in the starting $SbCl_3$ compound. In the $SbCl_3 \cdot C_6H_6$, the amount of charge transfer was small [311]. Electron density is reported to be transferred from benzene to the antimony p_z orbital, leading to an increase in the antimony QCC value upon complexation. Polarization interactions (dipole—dipole, ion—dipole), important in weak complexes, are also considered [311] to increase the Sb QCC value.

In the complex $SbCl_3 \cdot C_6H_5NH_2$, formation of three-centre four-electron $Cl_{axial}-Sb-N$ bonds causes transmittance of the electron density transferred from the ligand through the antimony p_z orbital, to the *trans*-chlorine atom. This factor, in company with rearrangement of the acceptor geometry produces [311] a significant decrease in value of the $^{121,123}Sb$ e^2Qq/h in this complex with respect to the uncomplexed $SbCl_3$ component.

The nature of the donor—acceptor interaction is different in the two complexes [311]. While complex $SbCl_3 \cdot C_6H_6$ is a typical Menshutkin complex, the $SbCl_3$ complex with aniline is of the $n\sigma$-type [315, 316] consistent with a fairly large amount of charge transfer [311]. Complexes of $SbBr_3$ and $SbCl_3$ with anisole and $SbCl_3$ with phenylchloride have also been reported to be of the $n\sigma$-type [305, 317].

Ishihara has reported [555] an NQR study of several n-complexes of type $SbCl_3 \cdot 2L$ ($L = (C_6H_5)_3PO$, $C_8H_6O_2$, $C_4H_8S_2$, $C_6H_5NH_2$). Some, together with previously studied $\pi\sigma$-complexes have been investigated using the single crystal Zeeman analysis. The temperature dependence of their NQR spectra have been measured to study the effect of intermolecular interactions and the motions of constituent fragments on the EFG at the Cl and Sb atoms.

In these complexes the configuration around the Sb atom appears to be distorted pyramidal, the Sb—Cl (basal) bond opposite to the ligand being longer than the Sb—Cl (apical) bond. It was found that the angle between the Sb—Cl (apical) bond and the principal z-axis of the EFG at the Sb atom depended on the strength of the coordination bond. As the ligand coordinated more strongly to $SbCl_3$, the EFG z-axis approached the Sb—Cl (apical) bond.

While AsX_3 and SbX_3 act as acceptors of n- and π-donors, arsenic and antimony can also be donors in complexes of $AsMe_3$, $AsEt_3$ and $SbMe_3$ with trichlorides of Group III metals (Al, Ga, In) ([274] and refs. cited therein). In the $GaCl_3$ complexes of Me_3As and Et_3As the donor power of the arsenic derivatives is nearly as high as that of Cl^- [318].

Earlier NQR data on $BiCl_3$ complexes with several ligands (acetone, acetonitrile, anisole, chloropyridines, etc.) were briefly reviewed in [274]. The spectra of these complexes have been analyzed and compared with the NQR spectrum of pure $BiCl_3$ discussed in detail in the preceding chapter. Conclusions have been drawn on the importance of spectroscopic shifts produced by the geometric rearrangement of the $BiCl_3$ molecule due to complexation. It was difficult to obtain definite information about charge transfer in these complexes. In complexes with various chloropyridines, $BiCl_3$ was found [291] to be an acceptor of the strength comparable to $SnCl_4$.

More recent data on $BiCl_3$ n- and π-complexes with a number of ligands, are listed in Table 2.25. Unfortunately, no X-ray data are available on their geometry. It has been [319, 320] supposed from the ^{35}Cl spectroscopic patterns, that the crystalline structure of pure $BiCl_3$ does not change too radically when forming complexes. Thus, the ^{35}Cl NQR spectra of complexes contain, as in

TABLE 2.25

NQR data on complexes of the type $BiCl_3 \cdot L$ and $2BiCl_3 \cdot L$ at 77 K (relative intensities of lines in parentheses)

Compound	^{35}Cl ν (MHz)	^{209}Bi (MHz) $e^2Qq \cdot h^{-1}$	η (%)	Ref.
$BiCl_3$	19.54 15.82 (2)	325.5	58.5	319
$CH_3CN \cdot BiCl_3$		372.0	25.7	
		372.8	30.1	319
		373.3	21.4	
$CH_3CN \cdot 2BiCl_3$	17.67; 14.34 (2)	380.2	30.5	309
	19.72; 15.40 (2)	240.3	78.0	
$ClCH_2CN \cdot BiCl_3$	18.57; 15.68 (2)	432.1	17.0	319
$CH_3CH_2CN \cdot BiCl_3$	17.74; 14.89 (2)	378.1	64.6	319
$C_6H_5CN \cdot BiCl_3$	18.503; 16.83; 16.64	420.0	19.3	319
	18.03; 15.50; 15.36	389.1	18.0	
$C_6H_5CN \cdot 2BiCl_3$	17.53; 14.66 (2)	410.8	23.0	319
	20.08; 16.12; 15.83	307.1	79.0	
$p\text{-}BrC_6H_4CN \cdot BiCl_3$	20.21; 14.75 (2)	445.4	65.0	319
	19.92; 15.63 (2)	440.1	61.0	
$NCC_6H_4CN \cdot 2BiCl_3$	18.70; 16.79 (2)	404.7	47.5	319
	16.93; 14.90; 14.34	331.1	10.2	
$CH_3COC_6H_5 \cdot BiCl_3$	16.69; 14.72; 14.48	392.8	58.0	319
$C_6H_6 \cdot BiCl_3$	19.20; 17.15 16.94; 19.47 16.74; 16.60	417.1	36.4	320
$CH_3C_6H_5 \cdot BiCl_3$	18.51; 17.74; 16.87	383.7	35.5	320
$1,2\text{-}(CH_3)_2C_6H_4 \cdot BiCl_3$	19.28; 15.28 (2)	390.5	13.7	320
		356.8	39.5	
$1,4\text{-}(CH_3)_2C_6H_4 \cdot BiCl_3$	17.82; 15.98; 15.84	400.1	33.5	320
		393.84	37.5	
$1,3,5\text{-}(CH_3)_3C_6H_3 \cdot BiCl_3$	19.37; 18.78; 18.50 19.10; 17.39; 17.06 19.01; 17.24; 16.94; 15.53; 15.12	432.7 372.5	26.0 6.0	320
$2,3,5,6\text{-}(CH_3)_4C_6H_4 \cdot BiCl_3$	18.49; 15.54 (2)	359.2	44.0	320
$GaCl_3 \cdot BiCl_3$	21.14; 16.17 (2)	628.47	24.5	321

the initial $BiCl_3$ spectrum, two lower frequency lines sometimes at frequencies coincident with one another. These have been assigned to Cl atoms which have a higher coordination number due to formation of secondary bonds. The higher ^{35}Cl frequency singlet, assigned in pure $BiCl_3$ to a relatively short $Bi-Cl$

bond, is also present in the spectra. The frequency shifted to greatest extent due to complex formation, occurs at this very Cl atom [319].

In all the 1:1 complexes (Table 2.25) an increase in the ^{209}Bi QCC value is accompanied by a reduction of η with respect to uncomplexed $BiCl_3$. According to the shift in the ^{35}Cl frequencies charge transfer occurs largely along the direction of the shortest Bi—Cl bond. This does not coincide with the direction of the q_{zz} component at the Bi site, suggesting that this noncoincidence could account for the increase in the value of the ^{209}Bi e^2Qq/h upon complexation [320].

The spectroscopic parameters of the two $BiCl_3$ groups in the 2:1 complexes differ considerably from each other, suggesting chemical inequivalence for these groups. One possible reason [319] for this is the formation of associates of the type $L \rightarrow {}_1BiCl_3 \rightarrow {}_2BiCl_3$ where $_1BiCl_3$ acts as a donor towards $_2BiCl_3$. In this case the higher ^{209}Bi QCC value is to be assigned to the $_1$Bi atom. However as alternative, versions of the ionic nature of these complexes are not excluded.

One interesting but rare example where $BiCl_3$ acts as a donor, is the complex $GaCl_3 \cdot BiCl_3$ (Table 2.25). The ^{35}Cl, ^{69}Ga and ^{209}Bi NQR spectra of this complex have been interpreted [321] in terms of the formation of a fairly strong complex with the Ga—Bi donor—acceptor bond.

(ii) Complexes of the type $M^{IV}X_4 \cdot nL$ ($M^{IV} = Te, Ti, Zr, Hf$)

These complexes though studied less than the $MX_3 \cdot L$ give an example of more complicated structural problem to examine with NQR. The dual functions of $TeCl_4$ are exhibited more clearly than those of SbX_3 or BiX_3. The central Te atom having from one hand a lone pair of electrons, and on the other, low-lying d-orbitals, permits $TeCl_4$ to show donor properties with respect to strong acceptors such as AlX_3 [225] and $GaCl_3$ [323] and acceptor properties with respect to n-donors such as ethers, ketones, sulphides, and sulphoxides ([325] and refs. cited therein). It is therefore interesting first to consider NQR results for the pure tellurium tetrahalides.
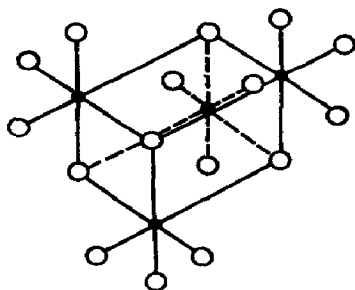

Figure 2.15 Schematic drawing of the atomic arrangement in $TeCl_4$ [327].
● Te; ○ Cl.

The [35]Cl NQR spectrum of $TeCl_4$ [322] contains 6 lines of equal intensity in agreement with X-ray data [327] and the occurrence of tetrameric units $(TeCl_3^+ \cdot Cl^-)_4$ in solid $TeCl_4$ (Fig. 2.15). The six observed resonances were assigned to the two species of $TeCl_3^+$ (Table 2.26). The signals from triply bridging

TABLE 2.26

[35]Cl and [81]Br NQR spectra of TeX_4 (X = Cl, Br) and some of their complexes (relative intensities of lines in parentheses)

Compound	T (K)	ν (MHz)	$\dfrac{e^2Qq}{h}$ (MHz)	η (%)	Assignment of lines	Ref.
$TeCl_4$	299	26.782	53.36	2.4		322
		26.947	53.87	up to 5.0		
		27.024	54.04	3.0	Cl-terminal	
		27.471	54.93	2.8		
		27.684	55.36	1.9		
		27.968	55.93	2.5		
$TeBr_4$	299	185.18	370.22	4.5		225
		187.68	373.5	up to 5.0		
		187.81			Br-terminal	
		190.91	381.74			
		195.36	390.71	1.5		
		197.34	394.63	2.7		
	293	13.539				
		12.513 (2)			Br-pyramidal	324
		12.625				
$TeCl_4 \cdot AlCl_3$	298	30.570			$[TeCl_3]^+$	225
		29.574				
$(TeCl_3^+ \cdot AlCl_4^-)$		29.420				
$TeBr_4 \cdot AlBr_3$	298	207.33			$[TeBr_3]^+$	225
		207.67				
$(TeBr_3^+ \cdot AlBr_4^-)$		208.12				
		208.90				
		212.45				
		214.37				
$TeCl_4 \cdot (C_3H_7)_2S$	77	30.66 (2)				325
		22.45				
		21.31				
$TeCl_4 \, 2(CH_3)_2SO$	77	31.47 (2)				325
		23.34				
$TeCl_4 \cdot POCl_3$	77	29.994 (2)				326
		26.754			Te—Cl	
		24.822				
		29.700			P—Cl	
		29.570 (2)				

or "pyramidal" Cl atoms were not detected, probably, because they fall in a low frequency region. Zeeman NQR effects have been analyzed [225] for TeCl$_4$ and TeBr$_4$. The zero-splitting patterns of both compounds were very much alike so TeBr$_4$ consists of tetramers (TeBr$_3^+ \cdot$ Br$^-$)$_4$ in accordance with X-ray diffraction data which show that TeBr$_4$ and TeCl$_4$ are isomorphous. Later the signals from triply bridging bromine atoms were also detected [324] (Table 2.26). One therefore sees that the potential ability for TeX$_4$ compounds to exhibit dual functions, is already reflected in their crystalline structure. On one hand, ionic [TeX$_3$]$^+$ groups are seen distinctly in tetrameric units which shows that TeX$_4$ is a potential donor of Cl$^-$ ions. On the other hand, the central Te atoms have a distorted octahedral environment in the crystal lattice, so one also expects the donor properties for TeX$_4$.

Table 2.26 contains NQR spectra for complexes illustrating the dual role played by tellurium tetrahalides. In complexes with AlCl$_3$ and AlBr$_3$ they are donors of halogen ions so that the complexes have ionic structures and are formulated [TeX$_3$]$^+ \cdot$ [AlX$_4$]$^-$. The resonances [225] are assigned to the [TeX$_3$]$^+$ species, those from the anion lying in a lower frequency region (Table 2.26).
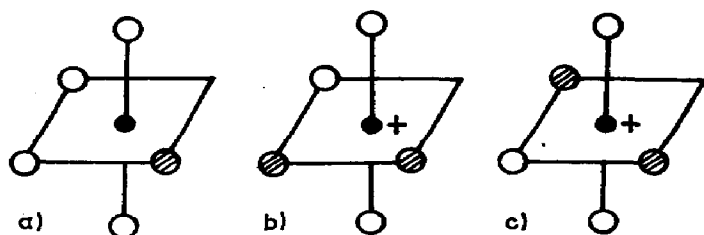
Figure 2.16   Assumed configurations of the complexes TeCl$_4 \cdot$ (C$_3$H$_7$)$_2$S (a) and [TeCl$_3 \cdot$ 2DMSO]$^+ \cdot$ Cl$^-$ (b or c) according to the data [325].

● Te ; ◉ ligand molecules ; ○ Cl.

The ^{35}Cl NQR spectrum of TeCl$_4 \cdot$ (C$_3$H$_7$)$_2$S contains three lines with intensity ratio 2:1:1. Taking into account the low conductivity of benzene solutions of this complex, the molecular structure shown in Figure 2.16a is proposed [325]. Thus, TeCl$_4$ appears here, and in the next few examples as an acceptor. As often pointed out, the axial Cl atoms give rise to a higher frequency line of double intensity. The complex TeCl$_4 \cdot$ 2DMSO gives only two resonances with intensity ratio 2:1. Unlike the constituent components, the compound is insoluble in benzene. A solution of TeCl$_4$ in DMSO shows high conductivity. The complex apparently has the ionic structure (TeCl$_3 \cdot$ 2DMSO)$^+ \cdot$ Cl$^-$ while the [TeCl$_3$]$^+$ moiety acts as an acceptor [325]. A possible cationic structure for this compound is depicted in Figure 2.16, b.

According to an NQR study [326], TeCl$_4$ also acts as an acceptor with respect to POCl$_3$, forming an octahedral complex of 1:1 composition. The high frequency line of double intensity (Table 2.26) was assigned, by analogy

with the spectrum of $TeCl_4 \cdot (C_3H_7)_2S$, to the axial chlorine atoms. The two lower frequency lines were assigned to equatorial Cl atoms, the remaining equatorial positions being occupied by a ligand molecule and a lone pair of tellurium electrons. The assignment of the higher frequency resonances to either donor or to acceptor moieties was made from a study of the temperature dependence of the ^{35}Cl NQR frequencies. The $POCl_3$ ^{35}Cl signals changed their multiplicity when the temperature was raised and vanished near room temperature due probably to hindered rotation of the PCl_3 group [326].

TABLE 2.27

^{35}Cl NQR spectra of complexes of the $TiCl_4 \cdot nL$ type $(n = 1, 2)$
([328] and refs. therein)

Compound	T (K)	ν (MHz)		
		$Cl^{(cis)}_{terminal}$	$Cl^{(trans)}_{terminal}$	$Cl_{bridging}$
$TiCl_4 \cdot MeCN$	77	7.643; 7.672	8.227	10.353; 10.389
$TiCl_4 \cdot POCl_3$	77	8.152; 7.936	7.622	10.076
	293	8.233; 8.051	7.727	9.946
$TiCl_4 \cdot MeNO_2$	77	7.585; 7.895	7.251; 7.367	9.605; 9.706; 9.752
$TiCl_4 \cdot py$	77	7.673; 7.700	7.323	10.058
$TiCl_4THF$	77	7.674; 7.764	7.998	9.814
$TiCl_4 \cdot MeCOOEt$	77	8.008	8.202	10.392
$TiCl_4 \cdot DMFA$	77	8.684	9.429	10.433
$TiCl_4 \cdot Hmpa^{a})$	77	9.573	9.218	10.756
$TiCl_4$	77	5.9802; 6.0380 6.0807; 6.1118		

Compound	T (K)	ν (MHz)		Isomer
		Cl_{axial}	$Cl_{equatorial}$	
$TiCl_4 \cdot 2MeCN$	77	8.125; 8.177	8.882; 9.060	cis-
	293	8.147; 8.238	8.980; 9.060	cis-
$TiCl_4 \cdot 2POCl_3$	77	8.141; 8.310	8.922; 9.047	cis-
$TiCl_4 \cdot 2py$	77	8.400		trans-
$TiCl_4 \cdot 2THF$	77	8.150; 8.483 8.663; 9.141		trans-
$TiCl_4 \cdot 2DMFA$	77	8.286; 8.603 8.782		trans-
$TiCl_4 \cdot 2Hmpa^{a})$	77	9.416; 9.775		trans-

a) Hmpa hexamethyltriamide of phosphoric acid.

Several more ^{35}Cl NQR $TeCl_4 \cdot nL$ spectra were reported in [226]. The 1:1 complexes with L = $FeCl_3$, $MoCl_5$, $NbCl_5$, $TaCl_5$ and $GaCl_3$ were concluded to be ionic, of the $[TeCl_3]^+ \cdot [M^xCl_{x+1}]^-$ type. The complexes $ZrCl_4 \cdot 2TeCl_4$ and $HfCl_4 \cdot 2TeCl_4$ were suggested to be molecular adducts although there is some doubt because of the weak intensities of resonances [226].

The NQR spectra of transition metal halide complexes can be interpreted self-consistently, assuming non-zero $p_\pi - d_\pi$ character in their terminal M—Cl bonds. According to X-ray results, the Ti—Cl bond distances increase and hence the covalency of Ti—Cl bonds decreases in the direction $TiCl_4$ [329] < $TiCl_4 \cdot POCl_3$ [330] < Rb_2TiCl_6 [331]. The ^{35}Cl NQR frequencies however shift higher in the same direction (Table 2.27) in contrast to what is observed in compounds of non-transition elements. Provided the chlorine p_π electrons participate in chemical bonding with the titanium vacant d-orbitals of appropriate symmetry, the increase in Ti—Cl bond length causes an increase in σ-ionic character of this bond (or increase in occupancy of the chlorine $3p_\sigma$ orbital) accompanied by a reduction of the ^{35}Cl frequency. A decrease in its $p_\pi - d_\pi$ character (or increase in occupancy of the chlorine $3p_\pi$ orbitals) is accompanied by a frequency increase. If the latter of the two competing contributions prevails one observes a net increase in the chlorine resonance frequency with an increase in bonding distance. For the same reason in bridging transition element compounds ($NbCl_5$, $TaCl_5$, etc.), where apart from the M—Cl terminal bonds, there exist much longer bridging M—Cl—M bonds whose $p_\pi - d_\pi$ character is insignificant, the lower frequency NQR lines are assigned to the terminal Cl atoms [149]. The opposite situation takes place with non-transition element bridging halides ($GaCl_3$ [346]). X-ray data available for $TiCl_4 \cdot MeCOOEt$, $TiCl_4 \cdot POCl_3$ and $TiCl_4 \cdot MeNO_2$ ([328] and refs. cited therein) show they are also dimeric with two Cl atoms bridging between two Ti atoms in a distorted octahedral environment (Fig. 2.17). Their NQR spectra (Table 2.27) contain a high frequency group of lines in the 10 MHz range which
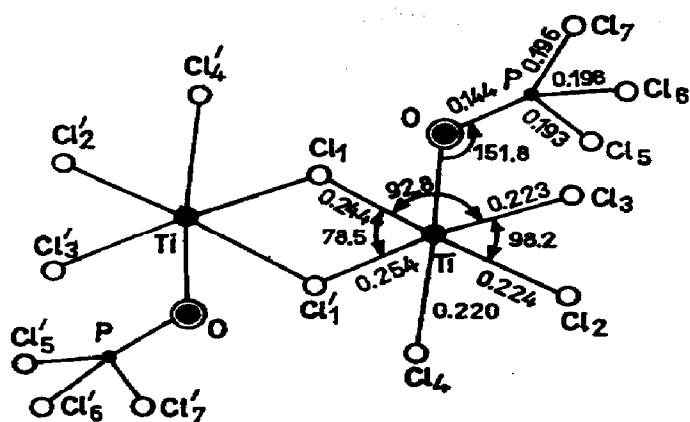

Figure 2.17 Atomic arrangement in $TiCl_4 \cdot POCl_3$ [330].

must be assigned, in accordance with the intensity ratio of the lines to bridging chlorine atoms, and low frequency multiplets which must be assigned to terminal Cl atoms. The latter have been assigned to atoms either *cis* or *trans* with respect to the ligand L, based on their multiplicity and relative intensity. The NQR patterns of the remaining 1:1 complexes, with unknown structures, are similar (Table 2.27); all are suggested to be dimeric [328].

Using the sp^3 hybrid MO orbitals of C_{3v} symmetry centered at bridging Cl atoms, and the Townes and Dailey approach (Table 1.8, eqns. (15*, 16*)) the occupancies of the bridging Cl—Ti orbitals and the net charges on Cl bridges were calculated in 1:1 complexes of known structure. The increase in donor ability of the ligands is accompanied by a decrease in the net charge on the bridging Cl atom, and hence by a decrease in occupation of the bridging Cl—Ti orbital. In other words, the bridge bonds increase in strength with increasing donor ability of the ligands. Table 2.27 also lists ^{35}Cl NQR frequencies for complexes of the type $TiCl_4 \cdot 2L$ with the same ligands as those in 1:1 complexes. X-ray data for $TiCl_4 \cdot 2POCl_3$ [332] show it has a *cis*-octahedral configuration, as does the $SnCl_4 \cdot 2POCl_3$ complex. The axial Sn—Cl bonds [279] give lower frequency signals in the NQR spectra of $SnCl_4 \cdot 2L$ complexes, being relatively less covalent than the equatorial bonds. Assuming a similar bond arrangement occurs in $TiCl_4 \cdot 2POCl_3$, the lower frequency doublet is assigned to the equatorial Cl atoms taking into account the $p_\pi - d_\pi$ contribution to the Ti—Cl bond. The NQR spectra of the remaining 1:2 $TiCl_4$ complexes in Table 2.27 were assigned [328] either to *cis*- or *trans*-isomers depending on the extent of spectroscopic splitting.

Attempts to compare the donor power of ligands in $TiCl_4 \cdot nL$ complexes, were made [328] based on their ^{35}Cl NQR frequencies. The ligand order obtained from either bridging or terminal ^{35}Cl resonances in 1:1 complexes, as well as in 1:2 complexes, differ from each other, and do not look very reasonable. They also differ from the order of the same ligands established using NQR data for $SnCl_4 \cdot 2L$ and $SbCl_5 \cdot L$ complexes. $TiCl_4 \cdot nL$ complexes therefore look less favourable for the comparative study of ligands than non-transition element adducts. Their structures have not been studied sufficiently by X-ray methods, and the relationship between NQR frequency shifts, and the charge distribution is less direct than in non-transition element halide complexes. Indeed, the NQR spectroscopic parameters for bridging halogen atoms depend on the interbond M—Cl—M angle which in the majority of complexes, is not known. The frequency shifts on terminal halogen atoms are governed by two contributions of opposite signs: the change in σ-covalent character (p_z orbital occupancy) and the change in p_π orbital occupancy. Their relative importance varies of course from complex to complex, and even from atom to atom, within the same complex, depending on its position with respect to the ligand. It is however difficult to take into account this variation at this semiquantitative level when X-ray data are not available.

Data for several more $MCl_4 \cdot nL$ complexes are listed in Table 2.28. Some $1:2$ complexes have been assigned to *cis*- or *trans*-isomers, on the basis of ^{35}Cl spectroscopic splitting in the MCl_4 moieties.

In other compounds the ^{35}Cl frequencies of the donor $POCl_3$ moiety have been measured. The shift to higher frequency of the $POCl_3$ ligand resonance was compared [334] with a number of metal chloride complexes, in addition to those listed in Table 2.28, to learn about the accepting power of various metal chlorides, in their higher oxidation states resulting in the sequence:

$$B > Sb > Al > Ga > Ta > Nb > Sn > Hf > Zr > Ti \tag{99}$$
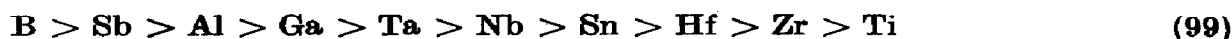
The relative Lewis acid strengths based upon NQR results for ligand moieties, agree well with those basing on other methods, such as IR spectroscopy, or

TABLE 2.28

^{35}Cl NQR spectra of complexes of the type $MCl_4 \cdot nL$ (relative intensities of lines in parentheses)

Compound	T (K)	Resonance frequencies ν (MHz)	Assignment	Ref.
$ZrCl_4 \cdot 2MeCN$ (*cis*)	77	5.056 (2); 5.395; 5.493	Zr—Cl	333
$HfCl_4 \cdot 2MeCN$ (*cis*)	77	5.757 (2); 6.043; 6.099	Zr—Cl	333
$MoCl_4 \cdot 2MeCN$ (*trans*)	77	10.789; 10.798	Mo—Cl	333
$ZrCl_4 \cdot POCl_3$	77	30.087; 30.208; 30.453	P—Cl	334
$ZrCl_4 \cdot 2POCl_3$	77	29.981; 30.067; 30.219	P—Cl	334
$HfCl_4 \cdot POCl_3$	77	30.168; 30.280; 30.552	P—Cl	334
$HfCl_4 \cdot 2POCl_3$	77	29.956; 30.124; 30.275	P—Cl	334
$HfCl_4 \cdot 3POCl_3$	77	28.622; 28.705; 28.942; 29.034; 29.939; 29.981; 30.126; 30.451	P—Cl	334
$ZrCl_4 \cdot 2POCl_3$	77	30.288 (2); 30.168 (×1)[a]; 30.054 (2); 30.024 (×6)[a]; 29.922; 29.856 (2) (×4)[a]; 29.030; 28.930; 28.680; 28.600 (2); 28.566	P—Cl; P—Cl; $POCl_3$	326

[a]) Relative intensity of doublet groups.

9*

the determination of enthalpies of complex formation in gaseous phase or in solutions.

NQR results for Group IV and V metal chlorides, the latter with metal atom valence basis $5s5p(5d)$ (Sn, Sb), possess the highest accepting power; then follow metal chlorides with valence basis M $5d6s6p$ (Hf, Ta) and finally those with $4d5s5p$ (Zr, Nb).

According to the ^{35}Cl frequency shifts of coordinated $POCl_3$ in the complexes $MCl_x \cdot nPOCl_3$ the accepting power of MCl_5 changes more strongly from metal to metal (Nb < Ta < Sb) than that of MCl_4 (Zr < Hf < Sn). In the Group IV transition metal complexes the order of increasing accepting power is the same (Ti < Zr < Hf) for both 1:1 and 1:2 complexes.

The ^{35}Cl NQR spectrum of $HfCl_4 \cdot 3POCl_3$ provides [334] evidence for formulating this complex as $HfCl_4 \cdot 2POCl_3 \cdot POCl_3$. The outer sphere $POCl_3$ molecule was suggested to come into $Cl\cdots Cl$ contact with the coordinated $POCl_3$ molecules. A very complicated ligand moiety ^{35}Cl NQR spectrum was reported [326] to be given by a compound of net composition $ZrCl_4 \cdot 2POCl_3$, prepared by dissolving $ZrCl_4$ in excess $POCl_3$. The sample probably contained a mixture of 1:1, and 1:2 $POCl_3$ complexes with an excess of $ZrCl_4 \cdot 2POCl_3$. $POCl_3$ molecules may also reside in interstitial sites of the structure (Table 2.28).

(iii) Complexes of the type $MCl_5 \cdot L$ (M = Nb, Ta)

The NQR spectra of transition metal $NbCl_5 \cdot L$ and $TaCl_5 \cdot L$ complexes are presented in Tables 2.29 and 2.30. The ^{35}Cl spectroscopic patterns of the niobium and tantalum complexes, with the same donors, bear a great resemblance in both splitting and intensity ratio, providing evidence for the close structural similarity of these compounds.

TABLE 2.29

^{181}Ta and ^{35}Cl NQR spectra of $TaCl_5 \cdot L$ complexes [335]. (The calculated values in parentheses)

Compound	T(K)	Isotope	ν (MHz)			$\dfrac{e^2Qq}{h}$ (MHz)	η (%)
			1/2—3/2	3/2—5/2	5/2—7/2		
$TaCl_5 \cdot POCl_3$	77	^{181}Ta	157.76	111.808	160.533	836.70	97.5
	293			117.424			
$TaCl_5 \cdot POCl_3$	77	^{35}Cl	7.337				
			8.069ª)				
			8.149				
			9.695				
	293	^{35}Cl	7.568				
			8.178				

TABLE 2.29 (continued)

Compound	T(K)	Iso-tope	ν (MHz)			$\dfrac{e^2Qq}{h}$ (MHz)	η (%)
			1/2—3/2	3/2—5/2	5/2—7/2		
			8.534				
			9.613				
$TaCl_5 \cdot (C_2H_5)_2O$	77	^{181}Ta	70.698	119.082	(182.041)	853.58	21.9
$TaCl_5 \cdot CH_3CN$	77	^{181}Ta	52.889	90.128	137.591	644.98	21.0
	293		53.65	99.345	150.289	702.76	14.0
	77	^{35}Cl	7.000				
			8.519				
			8.619				
			9.203				
			9.318				
	293	^{35}Cl	7.258				
			8.550				
			8.675				
			9.149				
			9.355				
$TaCl_5 \cdot C_6H_5CN$	77	^{181}Ta	51.38	99.17	149.34	697.59	9.3
	293		55.34	106.93	(161.02)	752.04	9.2
	77	^{35}Cl	6.64				
			8.87[a]				
			9.06[a]				
	293	^{35}Cl	6.88				
			8.94				
			9.08				
$TaCl_5 \cdot C_6H_5CH_2CN$	77	^{181}Ta	52.25	104.20	(156.35)	729.67	2.6
	77	^{35}Cl	6.450				
			9.000[b]				
			9.284				
$TaCl_5 \cdot CH_2{=}CHCH_2CN$	77	^{181}Ta	53.742	107.160	(160.795)	750.42	2.7
	77	^{35}Cl	6.865				
			8.650				
			8.829				
			8.999				
			9.304				
	293	^{35}Cl	7.098				
			7.676				
			8.895				
			9.020				
			9.254				

[a]) The lines of double intensity; [b]) the line of triple intensity.

TABLE 2.30

^{93}Nb and ^{35}Cl NQR spectra of NbCl$_5$ · L complexes [336]. (The calculated values parentheses)

Compound	T(K)	Iso-tope	ν (MHz)				$\dfrac{e^2Qq}{h}$ (MHz)	η (%)
			1/2—3/2	3/2—5/2	5/2—7/2	7/2—9/2		
NbCl$_5$ · POCl$_3$	77	^{93}Nb	5.772	3.958	4.685	6.768	43.13	83.1
	293		5.340	(3.863)	5.298	7.474	46.60	67.0
	77	^{35}Cl	6.654					
			7.697^a)					
			7.808					
			9.393					
	293	^{35}Cl	7.007					
			7.810					
			7.936					
			9.329					
NbCl$_5$ · (C$_2$H$_5$)$_2$O	77	^{93}Nb	(2.286)	(3.277)	5.090	6.820	41.07	21.1
	77	^{35}Cl	7.083					
			7.750					
			8.094^b)					
NbCl$_5$ · CH$_3$CN	77	^{93}Nb				4.900	(29.51)	21.0
	77	^{35}Cl	6.182					
			8.287					
			8.393					
			8.856					
			9.200					
	293	^{35}Cl	6.530					
			8.340					
			8.416					
			8.824					
			9.239					
NbCl$_5$ · C$_6$H$_5$CN	77	^{93}Nb	(1.455)	(2.758)	4.16	5.55	33.32	7.4
	293		(1.549)	(2.931)	4.42	5.90	35.43	7.5
	77	^{35}Cl	5.79					
			8.49^a)					
			8.68^a)					
	293	^{35}Cl	6.09					
			8.59					
			8.77					
NbCl$_5$ · C$_6$H$_5$CH$_2$CN	77	^{93}Nb	(1.470)	(2.808)	4.234	5.648	33.90	6.8
	293		(1.593)	(3.021)	4.559	6.082	36.54	7.3
	77	^{35}Cl	5.670					
			8.645^a)					
			8.748					
			9.099					

TABLE 2.30 (continued)

Compound	T(K)	Iso-tope	ν (MHz)				$\dfrac{e^2Qq}{h}$ (MHz)	η (%)
			1/2—3/2	3/2—5/2	5/2—7/2	7/2—9/2		
NbCl$_5$								
· CH$_2$=CHCH$_2$CN	77	^{93}Nb	(1.487)	(2.859)	4.307	5.745	34.48	6.3
	293		(1.610)	(3.056)	4.610	6.150	36.92	7.3
	77	^{35}Cl	6.094					
			8.293					
			8.589					
			8.720					
			9.231					
	293	^{35}Cl	6.419					
			8.324					
			8.672					
			8.764					
			9.172					

a) The lines of double intensity;
b) the line of triple intensity.

The NQR spectrum of NbCl$_5$ · POCl$_3$ agrees with X-ray data [337] on the complex: two Cl atoms lie in crystallographically equivalent axial positions, giving rise to a resonance of double intensity (Table 2.30).

A partial transfer of electron density from the chlorine p_π orbitals to the central metal vacant d orbitals of symmetry t_{2g} (d_{xy}, d_{xz}, d_{yz}) is also very important. The p_π — d_π interaction [335, 336] contributes to the anomalous temperature dependence of the ^{35}Cl NQR frequencies (Tables 2.29, 2.30) in a manner previously suggested by Brown and Kent [141]. With a temperature rise, the overlap between chlorine $3p_\pi$ orbitals and the central metal d_π orbitals, decreases, due to anharmonicity of the M—Cl bending vibrations leading to an increase in equilibrium bonding length, thus increasing the chlorine $3p_x$, $3p_y$ orbital occupancies and hence the resonance frequency. The p_π — d_π interactions were reported [336] to account for linear correlation between the lengthening of Nb—Cl bond distances, and the increase in ^{35}Cl resonance frequency (Fig. 2.18) observed in the structurally studied NbCl$_5$ and NbCl$_5$ · POCl$_3$ compounds. The temperature coefficient $\partial\nu/\partial T$ also showed a tendency to become less negative in the same direction. For Nb—Cl distances (r) shorter than 0.234 nm a linear correlation is observed between $\partial\nu/\partial T$ and r which is explained by the dominating contribution to the frequency of the rising $3p_\pi$ orbital occupancy as it increases with temperature. When the bond distance increases beyond 0.234 nm (corresponding to ^{35}Cl frequencies higher than

8.8—9.0 MHz in the Figure 2.18) the relative importance of the Bayer mechanism becomes greater. The growing importance of the alternative frequency temperature dependence mechanism causes a slower increase in the value of the temperature coefficient $\partial \nu / \partial T$ with r, making the correlation non-linear.

$NbCl_5 \cdot NCCl$ and $TaCl_5 \cdot NCCl$ have been studied [338] using ^{35}Cl NQR of the coordinated nitrile. Single peaks have been detected in both compounds, their frequencies being very similar to each other at temperatures between 77 and 300 K. At 77 K they are 41.930 MHz in niobium and 41.945 MHz in
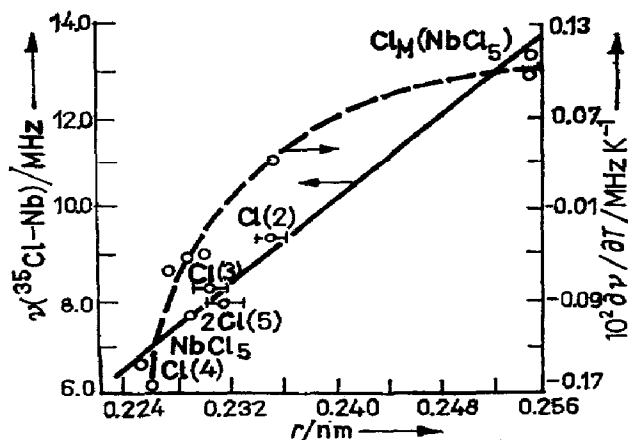
Figure 2.18 ^{35}Cl NQR frequency temperature coefficients $(\partial \nu / \partial T)$ and ^{35}Cl resonance frequencies (ν) for $NbCl_5$ and $NbCl_5 \cdot POCl_3$ vs Nb—Cl bond distance [337].

tantalum. These values are slightly greater than the ^{35}Cl frequency in free cyanogen chloride (41.7 MHz at 77 K) although the ligand is coordinated through the nitrogen atom and the chlorine atom is separated from the coordination centre. We have already mentioned above that NQR also provides evidence for electron shift density in coordinated ligands involving distant atoms, not acting as coordination centres. This shift must evidently increase with increase of accepting power of the metal chloride, providing a measure for comparison of the metal chlorides as acceptors. According to the results [338] on complexes with cyanogen chloride one can assume that the accepting power of $TaCl_5$ slightly exceeds that of $NbCl_5$ agreeing with conclusions from other NQR studies (eqn. 99). One cannot however, exclude the possibility that the shifts, of such small magnitude may originate from crystal lattice effects [338].

CHAPTER 3

COMPOUNDS WITH POLYMER FRAGMENTS IN CRYSTAL LATTICE

From the very outset, NQR developed as a method for studying the molecular crystals of organic and organoelement compounds containing halogen atom nuclei. This is easy to understand since the c.w. technique, the only one used in the past and one still practised at present, requires samples to be free of structural imperfections (see Chapter 1). Inorganic compounds are mostly coordination polymers often containing non-removable lattice defects such as local distortions, vacancies, admixtures, etc. Typically, their NQR line widths of about 70 kHz in the frequency range 50 to 100 MHz. Pulsed techniques have greatly facilitated studies of inorganic compounds, although their number still remains more limited than the number of organoelement compounds studied by NQR.

This chapter is devoted to the discussion of NQR data on solids containing polymeric fragments in crystal lattices. Such compounds (coordination crystals) represent aggregates of molecules or ions linked into chains (ribbons), layers, or three-dimensional networks. In these structures the relative contributions from inter- and intramolecular interactions vary widely and are in certain cases of comparable importance, meaning that one may only conventionally subdivide such compounds into constituent molecules. Their chemical formulae merely describe composition ratios.

NQR data on these compounds are much less extensive than on molecular compounds, though many naturally occurring minerals including those widely abundant ones have polymer structures. Many possess valuable physical properties. It is therefore very important to consider the relationship between NQR spectroscopic parameters, and crystallochemical features of these compounds.

The problems that arise in studies of coordination polymers bear mostly on the relative number and types of coordination polyhedra present in the crystal lattice, the quadrupole atoms' nearest environment, the ability to form additional donor-acceptor bond by the quadrupole atoms, lattice imperfections as indicated by NQR spectra, etc.

A. CHEMICALLY NON-EQUIVALENT BONDS IN BRIDGING DIMERIC COMPOUNDS

Because of the high sensitivity to the valence shell electron structure of quadrupole atoms, NQR is very effective for the study of compounds with chemically different bonds between the central atom and ligands of the same sort, such as bridging dimeric metal halides. Dimeric halides of transition and non-transition elements ($GaCl_3$, InI_3, $TaCl_5$, etc.) have been attractive for NQR investigators, for a long time because of the striking differences between the spectroscopic values of the terminal and bridging halogen atoms within dimeric molecules, as well as between the resonance frequencies of terminal halogens in transition and non-transition metal dimers. Both sorts of dimers have similar types of structure, with two equivalent bridging $M-hal-M$ bonds and the metal atoms located in either distorted tetrahedral (in trihalide dimers MX_3) or distorted octahedral (in pentahalide dimers MX_5) environments. Their NQR spectra contain two widely separated groups of lines, whose intensities are related to each other as the numbers of bridging and terminal halogen atoms. However while the resonances from bridging atoms, of the same halogen, in both types of dimers are relatively close to each other, the frequencies from terminal atoms are greatly different for transition and non-transition metal dimers. They appear at about half the bridging atom frequencies in TaX_5 and NbX_5 while in GaX_3 dimers they are found considerably higher than the frequencies of their bridging atoms (Tables 3.1 and 3.4).

Before discussing the reason for this difference we consider in more detail dimers of non-transition elements.

(i) Bridging dimers of non-transition elements

Bridging dimeric structures have been established by X-ray analysis for $GaCl_3$ [302], $AlBr_3$ [304], InI_3 [303] and ICl_3 [364]. Their NQR spectra are listed in Table 3.1. They are characterized by higher frequency terminal halogen resonances as compared to bridging halogen frequencies. The terminal and bridging group resonances have an intensity ratio 2:1. Asymmetry parameter values (η), whenever available, are always much higher for bridging than for terminal atoms, thus confirming X-ray data on interbond angles changing within the range 86 to 101° in the compounds discussed.

The spectroscopic patterns of other metal trihalides presented in Table 3.1 bear a great resemblance to those of the dimers whose structures are known. This provides evidence for the bridging dimeric structure of these compounds also. $SbCl_5$ seems to be dimeric at low temperatures considering its ^{35}Cl NQR spectrum, which is quite typical for bridging compounds.

For the compounds listed in Table 3.1 the spectroscopic splitting between the bridging and terminal halogen atom resonances is large enough that the assign-

ment is facile whether values of η are available or not. There are, however, aluminium heptabromide anions $[Al_2Br_7]^-$ composed according to X-ray data, ([208] and refs. cited therein) of two tetrahedra sharing one apex (Fig. 3.1) which give $^{79,81}Br$ resonances distributed more or less uniformly over a relatively

TABLE 3.1

NQR spectra of dimeric non-transition element halides (relative intensities of lines in parentheses)

Compound	Isotope	T (K)	Terminal atoms			Bridging atoms			Ref.
			1/2—3/2 ν (MHz)	e^2Qq/h (MHz)	η (%)	1/2—3/2 ν (MHz)	e^2Qq/h (MHz)	η (%)	
GaCl₃	³⁵Cl	305.2	19.084	38.12	8.9	14.667	28.30	47.3	
			20.225	40.43	3.4				
		77	19.543			15.139			346
			21.014						
GaBr₃	⁸¹Br	298	137.45			98.43			356
			137.53			98.40			
			137.72						
			137.78						
GaI₃	¹²⁷I	77	176.496	1176.53	0.9	135.719	853.92	27.3	357
			177.438	1186.91	2.8				
AlBr₃	⁸¹Br	301	92.36	184.6	7.3	79.85	158.1	24.8	344
			93.47	186.6	10.6				
		77	95.05ᵃ)			81.82ᵃ)			357
			95.61ᵃ)						
AlI₃	¹²⁷I	77	131.371	876.52	0.0	112.314	723.38	18.1	357
			131.844	879.33	0.0				
InI₃	¹²⁷I	297	173.177	1154.33	1.1	122.728	772.25	23.7	356—358
			173.633	1157.66	0.0				
ICl₃	³⁵Cl	297	33.916			13.740			192, 359
			35.680						
AuCl₃	³⁵Cl	77	33.340			23.285			195
			36.116						
SbCl₅	³⁵Cl	77	27.42			18.710 (2)			162, 170,
			27.85			18.732			360
			27.95						
			28.02						
			29.78 (2)						
			29.95 (2)						
			30.38 (2)						
			30.48 (2)						

TABLE 3.1 (continued)

Com-pound	Iso-tope	T(K)	ν (MHz)				e^2Qq/h (MHz)	η (%)	Ref.
			1/2—3/2	3/2—5/2	5/2—7/2	7/2—9/2			
GaCl₃	⁶⁹Ga	304.8	29.065				51.93	68.7	346
GaBr₃	⁶⁹Ga	77	26.494						356
GaI₃	⁶⁹Ga	77	21.586						356
AlBr₃	²⁷Al	77					13.858	72.85	123
InI₃	¹¹⁵In	77.3	36.718	26.864	37.420		327.20	65.04	356
ICl₃	¹²⁷I	77	458.19	909.37			3034.9	7.72	361, 363
SbCl₅	¹²¹Sb	77	42.90	51.10			186.70	79.3	
	¹²³Sb		38.41	30.98	47.57		237.99	79.3	360,
	¹²¹Sb		39.59	47.34			172.80	79.0	170,
	¹²³Sb		35.43	28.67	44.10		220.30	79.0	162

ᵃ) Recalculated from ⁷⁹Br frequencies according to $eQ(^{79}Br)/eQ(^{81}Br) = 1.1971$.

narrow frequency range (Table 3.2). One cannot therefore assign any specific resonance to the bridging halogen atom unless the asymmetry parameters are measured. Two exceptions are CsAl₂Br₇ having C_2 or C_S (⊥) anion symmetry, and intensity ratio 1:2:2:2 from the lowest frequency, and LiAl₂Br₇ (β) with anion symmetry C_{2v}, having the intensity ratio 2:4:1 from the lowest frequency. In both cases, the lines of unit intensity are to be assigned to bridging halogen atoms [208].

The spectroscopic patterns for related Ga₂X₇⁻ anions show a much larger splitting of frequencies (Table 3.2), the low frequency signal being assigned to a bridging halogen atom [194, 199]. The intensity ratio of the terminal-to-bridging halogen resonances was found to be 6:1 consistent with the corner-sharing tetrahedral structure of the anion ([192] and refs. cited therein). Assignment of resonances in gallium dimeric units is usually unambiguous and does not require additional experiments.
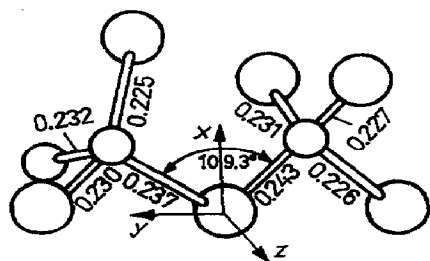
Figure 3.1 Atomic arrangement in the aluminium(III) heptabromide anion of KAl₂Br₇ and the EFG axes at the bridging Br atom [208]
○ Al; ◯ Br.

TABLE 3.2

NQR spectra (MHz) of dimeric bridging anions of type $[M_2X_7]^-$ (relative intensities of lines in parentheses; *RT* room temperature).

Compound	Isotope	T (K)	Terminal atoms			Bridging atoms			Ref.
			1/2–3/2 ν (MHz)	e²Qq/h (MHz)	η (%)	1/2–3/2 ν (MHz)	e²Qq/h (MHz)	η (%)	
Na₂Al₂Br₇	⁸¹Br	296	79.757	158.8	16.1	83.932	149.7	88.0	208
		250	80.895						
		296	80.601	160.3	18.8		9.64ᵇ	12.0ᵇ	
		250	81.511						
		296	84.308	168.4	9.1				
KAl₂Br₇	⁸¹Br	298	82.140	164.0	10.0	84.067	149.1	90.2	208
			83.386	166.7	5.0		10.4ᵇ	19.0ᵇ	
			83.456	166.7	9.1		8.7ᵇ	9.0ᵇ	
			84.089	168.1	4.3				
			85.084	169.7	13.6				
			88.116	175.9	10.4				
NH₄Al₂Br₇	⁸¹Br	296	84.365	168.3	11.9	84.723	156.3	72.0	208
			84.801	168.0	24.0				
			84.935	169.3	14.4		10.28ᵇ	4.0ᵇ	
			85.437	170.0	17.6		9.84ᵇ	13.0ᵇ	
			86.586	173.0	7.2				
			89.211	177.7	11.2				
CsAl₂Br₇	⁸¹Br	297	84.546 (2)			83.832 (1)			208
			84.546 (2)						
			85.298 (2)						
(Ne₄M)Al₂Br₇	⁸¹Br	296	⟨84.818⟩			78.226	139.6	87.8	208

TABLE 3.2 (continued)

Compound	Isotope	T (K)	Terminal atoms			Bridging atoms			Ref.
			$1/2-3/2$ [a] ν (MHz)	e^2Qq/h (MHz)	η (%)	$1/2-3/2$ ν (MHz)	e^2Qq/h (MHz)	η (%)	
LiAl₂Br₇ (polymorph α)	^{81}Br	296	80.003 81.228 83.030 85.329	Assignment of lines was not performed					208
LiAl₂Br₇ (polymorph β)	^{81}Br	333	79.061 (2) 80.820 (4)			82.992 (1)			208
NaGa₂Cl₇	^{35}Cl ^{69}Ga	77	⟨18.253⟩ ⟨19.566⟩			15.553			199
KGa₂Cl₇	^{35}Cl ^{69}Ga	77	⟨18.034⟩ ⟨20.600⟩			15.371			199
RbGa₂Cl₇	^{35}Cl ^{69}Ga	77	⟨18.089⟩ ⟨21.190⟩			15.092			199
Ga[Ga₂Cl₇]	^{35}Cl ^{69}Ga	77	⟨17.767⟩ ⟨19.500⟩			15.738			199
KGa₂Br₇	^{81}Br ^{69}Ga	RT	⟨120.99⟩ ⟨18.112⟩			99.59			194
NH₄Ga₂Br₇	^{81}Br ^{69}Ga	RT	⟨120.84⟩ ⟨18.297⟩			98.84			194
RbGa₂Br₇ (phase I)	^{81}Br ^{69}Ga	RT	⟨121.41⟩ ⟨18.82⟩			98.06			194
CsGa₂Br₇	^{81}Br ^{69}Ga	RT	⟨120.30⟩ ⟨18.456⟩			98.51			194
CsGa₂I₇	^{127}I ^{69}Ga	297	⟨156.89⟩ 15.88			160.69	767.7	66.3	194

a) ⟨ν⟩ (MHz) average NQR frequency; b) data for ^{27}Al at 284 K.

In order to make an unequivocal assignment in $[Al_2Br_7]^-$ species, Yamada [208] examined the ^{81}Br NQR Zeeman splitting patterns and ^{27}Al NMR rotation patterns of several compounds. Distinguishing between terminal and bridging halogens (Table 3.2) he obtained information concerning details of geometry and electron distribution.

The single crystal NQR Zeeman experiment allowed [208] the orientation of the bridging bromine EFG principal axes to be determined with respect to the Al—Br—Al plane (Fig. 3.1) as well as the EFG z-axes of the ^{27}Al nuclei. On the basis of the Townes and Dailey theory approximation, the effective charges and the σ-orbital populations in $[Al_2Br_7]^-$ ions were estimated. Assuming the sp^3 hybrid orbitals of C_{2v} symmetry are centred at the bridging Br atoms, the Al—Br—Al angles estimated from the η values using equation (16*) (Table 1.8) appeared to be in good agreement with those determined by the X-ray method. They are given below together with the bridging bonding orbital occupations (a_b) and the net electron charges on the bridging Br atoms (δ_b) calculated according to equation (15*).

	Al—Br—Al θ (deg)	a_b	δ_b
$NaAl_2Br_7$	107.1	1.68	−0.36
KAl_2Br_7	107.5	1.68	−0.36
$NH_4Al_2Br_7$	103.9	1.68	−0.36
$(CH_3)_4NAl_2Br_7$	107.0	1.70	−0.40

Hybrid sp^3 orbitals of C_{3v} symmetry were centered at the Al atom. Figure 3.2 shows the atomic arrangement and the occupation numbers of the bonding σ-orbitals in $[Al_2Br_7]^-$ anions. One can use equations similar to (73, 78—81) where $\theta = 106.6°$ for KAl_2Br_7, $\varepsilon(Al) = 0.25$, $\varepsilon(Br) = 0.15$, ^{27}Al $e^2Qq_p/h = -37.52$ MHz, and the total charge of the anion is equal to -1. If δ_t, δ_b and δ_M are charges on the terminal and bridging Br atoms and Al atom, respectively, then

$$-\delta_b - 6\delta_t + 2\delta_M = -1 \tag{100}$$
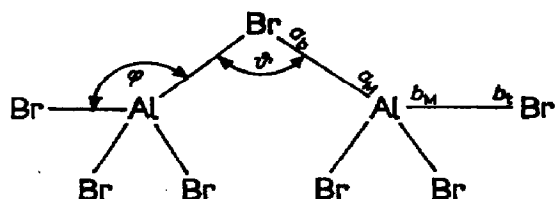
Figure 3.2 Occupation numbers of σ-bonding orbitals in $[Al_2Br_7]^-$ anions.

The following σ-bonding orbital populations and atomic charges in KAl_2Br_7 are then obtained [208]:

δ_t	δ_M	δ_b	b_t	b_M	a_M	a_b
-0.66	$+1.66$	-0.36	1.66	0.38	0.19	1.68

Various reasons have been suggested for so different frequency values for the bridging and terminal halogens in gallium and aluminium heptabromide ions (Table 3.2). According to Yamada [208], the large asymmetry parameters at the bridging Br atoms in aluminium compounds shift their NQR frequencies up, in accordance with the equations of Table 1.8, decreasing the separation between the terminal and bridging resonances.

Deeg and Weiss [199] however, suggest a weak degree of $(p-d)_\pi$ bonding is involved in the terminal $M-X$ bonding, the vacant $3d$ orbitals of aluminium being more favourable for accepting bromine p_π-electrons than the vacant $4d$ orbitals of gallium. Thus according to equation (51) (cf. (2*) in Table 1.8) the resonance frequency of the terminal Br atom is lowered as the population of the p_x and p_y orbitals decreases. Consequently a smaller value of $\bar{\nu}_t/\nu_b$ is found for Al compounds than for Ga compounds. Quantitative estimations of the π-bond character are however difficult in these compounds, since the transfer of π-electrons might affect the covalency of the σ-bonds [199].

Table 3.3 gives NQR spectra for compounds containing dimeric halide anions of general composition $[M_2X_9]^{3-}$ ($M=$ Sb, Bi; $X=$ Cl, Br, I), based on two octahedra sharing a face. In accordance with such an atomic arrangement, the intensity ratio of the terminal-to-bridging halogen resonances, must be $2:1$, which was observed in experiment (Table 3.3). The NQR spectra of many bismuth compounds, seem to be incomplete [173]. The spectra of the $Cs_3Sb_2X_9$ compounds appear quite consistent with the X-ray data available [342]. They correspond to the presence of one crystallographic type of antimony octahedron with $\eta = 0$, in the crystal lattice and two sorts of halogen atoms, terminal and bridging, in the ratio $2:1$. In the iodine compound, the NQR signals of both types of halogen, were found to have similarly high asymmetry parameters (Table 3.3). Unfortunately, no reasons for that unexpected observation were suggested [339].

The other compounds studied by NQR ($Rb_3Sb_2I_9$, $(NH_4)_3Sb_2I_9$) evidently belong to another structural type, probably to that of $(Ph_4P)_3Bi_2Br_9$ [343] in view of spectroscopic multiplicity and intensity ratio [339a].

An interesting opportunity, to compare chemical bonding in dimers containing the same central metal in various oxidation states, is presented by the NQR spectra of several tetra-alkylammonium hexahalogenogallates(II) (Table 3.3) and GaX_3 ($X=$ Cl, Br) (Table 3.1). The former compounds possess an

TABLE 3.3

NQR spectra (MHz) of dimeric anions of type $[M_2X_9]^{3-}$ and $[M_2X_6]^{2-}$

Compound	Isotope	T (K)	ν (MHz) 1/2–3/2	3/2–5/2	5/2–7/2	e^2Qq/h (MHz)	η (%)	Type of X[a]	Ref.
Cs₃Sb₂Cl₉	¹²¹Sb	77	14.644	29.268		97.6	0.0		340
	¹²³Sb		8.85	17.747	26.647	123.9	0.0		
	³⁵Cl	77	13.476					t	
Cs₃Sb₂Br₉	¹²¹Sb	77	10.3	20.62		68.7	0.8		339b,
	¹²³Sb		6.22	12.45	18.68	87.1	0.8		426
	⁸¹Br^b)	77	96.67					t	
			71.74					b	
(CH₃NH₃)₃Sb₂Br₉	⁸¹Br		101.5; 101.8					t	341
			64.78					b	
Cs₃Sb₂I₉	¹²¹Sb	77	8.63	17.26		57.5	0.0		339a
	¹²³Sb		5.24	10.481	15.72	73.3	0.0		
	¹²⁷I	77	130.65	208.67		722.1	45.8	t	
			67.80	103.29		360.5	51.4	b	
[(CH₃)₄N]₃Bi₂Cl₉	³⁵Cl	300	12.842					t	173
[(CH₃)₄N]₃Bi₂Br₉	⁸¹Br	300	91.75					t	173
			41.42					b	
(CH₃NH₃)₃Bi₂Cl₉	³⁵Cl	300	12.653; 12.710					t	173
			9.200					b	
	²⁰⁹Bi	300	13.44						
			14.08						
			18.77						
(CH₃NH₃)₃Bi₂Br₉	⁸¹Br	300	92.519					t	173
			65.139					b	

TABLE 3.3 (continued)

Compound	Isotope	T (K)	ν (MHz)			e^2Qq/h (MHz)	η(%)	Type of X[a]	Ref.
			1/2—3/2	3/2—5/2	5/2—7/2				
[(CH₃)₄N]₂Ga₂Cl₆	³⁵Cl	77	13.42					t	372
	⁶⁹Ga		23.46						
[(CH₃)₄N]₂Ga₂Br₆	⁸¹Br	77	89.94; 93.94 95.19; 96.41 100.49					t	372
	⁶⁹Ga		22.47; 23.9; 23.31						
[(C₂H₅)₄N]₂Ga₂Cl₆	³⁵Cl	77	13.25; 13.45; 13.57; 13.65; 13.87; 14.05					t	372
	⁶⁹Ga		23.27; 23.48						
[(C₂H₅)₄N]₂Ga₂Br₆	⁸¹Br	77	93.13; 94.13; 94.61					t	372
	⁶⁹Ga		22.30						

a) t terminal; b bridging;
b) recalculated from ⁷⁹Br frequencies according to $eQ(^{79}Br)/eQ(^{81}Br) = 1.1971$.

ethane-like dimeric structure [372] with Ga—Ga bonds and tetrahedral geometry about the Ga atom with oxidation number $+2$. The ^{35}Cl resonances appeared considerably lower in these compounds than the corresponding ^{35}Cl resonances in the Ga_2Cl_6 dimers where the gallium oxidation number is $+3$. The Townes and Dailey analysis of the electron distribution in these two types of dimer [372] gave the following results: ($\delta(Ga)$ = net electron charge on the Ga atom; $\delta(X)$ = negative charge on the halogen atom; a_{Ga} = occupancy of the terminal gallium orbital directed to the Cl atom; a_x = occupancy of the terminal halogen orbital directed to the Ga atom; b_{Ga} = occupancy of the Ga—Ga orbital)

	$\delta(Ga)$ (e)	$\delta(X)$ (e)	$a_{Ga}(e)$	$a_x(e)$	$b_{Ga}(e)$
$(Me_4N)_2Ga_2Cl_6$	1.05	—0.68	0.57	1.68	0.83
$(Me_4N)_2Ga_2Br_6$	0.88	—0.63	0.42	1.63	0.87
Ga_2Cl_6	1.57	—0.58	0.56	1.58	
Ga_2Br_6	1.28	—0.48	0.66	1.48	

The results are in agreement with the fact that the Ga—Cl bonds have higher ionicities in compounds with central metals in lower oxidation states. This is also consistent with X-ray data. Indeed, the terminal Ga—Cl bond distance is 0.206 nm in Ga_2Cl_6 [302] and 0.219 nm in $(Me_4N)_2Ga_2Cl_6$ [428].

(ii) Transition metal halides with dimeric units

NQR spectra of dimeric transition metal pentahalides are listed in Table 3.4. According to the X-ray data available on $NbCl_5$, $TaCl_5$, $NbBr_5$ [351], $MoCl_5$ [353] and $ReCl_5$ [352] the compounds are based on two distorted octahedra sharing an edge, so that one can expect, in their spectra, the terminal and bridging groups of halogen resonances in intensity ratio 4:1. This was observed for compounds whose spectra are complete (Table 3.4).

Let us now consider the structure-spectrum relationship for $NbCl_5$. According to the X-ray results [351] the Nb_2Cl_{10} molecules crystallize in a monoclinic lattice and occupy two sites of different symmetry in the crystal. The site of symmetry 2/m is occupied by n molecules, so that the Nb atoms lie on a two-fold symmetry axis while the two bridged Cl atoms are located in the mirror plane m, perpendicular to this axis. These molecules should therefore give rise to an NQR singlet from the two equivalent bridged Cl atoms and two signals, twice as intense as the singlet, from eight terminal Cl atoms, occupying two crystallographically non-equivalent positions. The separation between the bridging and terminal resonances must evidently be larger than those between crystallographically inequivalent terminal Cl atoms (Fig. 3.3a).

TABLE 3.4

NQR spectra of dimeric transition metal pentahalides (relative intensities of lines in parentheses; *RT* room temperature)

Halogen atoms

Compound	Isotope	T (K)	ν (MHz) 1/2—3/2 Terminal atoms	Bridging atoms	Ref.
NbCl$_5$ (I) (195°C)a)	35Cl	296	7.219; 7.365; 7.721	13.058	347, 349
NbCl$_5$ (II) (150°C)	35Cl	296	7.089 (2); 7.100 (4); 7.666 (2); 7.731 (2); 7.769 (2)	13.090 (2); 13.140	347
NbBr$_5$ (I)	81Br	300	50.53 (8); 52.11 (4)	87.96; 88.39; 89.07	149
NbBr$_5$	81Brb)	300	50.49; 50.58 (2); 50.68 (2); 51.77; 52.04; 52.16 (2); 52.49	87.96; 88.34 (2); 88.68; 89.07	151
TaCl$_5$	35Cl		7.598 (2); 7.641 (2); 7.663 (2); 8.141 (2); 8.231 (2); 8.261 (2)	13.334; 13.356; 13.347	48, 151
TaBr$_5$ (I)	81Br	77	54.18; 54.27; 54.40; 54.97	91.48	149
	81Br	300	54.98 (2); 55.30; 56.59	90.90	
TaBr$_5$ (II)	81Br	77	54.16; 54.28; 54.43; 54.48; 55.06; 55.33	91.30; 91.42; 91.57	151
	81Brb)	300	55.02 (2); 55.15 (2); 55.28 (2); 56.19 (2); 56.69 (2); 56.95 (2)	90.13; 90.32; 90.43	
WCl$_5$	35Cl	296	9.250 (4); 9.368 (4); 9.444 (4)	14.338; 14.370; 14.383	347
WCl$_5$	35Cl	297	9.254; 9.371; 9.444; 12.226	14.327; 14.362; 14.374	150
WBr$_5$	81Br	77	75.58; 76.34	96.57	150
MoCl$_5$	35Cl	77	8.938 (4)e)	14.035c)	347, 141
(unannealed)		296	9.009 (2); 9.022 (2); 9.057 (2)	14.047; 14.089	
MoCl$_5$ (I)	35Cl	77		14.471; 14.206; 14.063	348
MoCl$_5$ (II)e)	35Cl	77		12.18d); 14.27	

Compound	Isotope	T (K)	1/2—3/2	3/2—5/2	e²Qq/h	η (%)	1/2—3/2	3/2—5/2	e²Qq/h	η (%)	Ref.
ReCl₅ (I)	³⁵Cl	297	13.155; 13.202; 13.277; 13.291; 15.731; 15.891				17.318; 17.104 16.312ᵈ) 16.387				150
ReCl₅ (II) (150, 200 °C)ᵃ	³⁵Cl	296	15.609 (2); 15.782 (2); 15.684 (2); 16.174 (2); 16.320 (2); 16.420 (2)				17.165; 17.225; 17.253				347
NbI₅	¹²⁷I	77	48.69	93.44	313.4	18.0	119	188	656	47.0	150
			49.60	93.63	314.9	22.0					
TaI₅	¹²⁷I	77	70.50	140.5	468.6	5.1	122.77	215.2	732.9	33.7	
			71.43	142.2	474.3	6.0	123.61	216.8	738.3	33.6	
	¹²⁷I	RT	71.98	143.4	478.0	6.0	123.21	216.0	735.6	33.65	150
			72.69	144.6	482.6	6.0	123.3	211.6	723.2	37.0	

Central metal atoms

Compound	Isotope	T (K)	ν (MHz)				e²Qq/h (MHz)	η (%)	Ref.
			1/2—3/2	3/2—5/2	5/2—7/2	7/2—9/2			
NbCl₅ (I)	⁹³Nb	77	5.715	6.052	9.547	12.913	78.28	34.9	323, 347, 349
NbCl₅ (II)	⁹³Nb	296	5.251	6.047	9.534	12.852	77.71	30.8	347
			5.492	5.992	9.455	12.773	77.34	33.5	
NbBr₅	⁹³Nb	297			7.270	9.891	60.01	40.0	150
NbBr₅ (I)	⁹³Nb	300	5.076	4.616	7.196	9.822	59.87	43.8	151
			5.017	4.648	7.266	9.904	60.32	42.6	
TaCl₅	¹⁸¹Ta	77	190.40	239.78			1789.5	41.6	151
			185.58	241.80			1796.5	39.3	
		RT	177.6				1786	36.0	150
			183.0	241.4			1795	38.0	

TABLE 3.4 (continued)

Central metal atoms

Compound	Isotope	T (K)	ν (MHz)				e²Qq/h (MHz)	η (%)	Ref.
			1/2—3/2	3/2—5/2	5/2—7/2	7/2—9/2			
TaBr₅	¹⁸¹Ta	77	163.10	181.46	286.93		1375.13	50.3	151
			167.29	179.76	284.08		1367.09	52.7	
TaBr₅ (II)	¹⁸¹Ta	77	167.22	187.28	295.98		1418.1	49.8	
			163.05	189.00	298.27		1425.5	47.3	150
		300	156.7	190.0			1421	45.0	
			161.1				1436	46.0	
TaI₅	¹⁸¹Ta	77	84.78	110.78			822.8	39.1	
			85.36	111.28			826.6	39.3	
		RT	87.4	116.3			861	38.0	150
				117.3			870	37.0	

a) Temperature of annealing is shown in parentheses;
b) recalculated from ⁷⁹Br according to the ratio eQ (⁷⁹Br)$/eQ$ (⁸¹Br) = 1.1971;
c) vanishes after annealing;
d) lines are unassigned;
e) low-temperature phase.

The other symmetry site is occupied by $2n$ molecules, so that two bridged Cl atoms are crystallographically different. They must give rise to two lines, each of double intensity, taking into account the doubled occupation of this site compared to the site of 2/m symmetry. Four crystallographically non-equivalent positions exist in this site, and in accordance with the requirements of symmetry m, are occupied by eight terminal chlorines giving rise to four signals, each being twice as intense as the resonances from the bridging atoms (Fig. 3.3 b).
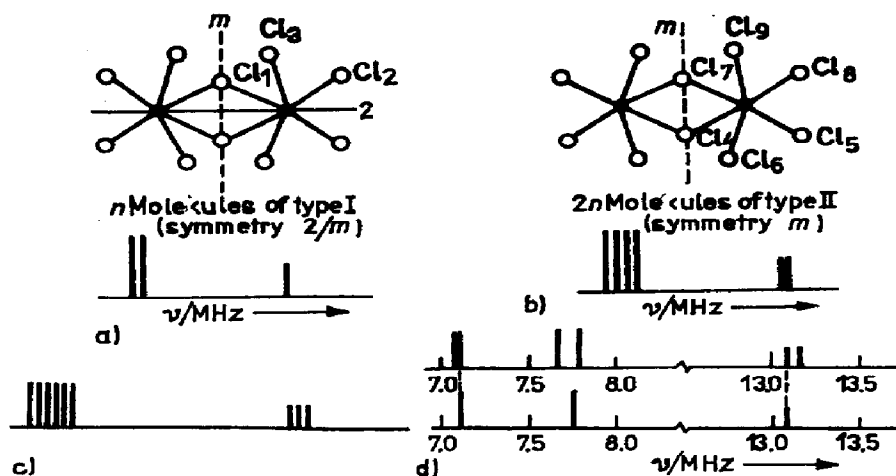
Figure 3.3 Two types of Nb_2Cl_{10} molecule in the $NbCl_5$ crystal lattice [351] and their hypothetical NQR spectra (a and b);
c) Hypothetical total ^{35}Cl spectroscopic pattern for $NbCl_5$;
d) assumed coincidence of spectroscopic lines to account for the ^{35}Cl NQR spectrum of $NbCl_5$(II) in terms of the structural data [351].

The net spectroscopic pattern should therefore consist of three equally intense lines from bridging Cl atoms separated far from a group of six lines from the terminal Cl atoms, the latter being twice as intense as the signals from the bridging Cl atoms (Fig. 3.3 c).

The same structure was established [351] for $NbBr_5$ and $TaCl_5$ which are therefore expected to give similar spectroscopic patterns. One can however see from Table 3.4 that at least two sets of NQR lines have been reported by various groups of authors for both $NbCl_5$ and $NbBr_5$ compounds, evidence for polymorphism in the dimers discussed. None of the $NbCl_5$ or $NbBr_5$ polymorphs studied have, however, given a halogen NQR spectrum exactly corresponding to that theoretically predicted. The only compounds which gave spectra completely consistent with expectation from X-ray data [351] were $TaCl_5$ and $TaBr_5$(II). A similar spectroscopic pattern was observed for an annealed $ReCl_5$ [347], although an unannealed sample of $ReCl_5$ gave a ^{35}Cl NQR spec-

trum nominally consistent (in total number of resonances) with that expected from X-ray data [352].

One could assume however that in the spectrum of $NbCl_5(II)$, two pairs of ^{35}Cl frequencies (one containing the two bridging signals from each type of dimer ($2/m$ and m) and another pair including the terminal signals from each type of dimer) appear accidentally coincident (Fig. 3.3d), the coincidence existing through the whole temperature range studied ($77 - 296$ K). With this assumption, the ^{35}Cl NQR spectrum of $NbCl_5(II)$ agrees with the monoclinic structure studied in [351]. The crystal structure of $NbCl_5(I)$ is unknown. A similar structure according to NQR (Table 3.4) can be ascribed to $TaBr_5(I)$. The halogen NQR spectra of $NbBr_5(I)$ and TaI_5 at 77 K are also similar to each other, and their structures are probably closely related.

Several different sets of spectroscopic lines have been reported for $MoCl_5$ by various authors [141, 347, 348] but no discussion of the correspondence between spectra and structure is available. As a whole it is seen, from NQR, that the polymorphism of heavy metal pentahalides is a characteristic property of these compounds. All of the polymorphs seem to have a dimeric structure, their NQR spectra showing average frequency values very close to each other. $^{79,81}Br$ NQR spectra were observed from several samples of $TaBr_5$ prepared according to the same procedure but showing different multiplicity. This varied from 5 to 10, for different samples, suggesting the existence of two polymorphs (I) and (II) for this compound (Table 3.4), some samples containing mixtures in various ratios of constituent. The $^{79,81}Br$ NQR spectra of $NbBr_5(I)$ and $TaBr_5(I)$ [149] were later reinvestigated by Edwards and McCarley [150] who reproduce the results [149]. After measuring the $^{79,81}Br$ spectrum, $TaBr_5(I)$ was annealed [150] to measure its ^{181}Ta spectrum. The latter, however, corresponds to $TaBr_5(II)$ (Table 3.4), conversion $TaBr_5(I)$ $\rightarrow TaBr_5(II)$ presumably occurring with annealing. The halogen frequencies of both polymorphs are very near to each other, so that minor variations in conditions of preparation may direct the process to formation of either of the polymorphs or of their mixtures. The NQR spectrum of $NbBr_5$, reported in [151], provides evidence for a mixture of polymorphs contained in the sample studied (Table 3.4). The ^{181}Ta NQR spectrum of $TaBr_5$ [151] is different from that of $TaBr_5(II)$ measured at our laboratory and by others [150].

We now return to comparing the spectroscopic patterns of transition and non-transition metal dimeric halides (Tables 3.1 and 3.4). The most obvious difference between them consists of the relative positions of the terminal halogen resonances which appear in transition metal pentahalides at frequencies much lower than those assigned to their bridging halogen atoms. In non-transition metal halides they were however always higher than the frequencies of bridging atoms. The other significant difference is seen in the temperature dependence of the terminal frequencies. While bridging halogen atom frequencies show a normal temperature dependence in both types of dimer, the ter-

minal halogen frequencies in transition metal compounds shift upwards with temperature rise, while in non-transition element dimers, they show a normal temperature dependence.

The explanation for the specific features observed with transition element compounds lies, of course, in the nature of the transition metal valence shells. The d^0 configuration in TaX_5 and NbX_5 dimers allows a considerable probability of electron transfer from the halogen valence p_π orbitals to the vacant d_π orbitals of the central atoms. In the framework of the Townes and Dailey theory, this means an effective lowering of the resonance frequency, due to the decrease in p_x, p_y orbital populations of the terminal halogens. The longer bridging bonds, being presumably σ-character, do not differ in their spectroscopic behaviour from those in non-transition metal dimers.

The basic differences between the spectra of the two classes of dimeric halide are reflected most clearly in an example where the central atoms possess similar electronegativity values.

	T (K)	Terminal atom		Bridging atom	
		e^2Qq/h (MHz)	η (%)	e^2Qq/h (MHz)	η (%)
InI$_3$	77	1154.3	1.1	772.25	23.7
		1157.7	0.0		
TaI$_5$	77	468.6	5.1	738.3	33.6
		474.3	6.0	735.6	33.65
				732.9	33.7

The close similarity in the QCC values observed for the bridging iodine atoms in both dimers, is not surprizing in view of the similar electronegativities of the metal atoms. Evidently the $M-I-M$ bonds have dominantly σ-bonding character, the long bridging bond distances [303, 351] and the departure of interbond angles from 180° (they fall within 86 − 111° in all the bridging dimers studied) making the formation of multiple bridging bonds unfavourable.

The positive temperature coefficient of the terminal halogen resonances in transition metal dimers (Table 3.4) is usually considered support for significant $p_\pi-d_\pi$ character in the appropriate bonds. A weakening of the π-bonds, due to thermal vibrations, leads, according to this viewpoint, to an increased population of halogen p_π orbitals with temperature and hence to an increase in resonance frequency. Since the bridging $M-X$ bonds have insignificant π-character the temperature behaviour is governed by the Bayer mechanism so that negative temperature coefficients are observed. The intensity ratio and the sign of the temperature coefficients can be used as criteria for the assignment of halogen resonances to bridging or terminal atoms in the NQR spectra of transition metal dimeric compounds [149, 150].

TABLE 3.5

Chemical bonding parameters (i ionic character, σ covalent character, π double bond character) in bridging dimers of transition metals according to ^{35}Cl, ^{79}Br, ^{127}I NQR data at 77 K [362]. (The numbering of polymorphs is the same as in Table 3.4. *RT* room temperature)

Compound	Terminal atoms					Bridging atoms				
	$\langle\nu\rangle$ (MHz)[a]	$d\nu/dT$c (kHz·K⁻¹)	i	σ	π	$\langle\nu\rangle$ (MHz)	$d\nu/dT$c (kHz·K⁻¹)	i	σ	π
NbCl₅ (I)	7.27 ● ax	0.25	0.39	0.324	0.286	13.29	−1.06	0.39	0.585	0.025
	7.40 eq	1.23		0.326	0.284					
NbCl₅ (II)	6.97 ax	0.56	0.39	0.320	0.290	13.31	−0.88	0.39	0.585	0.025
	7.44 eq	1.30		0.326	0.284					
NbBr₅	59.2 ax	6.3	0.30	0.373	0.327	107.5	−6.9	0.30	0.673	0.027
	60.0 eq	11.5		0.375	0.325					
NbI₅	(315)[b] ax	37.0	0.18	0.405	0.415	(655)[b]	−58.0	0.18	0.727	0.093
	(313)[b] eq	64.0		0.405	0.415					
TaCl₅	7.56 ax	0.32	0.43	0.313	0.257	13.55	−0.88	0.43	0.577	−0.007
	8.00 eq	0.94		0.319	0.251					
TaBr₅ (II)	65.1 ax	4.09	0.34	0.370	0.290	109.5	−6.12	0.34	0.666	−0.006
	65.8 eq	9.03		0.371	0.289					
TaI₅(*RT*)	(483)[b] ax	...	0.22	0.445	0.335	(723)[b]	...	0.22	0.756	0.025
	(478)[b] eq	...		0.443	0.337					
MoCl₅	8.79	1.33	0.30	0.378	0.322	14.19	−9.4	0.30	0.642	0.058

WCl₅	12.23 ax	~ 0	0.409	0.251					
	9.36 eq	> 0	0.371	0.289	14.48	< 0	0.34	0.635	0.025
ReCl₅ (II)	16.39 ax	−0.40	0.495	0.245					
	15.56 eq	0.89	0.484	0.256	17.33	−0.51	0.26	0.742	−0.002

0.34 0.26

ᵃ) ⟨ν⟩ average frequency values; ax and eq stand for axial and equatorial atoms, respectively;
ᵇ) the values of ¹²⁷I e^2Qq/h are given in parentheses;
ᶜ) temperature coefficient of resonance frequency.

Okubo [362] has attempted to estimate, within the framework of the Townes and Dailey theory, the chemical characteristics of metal—halogen bonds in transition metal compounds (Table 3.5). Values of σ and π have been calculated using the equation $i + \sigma + \pi = 1$; value i was estimated from the electronegativity difference of the atom-partners. The reliability of the ionic character so estimated is of course not very high, not indeed are the numerical values for σ- and π-bonding character. They may, nevertheless, be useful for comparing trends in chemical bonding among a series of related compounds.

Negligible values for the π-character were obtained, as expected, for the bridging bonds in pentahalides. The amount of π-character in the terminal Nb—Cl bond was not too different from $5.4\% \times 6$, 6 being the number of vacancies in the d_ε orbitals of the central metal [362]. The value of 5.4% per vacancy was also adopted, on the basis of ESR data [125], for $[IrCl_6]^{2-}$ anions.
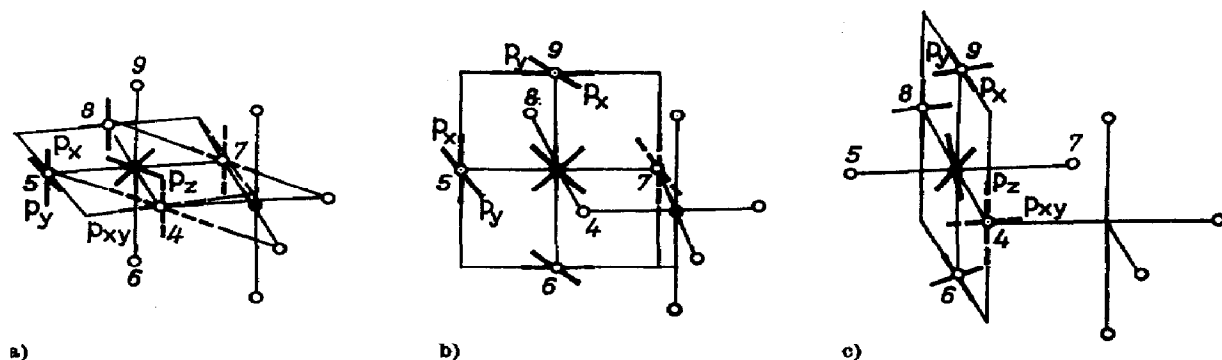
Figure 3.4 The p_π—d_π bonds in $NbCl_5$ illustrated for the octahedron $NbCl_4 \cdots Cl_2$ of Fig. 3.3 [362]. The bonding of the bridging Cl_4 and Cl_7 atoms with the Nb atom is indicated by the broken lines.

a) $d_{x^2-y^2}$-plane; b) $(d_{xz} + d_{yz})/\sqrt{2}$-plane; c) $(d_{xz} - d_{yz})/\sqrt{2}$-plane.

Assuming a close relationship between the value of the temperature coefficient ($d\nu/dT$) and the value of π-character of the corresponding bonds, Okubo assigned terminal halogen frequencies to axial (ax) and equatorial (eq) atoms (Table 3.5). According to the structural data ($Nb-Cl_{eq} = 0.225$ nm and $Nb-Cl_{ax} = 0.230$ nm [351]), and geometry of the overlapping π-orbitals (Fig. 3.4) the equatorial Nb—Cl bonds should be of higher π-character than the axial bonds. The resonances of the largest temperature coefficient $d\nu/dT$ have therefore been assigned to equatorial halogen atoms.

The increase in π-character of bridging bonds, as the halogen atom is varied from Cl to I (Table 3.5) has been attributed [362] to the approach of the central metal environment to octahedral symmetry. Octahedral symmetry is associated with the ratio of the stretching force constants for bridging and terminal bonds [350] approaching 1. The NQR spectra of several other compounds

TABLE 3.6

NQR spectra of transition metal bridging dimeric halides (relative intensities of resonances in parentheses, *RT* room temperature)

Halogen atoms

Compound	Isotope	T (K)	Terminal atoms			Bridging atoms				Ref.
			1/2—3/2 ν (MHz)	e²Qq/h (MHz)	η (%)	1/2—3/2 ν (MHz)	3/2—5/2	e²Qq/h (MHz)	η (%)	
NbOCl₃	³⁵Cl	77	8.763(2)			11.555				347
		296	8.843(2)			11.458				
WOCl₃	³⁵Cl	77	12.311(2)			13.085				
NbOBr₃	⁸¹Br	77	60.69			78.57				149
			61.05(2)							
			61.57							
		300	61.29			78.36				
			61.68							
			62.14							
MoOCl₄	³⁵Cl	77	12.567			15.817				347
			12.997							
			13.157							
		296	12.757			15.658				
			12.904							
			13.088							
Cu₂Br₂(PPh₃)₃	⁸¹Br	RT				47.52		82.38	99.7	350
						49.53		86.06	98.7	
Cu₂I₂(PPh₃)₃	¹²⁷I	RT				88.55	90.67	339.7	94.0	350
						91.76	93.56	352.3	98.0	

TABLE 3.6 (continued)

Halogen atoms

Compound	Isotope	T (K)	Terminal atoms			Bridging atoms				Ref.
			1/2—3/2 ν (MHz)	e^2Qq/h (MHz)	η (%)	1/2—3/2 ν (MHz)	3/2—5/2	e^2Qq/h (MHz)	η (%)	
$Nb_2Cl_6(SC_4H_8)_3$	^{35}Cl	298	8.547			9.047				354
			8.603							
			8.613							
			8.981							
			8.989							
$Nb_2Br_6(SC_4H_8)_3$	^{81}Br	298	59.11			67.35				354
			59.48			69.85				
			59.70							
			60.86							
$Ta_2Cl_6(SC_4H_8)_3$	^{35}Cl	298	9.230			10.321				354
			9.286			10.623				
			9.356							
$Ta_2Br_6(SC_4H_8)_3$	^{81}Br	298	62.78			71.47				354
			63.22			73.94				
			63.83							
			64.70							
$Nb_2I_6(SC_4H_8)_3$	^{127}I	298	90.61	522.7	39.3	120.7	195.2	673.8	44.3	354
			90.75	533.0	36.7	121.3	196.9	679.3	43.8	
			94.95	542.5	40.7					

Central metal atoms

Central metal atoms									
NbOCl$_3$	^{93}Nb	77	7.805	8.494	13.395	18.075	109.60	33.4	347
Cu$_2$Cl$_2$(PPh$_3$)$_3$	^{63}Cu	*RT*	29.95(3)[a]				59.08	28.9	350
			13.47(4)[a]						
Cu$_2$Br$_2$(PPh$_3$)$_3$	^{63}Cu	*RT*	28.36(3)[a]				55.82	30.7	350
			14.31(4)[a]						
Cu$_2$I$_2$(PPh$_3$)$_3$	^{63}Cu	*RT*	27.35(3)[a]				53.72	33.2	350
			15.87(4)[a]						
Nb$_2$Cl$_4$(SC$_4$H$_8$)$_3$	^{93}Nb	298	6.499	7.364	11.603	15.650	94.65	31.0	
			6.389	6.940	10.951	14.810	89.72	34.0	354
			6.888	6.821	10.712	14.563	88.49	39.0	
Nb$_2$Br$_6$(SC$_4$H$_8$)$_3$	^{93}Nb	298		8.207	12.787	17.145	103.29	22.0	354
			6.156	7.808	12.244	16.452	99.26	26.0	
Nb$_2$I$_6$(SC$_4$H$_8$)$_3$	^{93}Nb	298		8.319	12.815	17.150	103.18	18.0	354
				8.487	12.834	17.124	102.80	8.0	

a) The numbers in parentheses are the coordination numbers of the Cu atom.

having dimeric halides as basic structural units are shown in Table 3.6. Such a structure was established for $NbOCl_3$ (Fig. 3.5a, [355]) and may according to NQR data, be suggested for $WOCl_4$. $NbOBr_3$ also seems to have a bridging dimeric structure but its spectroscopy differs in detail from the structure of $NbOCl_3$. NQR and IR spectra [347] are showing that $MoOCl_4$ forms dimers bridged through two Cl atoms while the oxygens atoms are terminal (Fig. 3.5b). It is important to note that opposite signs for the frequency temperature dependences for bridging and terminal halogens have been observed for the compounds listed in Table 3.6.

a)   b)   c)
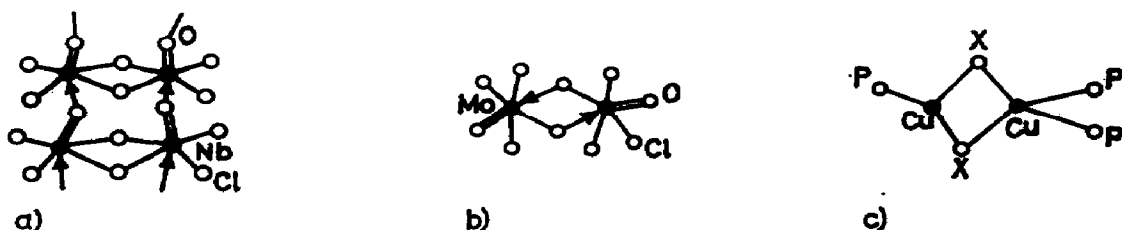
Figure 3.5   Schematic drawing of atomic arrangement in a) $NbOCl_3$; b) $MoOCl_4$; c) the $Cu_2X_2P_3$ core of $Cu_2X_2(PPh_3)_3$ (X = Cl, Br, I)

Complexes of copper(I) halides with triphenylphosphine were found ([350] and refs. cited therein) to have a binuclear structure. Two bridging halogen atoms in this complex connect with two copper atoms, one having a distorted tetrahedral coordination and the other approximately trigonal-planar (Fig. 3.5c). The decrease in ^{63}Cu QCC values from the chloride to the iodide complexes was discussed [350] with the high asymmetry parameters for the bridging Br atoms, in terms of $p_\pi - p_\pi$ halogen —copper interactions. Delocalized π-bonding occurs along the trigonal-planar coordination axis of the copper atom by mixing of copper $4p_z$ and $3d_{z^2}$ orbitals. The high η values of the EFG on the bridging halogen atoms are consistent with a $Cu_1 - X - Cu_2$ interbond angle close to 70.5° (according to eqn. (16*) (Table 1.8) $\eta \sim 1$ at $\theta = 70.5°$).

Dimeric tantalum(III) and niobium(III) halide adducts $M_2X_6(SC_4H_8)_3$ were studied by ^{35}Cl, ^{81}Br, ^{127}I and ^{93}Nb NQR [354] (Table 3.6) allowing one to compare the spectroscopic patterns of dimers with central metals in different oxidation states, $+3$ and $+5$. The diamagnetic dimers with tetrahydrothiophene are related to the metal —metal bonded cofacial octahedral structure consisting of two halogen atoms and the sulphur of one tetrahydrothiophene ligand bridging between the two metal atoms, while two halogen atoms and one tetrahydrothiophene are bound as terminal ligands to each metal [354].

As the oxidation state of the metal increases, greater covalency is expected in the metal —halogen bonds, and this is consistent with the difference in the halogen resonance frequencies in the NQR spectra of $Ta_2X_6(SC_4H_8)_3$ (I) (X = Cl, Br; Table 3.6) and Ta_2X_{10} (II) (X = Cl, Br; Table 3.4). Higher bridg-

ing halogen frequencies in (II) than in (I), agreed with the increased covalency of the metal—bridging halogen bonds in (II), which are of essentially σ-character. The decrease of the terminal halogen frequencies in (II) as the oxidation state of the metal increases is explained by a significant π-contribution to the terminal halide bonding to the metal. Indeed, the σ-covalency of the terminal bond increases as the metal is oxidized but in addition π-bonding will also increase. If the total change in π-donation exceeds the σ-donation change upon oxidation, then the resonance frequency will decrease and this is evidently the case for the terminal halogen frequencies in (I) and (II). The ^{93}Nb NQR coupling constants of the three niobium dimers increase in the order Cl < Br < I. This order is consistent with a nearly constant contribution over the series to the ^{93}Nb EFG from d-electrons involved in metal—metal bonding and decreasing contribution to the net ^{93}Nb EFG from d-electrons involved in metal—ligand bonding [354].

B. CHAIN (RIBBON) POLYMERS

(i) Infinite chains formed by metal halides

A large number of polymeric compounds containing infinite chains involve products of interaction between antimony trifluoride and alkali metal or ammonium halides.

The majority of the compounds form anionic chains composed of antimony polyhedra having various geometric configurations. The high environmental sensitivity of NQR makes it very effective for the study of these polymers (Table 3.7). The correlation between the spectroscopic parameters and configuration of antimony polyhedra enables one to identify the latter in compounds of unknown structure.

Caution should be exercized in that the central atom (Sb) QCC and η values vary within groups of similar coordination geometry, depending on variations in bond lengths, valence angles, electric charges on atoms, cation contributions, etc. Comparison of the spectroscopic parameters and available structure data leads however to definite limits in variations of NQR parameters within series of coordination groups of the same type.

Coordination polyhedra in these complexes have more or less rigid geometries, so that the spectroscopic parameters for a given coordination unit might be characteristic for a series of compounds which might contain these units.

Now let us compare the ^{121,123}Sb NQR [340] and X-ray data [367] for KSb_2F_7. Crystals of the latter contain Sb coordination polyhedra of two types ψ-octahedra (I) and trigonal ψ-bipyramids (II) (Fig. 3.6). The bridging Sb(I)—F bonds are much longer than all other bonds in the octahedra (I). For this reason the coordination polyhedra (I) are considered [367] as isolated ψ-tetrahedra (or SbF_3 groups). In agreement with structural data, the NQR spectrum of

TABLE 3.7

^{121,123}Sb NQR data for antimony trifluoride complexes with alkali metal halides at 77 K [340]

Compound		Resonance transition frequencies (MHz)					e^2Qq/h (MHz)		η (%)
		^{121}Sb		^{123}Sb			^{121}Sb	^{123}Sb	
		1/2—3/2	3/2—5/2	1/2—3/2	3/2—5/2	5/2—7/2			
SbF$_3$		80.66	160.9^a)	49.17	97.64^a)	146.59	536.7	684.2^b)	4.3^b)
KSb$_2$F$_7$	(I)	79.99	158.5	49.48	95.90	144.32	529.1	674.1^b)	8.7^b)
	(II)	83.14	165.0	51.16	100.08	150.51	550.8	702.6^b)	7.3^b)
KSbClF$_3$		79.78	158.9	49.15	95.92	144.22	530.1	674.1^b)	7.2^b)
RbSb$_2$F$_7$	(I)	79.90	157.5	49.68	95.54	143.97	526.1	672.5	9.8
	(II)	82.37	163.2	50.95	98.88	148.77	544.8	694.9	8.6
RbSb$_2$ClF$_6$	(I)	79.89	157.8	49.60	95.53	143.90	527.2	672.1	9.7
	(II)	82.40	163.2	50.95	98.84	148.80	544.8	694.7	8.7
NH$_4$Sb$_2$F$_7$	(I)	79.93	159.1	48.97	96.53	145.02	530.8	677.0	5.9
	(II)	80.94	161.3	49.63	97.65	146.67	538.0	684.9	6.3
CsSb$_2$F$_7$		79.42	154.9	50.44	93.56	141.55	518.5	661.8	13.8
CsSb$_2$ClF$_6$	(I)	79.44	155.0	50.44	93.54	141.56	518.5	660.9	14.3
	(II)	82.08			105.08				
CsSb$_4$F$_{13}$	(I)	79.47	155.1	50.44	93.55	141.53	519.0	661.6	13.8
	(II)	83.12	163.1	52.26	98.50	148.80	545.3	695.2	12.2
NaSb$_2$F$_7$		80.31	160.3	48.92	97.33	146.05	534.7	681.7	3.5
NaSbF$_4$		78.81	144.5	54.75	86.05	132.50	488.5	622.8	26.8
NaSbClF$_3\cdot$H$_2$O		73.16	143.5	46.13	86.56	130.78	479.8	611.2	12.7
KSbF$_4$	(I)	73.25	139.2	48.69	83.33	127.33	467.8	596.2	20.7
	(II)	78.29	154.3	48.90	93.58	141.05	517.0	659.0	10.4
	(III)	78.85	150.6	51.73	90.47	137.81	505.4	644.4	19.4
	(IV)	82.76	165.1	50.44	100.09	150.27	550.2	701.3	4.4
RbSbF$_4$		80.71	159.9	49.94	96.75	145.62	533.9	680.2	8.8
RbSbClF$_3$		80.41	159.5	49.27	97.00	145.90	533.8	679.2	7.9
CsSbF$_4$	(I)	76.38	152.4	46.60	92.48	138.86	508.4	648.1	4.3
	(II)	79.02	156.8	48.70	95.02	142.70	523.3	667.1	7.7
CsSbClF$_3$		75.18	150.4	45.77	91.22	136.90	501.2	638.9	2.8
NH$_4$SbF$_4$	(I)	75.28	148.9	46.61	90.17	135.65	497.3	633.9	9.0
	(II)	80.01	158.9	48.98	96.43	144.92	530.3	676.4	6.2
NH$_4$SbClF$_3$		78.03	155.7	47.57	94.46	141.80	519.3	661.9	4.0
NH$_4$Sb$_4$F$_{13}$	(I)	75.93	149.8	47.47	90.97	137.12	500.4	640.4	10.3
	(II)	81.01	160.7	49.89	97.26	146.33	536.4	683.2	7.9
KSbF$_4$	(I)							668.6^b)	4.9^b)
	(II)							701.5^b)	5.0^b)

^{a}) Frequencies reported earlier [365]; ^{b}) the data reported independently in [366].

KSb_2F_7 shows two types of Sb atom (Table 3.7). It is interesting that the antimony QCC and η values of the complex $KCl \cdot SbF_3$ ($KSbClF_3$) coincide almost exactly with the Sb(I) QCC and η of KSb_2F_7, which shows that SbF_3 units of the ψ-tetrahedral configuration with closely similar geometry, are present in both complexes. As in KSb_2F_7, these units in $KSbClF_3$ are only weakly bound into polymer chains through halogen bridges which however, involve in the latter case, the chlorine atoms. This suggestion was later confirmed by X-ray analysis [371].

Figure 3.6 Anionic chains in KSb_2F_7 [367].
● Sb; ○ F.

The close similarity of the antimony QCC values for SbF_3 units observed in the two compounds, confirms the assignment of KSb_2F_7 spectroscopic parameters to the groups (I) and (II) (Table 3.7). It also explained why the replacement of F atoms with Cl atoms had no marked effect on the antimony spectra in the respective coordination units. The chlorine bridges $\cdots F_3Sb\cdots Cl^-\cdots F_3Sb\cdots$ being, as in KSb_2F_7, of essentially ionic nature, produce, similarly to the fluorine bridges in the latter compound, a purely electrostatic contribution to the EFG at the Sb site. The ^{35}Cl NQR frequencies then evidently fall into a low-frequency range, where the spectrometer used was not sufficiently effective to detect them.

According to the $^{121,123}Sb$ NQR data selected from Table 3.7 and listed below, the following compounds may also contain, ψ-tetrahedral SbF_3 groups linked to adjacent coordination polyhedra by two long bridging bonds.

	$^{123}Sb\ e^2Qq/h$ (MHz)	η (%)
KSb_2F_7 (I)	674.1	8.7
$KSbClF_3$	674.1	7.2
$RbSb_2F_7$ (I)	672.5	9.8
$RbSb_2ClF_6$ (I)	672.1	9.7
$NH_4Sb_2F_7$ (I)	677.0	5.9
NH_4SbF_4 (II)	676.4	6.2

Trigonal ψ-pyramidal groups similar to Sb(II) polyhedra in KSb_2F_7 seem also to be present in $RbSb_2F_7$, $RbSb_2ClF_6$, $KSbF_4$ and $CsSb_4F_{13}$. The corresponding ^{123}Sb QCC values fall in the range $695-703$ MHz. The NQR data there-

fore suggest that the complex $RbSb_2F_7$ has a similar structure to KSb_2F_7. For the corresponding chlorofluoro derivative $RbSb_2ClF_6(2SbF_3 \cdot RbCl)$, NQR shows practically no difference in the nearest environment of each Sb atom. The latter structure may contain alternating chloro and fluoro bridges between Sb(I) and Sb(II) polyhedra. The corresponding bonds are expected to be rather weak to explain the nearly identical EFG on Sb in the fluoro and chlorofluoro complexes. Note that $RbSb_2F_7$ is isostructural [369] to $NH_4Sb_2F_7$, which does not contradict NQR data (Table 3.7).

X-ray data [368] for the complex $CsSb_2F_7$ show it is dimeric, containing two identical trigonal $\psi =$ bipyramids (Fig. 3.7). In agreement, [368] the ^{121,123}Sb
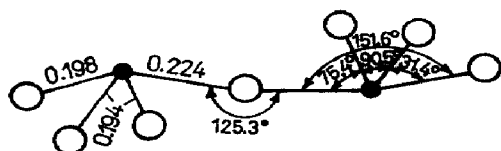

Figure 3.7   Atomic arrangement in the anionic part of $CsSb_2F_7$ [368].
● Sb; ○ F.

NQR spectra show that all the Sb occupy equivalent positions. Comparison of these results with the NQR spectrum of $CsSb_4F_{13}$ ($4SbF_3 \cdot CsF$) (Table 3.7) shows that one Sb atom (Sb(I)) in the latter, has the same nearest environment configuration as in $CsSb_2F_7$. The Sb atoms of the second sort, as suggested above, have the ψ-bipyramidal configuration similar to the Sb(II) polyhedra in KSb_2F_7. Thus the net structure of $[Sb_4F_{13}]^-$ ion is built up of dimerized $[Sb_2F_7]^-$ anions as shown in Figure 3.8. Based on NQR data (Table 3.7) the nearest coordination environment of antimony in NH_4SbClF_3 is very similar to that in $CsSb_2F_7$.

The antimony QCC values for $NaSb_2F_7$, $RbSbF_4$ and $RbSbClF_3$ do not differ significantly from that for pure SbF_3. The anionic chains of the two latter compounds are suggested to contain SbF_3 units weakly bridged through halogen anions (F^- or Cl^-) while in $NaSb_2F_7$ the SbF_3 groups might be very weakly dimerized through $Sb \cdots F \cdots Sb$ bridges.

The ^{121,123}Sb NQR data for $CsSbF_4$ and $CsSbClF_3$ suggest antimony environment patterns different from those discussed until now.

Indeed, the X-ray data have become available which show that $CsSbF_4$ possesses a dimeric structure [379] built up of two crystallographically different SbF_3 groups (Table 3.7) asymmetrically bridged by two fluorine atoms.
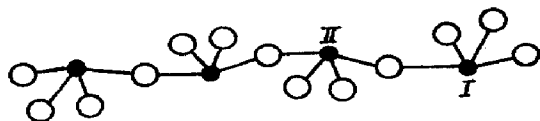

Figure 3.8   Assumed atomic arrangement in the anionic part of $CsSb_4F_{13}$ (see text)
● Sb; ○ F.

The crystal structure of $CsSbClF_3$ consists of quadrinuclear $[Sb_4Cl_4F_{12}]^{4-}$ isolated complexes forming layers [380]. The anionic complexes are built of SbF_3 groups linked by chlorine bridges.

Different sets of NQR [121,123]Sb frequencies have been detected for $KSbF_4$ by two groups [340, 366] (Table 3.7) neither, however, looking quite consistent with the X-ray data [370]. According to the latter, the $KSbF_4$ anionic fragment contains only SbF_5 ψ-octahedra linked into $[Sb_4F_{16}]^{4-}$ rings.

Therefore NQR data, in addition to X-ray data, do distinguish between the variety of configurations formed by antimony polyhedra in $SbF_3 \cdot x M^I hal$ complexes. The majority form anionic chains composed of ψ-octahedra, trigonal ψ-bipyramids and SbF_3 groups (ψ-tetrahedra). The other form dimers bridged by either one or two halogen atoms or multinuclear anionic complexes.

In general, the NQR data are useful to provide insight into the crystallochemical features of the polymers. They may also serve as a basis for the structural predictions. The latter are, however, more reliable if, in a series of closely related compounds, some members are previously studied by X-ray methods.

Table 3.8 contains NQR data for some other metal halides having infinite chain structures. Some, such as ZrX_4 (HfX_4), contain both bridging and terminal halogen atoms, while others, like MO_2Cl_2 (M = Mo, Cr, W), have either terminal halogens only, the chains being formed by the metal—oxygen bonds, or only bridging halogen atoms, like HgX_2 (X = Cl, Br, I). The NQR spectra readily reflect these features.

The $ZrCl_4$ ($HfCl_4$) compounds are known [385] to form chains made up from MCl_6 octahedra sharing edges. The intensity ratio of terminal-to-bridging resonances are expected to be $1:1$, consistent with the NQR data (Table 3.8). The latter also give a reason to suggest a similar structure for $ZrBr_4$ ($HfBr_4$). The X-ray data for ZrI_4 [386] and HfI_4 [387] show that both compounds consist of infinite chains of MI_6 octahedra sharing non-opposite edges. The chains however differ from each other and from the chains in the $ZrCl_4$ structure. A helical arrangement of ZrI_6 octahedra results in an identity period of 6 octahedra in ZrI_4. In $ZrCl_4$ this period equals 2 octahedra and in HfI_4 it is 4 units (Fig. 3.9). X-ray [386, 387] and the NQR data (Table 3.8) show that both types of iodine atoms, terminal and bridging, are crystallographically inequivalent in the tetraiodide compounds. However more complicated [79,81]Br and [127]I NQR spectra have been observed [376], those listed in Table 3.8 evidence for the presence of several polymorphs in the samples studied. The [127]I NQR spectra in Table 3.8 therefore give average frequency values. Rhombic and tetragonal modifications have been identified [376] in the X-ray powder patterns of the ZrI_4 samples, but their NQR lines are not assigned. X-ray analysis [386] determined the structure of ZrI_4 as monoclinic with space group $P2/c$.

The spectroscopic patterns of zirconium (hafnium) tetrahalides all have characteristic features discussed above for the transition metal bridging halides.

TABLE 3.8

NQR spectra of metal halides having a chain polymer structure (relative intensities of lines in parentheses)

Compounds	Isotope	T (K)	Terminal atoms				Bridging atoms				Ref.
			Res. frequencies (MHz)		e^2Qq/h (MHz)	η (%)	Res. frequencies (MHz)		e^2Qq/h (MHz)	η (%)	
			1/2–3/2	3/2–5/2			1/2–3/2	3/2–5/2			
$ZrCl_4$	^{35}Cl	77	4.583				7.500				376
$HfCl_4$	^{35}Cl	77					8.142				376
		300	4.677				8.055				
$ZrBr_4$	^{81}Br	77	28.50				51.97				377, 378
		296	29.34				51.11				377, 378
$HfBr_4$	^{81}Br	77	34.42				55.75				377, 378
		296	35.10				55.15				
ZrI_4	^{127}I	77	48.79	64.56	231.2	67.4	74.38	128.28	438.0	36.0	376
			51.89	66.53	239.7	71.0	73.16	126.95	433.1	35.1	
		296	49.36	68.26	242.5	62.5	74.26	124.43	427.0	39.8	
			52.45	69.99	250.3	66.5	75.38	125.53	431.3	40.6	
HfI_4	^{127}I	77	57.82	86.31	302.3	53.8	81.68	134.29	462.4	42.2	376
			54.66	84.89	295.3	49.1	82.55	135.51	466.7	42.4	
MoO_2Cl_2	^{35}Cl	83	15.40								275
CrO_2Cl_2	^{35}Cl	83	15.68								275
WO_2Cl_2	^{35}Cl	77	14.857								347
$WOCl_4$	^{35}Cl	77	12.998								347
$WOCl_3$	^{35}Cl	77	12.311(2)				13.085				347
$\alpha\text{-}PdCl_2$	^{35}Cl	296					18.069				374
$\beta\text{-}PdCl_2$	^{35}Cl	296					20.242				374
$\beta\text{-}PdCl_2$	^{35}Cl	296					23.615				374
$\beta\text{-}PtCl_2$	^{35}Cl	296					23.035				374

Compound	Isotope	T									Ref.
HgCl₂	³⁵Cl	77	22.522								427
			22.874								423 b
HgBr₂	⁸¹Br	77	129.907								211
			130.933								
HgI(red)						151.62	237.60	825.0	48.1		210
KHgI₃·H₂O	¹²⁷I	77	125.27	248.35	8.2	108.39	154.49	547.7	59.1		210
			135.45	267.94	5.2						
Me₄NHgI₃	¹²⁷I	77	122.80	234.60	8.0	102.04	159.03	553.0	48.6		210
			137.54	270.00	1.5	103.72	174.96	590.8	38.9		
			139.04	276.30	7.1						
			152.94	305.78	1.6						
CuCl₂	³⁵Cl	295				9.83					375
CuBr₂	⁸¹Br	295				69.98					375
SnCl₂	³⁵Cl	302				4.54					383
		297	5.79								
SnBr₂	⁸¹Br	77	63.72			40.91					381
PbBr₂	⁸¹Br	77	27.83			20.67					384
γ-ZnCl₂	³⁵Cl	77				12.83					381
ZnBr₂	⁸¹Br	77				81.42					
						83.09					
						84.13					384
ZnI₂	¹²⁷I	295				123.65	176.52	623.3	58.8		382
						127.36(2) ·	184.99(2)	651.3	57.0		
						142.28	179.54	649.4	72.7		

a) Recalculated from ^{79}Br frequencies according to $eQ(^{79}Br)/eQ(^{81}Br) = 1.1971$.

The assignment of resonance lines to bridging and terminal atoms has been made based on the same arguments. The bridging halogen atoms showed resonances at relatively higher frequencies with negative temperature coefficients. The lower frequency lines, with positive temperature coefficients, are assigned to the terminal halogen atoms. The suggestion concerning considerable $(p-d)_\pi$ character in the terminal $M-X$ bonds, in transition metal halides with the vacant d-orbitals, is supported by the high asymmetry parameter magnitudes (η) measured at the terminal iodine atoms in both zirconium and hafnium tetraiodides (Table 3.8).
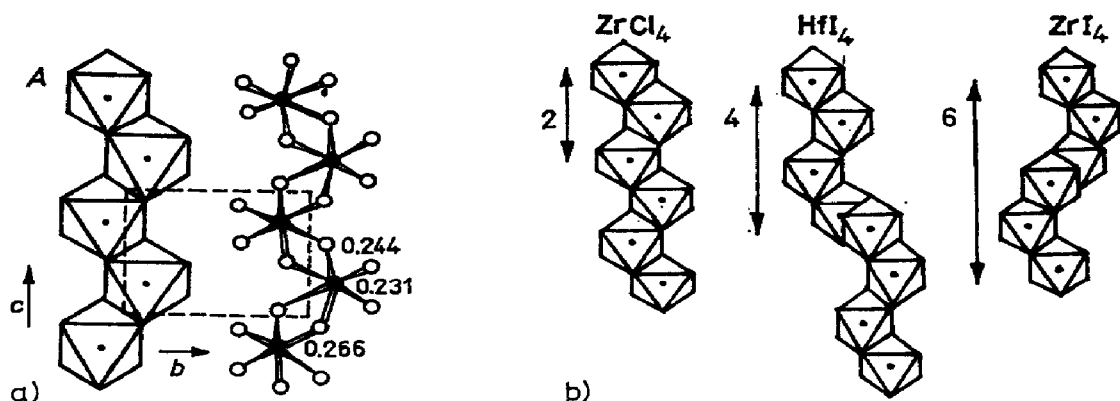

Figure 3.9   Linkage of octahedra to chains: a) in $ZrCl_4$ [385]; b) identity periods are shown in the arrangement of $Zrhal_6$ octahedra in $Zrhal_4$ crystals [385—387].

The reverse frequency ordering is found in NQR spectra of transition metal complexes with filled d-subshells. The terminal halogen frequencies in the mercury chain compounds $KHgI_3 \cdot H_2O$ and $(CH_3)_4NHgI_3$, built up from HgI_4 tetrahedra sharing vertices [388, 389] exceed their bridging atoms frequencies.

The NQR spectra of $PtCl_2$, $PdCl_2$, HgX_2 and CuX_2 show only bridging halogens in agreement with their structures consisting of infinite chains of edge-sharing tetrahedra $[MX_4]^{2-}$. A similar type of atomic arrangement (HgI_2-type structure) has been established for γ-$ZnCl_2$ [390, 391]. The halogen environment in $ZnBr_2$ and ZnI_2 (Table 3.8) is not very different from the Cl atom environment in the $ZnCl_2$ [381]. This suggestion agrees with X-ray data [392] for ZnI_2.

The $SnCl_2$ structure [393] is known to consist of $[Sn-Cl]_\infty$ chains running along the c-axis. One more Cl atom (terminal) is bound to each Sn atom. The NQR spectra of $SnCl_2$, $SnBr_2$ and $PbBr_2$ are consistent with this structure (Table 3.8).

(ii) Polymeric chalcogenides of Group V non-transition elements; ternary compounds

Group V non-transition element chalcogenides of the composition A_2B_3 such as As_2B_3 (B = S, Se, Te); Sb_2B_3 (B = S, Se) and Bi_2S_3 are known [394—401] to be coordination polymers (chains, ribbons) built up of two crystallochemically different coordination polyhedra. While one of them (say, formed by A^I) is a regular or slightly distorted trigonal pyramid AB_3, the other (formed by A^{II}) has lower symmetry due to the tendency of the A^{II} atoms to make secondary bonds with the chalcogen atoms of neighbouring polyhedra. The schematic arrangement of ribbons which is fairly close to the real structural patterns of Sb_2B_3 and Bi_2S_3 is given in Figure 3.10.
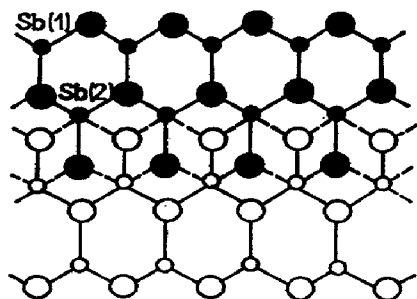

Figure 3.10   Atomic arrangement in Sb_2S_3 [442]
o Sb; ○ S.

The crystal structure of Sb_2S_3 (antimonite) [394, 395] consists of infinite ribbons $(Sb_4S_6)_n$ parallel to the c axis, which are only weakly linked together. The ribbon is built up from two types of chains, the middle part consisting of the $Sb^{II}S_5$ coordination polyhedra. On both sides of these chains, there are Sb^IS_3 polyhedra (Fig. 3.10). The Sb^I atoms are therefore in a trigonal pyramidal environment while the configuration of the $Sb^{II}S_5$ polyhedra is a distorted square pyramid. The Sb^{II} atom has, in addition to the three sulphur atoms at distances of 0.249 and 0.268 nm, two more separated S atoms (Sb—S = 0.282 nm), the latter distance however being shorter than the sum of the van der Waals radii. Such a geometry favours the suggestion that the antimony lone pair electrons occupy the sixth octahedral place of the $Sb^{II}S_5$ polyhedron. A 0.012 nm displacement of the Sb^{II} atom downwards from the pyramid bottom is explained by repulsion between the Sb^{II} lone pair of electrons and the valence bond electron pairs [394, 402]. For the same reason, some of the bond angles at the Sb^{II} atom are narrowed from 90°. The Sb^{II} polyhedron is considered to be a distorted ψ-octahedron. This is consistent with the decrease in $^{121,123}Sb$ QCC value for the Sb^{II} atom compared to that for Sb^I (Table 3.9).

Other A_2B_3 (A = Sb, Bi) compounds listed in Table 3.9 show similar structural features, and the crystallographic differences between the two coordina-

TABLE 3.9

NQR spectra of Group V element binary polymeric chalcogenides

	T (K)	Isotope, site	Transition frequencies (MHz)				e^2Qq/h (MHz)	η (%)	Ref.
			1/2—3/2	3/2—5/2	5/2—7/2	7/2—9/2			
Sb_2S_3	77	$^{121}Sb^I$	47.71	95.41			318.0		403,
		$^{123}Sb^I$	28.96	57.90	86.86		405.4	0.8	404
		$^{121}Sb^{II}$	42.98	73.29			250.7		
		$^{123}Sb^{II}$	32.27	43.13	67.45		319.4	37.7	
	300	$^{121}Sb^I$	44.35	88.69			295.6		
		$^{123}Sb^I$	26.93	53.85	80.86		376.9	2.0	
		$^{121}Sb^{II}$	40.99	69.59			238.3		
		$^{123}Sb^{II}$	30.84	40.99	64.19		303.8	38.3	
Sb_2Se_3	77	$^{121}Sb^I$	40.91	81.78			272.7		404
		$^{123}Sb^I$	24.83	49.68	74.51		347.0	0.0	
		$^{121}Sb^{II}$	34.98	57.73			198.6		
		$^{123}Sb^{II}$	27.02	33.92	53.30		253.3	41.8	
	300	$^{121}Sb^I$	38.07	76.09			253.7		
		$^{123}Sb^I$	23.10	46.10	69.17		327.5	0.9	
		$^{121}Sb^{II}$	33.10	54.51			187.7		
		$^{123}Sb^{II}$	25.44	31.94	50.20		238.4	41.9	
Bi_2S_3	77	$^{209}Bi^I$	14.25	28.29	42.25	56.63	339.6	3.0	403,
		$^{209}Bi^{II}$	21.50	14.73	16.32	23.77	152.75	88.9	404
As_2S_3	300	$^{75}As^I$	71.92				141.1	34.3	405,
		$^{75}As^{II}$	69.53				135.9	37.4	406
As_2Se_3	77	$^{75}As^I$	60.25						407
		$^{75}As^{II}$	56.07						
As_2Te_3	300	$^{75}As^I$	41.12						407

tion groups in every compound, are clearly reflected in their NQR spectra. In Sb_2S_3, the participation of Sb^{II} atoms in secondary bonding results in a decrease of the corresponding e^2Qq/h value by 21% from that of Sb^I, while the asymmetry parameter increases from 0.8 to 37.7% passing from Sb^I to Sb^{II}. The splitting amounts to 27% in Sb_2Se_3 indicative of a still greater difference between the two types of Sb atoms. In the spectrum of Bi_2S_3 the two ^{209}Bi e^2Qq/h values differ by 55%. The X-ray data [397] show that Bi_2S_3 features in fact, the greatest structural difference between the (I) and (II) units of all the A_2B_3 compounds studied.

X-ray data on arsenic chalcogenides As_2B_3 [398—401] show them to have crystallochemical features similar to those of Sb_2B_3 and Bi_2S_3. Their ^{75}As NQR spectra are also given in Table 3.9. By analogy with the antimony and bismuth compounds, the higher ^{75}As NQR frequencies are assigned to the As^I sites of relatively higher symmetry, while the lower frequency lines were assigned to As^{II} sites characterized by higher coordination number. In agreement with the structural differences between the As^I and As^{II} polyhedra increasing from As_2S_3 to As_2Te_3 [398—401] the NQR spectroscopic splitting increases from As_2S_3 to As_2Se_3. In the As_2Te_3 structure [401] the tendency to increase the coordination number is shown by the As^{II} atoms which form an octahedral configuration. This may probably be the reason for the failure to observe the As^{II} resonance in the ^{75}As NQR spectrum of As_2Te_3 [407].

Comparison of structural and NQR data for binary chalcogenides A_2B_3 shows that the NQR spectra distinctly reflect the ability of the A^{II} elements to form secondary bonds with chalcogen atoms thus increasing their coordination number. The shift of the A^{II} QCC value to lower frequency with respect to that of A^I may serve as a measure of this ability. According to the NQR results (Table 3.9) the A^{II} atoms show a tendency which grows with an increase in atomic radii of both, A and B atoms, to form secondary bonds accompanied by the increase of their coordination number. This is confirmed by the increasing NQR spectroscopic splitting along the As_2S_3—As_2Se_3—As_2Te_3 direction and by X-ray data [398—401] which reveal the increasing structural difference between the As^I and As^{II} polyhedra in the same direction. A similar increase in spectroscopic splitting has been observed, consistent with the X-ray results [394—397], between the QCC values at the A^I and A^{II} sites, in the series As_2S_3—Sb_2S_3—Bi_2S_3 (Table 3.9). This tendency might possibly be responsible for the crystallization of Sb_2Te_3, Bi_2Se_3 and Bi_2Te_3 in different structural types. They are known to form layer lattices, with the A atoms residing in octahedral sites [408].

Table 3.10 shows the NQR spectra of ternary chalcogenides. Many of them exist as natural minerals whose structures are built up from various polymeric patterns. The AB_3 trigonal pyramids are established as basic structural units in the majority of minerals. In Cu, Ag and Tl salts of metathioarsenous $HAsS_2$ (metathioantimonous $HSbS_2$) acid the AB_3 pyramidal groups are bound to $(AB_2)_n$ rings or infinite chains $(AB_2)_\infty$ through sulphur bridges. Smithite $AgAsS_2$ [431], lorandite $TlAsS_2$ [432], and miargyrite $AgSbS_2$ [433] may serve as examples. Wolfsbergite $CuSbS_2$ contains double layers of $(SbS_2)_\infty$ chains linked through Cu atoms tetrahedrally bound to sulphur atoms [434]. The spectroscopic analogies (Table 3.10) enable one to predict similar structures for some related compounds with unknown structures [410]: $CuSbS_2$—$CuSbSe_2$; Ag_3AsS_3—Ag_3AsSe_3; Tl_3SbS_3—Tl_3SbSe_3; Tl_3AsS_3—Tl_3AsSe_3—Tl_3SbSe_3.

The pyramidal AB_3 configuration is also typical for the chalcogenides of R_3AB_3 composition (R = Cu, Ag, Tl; A = As, Sb, Bi; B = S, Se [410] and

TABLE 3.10

[75]As, [121]Sb and [209]Bi NQR spectra of ternary Group V element chalcogenides at 77 K

Compound	e^2Qq/h (MHz)	η (%)	Ref.	Compound	ν (MHz)	Ref.
Ag_3SbS_3 pyrargyrite	332.3	0.0	409	Ag_3AsS_3 proustite	67.34	409
Cu_3SbS_3	344.9	10.0	413	Ag_3AsSe_3	54.62	435, 410
Cu_3BiS_3 wittichenite	544.1	17.6	416			
Tl_3SbS_3	345.8	0.0	410	Tl_3AsS_3 ellisite	68.93	410
Tl_3SbSe_3	265.3	0.0	410	Tl_3AsSe_3	58.82	411
Na_3SbS_3	357.9	0.0	419			
$CuSbSr_2$ wolfsbergite	379.3	1.6	412			
$CuSbSe_2$	324.7	2.0	410			
$AgSbS_2$ myargyrite	321.8	34.0	417	$AgAsS_2$ smithite	67.99; 68.56 71.64	435, 414
$TlSbS_2$	364.6 392.3	64.5 55.3	415	$TlAsS_2$ lorandite	81.14 84.12	411
Ag_5SbS_4 stephanite	361.8	10.7	420	$TlAsSe_2$	64.00 65.57	411

	ν (MHz)		e^2Qq/h (MHz)	η (%)	Ref.
	1/2—3/2	3/2—5/2			
$LiSbS_2$	85.15	89.62	335.4	93.8	436, 418
α-$NaSbS_2$	92.29	99.84	371.1	90.7	419, 435
$KSbS_2$	98.15	108.84	403.3	87.6	435, 418
$RbSbS_2$ (I)	89.17	115.43	415.2	69.8	435, 418
(II)	102.93	119.24	438.1	82.5	
$KSbSe_2$ (I)	77.92	96.19	349.1	75.3	435, 418
(II)	90.91	95.40	357.3	94.1	

refs. cited therein). The stability of this configuration is reflected in a relatively small scatter of QCC values over the compounds listed. The NQR spectra of chalcogenides containing regular AX_3 pyramids, with the central atom A located at the lattice site of point group symmetry 3m, show a zero asymmetry parameter (Table 3.10).

The Townes and Dailey approach [95] yields, after trivial transformations of equations (24*), (25*) of Table 1.8, relationships for the pyramidally coordi-

nated Group V atoms

$$U_p = -3(b - a)\frac{\cos \alpha}{1 - \cos \alpha} = (b - a)(1 - 2\cot^2 \theta) \qquad (101)$$

Here a is the occupation number of the central atom MO occupied by a lone pair of electrons, b is the occupancy of the MO directed to the three chalcogen atoms, α is the B—A—B angle, θ is the angle between the z axis and the direction of the AB bond (Fig. 3 in Table 1.8). If the lone pair of electrons is stereochemically inactive ($b = 2$), the equation (101) becomes

$$U_p = -\frac{3\cos \alpha}{1 - \cos \alpha}(1 + i) \qquad (102)$$

where i is the AB bond ionicity.

From equation (102), the QCC value at the AB_3 central atom is mainly determined by the geometry of this group and the ionic character of the AB bonding.

However these factors do not completely explain the variations in the experimental magnitudes of the arsenic or antimony QCC in the compounds discussed. The estimation of angular terms of equation (102) in the two structurally studied compounds, pyrargyrite Ag_3SbS_3 ($\alpha = 96° 20'$, Sb—S = 0.246 nm [318]) and stephanite Ag_5SbS_4 ($\alpha_1 = 93.8°$; $\alpha_2 = 94.5°$; Sb—S$_1$(2) = 0.247 nm; Sb—S$_2$ = 0.248 nm [346]) leads to the conclusion that the observed difference in the ^{121,123}Sb e^2Qq/h magnitudes in these compounds is fitted by at least a 45% difference in the Sb—S bond ionicities. This does not seem reasonable considering the nearly identical Sb—S bond distances which are close to the sum of their covalent radii (0.245 nm) in both compounds. A partial reason for the discrepancy might be an incorrect use of the Townes and Dailey approach which requires the pyramidal groups to be isolated, while they are not in the real structures. The other reason may lie in the stereochemical activity of the arsenic (antimony) lone pair of electrons [435] which means $b < 2$ in equation (101). The polarization effects due to the presence of metal atoms (Cu, Ag, Tl) also contribute to the EFG at the As (Sb) atom.

The electron density distribution in several antimony and arsenic chalcogenides (As_3SbS_3, Ag_5SbS_4, $CuSbS_2$, Ag_3AsS_3) were calculated within the MO LCAO CNDO approximations [436]. Partial delocalization of the antimony and arsenic lone pair electrons over the antibonding sulphur orbitals was postulated. The results show that delocalization of this type has a marked effect on the EFG value at the Sb atom and has to be considered when interpreting NQR spectra. It is worthwhile mentioning that satisfactory agreement between the theoretical and experimental e^2Qq/h values may be achieved merely by taking into consideration the delocalization effect, although a more rigorous treatment, of course, requires total energy minimization over all the Pauling's AO coefficients in the expansion of the Hartree-Fock one-electron orbitals.

The idea of the participation of lone pair electrons in chemical bonding finds support in some ab initio calculations [104a, 437] which show that the traditional view, according to which the lone pairs occupy non-bonding orbitals on halogen, nitrogen, etc. atoms is often not justified.

The other type of Sb atom environment established in ternary chalcogenides is SbB_4-ψ-trigonal bipyramid. This was detected in $TlSbS_2$ [438] and in several compounds of the same composition ($RSbB_2$) with alkali metal atoms for R: α-$NaSbS_2$ [439, 480], $KSbSe_2$ [439], $KSbS_2$ [440], and $RbSbS_2$ [441]. Their ^{121}Sb NQR spectra are listed in Table 3.10. The ^{123}Sb NQR signals were also observed in all the compounds shown in Table 3.10.
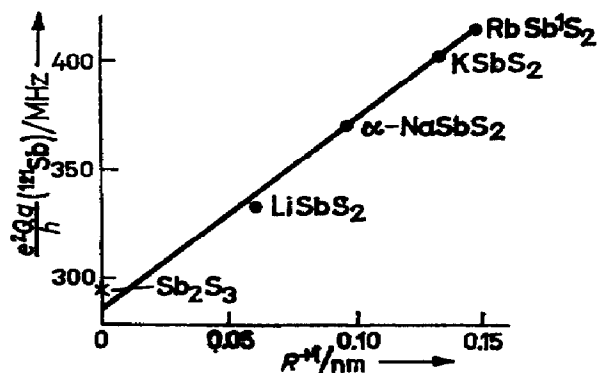
Figure 3.11 ^{121}Sb QCC values in $RSbS_2$ vs alkali metal ionic radii (R^{+1}).

In the series $LiSbS_2$, α-$NaSbS_2$, $KSbS_2$ and $RbSbS_2$ (Sb(I)) the antimony QCC values increase almost linearly with the alkali metal ionic radii (R^+) (Fig. 3.11) thus reflecting the cation influence on the Sb QCC. Bearing in mind that the alkali atom electronegativity decreases in the series Li > Na > K > Rb with increase of their ionic radii one can expect an increase in the effective positive charge on the alkali atoms in the same direction. The influence of cations on the Sb e^2Qq/h may then be attributed to increasing Sb—S bond ionicities along the series, which is followed by an increase in the Sb QCC (eqn. (102)). Extrapolation of the straight line in Figure 3.11 to intersection with the ordinate axis, gives an e^2Qq/h value near that observed for Sb(I) in Sb_2S_3 (Table 3.9).

X-ray data on $RbSbS_2$ [441] give 4 types of crystallographically independent positions for the Sb atoms in the crystal, while the NQR detected only two, with the signal-to-noise ratio of resonances exceeding 50 [418, 435]. Some of the compounds appeared to partially decompose with time although stored in sealed ampoules. Thus, in the NQR spectrum of α-$NaSbS_2$, Sb_2S_3 resonances, which were formerly absent, appeared with time. Resonances in $CsSbS_2$, which became observable after prolonged homogenizing and annealing, vanished again after several months, and did not appear after repeated annealing.

This instability gives some reason to suppose that the structure of $RbSbS_2$ changes with the loss of some symmetry elements, under the action of X-rays.

In general, chalcogenides of type RAX_2, where R is an alkali metal atom, show crystallochemical properties similar to those of other ternary chalcogenides of the same composition. Their structures become more complicated as the radii of the constituent atoms increase. The spectroscopic multiplicity shows two crystallographically independent positions for the Sb atoms in $RbSbS_2$ and $KSbSe_2$ while all the Sb atoms are equivalent in $LiSbS_2$, α-$NaSbS_2$ and $KSbS_2$. The NQR spectrum of $CsSbS_2$ detected four inequivalent Sb atoms. The magnitudes of their ^{121}Sb QCC and η values, are as follows: (I) 293.8 MHz, $\eta = 47.7\%$; (II) 336.4 MHz, $\eta = 36.0\%$; (III) 449.1 MHz, $\eta = 38.5\%$; (IV) 482.0 MHz, $\eta = 35.8\%$.

NQR results for ternary chalcogenides are as a whole, in satisfactory agreement with the X-ray data available. They also supply additional crystallochemical information. The NQR spectra of the compounds (Table 3.10) indicate that the EFG at arsenic (antimony) atoms does not vary considerably within the coordination polyhedra of similar types. The same is seemingly valid for the average bonding state within the polyhedra, although the crystal structures of the compounds may differ considerably in detail.

The NQR data suggest, as indicated above, the participation of antimony (arsenic) lone pairs in chemical bonding. This is agreed with the structure data available. X-ray data for $TlAsS_2$ [432], for example, show shortened As—S bond distances in both types of AsS_3 coordination polyhedra. They are 0.215 and 0.216 nm in AsS_3(I) and 0.205 nm in AsS_3(II) which is shorter than the sum of the corresponding covalent radii (0.220 nm). The antimony lone pair of electrons is also stereochemically active in $TlSbS_2$ [438].

This lone pair activity evidently enhances the valence potentialities of the antimony (arsenic) atoms. Their valence resources can then be enhanced by the formation of secondary bonds and hence by an increase in coordination number. Such an increase was established in myargyrite $AgSbS_2$ [433] and smithite $AgAsS_2$ [431]. Their antimony (arsenic) atoms possess, in addition to the three nearest neighbour sulphur atoms, three next neighbour sulphur atoms at distances shorter than the sum of van der Waals radii. This is reflected in lower Sb (As) NQR frequencies in their spectra, compared to the spectra of other compounds having the same composition (Table 3.10).

C. COMPOUNDS WITH LAYER STRUCTURE

Substances which form layer lattices include crystals of diverse structural types. Some, such as perovskite compounds, "sandwiches" or other double oxides possess valuable physical properties. We shall discuss here compounds which have been most extensively studied by NQR.

(i) Metal halides and oxyhalides with a "sandwich" lattice

The most numerous family of "sandwich" compounds is formed by the halides of non-transition and transition metals in oxidation states $+2$ and $+3$. The metals are often located in an octahedral environment of halogen atoms. The arrangement of the latter (as well as of metal atoms) is a planar network formed by alternating sheets of coplanar atoms of the same sort. As a result metal layers and pairs of halogen atom layers, form a "sandwich" structure [442]. A simplified scheme for such a "sandwich" atomic arrangement, in metal dihalide crystals is shown in Fig. 3.12. The halogen atoms are seen to be tri-coordinate.
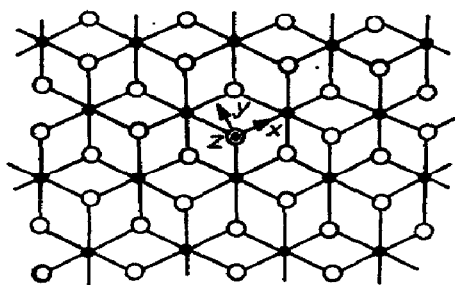
Figure 3.12   Spatial arrangement of the atoms in layer metal dihalides [442]. The orientation of the EFG axes at the halogen site is shown.

● metal atoms ; ○ halogen atoms.

The real structures of metal dihalides may, of course, be much more complicated in detail, with higher coordination numbers for all the atoms, due to various packing patterns. The crystal structure of $SrBr_2$ [451] contains, for example, 10 formula units in the unit cell of tetragonal symmetry $P4/n$ with four inequivalent bromine positions. Two are tetrahedrally coordinated by equivalent Sr atoms producing a vanishing EFG at these Br atoms. This might explain the failure to observe their NQR signals in the spectrum of $SrBr_2$ [449] (Table 3.11).

The structural types $CdCl_2$ and CdI_2 are, however, satisfactorily described by the scheme in Fig. 3.12.

Table 3.11 lists NQR spectra for metal dihalides and their hydrates. The halogen NQR frequencies are remarkably low in these compounds. In hydrated substances, water molecules readily enter the metal inner coordination sphere to increase the halogen atom asymmetry parameter (η). Their crystals retain, as a rule the layer structure. Thus in $BaBr_2 \cdot 2H_2O$ [450] the $Ba(H_2O)_2$- and Br- columns extend along the c-axis. Each Br atom is linked with three $Ba(H_2O)_2$ groups and has one Ba atom and two water molecules in its nearest environment. Both metal and halogen atoms occupy crystallographically equivalent positions in the crystal lattice of the compound. From the close resemblance of the NQR spectra for $BaBr_2 \cdot 2H_2O$ and $BaI_2 \cdot 2H_2O$ the two compounds

TABLE 3.11

NQR data on layer metal dihalides and hydrated compounds

Compound	Isotope	T(K)	ν (MHz) 1/2—3/2	ν (MHz) 3/2—5/2	e^2Qq/h (MHz)	η (%)	$e^2Qq/h(1-\gamma_\infty)$ ionic (MHz)	Ref.
$CaBr_2$ᵇ)	⁸¹Br	77	32.88					449
$CaBr_2 \cdot H_2O$ᵇ)	⁸¹Br	77	15.83					449
$CaI_2 \cdot 6H_2O$	¹²⁷I	77	15.52	27.97	94.81	29.6	18.96ᵃ)	449
$SrBr_2$ᵇ)	⁸¹Br	77	28.93					449
			14.88					
$SrBr_2 \cdot H_2O$ᵇ)	⁸¹Br	77	13.98					449
$SrI_2 \cdot 6H_2O$	¹²⁷I	77	24.82	48.79	163.04	11.7		
$BaCl_2 \cdot 2H_2O$	¹³⁷Ba	300	16.303		29.78	77.14		443a,b
$BaBr_2$	⁸¹Br	77	21.73					444
			12.19					
$BaBr_2 \cdot H_2O$	⁸¹Br	77	10.12					444
$BaBr_2 \cdot 2H_2O$	⁸¹Br	77	3.82					444
	¹³⁷Ba	77	25.83		44.8	73.0		445
$BaI_2 \cdot 2H_2O$	¹²⁷I	300	10.23	15.34	53.7	53.2		446
	¹³⁷Ba	300	24.46					
$CdBr_2$	⁸¹Br	297	14.34		26.68	0.0	5.9	447
CdI_2	¹²⁷I	297	14.49	29.02	96.6	0.0	7.17	447
			14.79	29.47	98.6	0.0		
$PbBr_2$	⁸¹Br	298	17.39					384
			26.15					
PbI_2	¹²⁷I	77	17.15	34.5	116.6	0.0		448
$TiCl_2$	³⁵Cl	300	4.17		8.34	0.0		447
$CrCl_2$	³⁵Cl	300	8.52		17.04	0.0		447
$CoCl_2$	³⁵Cl	4.2	2.62				0.11	467
$CoCl_2 \cdot 2H_2O$	³⁵Cl	76	5.2		9.866	44.0		468
$CoCl_2 \cdot 6H_2O$	³⁵Cl	77			5.508	8.0		469
$FeCl_2$	³⁵Cl	77	2.37				0.24	470

ᵃ) Data [447] on anhydrous compound; .
ᵇ) recalculated from the data on ⁷⁹Br according to $eQ(^{79}Br)/eQ(^{81}Br) = 1.1971$.

appear to be isostructural [446]. $BaCl_2 \cdot 2H_2O$ has a different structure ([446] and refs. cited therein) with two types of Cl position and a different coordination environment of Ba atoms, but it remains layered.

Only one halogen NQR signal was observed in $SrBr_2 \cdot H_2O$ [449] but the X-ray analysis [452] established two types of Br atom in the crystal. A similar situation was reported [444] for $BaBr_2 \cdot H_2O$. The probable reason for the discrepancy of the data on $SrBr_2 \cdot H_2O$ might be the effect on the environment

of one of the Br atoms of 3 Sr atoms and one O atom at nearly identical distances (0.331 – 0.332 nm) producing, as in anhydrous $SrBr_2$, a close to zero EFG at this Br atom.

Table 3.11 shows a remarkable variation in the NQR parameters with the number of water molecules in the crystalhydrates.

The coordination polyhedra in Figure 3.12 present the arrangement of atoms in metal dihalides where all the edges are shared. In metal trihalides (Fig. 3.13) only three edges are shared and halogen atoms are di-coordinate. This type of structure occurs in $AlCl_3$, $CrCl_3$ and $FeCl_3$, etc. The halogen NQR spectra of various metal trihalides are listed in Table 3.12. Their frequencies, in general, appear to be higher than in the corresponding metal dihalides, consistent with the difference in halogen environment in the two structures.
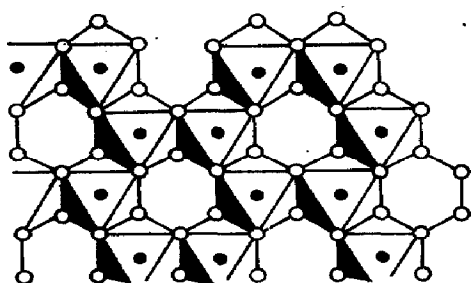
Figure 3.13   Scheme of spatial atomic arrangement in layer metal trihalides [442]. ● metal atoms; ○ halogen atoms.

At first sight, the low halogen atom NQR frequencies and QCC values favour a predominantly ionic nature for the metal—halogen bonds in the layer structures. The relative importance of the ionic lattice, and covalent bond models, contributing to the EFG value has been investigated by Barnes et al. [447], QCC values in covalent compounds being dependent on the halogen atom hybridization state and the partial ionic character of the metal—halogen bond. On the other hand, ionic compounds may feature high EFGs because of the antishielding effects. Thus both limiting models can yield spectroscopic parameters of comparable value. QCC values have been calculated for some layer metal halides on the basis of a purely ionic model. The model considered interactions of nuclear quadrupole moments with the EFG, due to the lattice of ionic cores enhanced by the antishielding effect of the core electrons of the halogen atom. The results are shown in Table 3.11 under "e^2Qq/h $(1 - \gamma_\infty)$ ionic". They show the ionic model to be a rather poor approximation, the calculated values being far below the experimental ones. The results could only be improved by using antishielding factor values, γ_∞, exceeding the theoretical values. At the same time, comparison of the calculation with the experimental QCC values for, e.g. two non-equivalent halogen atoms in CdI_2 shows that

TABLE 3.12

Halogen NQR data for layer metal trihalides (RT room temperature)

Compound	Isotope	T (K)	Transition frequency (MHz)		e^2Qq/h (MHz)	η (%)	Ref.
			1/2—3/2	3/2—5/2			
TiCl$_3$	^{35}Cl	297	7.39				447
VCl$_3$	^{35}Cl	297	9.40				447
FeCl$_3$	^{35}Cl	300	10.118				453
ScBr$_3$	^{81}Br	295	41.163				454
CrBr$_3$	^{81}Br	297	85.73				447
ScI$_3$	^{127}I	297	57.21	106.5	359.5	24.3	454
BiI$_3$	^{127}I	77	111.32	201.38	682.18	29.0	455
UCl$_3$	^{35}Cl	77	4.51				456a
NdBr$_3$ I	^{81}Br	RT	44.575		89.076	6.8	457
II			23.549		45.348	48.7	
UI$_3$ I	^{127}I	6.0	56.197	109.086	365.35	15.4	457
II			39.615	50.960	183.49	70.58	
CrCl$_3$	^{35}Cl	297	12.848				447
			12.812				
TlCl$_3$	^{35}Cl	300	14.812				456a
			14.756				458
RuCl$_3$	^{35}Cl	77	16.880				456b
			16.815				
YCl$_3$	^{35}Cl	4.2	4.273				456
			4.212				
TlBr$_3$	^{81}Br	297	125.9				195
			125.7				

more realistic empirical values for these factors amount to about $20-30\%$ of the theoretical values.

The Townes and Dailey theory has been used [447] to calculate the QCC at the halogen atom, assuming sp^3 hybridized MOs in metal dihalides, and sp^2 hybridized MOs at the halogen atom, in metal trihalides. For metal dihalides the EFG axes are shown in Figure 3.12. As a result the following relationship was obtained.

$$e^2Qq_{zz}/h = \frac{3s(1-i)}{1+3\varepsilon i} \cdot (e^2Qq_p/h)$$

(103)

where ε reflects the small contribution to EFG from the halogen atom charge. Based on electronegativity differences the ionicities i of the cadmium—halogen bonds were set equal to 50% which gave $s = 0.036$ [447]. Using further, the

equation $s = \dfrac{\cos \alpha}{\cos \alpha - 1}$ [97] the values of $\alpha(\text{Cd}-\text{hal}-\text{Cd})$ angles were predicted to compare with X-ray values. Thus, for CdI_2 this estimation gave $\alpha = 92°$ against $88°$ determined by the X-ray analysis ([447] and refs. cited therein). Comparison of the two models led to the conclusion that the covalent bond model should be preferred. The latter may be improved by inclusion of ionic lattice contributions to EFG. The total EFG value (q_t) should then be regarded as a sum of two terms: one describing the contributions from the charges of the lattice ionic cores (q_l) estimated from consideration of relative atom electronegativities and the other depending on the contributions from halogen atom valence sp orbitals (q_b) slightly differing from the pure p-orbitals:

$$q_t = q_b + q_l \tag{104}$$

Using empirical γ_∞ values and estimating the s-character with the help of equation (104), values of interbond α angles have again been calculated. It appeared that the inclusion of ionic contributions had no marked effect on the covalent parameter values. Generally speaking, the lattice term only leads to some enhancement of valence bond s-character and consequently to some increase in valence angles. It however improves agreement between the calculated and experimental values, in particular with the difference between the ^{127}I e^2Qq/h values in CdI_2. According to [447], the latter model is the most realistic. It is important that, though lattice contributions to EFGs may vary considerably from one compound to another (Table 3.11), their summary effect on QCC remains significantly smaller than the effect of the halogen atom p-orbitals.

Transition metal dihalides have been concluded [459] to be largely ionic (80% and higher), the higher halides being more covalent than the lower ones. Lyfar et al. [460] later reestimated the covalent and ionic contributions to q_{zz} at the halogen site in $CdBr_2$ and CdI_2. Using the relationship (103) when estimating the covalent contribution, they however took into account the fact that the ionicity or covalency portion of each of the three bonds formed by the halide ion with the three cadmium ions at about $90°$ could not be estimated merely from the electronegativity difference of the atoms.

Presenting the state Br^- (I^-) as a superposition of the three states where the halogen atom is bonded only with one of the three Cd^{2+} ions they have concluded that the degree of ionicity of each bond follows from the electronegativity difference of $Cd-\text{hal}$, but the mean electron density per bond is $\sigma = i/3$. The i values used in equation (103) were 0.60 for $CdBr_2$ and 0.52 for CdI_2. The values of s were 0.021 for $CdBr_2$ and 0.005 17 for CdI_2 using $91°14' \pm 5°$ and $90°14' \pm 5°$ for the corresponding α angles as determined by X-ray ([461] and refs. cited therein). The latter are, however considered insufficiently

exact, giving a marked uncertainty in the calculation of s and hence of q_b in equation (104).

This of course partly accounts for the discrepancy between the calculated and observed results, but the discrepancy is characterized by the systematic underestimation of q_b which does not result from the error in X-ray data.

The lattice contribution to the NQR frequency also appeared to be too small compared to the observed frequencies, the sign of q_l being opposite to that of q_b.

The inconsistency of the calculated e^2Qq/h values with those observed experimentally, may be accounted for by the strong polarization of the co-valent bonds by the internal electric field present in the layer crystals. Indeed, the strength of the internal electric field at the halogen site in PbI_2 possessing a "sandwich" structure was estimated [462] to be of the order of 4.2×10^8 Vcm^{-1}, typical for layer crystals.

Values of the electric field constants measured on single crystals of the Cdhal$_2$, and Pbhal$_2$ layer compounds gave, however, evidence that the contribution from the polarization of bonds by the electric field is an order of magnitude smaller than the contribution of ionic polarizability [461, 462].

Table 3.12 lists halogen NQR spectra for layer metal trihalides crystallizing in several structural types. The compounds $TiCl_3$ through BiI_3 crystallize in the $FeCl_3$ lattice [442] with hexagonal close packing of halogen atoms and metal atoms occupying 1/3 of the octahedral cavities (Fig. 3.13). Halogen atoms form bridges between pairs of metal atoms. The Townes and Dailey analysis gives for the iodine valence orbital occupancies in ScI_3 [454]: $N_s = 1.975$, $N_z = 1.831$, $N_y = 1.856$. Of the 8 electrons which might be present on the iodine atom if the structure were purely ionic, there are thus only 7.662 electrons according to the NQR estimate. A similar treatment for BiI_3 gives 7.308 electrons, and with UI_3 which crystallizes in the $PuBr_3$ type structure and contains two crystallographically independent I positions, the number of electrons on I(I) and I(II) are equal to 7.665 6 and 7.801 6, respectively.

Compounds $CrCl_3$ through $TlBr_3$ crystallize in the $AlCl_3$ lattice.

The valence angle estimates made in [447] for metal trihalides using equation (16*) of Table 1.8 range from 93 to 102°. The X-ray structural data gave values of about 90°. Thus it appears that the QCC values for metal trihalides also fit, to a reasonably good approximation, the model of partial covalent bonds having rather high ionicities and only small departure from pure p-configurations. As with metal dihalides, the inclusion of ionic contributions to the halogen atom EFGs leads to some increase of the valence angles and does not seriously affect the parameter values describing the covalent metal — halogen bonding.

Carlson et al. [456, 463—465], who have studied the ^{35}Cl NQR spectra of a large number of rare earth metal trichlorides belonging to various structural types (Table 3.13) also assume the possible presence of a small fraction of covalency in rare earth metal—halogen bonds in these compounds.

TABLE 3.13

[35]Cl NQR data on rare earth metal chlorides

Compound	T (K)	ν (MHz)	η (%)	Ref.
$PrCl_3$	4.2	4.5667	58 ± 2	463
$CeCl_3$	4.2	4.387		466
$NdCl_3$	4.2	4.729		466
$SmCl_3$	4.2	5.033		466
$LaCl_3$	4.2	4.167	50 ± 2	456a
$GdCl_3$	4.2	5.315	42.5 ± 0.1	464
$TbCl_3$	77	7.45		456b
		4.30		
$HoCl_3$	4.2	4.3071		456a
		4.3900		
$YbCl_3$	4.2	4.7903		456a
		4.8464		
$ErCl_3$	4.2	4.4566		456a
		4.5157		

Compounds having "sandwich" structure are the bismuth oxyhalides BiOX. They crystallize with a tetragonal PbFCl type lattice consisting of a central sheet of coplanar oxygen atoms with a sheet of halogen atoms on each side and the metal atoms between the oxygen and halogen atoms ([471] and refs. cited therein). Each Bi atom is surrounded by four oxygen and four halogen atoms. The [209]Bi NQR spectra are given in Table 3.14. The Bi atom asymmetry parameter values (η) are zero in accordance with the position of the latter at four-fold axially symmetric sites. None of the halogen resonances has been detected, due probably, to their highly ionic state in the crystal lattice.

In order to rationalize the bonding nature in the "sandwich" oxyhalides the adequacy of the ionic and covalent models was compared [471]. Two theoretical approaches were used; the self-consistent monopole-point dipole lattice-sum approach, and the simple MO LCAO method within the Townes and Dailey theory approximations.

The lattice sum calculation [471] was carried out over all the ions in a volume of $20 \times 20 \times 20$ unit cells, assuming the charges $+3e$, $-2e$ and $-e$ for the Bi^{3+}, O^{2-} and X^- ions, respectively. The monopole and dipolar contributions to the EFG at Bi and the X sites were calculated for this volume, using the optical polarizabilities of the halide ions and various assumed polarizabilities of the Bi^{3+} ions ($\alpha(Bi) = 2 \cdot 10^{-2}$, $4 \cdot 10^{-2}$, $8 \cdot 10^{-2}$ nm³. The results obtained when the reasonable value of α (Bi) $= 4 \cdot 10^{-2}$ was used, gave the EFG of the chloride, bromide and iodide compounds in about the right ratios, but the QCC values were only one-quarter of the experimental values.

TABLE 3.14

NQR spectra of several Group V element oxyhalides

Compound	T (K)	Isotope	Transition frequencies (MHz)				e²Qq/h (MHz)	η (%)	Ref.
			1/2—3/2	3/2—5/2	5/2—7/2	7/2—9/2			
BiOF	295	²⁰⁹Bi	11.44	22.76	34.07	45.49	272.94	0.0	471
BiOCl	295	²⁰⁹Bi	6.445	12.691	19.040	25.413	152.46	0.0	471
BiOBr	295	²⁰⁹Bi	5.001	10.004	14.976	19.931	119.58	0.0	471
BiOI	295	²⁰⁹Bi	...	...	11.404	15.210	91.26	0.0	471
Bi₃O₄Cl	77	(I)²⁰⁹Bi	20.8	25.32	39.68	53.30	321.55	25.8	472
		(II)	59.31	45.50	66.54	92.61	571.75	58.1	
Bi₃O₄Br	77	(I)²⁰⁹Bi	21.97	25.13	39.59	53.34	322.915	31.1	472
		(II)	58.04	43.39	61.92	86.63	536.87	61.7	
Sb₄O₅Cl₂		¹²¹Sb	82.48	...					
		(I)¹²³Sb	58.97	87.50	...		638.6	30.7	471
	77	¹²¹Sb	92.29	...					
		(II)¹²³Sb	70.25	91.13	...		677.5	39.6	
α-Sb₅O₇I		¹²¹Sb	112.82	159.13			563.3		479
		(I)¹²³Sb	95.56	93.60	147.99		718.0	60.2	
	77	¹²¹Sb	101.14	169.15			580.7		
		(II)¹²³Sb	77.19	99.50	156.00		740.3	40.0	
		¹²¹Sb	111.32	168.89			589.9		
		(III)¹²³Sb	90.93	98.98	156.63		752.0	51.9	
		¹²¹Sb	88.94	169.26			568.8		
		(IV)¹²³Sb	58.71	101.50	154.74		724.9	19.95	
		¹²¹Sb	89.79	171.26			574.5		
		(V)¹²³Sb	59.11	102.75	156.74		733.2	19.5	
		¹²⁷I	16.25	23.35			82.4	58.1	

A number of contributions to the EFG was neglected in this approach, among them the contributions from charges external to the ion, and those from the electronic charge distribution of the bismuth ion. The latter were considered in the MO calculations.

The model adopted [471] in the MO calculations was chosen on the basis of the structural data. According to this model the Bi atom formed strong directional bonds to the four nearest O atoms, making a pyramid with the Bi atom at the vertex, and was more weakly ionically bonded to the four nearest halogen atoms. A set of s^2p^3 hybrid orbitals of C_{4v} symmetry was then constructed, for a neutral Bi atom, with the z direction parallel to the c-axis of the unit cell. The p-orbital analysis (the d-orbital contribution was discarded) of these orbitals yields

$$e^2Qq/e^2Qq_p = (b - a)/(1 + \lambda^2) \tag{105}$$

Here a is the population of each of the four molecular orbitals pointing to the O atoms, b is the population of the molecular orbital directed toward the halogen layer; $e^2Qq_p/h \sim 1500$ MHz; λ is the undetermined coefficient, related to the angle between the Bi$-$O bond direction and the z axis

$$\lambda/(1 + \lambda^2)^{1/2} = \left(\sqrt{5} \sin \theta \cos \theta + \sqrt{2} \cos \theta\right)/\sin \theta \qquad (106)$$

Since the Bi$-$O distances and the O$-$Bi$-$O angles remain essentially constant, for the series of BiOX compounds, a and λ are also assumed constant for the four oxyhalides. Assuming further that $a > b$, because the Bi$-$O bonds are stronger than the Bi$-$X bonds, equation (105) predicts a decrease of the QCC as the halogen electronegativity decreases, i.e. b becomes greater gaining electrons in the series from iodide to fluoride, as observed. This explanation of the change in the ^{209}Bi QCC through the series is the only advantage of the Townes and Dailey approach, the disadvantages being uncertainties of the ground-state configuration, of spatial extent of the wave functions and contributions of d-orbitals [471].

The lattice sum method was concluded [471], in spite of its approximations, to be more satisfactory for yielding a basis for further refinement and testing as well as providing fair agreement with the observed trends in the QCC values.

(ii) Other layer oxyhalides of group V elements

In addition to the A^{V}OX compounds which are known to be the products of 1 : 1 composition formed in the systems A$_2^V$O$_3$ + A^{V}X$_3$, several other oxyhalides of various composition, formed in these systems, have been studied by NQR. Their spectra are also given in Table 3.14. The structure of both the listed antimony oxyhalides are available.

The compound of 5 : 2 composition (Sb$_4$O$_5$Cl$_2$) is built up from two types of distorted tetrahedra ψ-SbO$_3$, with the lone pairs of the antimony electrons at one corner. The coordination polyhedra share corners to form infinite [Sb$_4$O$_5$]$^{2+}$ layers parallel to the b plane, the Cl atoms being located between the layers [481]. They are in ionic state, considering the failure to observe their resonances in NQR spectra. In the spectrum of Sb$_4$O$_5$Cl$_2$, the antimony QCC values (as well as the η values) (Table 3.14) are not very different from those of valentinite Sb$_2$O$_3$ (690.3 MHz and 36.0%, respectively [365]) which is consistent with a similar type of coordination environment around the Sb atom in both compounds.

The antimony(III) oxide iodide Sb$_5$O$_7$I (7 Sb$_2$O$_3\cdot$1 SbI$_3$) is known [482a] to form 9 polytypes. The polytype 2MC of low-temperature phase α-Sb$_5$O$_7$I possesses ferro-elastic properties [482b]. Its crystal lattice is formed by Sb$_2$[Sb$_3$O$_7$]$^+$ layers connected by intermediate iodine atoms which are located at the centre of a slightly distorted cuboctahedron of Sb atoms. The nearest coordination environment of each Sb atom consists of three oxygen atoms

making a nearly equilateral triangle with the antimony atom above the base. There are altogether 5 crystallographically independent positions for the Sb atoms in the crystal of α-Sb_5O_7I [482b]. Three of them (I—III in Table 3.14) which form the structure units $[Sb_3O_7]^{5-}$ (Fig. 3.14) have, apart from the three nearest oxygen atoms, two more distant (0.39 nm) iodine atoms. The other two Sb atoms (IV and V in Table 3.14) are bound to three oxygen atoms above and below the $[Sb_3O_7]^{5-}$ units and have, in addition, three more distant (~ 0.39 nm) iodine atoms. This is readily reflected in the Sb atom asymmetry parameter values thus showing high sensitivity to the site symmetry, of the quadrupole atom. The η values are also known to be very sensitive to the external charge contribution. The QCC values at the Sb atoms seem to be less sensitive to these factors, as confirmed by comparison of the [121,123]Sb QCC values at the positions (I)—(V) in Table 3.14.
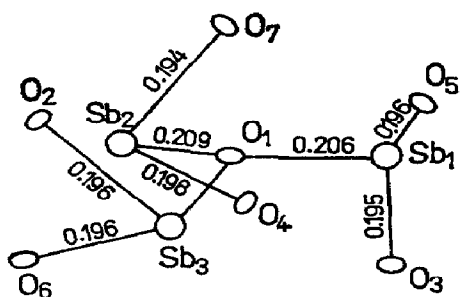
Figure 3.14 The structural units $[Sb_3O_7]^{5-}$ established by X-ray in α-Sb_5O_7I [482b].

Table 3.14 also gives the [209]Bi NQR spectra of two bismuth(III) oxyhalides Bi_3O_4X ($4\,Bi_2O_3 \cdot 1\,BiX_3$) of unknown structure. The X-ray powder diffraction analysis [483] only determined the monoclinic symmetry of crystal lattice for Bi_3O_4Cl and rhombohedral symmetry for Bi_3O_4Br as well as the unit cell dimensions for both compounds. Some structural predictions may, however, be made on the basis of NQR.

First, no halogen resonances have been detected in either compound. This suggests the presence of ionic halogens in the crystals, as in the known oxyhalides with layer structure (A^VOX, $A_4^VO_5X_2$).

Second, the [209]Bi NQR spectra of both compounds establish two crystallographically independent Bi atoms with coordination environments considerably different from each other. The Bi(I) position is characterized by relatively lower QCC and η values than Bi(II). Note also that the QCC and η values at Bi(I) are practically insensitive to the substitution of chlorine for bromine. We can therefore expect that no halogen atoms enter the nearest environment of the Bi(I) atoms and that the site symmetry of the latter is higher than that of the Bi(II) atoms' environment.

Third, the QCC and η values for Bi(II) are not greatly different from those in α-Bi$_2$O$_3$ (Bi^1:556.6 MHz, $\eta = 10.0\%$; Bi^2: 483.2 MHz, $\eta = 41.3\%$ [365, 404]). They decrease from chloride to bromide, so providing evidence for the presence of Bi(II)—halogen contacts in the structure of both compounds.

We can note in summary that as a whole the picture of the chemical bonding in layer compounds discussed in this section, is not yet definitive. This is largely accounted for by the compounds being more complicated objects for theoretical investigation than purely ionic or molecular crystals. They contain in the crystal lattice both coordination polyhedra formed by strong directional bonds and yet are linked with each other, into polymer patterns, through atoms, or groups of atoms, bearing considerable electric charges.

(iii) Layer oxides of Group V elements; double oxides and related compounds

All the layer compounds listed in Table 3.15 although they belong to various structural types, have a crystal chemistry much in common with each other. They can be described as double oxides $A^{III}A^VO_4$ containing the central atoms A in two oxidation states, $+3$ and $+5$. These central atoms may be the elements of the same group or may even be the atoms of the same element, as in case of Sb_2O_4.

The latter compound is known to exist in two crystal modifications, α and β. In β-Sb$_2$O$_4$ the crystal lattice of monoclinic symmetry contains Sb^V—O octahedra sharing corners, to form corrugated layers parallel to (100). Adjacent sheets are joined by the columns of Sb^{III} atoms trapped between them [484] (Fig. 3.15). The Sb^{III} atoms have a one-sided four-fold coordination of oxygen atoms, showing the presence of a stereochemically active lone pair.

In orthorhombic α-Sb$_2$O$_4$ the Sb atoms are also present in two oxidation states. The nearest environment of both types of antimony atoms is similar in α- and β-Sb$_2$O$_4$, the differences between the two forms consisting of relatively stronger distortion of the Sb^V-octahedra in the β-form [485] (Fig. 3.16).

All the features established by the structural studies for α- and β-Sb$_2$O$_4$ are definitely confirmed by their NQR spectra (Table 3.15). The latter gives, in addition, some support to the opinion reported in [486] that α- and β-Sb$_2$O$_4$ are individual phases with slightly different stoichiometry, β-Sb$_2$O$_4$ being an oxygen-deficient phase with respect to α-Sb$_2$O$_4$. In agreement with this report, the [121.123]Sb resonances in the NQR spectrum of α-Sb$_2$O$_4$ appeared to be abnormally wide (Fig. 3.17). This might be associated with a statistically disordered distribution of the excess oxygen atoms over the crystal lattice of α-Sb$_2$O$_4$.

A final answer to question about the nature of the difference between α- and β-Sb$_2$O$_4$ must however await for the reliable data on the range of thermodynamic stability of these compounds.

The structure of α-Sb$_2$O$_4$ appears to be typical for many Group V element

TABLE 3.15

NQR spectra of several Group V element oxides and related rare earth niobates at 77 K

Compound	Isotope	Oxidation state	Transition frequencies (MHz)				e^2Qq/h (MHz)	η (%)	Ref.
			1/2—3/2	3/2—5/2	5/2—7/2	7/2—9/2			
α-Sb$_2$O$_4$	^{121}Sb	(III)	72.3	138.5			464.8	18.5	473,
	^{123}Sb		47.3	83.2	126.6		592.8		474
	^{121}Sb	(V)	21.9	41.6			139.8	20.4	
	^{123}Sb		...	25.1	38.2		179.1		
β-Sb$_2$O$_4$	^{121}Sb	(III)	77.1	148.4			497.8	17.4	
	^{123}Sb		50.0	89.3	135.6		634.9		473
	^{121}Sb	(V)	22.0	43.7			145.9	6.6	
	^{123}Sb		...	26.5	39.9		186.1		
SbPO$_4$	^{121}Sb	(III)	76.605	151.530			505.980	9.25	474
	^{123}Sb		47.499	91.712	138.066		644.979		
SbTaO$_4$	^{121}Sb	(III)	80.18	142.75			484.91	31.4	474,
	^{123}Sb		57.54	84.60	131.14		618.11	31.3	475
SbNbO$_4$	^{121}Sb	(III)	81.6	142.5			484.5	34.0	475
	^{123}Sb		...	84.3	131.5		618.9	34.0	
BiNbO$_4$	^{209}Bi	(III)	41.871	42.631	67.247	91.064	552.74	37.0	475
BiTaO$_4$	^{209}Bi	(III)	41.946	42.654	67.197	91.080	555.16	37.0	475
BiVO$_4$	^{209}Bi	(III)	21.3	14.5	16	22	149.5	90.1	476
LuNbO$_4$	^{175}Lu	(III)	80.1	69.6	108.7		536.2	71.2	477
LaNbO$_4$	^{139}La	(III)	5.66	4.98	7.79		38.4	70.0	478
	^{93}Nb	(V)	4.02	7.40	11.18	14.92	100.1	9.0	478
YbNbO$_4$	^{93}Nb	(V)	6.4*)	6.4*)	10.12	13.73	101	38.0	478

*) Calculated frequencies.
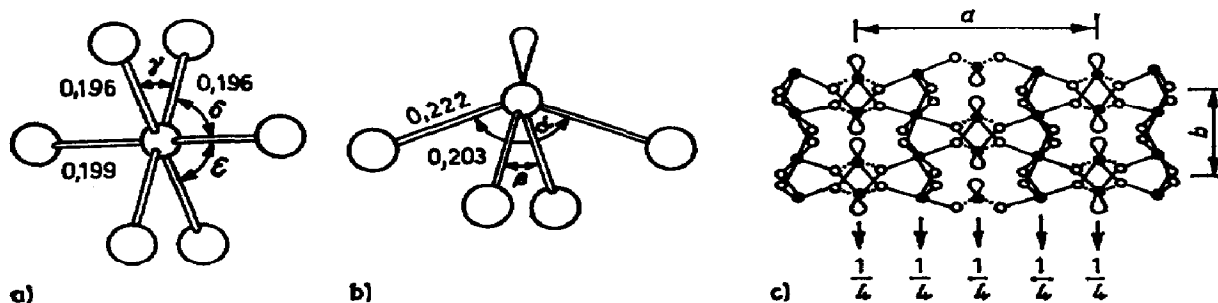
Figure 3.15   Atomic arrangement in β-Sb$_2$O$_4$ [484];
a) the antimony(V) coordination polyhedra ($\gamma = 88.7°$; $\delta = 89.8°$; $\varepsilon = 95.7°$);
b) the antimony(III) coordination polyhedra ($\alpha = 148.1°$; $\beta = 87.9°$);
c) [001] projection showing corrugated layers of Sb^V octahedra with Sb^{III} columns trapped between them.

double oxides. According to [487] the compounds $SbNbO_4$, $SbTaO_4$ and low-temperature orthorhombic forms of $BiNbO_4$ and $BiTaO_4$ are isostructural with α-Sb_2O_4, forming family of stibiotantalite structural type [488]. Structures of this type are built up from corrugated sheets of A^V—O (A^V = Sb, Nb, Ta) distorted octahedra linked by sharing corners, and running parallel to the
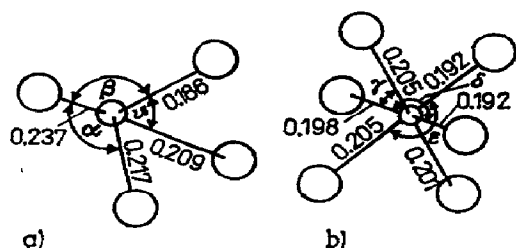
Figure 3.16   Coordination of the Sb atoms in α-Sb_2O_4 [485]:
a) the antimony(III) coordination polyhedra ($\alpha = 145.5°$; $\beta = 82.5°$; $\theta = 78.6°$);
b) the antimony(V) coordination polyhedra ($\gamma = 87.1°$; $\delta = 175.6°$; $\varepsilon = 176.6°$).

(001) plane. Adjacent sheets are joined by A^{III} atoms (A^{III} = Sb, Bi). The antimony phosphate $SbPO_4$ crystallizes in a monoclinic lattice [489] and is not isostructural with the compounds of the stibiotantalite structural type. It however also forms layers of composition $SbPO_4$, with the Sb atoms coordinated on one-side to four oxygen atoms, in a manner very similar to the coordination of the Sb^{III} atoms in the stibiotantalite compounds and in α-Sb_2O_4.
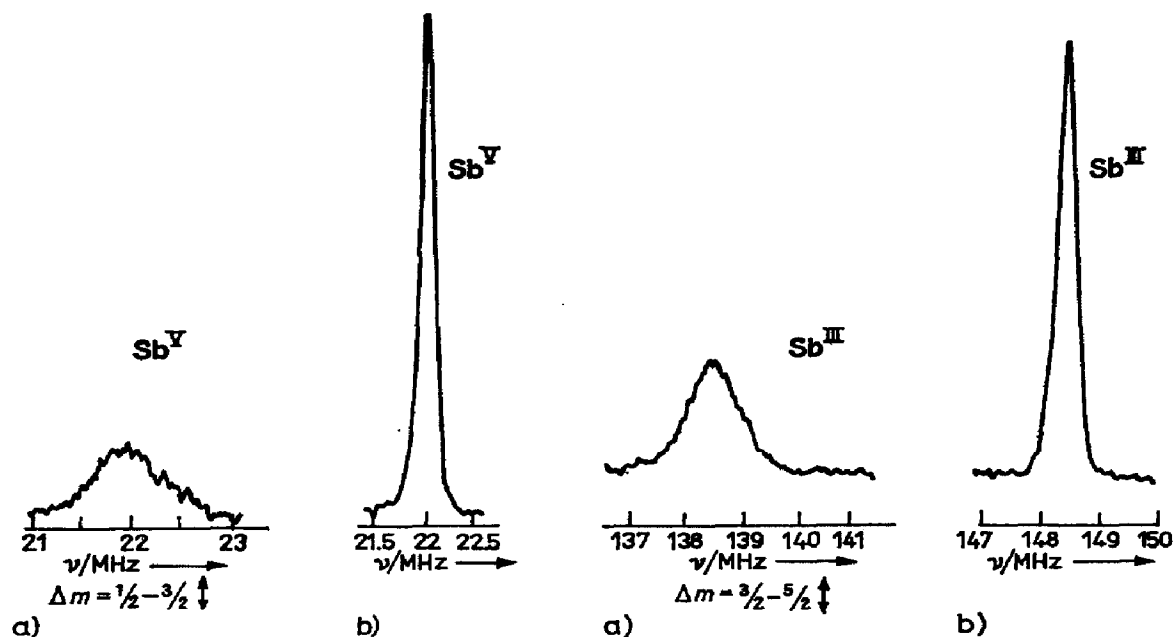
Figure 3.17 ^{121}Sb resonances in α-Sb_2O_4 (a) and β-Sb_2O_4 (b) [473].

The similarity of the coordination environment of the A^{III} atoms in the compounds enumerated, is reflected in the relatively small scatter of the QCC values at the A^{III} site in their NQR spectra (Table 3.15).

The spectroscopic parameters, however, change abruptly when the compounds of similar composition crystallize in fergusonite structural type. $BiVO_4$ (purcherite) and rare earth niobates are known to belong to this type [490, 491]. The decrease in the [209]Bi QCC was observed in $BiVO_4$ with respect to the [209]Bi QCC in $BiNbO_4$ and $BiTaO_4$ (Table 3.15) compatible with the difference between the two structural types.

The structure of purcherite can easily be obtained from the "sandwich" structure of BiOCl. The substitution of one half the number of Bi atoms with vanadium and all the Cl atoms with oxygen and a shift of alternate layers parallel to the b' axis, leads to the structure of purcherite [490]. In the latter, vanadium atoms are not in an octahedral environment as are the A^V atoms in the stibiotantalite structure. They are bonded to only four oxygen atoms, the tetrahedral environment being considerably distorted. The Bi atoms have two pairs of short Bi — O bonds (0.220 and 0.231 nm) and two pairs of long bonds (0.254 and 0.273 nm in their nearest environment, analogous to that in BiOCl. This accounts for the similarity of the [209]Bi QCC magnitudes in $BiVO_4$ and BiOCl as well as for the decrease with respect to the corresponding magnitudes in $BiNbO_4$ and $BiTaO_4$ (Tables 3.14 and 3.15).

In general, the atoms at the A position in the compounds ABO_4 with the fergusonite type of structure are characterized by considerable ionicity. The EFG at this site, although not large, is nevertheless important. It is associated with the internal electric fields usually present in the compounds related to ferroelectric materials, and responsible for the anomalies of dielectric properties in these compounds [477].

Many of double oxides listed in Table 3.15 reveal the physical properties valuable from the practical viewpoint. Thus $BiVO_4$ is antiferroelectric with a Curie temperature $T_c = 570\,^\circ C$ ([476] and refs. cited therein). Ferroelastic phase transitions have been detected in rare earth orthoniobates ([477, 478] and refs. cited therein). Ferro- and antiferroelectric properties were established in a number of compounds with the stibiotantalite structure ([492] and refs. cited therein).

Some other oxygen-containing compounds studied by NQR and important in applied fields are listed in Table 3.16. They belong to perovskite, perovskite-like and other structural types, characterized by layer or three-dimensional networks.

Ferroelectric ABO_3 crystals with a perovskite structure attracted considerable attention. An extended literature, is available concerning the phase transitions, the crystal modifications, NMR measurements, calculations of spontaneous polarization and internal electric fields (see, for example, the periodic "Ferroelectrics", Gordon and Breach Science Publishers Ltd, Great

TABLE 3.16

NQR spectra of double oxides (RT room temperature)

Compound	Isotope	T (K)	Transition frequencies (MHz)				e^2Qq/h (MHz)	η (%)	Ref.
			1/2—3/2	3/2—5/2	5/2—7/2	7/2—9/2			
LiNbO$_3$	^{93}Nb	77	0.988	1.958	2.942	3.950	23.516	3.0	496,
		298	0.924	1.842	2.763	3.685	22.10	3.0	497
LiTaO$_3$	^{181}Ta	77	19.2	37.9	56.9	...	266	5.0	478
NaNbO$_3$	^{93}Nb	RT					19.7	82.0	498
KNbO$_3$	^{93}Nb	298	3.03	2.085	2.527	3.648	23.12	80.6	499
		77		1.335	2.004	2.674	16.0	0.0	
Bi$_4$Ti$_3$O$_{12}$	^{209}Bi	77	32.24	31.16	48.92	66.49	404.3	40.0	500
			...	19.67	30.60	40.83	245.9	20.3	
Bi$_4$Si$_3$O$_{12}$	^{209}Bi	RT	19.6	39.2	59.0	78.4	470.4	0.0	501
Bi$_4$Ge$_3$O$_{12}$	^{209}Bi	RT	20.4	40.6	61.4	81.8	490.8	0.0	501
		77	21.18	42.31	63.47	84.61	507.8	1.1	
Bi$_{12}$SiO$_{20}$	^{209}Bi	77	34.29	56.02	85.95	114.77	690.3	15.4	500
Bi$_{12}$GeO$_{20}$	^{209}Bi	77	34.22	55.74	85.53*	114.34*	687.2	15.5	500
Bi$_2$WO$_6$	^{209}Bi	77	35.03	34.99	55.11	74.75	453.8	38.1	
			37.02	34.62	54.19	73.82	449.4	42.0	
Bi$_2$Mo$_3$O$_{12}$	^{209}Bi	77	20.68	35.9	54.7	73.05	438.8	12.5	
			28.74	26.5	41.4	56.45	343.9	42.9	
	^{209}Bi	300	33.7	25.7	37.3	52.0	321.1	59.4	

*) Calculated frequencies.

Britain). The NQR data provide experimental values for the internal electric field gradients and are very important in this respect. They may serve as a test for the choice and refinement of structure and bonding models thus shedding light on the mechanism of ferroelectricity in the compounds.

Discussion of these problems is however beyond the scope of this book, and we shall only mention here that according to most of the results the oxygen containing perovskite compounds are essentially ionic crystals. The calculation of the internal electric fields in the rhombohedral phase KNbO$_3$ [493] within an electrostatic point charge and dipole model leads to correct values for the QCC at the constituent atoms in the crystal.

Some members of a less numerous family of halogen-containing perovskites ABCl$_3$ are also ferroelectrics (CsGeCl$_3$, CsPbCl$_3$, etc.). Calculation of the EFG at their atoms within the electrostatic model, [494, 495] leads to the conclusion that the EFG at the chlorine site is determined mainly by contributions from external point charges, those from the dipolar polarizability of the ions being negligible. The overlap between the electron shells of the ions is also important in cubic perovskites since it determines some details of the quadrupole inter-

action under high hydrostatic pressure and during structural phase transitions [495].

The remaining compounds of Table 3.16 are represented by mixed bismuth oxides.

The compounds $Bi_4Ti_3O_{12}$, $Bi_{12}SiO_{20}$ and $Bi_{12}GeO_{20}$ show remarkable piezoactivity [500, 502]. According to [502] $Bi_{12}GeO_{20}$ crystallizes in a cubic lattice (I23) with the unit cell dimension $a = 1.015$ nm. The germanium atoms occupy the geometrically regular tetrahedral sites ($Ge-O = 0.172$ nm). The bismuth atoms are heptacoordinated, five oxygen atoms forming an incomplete octahedral arrangement, with the $Bi-O$ distances ranging from 0.208 to 0.264 nm and the two remaining O atoms being electrostatically coordinated from the side of a vacant octahedral apex (0.308 and 0.317 nm). The crystal is strongly optically active and photoconductive in the visible range. Low, room-temperature elastic wave losses have been reported as well as low propagation wave velocities ([502] and refs. cited therein). The isostructural $Bi_{12}SiO_{20}$ also finds an application in opto- and acoustoelectronics. The relationship between the physical properties of the compounds and NQR parameters have been studied by various groups [503, 504].

$Bi_4Ti_3O_{12}$ crystallizes in an orthorhombic lattice [505] which contains the $[Bi_2O_2]^+$ layers alternating with the perovskite-like double layers $[Bi_2Ti_3O_{10}]^{2-}$ corresponding to a hypothetical $BiTiO_3$ perovskite structure. In agreement with the X-ray data, the ^{209}Bi NQR spectrum of $Bi_4Ti_3O_{12}$ shows two sets of lines (Table 3.16). The set with the higher QCC value was assigned [500] to the Bi atoms in the $[Bi_2O_2]^{2+}$ layers. The Bi atoms occupying the spaces in the $Ti-O$ octahedral framework of the $[Bi_2Ti_3O_{10}]^{2-}$ units seem to give rise to a lower frequency set of resonances.

Similar structural patterns have been established by X-ray analysis for several other mixed bismuth oxides. $[Bi_2O_2]^{2+}$ layers alternating with sheets of oxygen polyhedra, formed by atoms of the second element (Ge, W), were found in $BiGeO_5$ [506] and $Bi_2W_2O_9$ [507]. Based on ^{209}Bi NQR spectra (Table 3.16) similar layers can be expected in Bi_2WO_6 and $Bi_2Mo_3O_{12}$.

The structures of $Bi_4Ge_3O_{12}$ and $Bi_4Si_3O_{12}$ (euletine) are different from that of $Bi_4Ti_3O_{12}$. According to [508] euletine crystallizes in a cubic lattice I43d ($a = 1.03$ nm). Each Bi atom is coordinated to a distorted octahedron of oxygen atoms, three close neighbours located at 0.215 nm and three more at 0.262 nm. The Bi atoms link discrete SiO_4 tetrahedra. The ^{209}Bi NQR spectra provide evidence for a close structural resemblance between $Bi_4Si_3O_{12}$ and $Bi_4Ge_3O_{12}$. Based on NQR spectral data, it is concluded [501] that the purely ionic model is inadequate to describe the EFG at the Bi site in these compounds.

Summarizing Chapter 3 we have to note that not only double oxides possess valuable practical properties. The majority of the chalcogenide polymers discussed here, also show interesting physical properties and are widely used in various fields. Thus, Sb_2S_3 is the commercial source of antimony and is a high-resistance

semiconductor. It displays ferroelectric properties below 420—490 K ([508] and refs. cited therein). Sb_2Se_3 is also a semiconductor. Lorandite ($TlAsS_2$) is a promising semiconducting pyro- and ferroelectric. Orpiment (As_2S_3) is used in radio and television engineering and in IR optics [509] on account of its high dielectric properties. Proustite (Ag_3AsS_3) and pyrargyrite (Ag_3SbS_3) are semiconductors, transparent in a wide range of the IR spectrum [510]. They show nonlinear optical properties and belong to pyro-, piezo- and ferroelectric materials [511—513]. Phase transitions in proustite and pyrargyrite have been extensively studied using NQR ([514, 515] and refs. cited therein). With the help of the latter, first order phase transitions have been detected in smithite ($AgAsS_2$) [414, 435] and in the selenium analogue of lorandite ($TlAsSe_2$) [407].

It is evident however that one has to consider a good deal of crystallo-chemical information in order to discover properties of interest and to specify their nature. Our intention was to show, in this respect, that nuclear quadrupole resonance is an effective tool for crystal chemistry investigation of great importance among methods of material research.

A further extension for NQR studies in the field of inorganic polymers and ionic compounds is expected for two reasons. First, it would facilitate and improve experimental techniques in this area of considerable complexity, and second, it would contribute to the development for industry of a larger number of materials with valuable physical properties.

CHAPTER 4

NQR APPLICATIONS TO MATERIALS RESEARCH

Here we give a short review of some less common applications of NQR spectroscopy. They bring to light methods which are not widely known but can give diverse subtle information in various aspects of materials research.

A. IMPURITIES AND MIXED CRYSTALS

NQR was successfully used by several groups, for the study of problems concerned with compounds possessing imperfect lattices, such as compounds with impurities, mixed crystals, etc. They studied the distribution of the impurities over the crystal and their interaction with atoms of the matrix.

The influence of various impurities on the NQR spectroscopic parameters of a large number of Group V element chalcogenides has been examined [516]. We recall that binary compounds of the $A_2^V B_3^{VI}$ type contain two crystallo-chemically different coordination polyhedra AB_3. Comparison of the variations in the spectroscopic parameters of these two groups in the presence of impurities showed that the latter affect them differently. The effect of each type of impurity on the NQR parameters is quite specific [516]. The spectroscopic variations are usually related to the form in which the impurity is present in the crystal lattice; as an inclusion phase in lattice vacancies, in the form of isomorphous substituent, localized in interlayer spaces, etc. One can analyze the impurity distribution by comparing the spectra of crystals with impurities to the spectra of pure crystals.

The introduction of small quantities of an impurity or a non-stoichiometric ion, may, under certain conditions, permit the isomorphous substitution of atoms of a given type in the crystal lattice. In this case, broadening of the NQR lines is observed. NQR study of solid substitution solutions $Sb_2S_3 + Bi_2S_3$ [517] reveals broadening of the $^{121,123}Sb$ resonances by up to several MHz, on introduction of Bi_2S_3 in concentrations below 10 mol%.

Proustite Ag_3AsS_3 and pyrargyrite Ag_3SbS_3 are known to display limited isomorphism. Natural samples of these minerals usually contain a small

amount of isomorphic atoms (Sb or As). The [75]As NQR signals were observed [409] from impurity arsenic atoms in pyrargyrite crystals where the content of the latter did not exceed 2%. NQR showed that the impurity affected the crystal lattice of the pyrargyrite matrix, due presumably to the difference in the dimensions of the As and Sb atoms. There is considerable broadening of the [75]As atom NQR line (300 kHz) compared to the line width in the standard proustite sample (24 kHz). In the sample under study, the [75]As NQR signal was observed [409] at a frequency slightly exceeding the frequency of the same signal in the standard Ag_3AsS_3 sample (67.58 against 67.31 MHz at 77 K). The small frequency shift was interpreted as the retention of symmetry in the vicinity of the As atoms in the pyrargyrite matrix, characteristic of isomorphic systems.

Direct observation of NQR from impurity atoms is, however, rare on account of their small concentration. It is more reasonable to take advantage of the sensitivity of NQR to crystallochemical changes produced by impurities in the matrix.

An effective approach to the study of the distribution of isomorphically substituted impurities consists of the systematic analysis of spectroscopic changes produced in the matrix, by continuous variation of the relevant sources of broadening. Mixed crystals of the A_xB_{1-x} type provide an example of such a model. The NQR spectrum of a molecule (atom) B reflects the influence of impurity molecules (atoms) A which can be treated as point defects if x is small.

In this respect the results of the above NQR study of the solid solution $Sb_2S_3 + Bi_2S_3$ [517] is worth discussing in more detail. Changes in the [121,123]Sb NQR spectra were observed as the relative Bi_2S_3 content varied. A dramatic broadening of the antimony resonances occurred even at low (under 10 mol %) concentration of the added second component. With an increase in the amount of Bi atoms, new satellites appeared in the vicinity of the undisturbed antimony resonances, dependent on the symmetry of the nearest environment and concentration ratio, (Fig. 4.1). The whole family shifted gradually with varying composition. The relative intensities of the multiplet components were also dependent on the composition of the solid solution. Similar features were observed in the NQR spectra of solid solutions formed by molecular crystals of halosubstituted benzenes ([518] and refs. cited therein). The composition dependent spectroscopic changes are determined mainly by electrostatic interactions. Short range interactions are responsible, together with symmetry and packing factors, for splitting of the spectroscopic multiplets, while line broadening reflects uncertainty in the mutual arrangement of the atoms. The concentration dependent shifts of the whole family of resonances are accounted for by the change in charge distribution in the vicinity of the resonance atoms via the change of packing coefficients. These conclusions do not, of course, explain all the diversity of experimental observations reported in the numerous publications devoted to this interesting but very complicated problem.

Upon introduction of certain other impurities (Cu, Zn) into Sb_2S_3 or Bi_2S_3, the spectroscopic parameters provide evidence that the impurities occupy vacancies (interstitial sites) in the lattice [516]. In this case the NQR lines are not broadened to such a degree as they were in the case of isomorphous substitution. These impurity sites do not seriously affect the crystal lattice of the matrix. The spectroscopic parameter most sensitive to the latter type of impurity is the spin—spin relaxation time T_2 [516]. An increased content of impurity may also lengthen the spin lattice relaxation time T_1.

Consider as an example, the NQR study of the chemisorption ability of antimonite (Sb_2S_3) [519]. The change in the T_2 ^{121}Sb value (transitions $\Delta m = 5/2 - 3/2$ were identified for both Sb positions) due to the action of chemisorbed material was recorded as a criterion of the chemisorption ability. It was
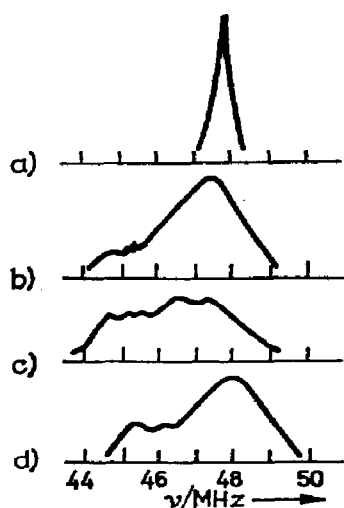
Figure 4.1 ^{121}Sb NQR line in solid solutions of $Sb_2S_3 + Bi_2S_3$ of various compositions [517].

a) Sb_2S_3; b) 10 mole % of Bi_2S_3; c) 25 mole % of Bi_2S_3; d) 80 mole % of Bi_2S_3.

concluded that cations shortened the T_2 value in the sequence Cu > Ag > Zn > Pb > xan[1]). The change of T_2 is greater for Sb atoms at position (I) with the lower coordination number and smaller asymmetry parameter (Table 3.9). Based on these observations one may conclude [519] that the chemisorbed species show a tendency to concentrate in the vicinity of the Sb^I atoms. The centres of chemisorption are reported to be of electron-donor nature. Sulphur atoms possessing lone pairs of electrons directed to the van der Waals (inter-ribbon) space of the structure, are responsible for the sorbent—sorbate donor—acceptor interactions. As a result of chemisorption, the concentration of current carriers increases, thus affecting the relaxation time T_2.

---

[1]) Xan = xanthogenate.

13*

Finally, impurities can localize in structural defects such as dislocations, intercrystallite boundaries, etc. Dislocation defects have been established in all the minerals discussed here. In low-symmetry crystals containing several inequivalent coordination groups of the same element, regions of dislocation distortions develop preferably within the groups of lower symmetry ([516] and refs. cited therein). Dislocations are the most dynamic of the defects, capable of displacement, closing, degeneration [524]. They can interact with impurities attracting them and forming concentration clouds, thus blocking the defect regions. The interaction is governed by the Coulomb forces between impurity atoms and dislocation fields. All the binary $A_2^V B_3$ chalcogenides, containing two types of coordination group (AB_3 and AB_{3+n}) of different symmetry, show distinctly differing line widths in their NQR spectra, assigned to positions A(I) and A(II). The resonances assigned to the A(II) atoms at groups of lower

TABLE 4.1

NQR frequencies ν ($\Delta m = 1/2-3/2$), asymmetry parameters η and linewidths $\Delta\nu$ in binary Group V chalcogenides

Compound	Coordination group	T (K)	Isotope	ν (MHz)	$\Delta\nu$ (kHz)	η (%)	Ref.
As_2S_3	I			71.94	100	34.3	405
	II	300	^{75}As	69.55	140	37.4	406
As_2Se_3	I			60.25	150		
	II	77	^{75}As	56.07	270		407
Sb_2S_3	I			47.70	70	0.8	
	II	77	^{121}Sb	42.98	120	37.7	403
Sb_2Se_3	I			40.91	35	0.0	
	II	77	^{121}Sb	34.98	50	41.8	404
Bi_2S_3	I			14.25	70	3.0	
	II	77		21.50	150	88.9	404

symmetry, were always considerably wider than those assigned to A(I) (Table 4.1, Fig. 4.2). The low-frequency line in the ^{75}As NQR spectrum of natural orpiment (α-As_2S_3) was considerably wider than the high-frequency line. It also remained wider in the spectrum of artificial α-As_2S_3 (Fig. 4.3) obtained from highly pure glass under the action of high pressure (40−70 kbar) and temperature (300−400 °C) [525]. This seems to be in agreement with the fact that the defects are intrinsic in crystal lattices so that they often cannot be removed by the usual methods such as annealing, for example [516, 524].

In the [209]Bi NQR spectra of α-Bi_2O_3, doped with boron, the resonances assigned to the lower symmetry polyhedra also suffered considerably more broadening due to doping, than the other lines [526]. This observation is explained by the selective distribution of dopant boron atoms over the α-Bi_2O_3 host lattice, suggesting that dopant atoms predominantly localize in the vicinity of the lower symmetry bismuth polyhedra [526].
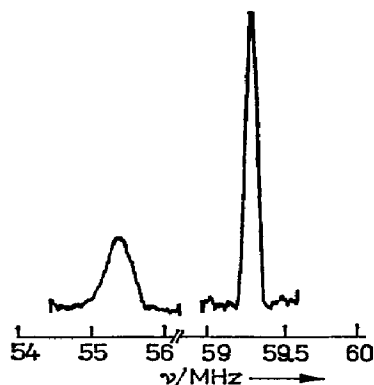
Figure 4.2   [75]As NQR signals in As_2Se_3 at room temperature.
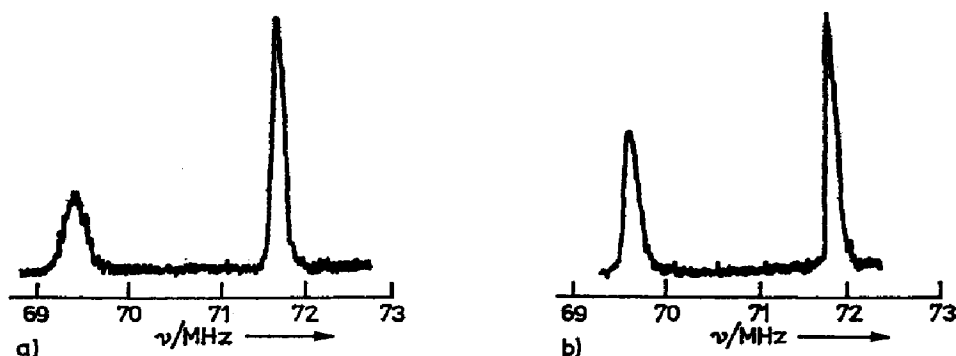
Figure 4.3   [75]As NQR spectra of two α-As_2S_3 samples at room temperature [525]
a) a sample of natural orpiment;
b) a sample crystallized from glass at high pressure and temperature.

B. NQR IN VITREOUS MATERIALS

The improvement of experimental technique and in particular of pulse instrumentation has opened for investigation a vast field of problems related to non-crystalline solids with the help of NQR. A series of pulsed [75]As NQR studies was carried out on glassy As_2S_3 and As_2Se_3 [520 — 522]. It is a difficult problem to detect NQR signals in glassy substances. The magnitude of the EFG at a certain atom is highly sensitive to the nearest atomic environment. In a glass,

the configuration and location of the neighbouring atoms vary from site to site thus producing considerable line broadening. The half width of the ^{75}As resonance observed in glassy As_2S_3 was ~ 3.5 MHz. In the As_2Se_3 glass, the halfwidth was ~ 6 MHz (see ref. [521]). The pulse technique has a distinct advantage over the continuous-wave (c.w.) method in detecting such wide NQR lines. We have mentioned in Chapter 1 that c.w. methods are unable to detect NQR signals in imperfect samples because it is impossible to use field or frequency modulation equal in magnitude to the line width, if the latter is as broad as, for example, in vitreous As_2S_3. The results obtained for vitreous samples were compared to ^{75}As NQR measurements in crystalline As_2S_3 and As_2Se_3. They provide deeper insight into the structure of glassy compounds. The most important conclusion is concerned with the fact that the local order in these two glasses is remarkably well preserved. The basic structural unit in glassy As_2X_3 (X = S, Se) is, as in the corresponding crystals, a trigonal AsX_3 pyramid. However, unlike in the crystals, this pyramid is characterized not by a fixed, but by an average $X - As - X$ pyramidal apex bonding angle $\Delta\alpha$ due to the scatter of its value over the sample volume. From the results of simple MO calculations, and measurements of the width of the ^{75}As NQR absorption spectrum, the striking conclusion arises, that in glassy As_2S_3, the average apex bonding angle $\Delta\alpha$ varies statistically throughout the glass, within the rather narrow limit from ± 0.5 to $\pm 1°$. For glassy As_2Se_3, where the data are less accurate, the corresponding $\Delta\alpha$ value is approximately $\pm 3°$.

NQR results in vitreous As_2S_3 and As_2Se_3 were best interpreted by assuming that layers are still retained in the amorphous phases of these materials.

Measurements on unannealed and strain-relieved As_2Se_3 indicated that at least some of the greater deviation in α over a long range than that which occurs locally, can be attributed to the presence of macroscopic strains [522]. The crystal chemistry of the amorphous state attracts considerable attention, being at the same time the subject of debate. As an example it is reported [520 b] that X-ray and neutron-diffraction data on glassy SiO_2, have variously been interpreted to support a structural arrangement based either on a random network of SiO_4 tetrahedra or on a more ordered network of distorted regions retaining substantial elements of the crystalline order.

Conclusions [520 − 522] based on the first NQR results of vitreous As_2S_3 and As_2Se_3 are therefore of fundamental importance in clarifying some structural aspects of vitreous inorganic compounds.

As_2S_3 and As_2Se_3 are highly valuable materials possessing the useful property of existing in both the crystalline and amorphous state. Only one other inorganic compound with such dual properties has been studied to our knowledge using NQR [523]. Pyrophosphorylchloride $P_2O_3Cl_4$ which is a liquid at room temperature, forms a transparent glass when cooled to liquid nitrogen temperature. It is possible to observe in the glassy compound the ^{35}Cl NQR signal which was naturally very broad (under ~ 1 MHz). Repeated melting and freezing

of the sample, followed by recording the NQR spectra, led to gradual crystallization of pyrophosphorylchloride. The process, in all its stages, was reflected distinctly in the NQR spectra (Fig. 4.4). Two crystalline modifications, one being metastable, have been identified in the crystalline phase [523].

Concerning to amorphous SiO_2, the latest results on the ^{17}O NMR study of this compound [552] indicate significant local order in the material. Quadrupole parameters (QCC and η) for the oxygen site, have been obtained from a computer simulation. The Townes and Dailey calculation related the quadrupole parameters to the charge density in the oxygen orbitals. This was consistent with the Si—O—Si bond angle ($\Delta\alpha$) having a distribution of values $130° \leqq \Delta\alpha \leqq 180°$.
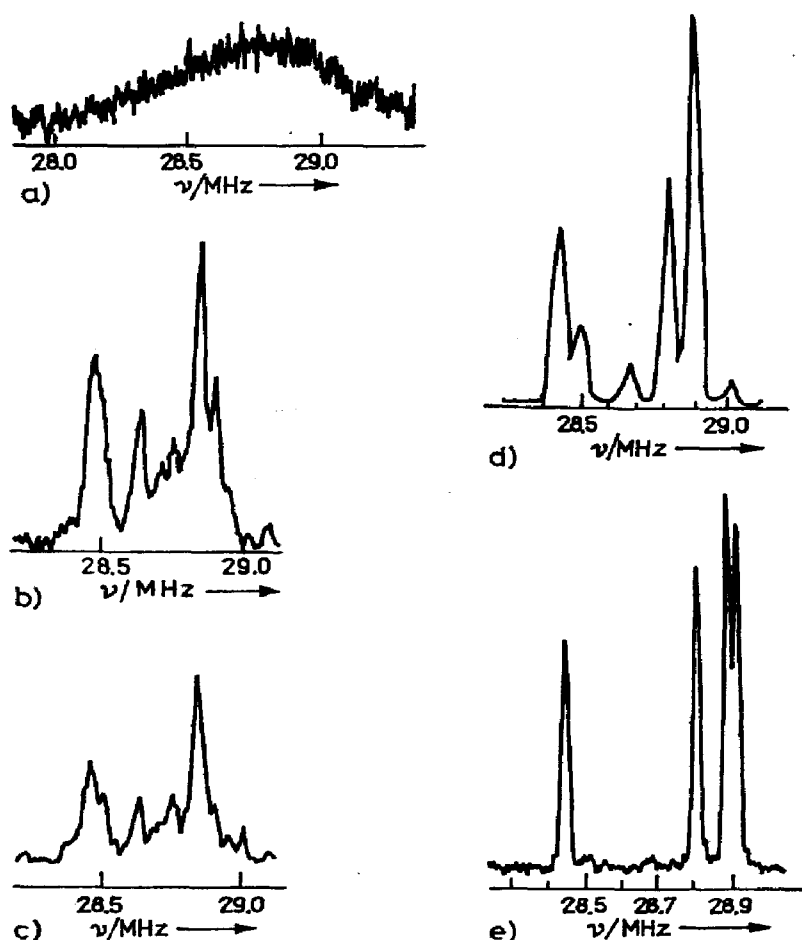
Figure 4.4   Change of the ^{35}Cl NQR spectrum of glassy $P_2O_3Cl_4$ (a) in the course of crystallization of the compound (b)—(e) [523]. ^{35}Cl resonances of two crystal modifications are seen in the spectrum (d).

C. NQR AS METHOD FOR PHYSICO-CHEMICAL ANALYSIS

The use of NQR for the study of the $Na_2S + Sb_2S_3$ system was attempted [419] in combination with traditional methods for physico-chemical analysis; differential thermal analysis (DTA) and X-ray phase analysis (XPA) [527, 528]. It was expected [419] that NQR would be effective in this experiment for several reasons: first, each compound formed in the system would give rise to an individual spectroscopic pattern; then, the relative intensities of the NQR lines from a certain compound, would evidently vary with concentration ratio giving a maximum at the composition corresponding to its stoichiometry; finally, the variation of line widths could, in principle, determine boundary compositions of solid solutions, if these are formed in the system. The presence of initial components in samples of non-stoichiometric composition could also be detected by NQR.
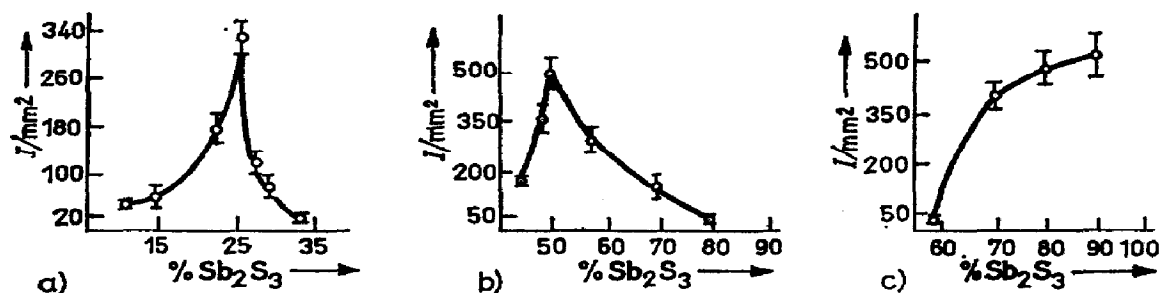
Figure 4.5   Resonance peak areas for the ^{123}Sb NQR transition $\Delta m = 5/2 - 3/2$ as a function of sample composition in the system $Na_2S + Sb_2S_3$ [419]:
a) in the NQR spectrum of Na_3SbS_3;
b) in the NQR spectrum of $NaSbS_2$;
c) in the NQR spectrum of Sb_2S_3.

According to the NQR data [419] compounds of the composition Na_3SbS_3 and $NaSbS_2$ were formed in the system (Fig. 4.5), the conclusion agreeing with the DTA and XPA data. The $^{121, 123}Sb$ NQR spectra of the compounds (Table 3.10) were discussed in the preceding chapter. One can see from Figure 4.5 that the NQR spectra of the samples containing 58, 70 and 80 mol % of Sb_2S_3 show resonances from the initial Sb_2S_3, in addition to those characteristic of $NaSbS_2$. It is also seen that the intensity curves for Na_3SbS_3 and $NaSbS_2$ are asymmetric with respect to their stoichiometric compositions (25 and 50 mol % of Sb_2S_3, respectively). In fact, a third compound, containing 40 mol % of Sb_2S_3 ($Na_6Sb_4S_9$) was detected in the $Na_2S + Sb_2S_3$ system by DTA and XPA methods [527, 528]. The abrupt decrease in the intensity curves at 40 mol % of Sb_2S_3 is therefore due to formation of the third compound in the system. Its $^{121, 123}Sb$ NQR spectrum has not however been detected, due probably to

one reason making NQR spectra unobservable (Chapter 1). For instance, the site, where the quadrupole atom resides may have cubic point symmetry.

The application of NQR nevertheless appeared useful since it enabled one to establish the formation of the two compounds, to determine their composition and to obtain certain crystallochemical characteristics, as well as to obtain indirect evidence for the formation of the third compound. The NQR study, combined with DTA and XPA techniques, evidently increases the efficiency of the latter, enlarges the amount of information received and makes the investigation less time consuming.
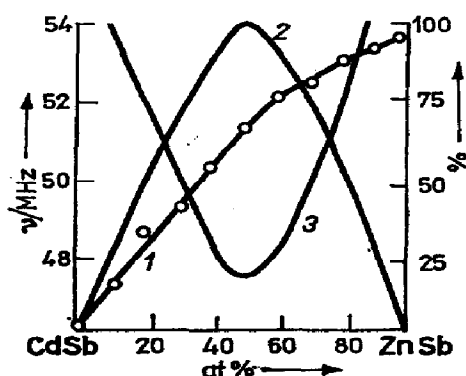
Figure 4.6   Variation of the NQR spectroscopic parameters for the system CdSb + ZnSb [529]:

1 ^{121}Sb NQR frequency ($\Delta m = 1/2 - 3/2$);
2 relative linewidth $\Delta\nu/\Delta\nu_{max}$;
3 relative amplitude of the ^{121}Sb resonance.

Results of the similar use of NQR for the study of CdSb + ZnSb alloys were reported later [529]. Several spectroscopic parameters varied [529] in samples containing annealed solid CdSb + ZnSb solutions of composition 1, 2, 10, 20, 30, 40, 50, 60, 70, 80 and 90 at. % of CdSb (Fig. 4.6). The ^{121,123}Sb NQR spectra of the starting components at 77 K are shown below.

	Isotope	Transition frequencies (MHz)			e^2Qq/h (MHz)	η (%)	Ref.
		1/2—3/2	3/2—5/2	5/2—7/2			
ZnSb	^{121}Sb	53.55	88.10		303.42	42.0	529
	^{123}Sb	41.42	51.76	81.31	386.72		
CdSb	^{121}Sb	46.30	84.82		286.75	27.0	530
	^{123}Sb	32.34	50.46	76.73	365.74		

ZnSb and CdSb were reported to be isostructural ([529] and refs. cited therein) which is consistent with the NQR data.

The most interesting result of the experiment [529] was the composition dependent smooth change of antimony resonance frequency between the end-member values which exceeded 7 MHz (Fig. 4.6). Evidently substitution of Zn atoms for Cd atoms in the solid solutions, generates a continuous variation in the EFG value at the antimony atoms in this system.

D. AFTER-EFFECTS IN MATERIALS SUBJECT TO THE INFLUENCE OF EXTREME CONDITIONS

The study of materials subject to the action of extreme conditions such as high pressure and temperature, shock compression, etc., is a promising field for the use of NQR. There are no especial limitations when NQR is used in this way and it can provide important informrtion for such investigations on the stability range of crystal modifications, local structural changes, the appearance of new crystal modifications and their crystal chemistry features.

The results of an ^{75}As NQR study of the changes in glassy As_2S_3 and As_2S_5 subject to high pressure (40—70 kbar) and temperature (up to 1 000 °C) were reported [525].

Glassy As_2S_3 first crystallized with the formation of an α-phase identical to natural orpiment which fact was unequivocally established by NQR (Fig. 4.3) in agreement with DTA and XPA. A further increase in temperature at constant pressure, resulted, according to XPA, in the polymorphic transitions α-$As_2S_3 \rightarrow \beta$-$As_2S_3 \rightarrow \gamma$-$As_2S_3$. The ^{75}As NQR spectra of the three modifications (see Figure 4.7) clearly show that the sample of β-As_2S_3 includes both
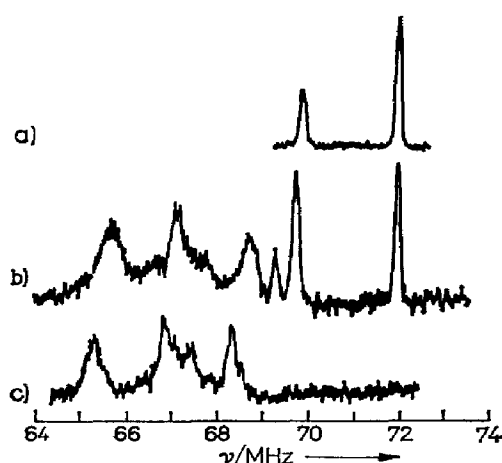
Figure 4.7   The ^{75}As NQR spectra of As_2S_3 crystal modifications obtained under high pressure and temperature (recorded at room temperature) [525]:
a) α-As_2S_3; b) β-As_2S_3; c) γ-As_2S_3.

the α- and γ-phases. Some weak additional lines in its spectrum, which were absent in the spectra of α-As_2S_3 and γ-As_2S_3 were interpreted [525] as evidence for the presence of a small amount of the associate α-As_2S_3 · γ-As_2S_3 formed presumably through bridging sulphur atoms ($As^\alpha\cdots S\cdots As^\gamma$).

The β-As_2S_3 and γ-As_2S_3 were further annealed at 180 °C for 2 months and their ^{75}As NQR spectra recorded again (Fig. 4.8). They distinctly reflect the local structural changes in the samples which occurred as a result of annealing. The structures became more ordered as demonstrated by the narrowed resonances. The intermediate As positions, which appeared during the α → β reorganization were redistributed between the two in γ-As_2S_3. In the ^{75}As NQR spectrum of β-As_2S_3, the resonances assigned to α-As_2S_3 showed a tendency to vanish, evidence for the conversion β → γ during annealing. Under constant pressure, and at temperatures of 700 — 1000 °C, γ-As_2S_3 can also be obtained from α-As_2S_3.
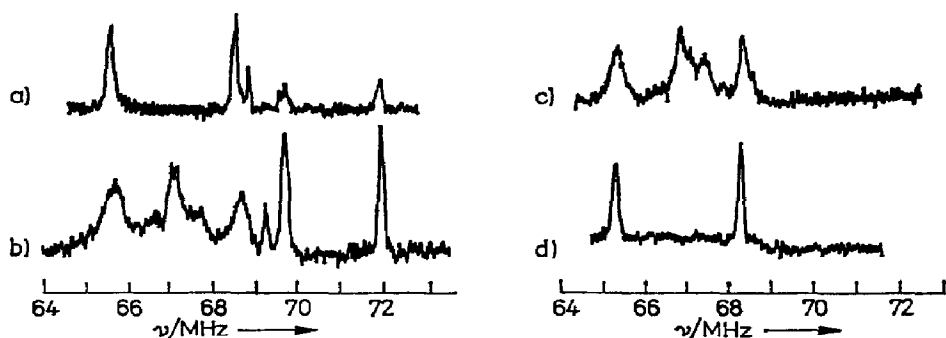
Figure 4.8 The change of the ^{75}As NQR spectra of As_2S_3 modifications due to annealing [525]:

a) the spectrum of β-As_2S_3 annealed; b) the spectrum of the same sample before annealing; c) the spectrum of γ-As_2S_3 before annealing; d) the spectrum of γ-As_2S_3 annealed.

According to NQR, both the α- and γ-phases have several crystallochemical features in common. Both possess two crystallographically independent As positions with the ^{75}As NQR frequencies typical for polymer arsenic chalcogenides. The shift of the NQR spectrum of γ-As_2S_3 to lower frequencies with respect to those of α-As_2S_3 was explained [525] as an increase in the coordination number of the arsenic atoms, due to a closer approach of chains under the action of high pressure.

A similar experiment was carried out with glassy As_2S_5 [525]. The latter crystallized at pressures of 40 — 70 kbar and temperatures within 300 — 600 °C. The ^{75}As spectra of crystalline α-As_2S_3 and As_2S_5 before, and after, annealing are given in Figure 4.9. It is evident that two crystal modifications are formed in the As_2S_5 sample under high pressure and temperature. One with an intense

doublet appears to be thermally unstable, undergoing structural transformation under annealing and diminishing in relative content. The other modification is thermally stable. It contains four crystallographically independent arsenic positions, their resonances lying within the frequency range typical for trivalent arsenic chain chalcogenide polymers.

Clearly NQR spectroscopy is very important in fields such as this. NQR evidence for the after-effects experienced by materials under extreme conditions, appears to be more useful than traditional DTA and XPA. The latter
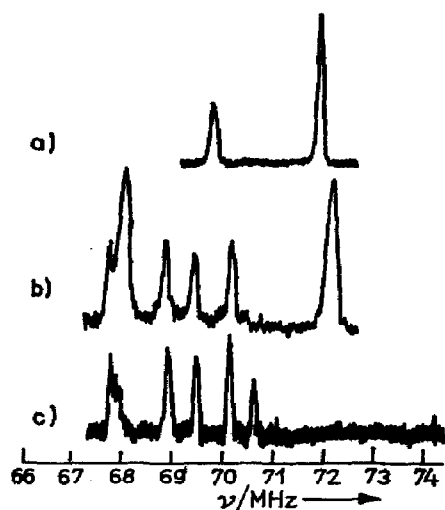
Figure 4.9   The ^{75}As NQR spectra of arsenic sulphides crystallized from glass at high pressure and temperature [525]:

a) α-As$_2$S$_3$; b) As$_2$S$_5$ unannealed; c) As$_2$S$_5$ annealed.

gave diffraction patterns of β- and γ-As$_2$S$_3$ too complicated for indexing. They were however considered [525] as evidence for β-As$_2$S$_3$ being an individual polymorph of orpiment. But NQR clearly showed that β-As$_2$S$_3$ was an intermediate state during the conversion α- → γ-As$_2$S$_3$. Under certain conditions, specified in [525] the high-temperature-pressure γ-phase is developed in α-As$_2$S$_3$ but the latter does not disappear. According to NQR the sample β-As$_2$S$_3$ contains α-As$_2$S$_3$, γ-As$_2$S$_3$ and presumably a small amount of the associate α-As$_2$S$_3 \cdot \gamma$-As$_2$S$_3$. ^{75}As NQR also yields information on the crystal chemistry of the new phases, γ-As$_2$S$_3$ and As$_2$S$_5$ formed under high pressure and temperature.

The sensitivity of NQR to structural changes is superior to X-ray diffraction patterns [531]. The relative broadening of the lines in both NQR and X-ray spectra were compared [531] after the samples of InSb and CdSb had been subject to shock compression with a peak pressure of 100 kbar. The defects produced in the samples due to shock loading strongly affected the NQR line widths while those in the X-ray diffraction patterns broadened insignifi-

cantly. With the help of NQR the appearance of piezoactivity induced by shock compression in CdSb and InSb was established [531].

Spectroscopic methods are now the most reliable sources of various information on the effect of extreme conditions upon materials. They supply such information from powder samples. The principal limitation of the X-ray experiment is the difficulty in growing single crystals. In any event, few crystals remain intact under the action of extreme conditions.

E. NQR IN THERMODYNAMICALLY UNSTABLE COMPLEXES

The sensitivity of NQR to alterations in the details of a structure such as the rearrangement of atomic positions and order-disorder phenomena, permits the observation of dynamic processes occurring in thermodynamically non-equilibrium systems, a study poorly accessible by other methods.

A convenient model of a non-equilibrium system is afforded by the *cis*-isomers of a number of diaminodihaloplatinite complexes. The total energy of the *cis*-isomers exceeds that of the corresponding *trans*-isomers, so that the formation of *cis*-isomers by these complexes is thermodynamically unfavourable [532, 533]. They therefore show a tendency to *cis-trans* isomerization at low activation energies.

Using NQR a number of phenomena were observed [534 — 536] to proceed in *cis*-isomers of platinum(II) complexes, processes such as thermoisomerization, the spontaneous conversion of crystalline modifications, and differences in thermal behaviour in samples prepared by different methods. The NQR spectra also permitted the detection of a previously unknown innersphere transformation in several complexes. The high thermodynamic instability is readily reflected in the ^{127}I NQR spectra displayed by *cis*-platinum(II) diaminodiiodides. Slow changes involving the continuous alteration of iodine resonance line widths and amplitudes could be observed for many hours after preparation (Fig. 4.10).

To stimulate thermoisomerization in *cis*-$Ptpy_2I_2$ it is sufficient to heat the sample for 1 hour at 140°C, the isomerization then proceeding at room temperature to complete conversion into the *trans*-form. This was monitored by NQR spectra over several days [534].

In a freshly prepared sample of *cis*-$Pt(buNH_2)_2I_2$, about 20% of the trans-form was detected by ^{127}I NQR and confirmed by polarography [536].

The controlled variation of conditions of preparation [534] mainly involved the duration of heating to completely convert the *cis*-isomer to the *trans*-form. For *cis*-$Pt(etNH_2)_2I_2$ the conversion varied from 2 to 9 hours depending on the component ratios Pt:KI:L [534].

Maintaining a precipitate in solution during preparation of the compounds has given some interesting results. A sample of *cis*-$Pt(meNH_2)_2I_2$, so obtained,

gave a completely different ^{127}I NQR spectrum after several months, its pattern however allowing one to suggest that the new crystalline *cis*-modification developed spontaneously during the storage time. The structural transformation $cis^{(1)}$-Pt(meNH$_2$)$_2$I$_2$ → $cis^{(2)}$-Pt(meNH$_2$)$_2$I$_2$ was accompanied by single crystal growth, so that a complete structure study of the new compound was made by X-ray [535]. While $cis^{(1)}$-Pt(meNH$_2$)$_2$I$_2$ converted into the *trans*-form at 140—150 °C and decomposed at above 170 °C, $cis^{(2)}$-Pt(meNH$_2$)$_2$I$_2$ showed no indications of either conversion to *trans*-Pt(meNH$_2$)$_2$I$_2$ or of decomposition on heating to 170 °C. Moreover, new resonances identical to those of *trans*-Pt(NH$_3$)$_2$I$_2$ were developed at 180 °C. They prevailed in intensity at 190 °C
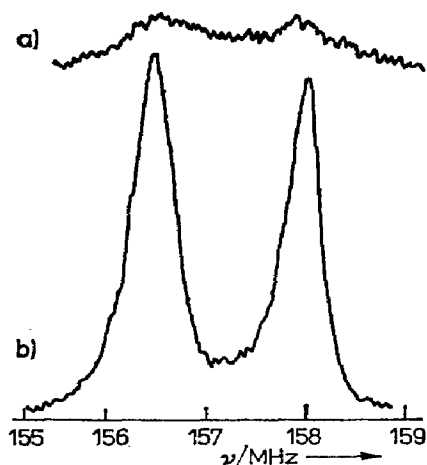
Figure 4.10 ^{127}I NQR lower frequency lines in *cis*-Pt(C$_5$H$_5$N)$_2$I$_2$ [535]: a) freshly prepared sample; b) the same sample after 24 hours.

and remained the only lines at 195 °C, evidencing for the inner sphere conversion $cis^{(2)}$-Pt(meNH$_2$)$_2$I$_2$ → *trans*-Pt(NH$_3$)$_2$I$_2$ occurring on heating this new compound [535]. The elemental analysis of the product confirmed the composition of the sample.

Another inner sphere conversion occurred in a sample of *cis*-Pt(etNH$_2$)$_2$I$_2$ which was also kept for a prolonged period (24 hours) in solution during preparation. After the first NQR study, the sample was stored for years in the same tube. Initially it was a fine powder, but during storage a number of single crystals grew inside the tube. The NQR test of the content of the tube showed that it became $cis^{(1)}$-Pt(meNH$_2$)$_2$I$_2$ suggesting the spontaneous transformation *cis*-Pt(etNH$_2$)$_2$I$_2$ → $cis^{(1)}$-Pt(meNH$_2$)$_2$I$_2$ proceeded during storage [535]. The single crystal X-ray study of the new content of the tube was also attempted to give the same lattice parameters as those earlier measured for the $cis^{(2)}$-Pt(meNH$_2$)$_2$I$_2$. This indicates that the structure conversion $cis^{(1)}$-Pt(meNH$_2$)$_2$I$_2$ → $cis^{(2)}$-Pt(meNH$_2$)$_2$I$_2$ took place under the action of X-ray irradiation [535].

The prolonged maintenance of samples in solution presumably promoted the formation of more thermodynamically stable compounds. One can believe that $cis^{(2)}$-Pt(meNH$_2$)$_2$I$_2$ is more thermodynamically stable than trans-Pt(meNH$_2$)$_2$I$_2$ but its energy is still higher than that of trans-Pt(NH$_3$)$_2$I$_2$, accounting for the observed thermoisomerization $cis^{(2)}$-Pt(meNH$_2$)$_2$I$_2$ → trans-Pt(NH$_3$)$_2$I$_2$ accompanied by inner sphere transformation.

According to NQR and in agreement with estimation of the isomerization energies [533], the cis-trans isomerization of PtL$_2$I$_2$ is favoured in following sequence: NH$_3 \gtrsim$ py $<$ meNH$_2 <$ etNH$_2$. This conclusion might account for the observed inner sphere conversion cis-Pt(etNH$_2$)$_2$I$_2$ → $cis^{(1)}$-Pt(meNH$_2$)$_2$I$_2$ governed by the tendency of the former complex to reduce its free energy. The tendency is realized under certain preparation conditions (maintaining the precipitate for a long time in solution).

F. POTENTIAL APPLICATIONS OF NQR TO THE GEOSCIENCES

A group of American authors [537] has reported their opinions on the long-term potential of NQR spectroscopy to the geosciences, many of which are associated with an in-depth understanding of mineralogy.

The limitations of widely used traditional methods for studying mineralogical problems, such as X-ray, electron and neutron diffraction, NMR, and electron microscopy are noted. They are not able to fully characterize the minerals, especially if they are polycrystalline.

NQR spectroscopy has advantages over the other methods providing a diversity of information about structure and bonding, order-disorder phenomena, and on atomic arrangement. Study of the temperature and pressure variations yields information on molecular dynamics and phase transitions as well as strain and stress. NQR also permits the study of some subtle aspects of crystal structures impossible to investigate by other techniques. Moreover NQR requires neither single crystals nor an external magnetic field [537].

Since the rocks and sediments composing the upper few kilometers of the earth's crust are made up principally of alumino-silicate minerals containing oxygen, silicon and aluminium initial investigations are centred on the problem of efficient detection of aluminium-27 NQR [537].

The potential applications of NQR to various energy technologies have been tabulated [537]. These include nuclear waste isolation, continental drilling, fossil fuel recovery, etc., and those technologies whose implementation may take many years of effort. Among them are the identification of lattice sites of radionuclides in glasses, synthetic and natural minerals; measurement of stress in salts and rock formations; measurement of stress at depth; evaluation of localized stress in non-isotropic materials; interpretation of ordering in minerals with respect to thermodynamic properties, continuous measurement

of the distribution of sulphur between organic and inorganic phases in coal; characterization of phase transitions in common rock-forming minerals, etc.

To make fuller use of the potentialities of the method, many experiments are to be undertaken [537]. This covers the development of ^{27}Al NQR instrumentation techniques including the detection of NQR lines of various intensities, widths and shapes; improved sensitivity; remote analysis and measurement of small samples. NQR research on other important probe nuclei (^{33}S, ^{235}U, ^{17}O, etc.) must be undertaken.

G. NQR STUDY OF INTERMETALLIC COMPOUNDS

The NQR spectra of metals are highly sensitive to superfine interactions between nuclei and conduction electrons, the spectroscopic parameters being related to the density of states at the Fermi level N(0). A series of ^{93}Nb NQR investigations were performed [540—542] on binary Nb_3X alloys (X = Al, Ga, Ge, Sn, Pt, Os, Ir, Sb). These alloys are known to have a crystal structure of type A-15 with niobium atoms occupying crystallographically equivalent positions 6(c), thus forming a system of orthogonal chains oriented along the [100], [010], [001] directions. The latter lie along the axes of a body-centered cubic sublattice formed by the atoms of the second component, occupying equivalent sites 2(a) ([541] and refs. cited therein).

Many intermetallic compounds which belong to this structural type, show anomalous magnetic, electric and elastic properties. Some are well-known high-temperature superconductors.

TABLE 4.2

^{93}Nb Quadrupole coupling constants and superconducting transition temperatures in intermetallic alloys [541, 542]

Compound	e^2Qq/h (MHz)	T_c (K)
Nb_3Al	113.1 ± 0.3	18.2
Nb_3Ga	101.4 ± 0.3	
Nb_3Ge	76.8 ± 0.2	
Nb_3Sn	44.7 ± 0.2	
Nb_3Sb	64	
Nb_3Ir	77.6 ± 0.5	
Nb_3Os	75.4 ± 0.5	
Nb_3Pt	72.0 ± 0.6	
$(Nb_{0.97}Zr_{0.03})_3Al$	110.4 ± 0.4	14.6
$Nb_3(Al_{0.9}Ga_{0.1})$	111.0 ± 0.4	19.1
$Nb_3(Al_{0.9}Sn_{0.1})$	113.0 ± 0.5	16.6
$Nb_3(Al_{0.95}Si_{0.05})$	110.4 ± 0.5	18.2

⁹³Nb NQR data for these alloys are shown in Table 4.2. The superconducting transition temperature T_c of the alloys appears to be varied by doping. ⁹³Nb NQR data for several doped alloys are also available in Table 4.2 together with their transition temperatures T_c. The Nb sites 6(c) have tetragonal symmetry. The point group is $D_{2d}(42m)$ requiring the asymmetry parameter at the niobium site to be zero. The ⁹³Nb NQR spectra of most compounds verified axial symmetry for the EFG. Only in Nb_3Os and Nb_3Ir did the resonances yield high asymmetry parameter values ($\eta \simeq 0.8$). This was interpreted as a result of disorder characteristic of niobium compounds with transition metals ([541] and refs. cited therein).

The wide range in ⁹³Nb QCC values in these Nb_3X compounds (Table 4.2) is related to the quasi uni-dimensional properties of these compounds [541]. A considerable dependence of the ⁹³Nb QCC values on the overlap between d-orbitals of the neighbouring Nb atoms is to be expected in such structures.

Non-negligible charge transfer from Nb to X atoms occurs in the A-15 compounds [541]. This leads to the increased coupling between the Nb and X atoms, thereby influencing the uni-dimensionality of the structure. The increasing charge transfer to Nb_3Ga and Nb_3Ge is accompanied by a reduction of the ⁹³Nb QCC value. The considerable charge transfer in Nb_3Ir and Nb_3Os was believed [541] to be responsible for the considerable difference in their electron distribution (non-axial EFG) compared to the other compounds of Table 4.2.

In ternary solid solutions obtained by doping the $NbAl_3$ alloys with Zr, Ga, Sn, Si, the substituting atoms occupied either 6(c) or 2(a) positions. When the Al atoms were substituted for Sn, Si, Ga, broadening of the ⁹³Nb resonances was observed. The latter, however was small in systems with Zr dopant atoms.

Substitution of Nb atoms in Nb_3Al was found to shift T_c much more effectively than substitution of Al atoms [542]. The ⁹³Nb QCC decreased with respect to Nb_3Al in the ternary systems of both types, $(Nb, A)_3Al$ and $Nb_3(Al, B)$ (Table 4.2).

The total EFG in metals may be represented as the sum

$$eq = eq_{latt}(1 - \gamma_\infty) + eq_{ce}(1 - R_Q)$$

where eq_{latt} is the point-charge contribution, $(1 - \gamma_\infty)$ and $(1 - R_Q)$ are the Sternheimer antishielding and shielding factors, respectively, and eq_{ce} is the EFG due to the conducting electrons. The contribution of eq_{ce} is proportional to the density of states at the Fermi level N(0) [542].

The decrease in ⁹³Nb QCC due to alloying was therefore considered [541, 542] to be due to a reduction of the density of the N(0) states of conduction electrons at the Fermi level. More detailed information was obtained [541, 542] from relaxation measurements.

H. NQR PULSE INSTRUMENTATION AND RELATED ECHO PHENOMENA

Pulse NQR spectrometers which operate in a wide frequency range, appear to be very suitable for the investigation of some other related echo phenomena. The possibility to observe piezoelectric resonances using NQR equipment, is widely known. In 1970 two groups of authors discovered a new phenomenon of electroacoustic echo (EAE) using NQR spectrometers [538, 539].

The effect has considerable potential in various areas of science and engineering. It can find many applications in the field of communication. The construction of controlled delay lines with extremely long delay times is possible using EAE. The most interesting property of materials possessing the EAE effect is the long-term storage of the response echo signal. This can be used in memory devices of a new type characterized by large information capacity, non-destructive reading, power-free storage of information, low cost and low energy consumption. The coherent signal accumulation, averaging, recording and erasing systems can also be constructed using the EAE phenomenon.

In more fundamental areas, the EAE effect may serve as a new method for the investigation of solids. Using EAE various nonlinear parameters may be measured. It is also an efficient tool for the study of acoustic attenuation (especially at superhigh frequencies), point defects, dislocations and impurity sites.

With this potential, the study of EAE has advanced to the research forefront of the physics and chemistry of solids. It is not appropriate to discuss the question here in detail, but it is necessary to comment briefly on some aspects insofar as they are closely related to NQR and its contribution to the investigation of new phenomena.

Having some phenomenological features in common with NQR spin echo, the EAE is quite different in nature. When a piezoelectric substance is excited by three electromagnetic pulses applied at the time moments $t = 0$, τ, T respectively, a response series of echo signals arises at the moments $t = (n + 1)\tau$ and $t = T + n\tau$ ($n = 1, 2, 3...$). The former signals make a two-pulse and the latter a three-pulse electroacoustic echo. The EAE can be observed in a wide frequency range, in single crystals, as well as in piezoelectric powders. In the latter substances, the dominating mechanism for echo formation, is determined by the nonlinear properties of the system of piezoelectric oscillators. The three-pulse echo possesses the property of long-term memory. When applying the pair of exciting pulses, a "record" of the electroacoustic echo signal can be made which can be stored for a long time (days or weeks). A repeated application of the third pulse, of the same filling frequency as that of the two first pulses and of an amplitude not exceeding the amplitudes of the two preceding pulses, can then permit the non-destructive "reading" of the stored signal. The first pair of exciting pulses is therefore called the "recording" pulses while the third pulse is called the "reading" pulse.

We refer the interested reader to the thesis by Petrosyan [543] for information on the more important theoretical and experimental EAE results as well as a systematic list of references on this problem and related aspects. The final purpose of the study [543] was a search and NQR investigation of crystals possessing the EAE effect.

Inorganic compounds and especially alkali metal halogenates contain numerous examples where the EAE effect was observed (α-HIO_3, $KBrO_3$, $CsBrO_3$, SbF_3, $CsIO_3$, Bi_8TiO_{14}, $Bi_{12}GeO_{20}$, etc.). Iodates are known to find a wide application in quantum electronics, nonlinear optics and piezoengineering [543]. The literature data available on these compounds, contained however many contradictions. Thus, there was considerable discord on the number, structure and NQR spectra of the crystalline modifications formed by acid potassium biiodate ($KIO_3 \cdot HIO_3$). There were also contradictions between the X-ray data on the centrosymmetric structure of iodate anhydride (I_2O_5) [546] and a report on the observation of the piezoelectric resonances and EAE in commercial samples of I_2O_5 ([543] and refs. cited therein).

Using NQR all the discrepancies in the data have been rationalized [543]. The compounds formed in the system $H_2O - I_2O_5$ have been studied systematically together with the related compounds ($RbIO_3 \cdot HIO_3$, $CsIO_3 \cdot HIO_3$, $LiBrO_3$, $LiBrO_3 \cdot H_2O$, etc.). The existence of α-HIO_3 which appeared to be metastable at room temperature, was confirmed. It was also found that commercial iodate anhydride (I_2O_5) contained, as a rule, a mixture of α-HIO_3 and $HIO_3 \cdot I_2O_5$, free I_2O_5 often being completely absent in the reagent. The ^{127}I NQR spectra consistently reported either some $HIO_3 \cdot I_2O_5$ resonances or the combined spectrum of α-HIO_3 and $HIO_3 \cdot I_2O_5$ [544, 545]. The true ^{127}I NQR spectrum of I_2O_5 was not known. The observed piezoresonances or EAE signals in commercial I_2O_5 have evidently been accounted for by the presence of α-HIO_3 in the samples used. In the pure sample of I_2O_5 [547, 548] both the piezoelectric resonances and the EAE signals were completely absent, and the ^{127}I NQR spectra appeared in complete agreement with the X-ray data [546].

All the crystal modifications (α, β, γ, δ) of acid potassium biiodate ($KIO_3 \cdot HIO_3$) have been prepared and investigated using NQR [543]. α-$KIO_3 \cdot HIO_3$ is ferroelectric, the first example in the acid iodate family. The order, mechanism and temperature of the ferroelectric phase transition (223 K) have been determined. A detailed study of the thermal behaviour of other modifications of acid potassium biiodate has been carried out in the temperature range near dehydration. This gave information [543] on the relative thermodynamic stability of the crystalline modifications of potassium biiodate.

The varied information was obtained [543] on a large number of compounds using NQR spectroscopy almost exclusively. As a result of this study EAE was observed for the first time in 60 piezo- and ferroelectric crystals.

Two ways of erasing the electroacoustic record were proposed [549] to

provide experimental confirmation of the composite nature of the three-pulse echo. The experiments provided evidence in favour of one of the disputed mechanisms responsible for the long-term memory of three-pulse echo, attributing the effect to a residual plastic deformation which develops in the piezoelectric substance due to the action of radiofrequency pulses [550].

CONCLUDING REMARKS

In this review the authors intended to cover, comprehensively, the diversity of information which can be obtained using NQR. Various classes of inorganic compounds were considered from the viewpoint of their geometry and chemical bonding.

Aiming at simplicity and clarity to non-specialists, the authors often limited themselves to a qualitative comparison of the results for as great a number of related compounds as possible.

A short review of promising applications is included for NQR in areas which have not yet become traditional.

The large field of NQR spectroscopy based on relaxation measurements was, however, beyond the scope of the present paper. Information obtained from measurement of relaxation rates, their temperature dependence and the temperature dependence of the resonance frequencies provides information concerning the dynamic properties of crystal lattices, molecules or ions. Investigation of the temperature behaviour of the spectroscopic parameters including relaxation times contributes considerably to our understanding of the nature and mechanisms of phase transitions. Consideration of these subjects would, however, greatly increase the size of this monograph, so the reader is referred to reviews [154, 551, 553, 554] devoted to these problems.

REFERENCES

1. a) H. G. Dehmelt and H. Krüger, Naturwiss., **37**, 111 (1950);
   b) H. G. Dehmelt and H. Krüger, Naturwiss., **38**, 921 (1950).
2. T. P. Das and E. L. Hahn, Solid State Physics, Suppl. 1 (1958).
3. E. A. C. Lucken, Nuclear Quadrupole Coupling Constants, Academic Press, New York, 1969.
4. G. K. Semin, T. A. Babushkina and G. G. Yakobson, Primenenie yadernogo kvadrupol'nogo rezonansa v khimii, Khimia, Leningrad, 1972.
5. V. S. Grechishkin, Yadernye kvadrupol'nye vzaimodeistviya v tverdykh telakh, Nauka, Moskva, 1973.
6. I. A. Safin and D. Ya. Osokin, Yaderny Kvadrupol'nyi Rezonans v Soeidineniyakh Azota, Nauka, Moskva, 1977.
7. E. R. Andrew, Nuclear Magnetic Resonance, Cambridge Univ. Press, London and New York, 1955.
8. J. A. S. Smith, J. Chem. Educ., **48**, No. 1, 39 (1971).
9. C. P. Slichter, Principles of Nuclear Magnetism, Harper and Row, New York, 1963.
10. N. F. Ramsey, Nuclear Moments, Wiley, New York, 1953.
11. M. H. Cohen, Phys. Rev., **96**, 1278 (1954).
12. A. S. Vigdorov and E. A. Kravchenko, Koord. Khim., **3**, 1275 (1977).
13. E. Schempp and P. J. Bray, Phys. Chem., **4**, 522 (1970).
14. C. Dean, Phys. Rev., **96**, 1053 (1954).
15. V. Rehn, J. Chem. Phys., **38**, 749 (1963).
16. E. L. Hahn and B. Herzog, Phys. Rev., **93**, 639 (1954).
17. A. A. Boguslavskii and V. V. Pechenov, Izv. Akad. Nauk SSSR, Ser. fiz., **45**, 540 (1981).
18. D. Giezendanner, S. Sengupta and G. Litzistorf, J. Mol. Struct., **58**, 519 (1980).
19. a) D. Giezendanner, S. Sengupta and E. A. C. Lucken, J. Mol. Struct., **58**, 229 (1980);
    b) G. Litzistorf, S. Sengupta and E. A. C. Lucken, J. Mol. Struct., **83**, 285 (1982).
20. Y. Morino and M. Toyama, J. Chem. Phys., **35**, 1289 (1961).
21. F. J. Adrian, J. Chem. Phys., **38**, 1258 (1963).
22. J. D. Graybeal and P. J. Green, J. Phys. Chem., **73**, 2948 (1969).
23. K. V. Raman and P. T. Narasimhan, Pure Appl. Chem., **32**, 271 (1972).

24 J. Darville, A. Gerard and M. T. Calende, J. Magnet. Res., **16**, 205 (1974).

25 H. R. Brooker and R. B. Greel, J. Chem. Phys., **61**, 3658 (1974).

26 a) S. Sengupta, D. Giezendanner and E. A. C. Lucken, J. Magnet. Res., **38**, 553 (1980);
b) S. Sengupta, G. Litzistorf and E. A. C. Lucken, J. Magn. Res. **42**, 45 (1981).

27 V. Harihara Subramanian and P. T. Narasimhan, J. Mol. Struct. **58**, 193 (1980).

28 Yu. E. Sapozhnikov and Ya. B. Yasman, Izv. Akad. Nauk SSSR, Ser. fiz., **42**, 2148 (1978).

29 M. I. Podgoretzkii and O. A. Khrustalev, Uspekhi fiz. nauk, **81**, 217 (1963).

30 W. B. Mims, Phys. Rev., **B5**, 2409 (1972).

31 A. A. Boguslavskii and V. V. Pechenov, Izv. Akad. Nauk SSSR, Ser. fiz., **35**, 2600 (1975).

32 D. V. Zakirov and I. A. Safin, Izv. Akad. Nauk SSSR, Ser. fiz., **45**, 546 (1981).

33 D. V. Zakirov and I. A. Safin, J. Mol. Struct., **83**, 253 (1982).

34 S. N. Aristov and B. V. Dresvyankin, Izv. Akad. Nauk SSSR, Ser. fiz., **45**, 1797 (1981).

35 V. P. Feshin, G. V. Dolgushin, M. G. Voronkov, B. V. Timokhin, V. K. Dmitriev, V. I. Dmitriev, V. N. Vengel'nikova, Yu. E. Sapozhnikov and Ya. B. Yasman, Dokl. Akad. Nauk SSSR, **261** (2), 436 (1981).

36 V. S. Grechishkin, G. B. Soifer, Prib. i tekhn. eksp., **1**, 5 (1963).

37 F. N. H. Robinson, J. Sci. Instrum., **36**, 481 (1959).

38 a) R. V. Pound, Phys. Rev., **79**, 685 (1950);
b) R. V. Pound and D. W. Knight, Rev. Sci. Instrum., **21**, 219 (1950).

39 G. Watkins and R. V. Pound, Phys. Rev., **85**, 1062 (1952).

40 F. N. H. Robinson, J. Sci. Instrum., **36**, 481 (1959).

41 J. R. Whitehead, Super-regenerative Receivers, Cambridge, 1950.

42 D. A. Tong, J. Sci. Instrum., **1**, 1153, 1162 (1968).

43 A. Lenovenko, Yu. Mochulskii and N. Kupchenko, Zavod. Lab., **39**, 1153 (1973).

44 M. Read, Adv. Nucl. Quadr. Res., **1**, 203 (1974).

45 J. C. Carter, J. A. S. Smith, J. W. R. Cook and P. M. Butcher, Adv. Nucl. Quadr. Res., **1**, 191 (1974).

46 a) F. Reiter and J. Voitländer, J. Phys. (E), **6**, 276 (1973);
b) H. Gotou, Y. Nishiyama and A. Shimauchi, J. Phys. (E): Sci. Instrum. **12**, 1979.

47 R. Moores, Adv. Nucl. Quadr. Res., **1**, 185 (1974).

48 I. A. Safin, A. Klebanov and I. S. Bondarenko, Prib. i tekhn. eksp., 150 (1970).

49 M. Bloom and R. E. Norberg, Phys. Rev., **93**, 638 (1954).

50 M. Bloom, E. L. Hahn and B. Herzog, Phys. Rev., **97**, 1699 (1955).

51 B. Herzog and E. L. Hahn, Phys. Rev., **103**, 148 (1956).

52 T. P. Das and A. K. Saha, Phys. Rev., **98**, 516 (1955).

53 I. J. Lowe and R. E. Norberg, Phys. Rev., **107**, 46 (1957).

54 D. E. Woessner and H. S. Gutowsky, J. Chem. Phys., **39**, 440 (1963).

55 I. A. Safin, Prib. i tekhn. eksp., 98 (1962).

56 I. A. Safin, Zh. strukt. khim., 267 (1963).

57 A. Tzalmona, Phys. Lett., **20**, 478 (1968).

58 Z. Borsutzkii, A. Gordeev, V. Grechishkin and I. Izmestiev, Sb. Radiospektroskopia, tr. ENI, PGU, 12 (1), 67 (1966).

59 B. N. Pavlov, I. A. Safin, G. K. Semin, E. I. Fedin and D. Ya. Shtern, Vestn. Akad. Nauk SSSR, 11, 40 (1964).

60 D. Ya. Shtern and B. N. Pavlov, in: Radiospektroskopia tverdogo tela, Moskva, 1967.

61 W. G. Clark, Rev. Sci. Instrum., 35, 316 (1964).

62 B. N. Pavlov, A. Klebanov and I. S. Bondarenko, Prib. i tekhn. eksp., 150 (1970).

63 I. A. Safin and D. Ya. Osokin, Prib. i tekhn. eksp., 1, 164 (1971).

64 D. Ya. Osokin, I. A. Safin and I. Nuretdinov, Dokl. Akad. Nauk SSSR, 186, 1128 (1969).

65 D. Ya. Osokin and I. A. Safin, Fiz. tverdogo tela, 11, 3608 (1969).

66 D. Ya. Osokin, I. A. Safin and I. Nuretdinov, Dokl. Akad. Nauk SSSR, 190, 357 (1970).

67 G. E. Peterson and T. Oja, Adv. Nucl. Quadr. Res., 1, 179 (1984).

68 B. N. Pavlov, Izv. Akad. Nauk SSSR, Ser. khim., 39, 2627 (1975).

69 Yu. Manzhura, V. Posadskii, A. Postnikov, L. Ryumin and V. Toporkov, Zavod. Lab., 39, 227 (1973).

70 B. Ignatov, A. Aleksandrov, L. Pososhenko and G. Semin, Izv. Akad. Nauk SSSR, Ser. fiz., 39, 2630 (1975).

71 J. C. Harding, jr., D. A. Wade, R. A. Morino, E. G. Sauer and S. M. Klainer, J. Magn. Res., 36, 21 (1979).

72 E. N. Kaufman, J. R. Brookeman, P. C. Canepa, T. A. Scott, D. H. Rasmussen and J. H. Perepezko, Solid State Commun., 29, 378 (1979).

73 D. E. Woessner and H. S. Gutowsky, J. Chem. Phys., 39, 440 (1963).

74 A. E. Mefed and B. N. Pavlov, J. Mol. Struct., 83, 131 (1982).

75 a) O. S. Zueva, J. Mol. Struct., 83, 379 (1982);
   b) O. S. Zueva and A. R. Kessel, J. Mol. Struct., 83, 383 (1982).

76 T. Ito and T. Hashi, J. Mol. Struct., 58, 389 (1980).

77 R. A. Marino and S. M. Klainer, J. Chem. Phys., 67, 3388 (1977).

78 R. Cantor and J. Waugh, J. Chem. Phys., 73, 1054 (1980).

79 a) D. Ya. Osokin, Phys. Stat. Solidi (b), 102, 681 (1980);
   b) D. Ya. Osokin, J. Mol. Struct., 83, 285 (1982).

80 B. N. Provotorov and V. Karnaukh, J. Mol. Struct., 83 (1982).

81 D. T. Edmonds, M. J. Hunt, A. L. Mockay and C. P. Summers, Adv. Nucl. Quadr. Res., 1, 145 (1974).

82 R. Blinc, Adv. Nucl. Quadr. Res., 2, 71 (1975).

83 D. T. Edmonds, Phys. Rep., C29, 233 (1977).

84 J. L. Ragle and G. L. Minott, Adv. Nucl. Quadr. Res., 3, 205 (1978).

85 V. P. Anferov, V. S. Grechishkin and S. V. Grechishkina, Izv. Akad. Nauk SSSR, Ser. khim., 42, 2164 (1978).

86 V. S. Grechishkin and V. P. Anferov, Adv. Nucl. Quadr. Res., 4, 71 (1980).

87 J. A. S. Smith, J. Mol. Struct., 58, 1 (1980).

88 a) S. G. P. Brosnan and D. T. Edmonds, J. Mol. Struct. 58, 23 (1980).
   b) S. G. P. Brosnan and D. T. Edmonds, J. Magn. Res., 38, 47 (1980).

89 I. J. F. Popplett, J. Magn. Res., 44, 488 (1981).

90   I. J. F. Popplett, J. Magn. Res., 50, 382 (1982).

91   I. J. F. Popplett, J. Magn. Res., 50, 397 (1982).

92   a) I. J. F. Popplett and J. A. S. Smith, J. Chem. Soc. Faraday Trans., 2, 77 (1981);
      b) J. Chem. Soc., Faraday Trans., 2, 1155 (1981).

93   V. P. Anferov, S. V. Anferova, V. S. Grechishkin and V. M. Mikhailov, J. Mol. Struct., 83, 135 (1982).

94   R. Ader and M. Shporer, J. Magn. Res., 47, 483 (1982).

95   C. H. Townes and B. P. Dailey, J. Chem. Phys., 17, 782 (1949).

96   R. M. Sternheimer, Phys. Rev., 80, 102 (1950); 84, 244 (1951); 86, 316 (1952); 95, 736 (1954); 105, 158 (1957); 130, 1423 (1963); 132, 637 (1963); 146, 140 (1966).

97   C. H. Townes and A. L. Shawlow, Microwave Spectroscopy, McGraw-Hill, New York, 1955.

98   D. Schoemaker, Phys. Rev., 149, 693 (1961).

99   M. A. Whitehead and H. Jaffe, J. Chem. Phys., 34, 2204 (1961).

100   T. P. Das, J. Chem. Phys., 27, 1 (1957).

101   F. Cotton and C. Harris, Proc. Nat. Acad. Sci., 56, 12 (1966).

102   P. A. Casabella and T. Oja, J. Chem. Phys., 50, 4814 (1969).

103   a) J. Richardson, Rev. Mod. Phys., 32, 461 (1960);
      b) J. Richardson, J. Chem. Phys., 35, 1829 (1961).

104   a) C. W. Kern and M. Karplus, J. Chem. Phys., 42, 1062 (1964);
      b) C. W. Kern and R. L. Matcha, J. Chem. Phys., 49, 2081 (1968).

105   E. Scrocco and J. Tomassi, Theoret. Chim. Acta, 2, 384 (1964); R. Bonaccorsi, E. Scrocco and J. Tomassi, J. Chem. Phys., 50, 2940 (1968).

106   a) P. Cade, Bull. Amer. Phys. Soc., 11, 11 (1966);
      b) D. Davies and W. Mackrodt, Chem. Commun., 1967, 1226 (1967).

107   a) E. Shempp and P. J. Bray, J. Chem. Phys., 48, 2381 (1968);
      b) C. T. O'Konski and Tae Kyu Ha, J. Chem. Phys., 49, 5354 (1968).

108   L. C. Snyder, J. Chem. Phys., 68, 291 (1978).

109   M. Redshaw, M. H. Palmer and R. H. Finlay, Z. Naturforsch., A34, 220 (1979).

110   M. Barber, S. M. Hayne and D. Hinchliffe, J. Mol. Struct., 62, 207 (1980).

111   A. Weiss, Fortschritte der chemischen Forschung, Topics in Current Chemistry, 30, 3 (1972).

112   R. Bersohn, J. Appl. Phys., 33, Suppl. 1, 286 (1962).

113   a) K. Shimomura, J. Phys. Soc. Jap., 12, 652 (1957).
      b) K. Shimomura, J. Sci. Hiroshima Univ., A21, 241 (1958).

114   Y. Morino and M. Toyama, J. Phys. Soc. Jap., 15, 288 (1960).

115   J. Milledge and L. M. Pant, Acta Crystallogr., 13, 285 (1960).

116   Y. Furukawa, J. Sci. Hiroshima Univ., A37, 357 (1973).

117   a) S. G. Nyburg, G. A. Ozin and J. T. Szymanski, Acta Crystallogr., B27, 2298 (1981);
      b) Acta Crystallogr. B28, 2885 (1972).

118   E. A. Kravchenko, Yu. K. Maksyutin, E. N. Guryanova and G. K. Semin, Izv. Akad. Nauk SSSR, Ser. khim., 1271 (1968).

119   A. I. Kuz'min and G. N. Zviadadze, Koord. Khim., 6, 1538 (1980).

120   I. Lindquist, Inorganic Adduct Molecules of Oxo-Compounds, Academic Press, New York, 1963.

121   I. R. Beattie, M. Milne, M. Webster, H. E. Blayden, P. J. Jones, R. C. G. Killean and J. L. Lawrence, J. Chem. Soc. A, 482 (1969).

122   T. J. Bastow, I. D. Campbell and H. J. Whitfield, Solid State Commun., 39, 307 (1981).

123   P. A. Casabella, P. J. Bray and R. G. Barnes, J. Chem. Phys., 30, 1393 (1959).

124   G. Wulfsberg and A. Weiss, Ber. Bunsenges. Phys. Chem., 84, 474 (1980).

125   M. Kubo and D. Nakamura, Adv. Inorg. Chem. Radiochem., 8, 257 (1966).

126   J. D. Graybeal, R. McKown and S. Ing, J. Phys. Chem., 74, 1814 (1970).

127   W. A. Welsh, T. B. Brill, P. Thomson, R. Wood and R. G. Gearhart, Inorg. Chem., 13, 1797 (1974).

128   a) T. B. Brill, R. G. Gearhart and W. A. Welsh, J. Magn. Res., 13, 27 (1974); b) T. B. Brill, J. Chem. Phys., 61, 424 (1974).

129   Y. Furukawa, L. S. Prabhumirashi, R. Ikeda and D. Nakamura, Bull. Chem. Soc. Jap., 55, 995 (1982).

130   T. B. Brill and W. A. Welsh, J. Chem. Soc. (Dalton), 357 (1973).

131   R. Ikeda, A. Sasane, D. Nakamura and M. Kubo, J. Phys. Chem., 70, 2926 (1966).

132   R. J. Gillespie and R. S. Nyholm, Quart. Rev. Chem. Soc., 11, 339 (1957).

133   D. Urch, J. Chem. Soc., Suppl. 1, 5775 (1964).

134   L. Ramakrishnan, S. Soundararajan, V. Sastry and J. Ramakrishna, Coord. Chem. Rev., 22, 123 (1977).

135   D. Nakamura, R. Ikeda and M. Kubo, Coord. Chem. Rev., 17, 281 (1975).

136   H. Bayer, Z. Phys., 130, 227 (1951).

137   a) T. Kushida, J. Sci. Hiroshima Univ., A19, 327 (1955); b) T. Kushida, G. Benedek and N. Bloembergen, Phys. Rev., 104, 1364 (1956).

138   J. E. Fergusson and D. E. Scaife, Inorg. Nucl. Chem. Lett., 7, 987 (1971).

139   P. J. Cresswell, J. E. Fergusson, B. R. Penfold and D. E. Scaife, J. Chem. Soc. (Dalton), 254 (1972).

140   T. Haas and E. Marram, J. Chem. Phys., 43, 3985 (1965).

141   T. L. Brown and L. G. Kent, J. Phys. Chem., 74, 3572 (1970).

142   G. P. O'Leary, Phys. Rev. Lett., 23, 782 (1969).

143   G. P. O'Leary and R. G. Wheeler, Phys. Rev., B1, 4409 (1970).

144   G. L. Baker and R. L. Armstrong, Can. J. Phys., 48, 1649 (1970).

145   K. R. Jeffrey, R. L. Armstrong and K. Kisman, Phys. Rev., B1, 3770 (1970).

146   R. L. Armstrong and G. L. Baker, Can. J. Phys., 48, 2411 (1970).

147   E. A. C. Lucken, J. Mol. Struct., 58, 121 (1980).

148   M. C. Day, jr. and J. Selbin, Theoretical Inorganic Chemistry, Reinhold Book Corporation, 1969.

149   Yu. A. Buslaev, E. A. Kravchenko, S. M. Sinitzyna and G. K. Semin, Izv. Akad. Nauk SSSR, Ser. khim., 2816 (1969).

150   P. A. Edwards and R. E. McCarley, Inorg. Chem., 12, 900 (1973).

151   G. K. Semin, S. I. Kuznetzov, I. M. Alimov, T. L. Khotsianova, E. V. Bryukhova, L. A. Nisselson and K. V. Tretyakova, Inorg. Chim. Acta, 13, 181 (1974).

152   R. L. Armstrong and H. M. van Driel, Adv. Nucl. Quadr. Res., 2, 179 (1975).

153   H. Chihara and N. Nakamura, Adv. Nucl. Quadr. Res., 4, 1 (1981).

154   R. Sh. Lotfullin, Izv. Akad. Nauk SSSR, Ser. fiz., 42, 2018 (1978).

155   H. Chihara, N. Nakamura and S. Seki, Bull. Chem. Soc. Jap., 40, 50 (1967).

156   J. V. Dilorenzo and R. F. Schneider, Inorg. Chem., 6, 766 (1967).

157   R. J. Lynch and T. C. Waddington, Adv. Nucl. Quadr. Res., 1, 37 (1974).

158   T. L. Brown, W. G. McDugle, jr., and L. G. Kent, J. Am. Chem. Soc., 92, 3645 (1970).

159   D. J. Merryman and J. Corbett, Inorg. Chem., 13, 1258 (1974).

160   S. Porter and R. Jacobson, Cryst. Struct. Commun., 1, 431 (1972).

161   C. Vonk and E. Wiebenga, Acta Crystallogr., 12, 859 (1959).

162   R. F. Schneider and J. V. DiLorenzo, J. Chem. Phys., 47, 2349 (1967).

163   H. Negita and Z. Hirano, Bull. Chem. Soc. Jap., 31, 660 (1958).

164   D. McCall and H. S. Gutowsky, J. Chem. Phys., 31, 1300 (1953).

165   J. V. DiLorenzo and R. F. Schneider, J. Phys. Chem., 72, 761 (1968).

166   R. M. Hart, M. A. Whitehead and L. Krause, J. Chem. Phys., 56, 3038 (1972).

167   Z. Fokina, S. Kuznetzov, N. Timoshenko and E. Bryukhova, Zh. fiz. khim., 53, 146 (1979).

168   a) L. Kolditz, T. Moya, U. Calov, E. Kravchenko and R. Stösser, Z. Chem., 21, 38 (1981); b) L. Kolditz, T. Moya, U. Calov, E. Kravchenko and Yu. Buslaev, Z. Chem., 24, 51 (1984).

169   A. I. Kuz'min, B. E. Dzevitzkii, G. N. Zviadadze, Zh. fiz. khim., 53, 167 (1979).

170   E. A. Kravchenko, B. V. Levin, S. Bananyarly and T. A. Toktomatov, Koord. Khim., 3, 374 (1972).

171   T. B. Brill and G. G. Long, J. Phys. Chem., 75, 1898 (1971).

172   T. Okuda, M. Hiura, E. Koshimizu, H. Ishihara, Y. Kushi and H. Negita, Chem. Lett., 1321 (1982).

173   A. G. Landers and T. B. Brill, Inorg. Chem., 19, 744 (1980).

174   H. Terao, J. Sci. Hiroshima Univ., A 46, 95 (1982).

175   S. Lawton and R. A. Jacobson, Inorg. Chem., 5, 743 (1966).

176   C. R. Hubbard and R. A. Jacobson, Proc. Iowa Acad. Sci., 75, 85 (1968).

177   A. T. Jensen and S. E. Rasmussen, Acta Chem. Scand., 9, 708 (1955).

178   a) J. D. Donaldson, M. J. Tricker and B. W. Dale, J. Chem. Soc. (Dalton), 893 (1972); b) J. D. Donaldson and M. J. K. Thomas, Inorg. Nucl. Chem. Lett., 14, 93 (1978).

179   B. M. Gimark, jr., J. F. Liebman and M. Kohn, J. Am. Chem. Soc., 100, 2334 (1978).

180   A. Sasane, T. Matuo, D. Nakamura and M. Kubo, J. Magn. Res., 4, 257 (1971).

181   C. W. Fryer and J. A. S. Smith, J. Chem. Soc. A, 1029 (1970).

182   E. P. Marram, E. J. McNiff and J. L. Ragle, J. Phys. Chem., 67, 1719 (1963).

183   K. Ito, D. Nakamura, Y. Kurita, K. Ito and M. Kubo, J. Am. Chem. Soc., 83, 4526 (1961).

184   H. Kashiwagi, D. Nakamura and M. Kubo, J. Phys. Chem., 71, 4443 (1967).

185   A. Sasane, T. Matuo, D. Nakamura and M. Kubo, Bull. Chem. Soc. Jap., 43, 1908 (1970).

186   A. Sasane, D. Nakamura and M. Kubo, J. Magn. Res., 8, 179 (1972).

187   G. Furlani, F. Capece, C. Sartori, Internat. Summer School on Theoretical Chemistry. NQR Spectroscopy, Italy, 1967.

188   D. Scaife, Austr. J. Chem., 24, 1993 (1971).

189   K. B. Dillon and T. C. Waddington, Inorg. Nucl. Chem. Lett., 14, 415 (1978).

190   C. D. Cornwell and R. S. Yamasaki, J. Chem. Phys., 27, 1060 (1957).

191   Y. Kurita, D. Nakamura and N. Hayakawa, J. Chem. Soc. Jap., Pure Chem. Sect., 79, 1093 (1958).

192   J. C. Evans and G. Y. S. Lo, Inorg. Chem., 6, 836 (1967).

193   W. Scheinert and A. Weiss, Z. Naturforsch., 31 a, 1354 (1976).

194   W. Fichtner and A. Weiss, Z. Naturforsch., 35 b, 170 (1980).

195   S. L. Segel and R. G. Barnes, Cataloge of Nuclear Quadrupole Interaction and Resonance Frequencies in Solids, US Atomic Energy Commission (1965).

196   D. J. Merryman, P. A. Edwards, J. D. Corbett and R. E. McCarley, Inorg. Chem., 13, 1471 (1974).

197   D. J. Merryman, J. D. Corbett and P. A. Edwards, Inorg. Chem., 14, 428 (1975).

198   D. E. Scaife, Aust. J. Chem., 23, 2205 (1970).

199   T. Deeg and A. Weiss, Ber. Bunsenges. Phys. Chem., 79, 497 (1975).

200   D. A. Tong, J. Chem. Soc., Chem. Commun., 790 (1969).

201   I. Alimov, E. Bryukhova, A. Grigoriev, L. Mikheeva and L. Komissarova, Izv. Akad. Nauk SSSR, Ser. khim., 982 (1975).

202   J. P. Huvenne, P. Legrand and W. Gabes, J. Mol. Str., 27, 357 (1975).

203   R. J. Elema, J. L. De Boer and A. Vos, Acta Crystallogr., 16, 243 (1963).

204   P. W. Smith and R. Stoessiger, Chem. Commun., 279 (1971).

205   a) W. J. Asker, D. E. Scaife and J. A. Watts, Aust. J. Chem., 25, 2301 (1972); b) D. E. Scaife, Austr. J. Chem., 24, 1315 (1971).

206   M. Hiura, J. Sci. Hiroshima Univ., A45, 383 (1982).

207   S. Plesco, R. Kind and H. Arend, Phys. Stat. Solidi (a), 61, 87 (1980).

208   K. Yamada, J. Sci. Hiroshima Univ., A41, 77 (1977).

209   D. E. Scaife, Austr. J. Chem., 24, 1753 (1971).

210   V. I. Pakhomov, P. M. Fedorov, I. M. Alimov, I. N. Ivanova-Korfini and G. K. Semin, Izv. Akad. Nauk SSSR, Ser. fiz., 39, 2519 (1975).

211   D. Nakamura, Y. Kurita, K. Ito and M. Kubo, J. Chem. Phys., 31, 1433 (1959).

212   P. K. Kadaba and D. E. O'Reily, J. Chem. Phys., 55, 5833 (1971).

213   I. P. Aleksandrova, J. Mol. Str., 83, 403 (1982).

214   A. K. Moskalev, I. A. Belobrova and I. P. Aleksandrova, Fiz. tverd. tela, 20, 3288 (1978).

215   F. Milia, Phys. Lett., 70A, 218 (1979).

216   I. A. Belobrova, I. P. Aleksandrova and A. K. Moskalev, Phys. Stat. Solidi (a), 66, K17 (1981).

217   I. A. Belobrova, A. K. Moskalev, N. V. Bizukina, S. V. Misul and I. P. Aleksandrova, Solid State Communs, 33, 1101 (1980).

218   S. Sawada, Y. Shiroishi, A. Yamamoto, M. Takashige and M. Matusuo, J. Phys. Soc. Jap., 43, 2089 (1977).

219   M. Izumi, J. D. Axe and G. Shirane, Phys. Rev., B15, 4392 (1977).

220   B. Morosin and E. C. Lingafelter, J. Phys. Chem., 65, 50 (1961).

221   H. P. Keng and L. Alexander, J. Am. Chem. Soc., 66, 1056 (1944).

222 R. P. van Stapele, H. G. Bongers and P. E. Zijlstra, J. Chem. Phys., **44**, 3719 (1966).

223 A. J. Edwards, J. Chem. Soc. (Dalton), 1723 (1978).

224 S. I. Trojanov, L. Kolditz and A. Radde, Z. Chem., **23**, 136 (1983).

225 V. W. Savodny, K. Rediess and V. Thewalt, Z. anorg. allg. Chem., **499**, 81 (1983).

226 Z. A. Fokina, S. I. Kuznetzov, N. I. Timoshenko and E. V. Bryukhova, Izv. Akad. Nauk SSSR, Ser. khim., 1946 (1982).

227 A. Finch, P. Gates, T. Page, K. B. Dillon, T. C. Waddington, J. Chem. Soc. (Dalton), 2401 (1980).

228 T. Okuda, K. Yamada, H. Ishihara and H. Negita, Bull. Chem. Soc. Jap., **50**, 3136 (1977).

229 A. I. Kuz'min, V. I. Shpanko, V. F. Sukhoverkhov, G. N. Zviadadze and B. E. Dzevitzkii, Zh. fiz. khim., **39**, 2555 (1975).

230 A. I. Kuz'min, V. I. Shpanko, V. F. Sukhoverkhov, G. N. Zviadadze and V. E. Dzevitzkii, Zh. fiz. khim., **53**, 160 (1979).

231 A. I. Kuz'min, V. F. Sukhoverkhov and A. V. Sharabarin, Zh. neorg. khim., **26**, 821 (1981).

232 A. J. Edwards and R. I. C. Sills, J. Chem. Soc., 2697 (1970).

233 H. Lynton and J. Passmore, Canad. J. Chem., **49**, 1539 (1971).

234 M. D. Lind and K. O. Christe, Inorg. Chem., **11**, 608 (1972).

235 A. I. Kuz'min, V. I. Shpanko, G. N. Zviadadze, V. F. Sukhoverkhov and B. E. Dzevitzkii, Zh. neorg. khim., **24**, 2127 (1979).

236 A. B. Neiding and V. B. Sokolov, Uspekhi khim., **43**, 2146 (1974).

237 A. J. Edwards and G. R. Jones, J. Chem. Soc., 1467 (1970).

238 T. L. Brown, Acc. Chem. Res., **7**, 408 (1974).

239 I. Watanabe, H. Tanaka and I. Shimizu, J. Chem. Phys., **52**, 4031 (1970).

240 a) H. Hartmann, M. Fleissner and H. Sillescu, Naturwiss., **50**, 591 (1963);
b) H. Hartmann, M. Fleissner and H. Sillescu, Theoret. Chim. Acta, **2**, 63 (1964).

241 I. Watanabe, J. Chem. Phys., **57**, 3014 (1972).

242 I. Watanabe and Y. Yamagata, J. Chem. Phys., **46**, 407 (1967).

243 I. Watanabe, J. Phys. Soc. Jap., **29**, 1204 (1970).

244 T. B. Brill and Z. Hugus, jr., J. Phys. Chem., **74**, 3022 (1970).

245 R. A. Johnson, M. T. Rogers and G. Leroi, J. Chem. Phys., **56**, 789 (1972).

246 W. M. Shirley and Z. Z. Hugus, jr., J. Magn. Res., **37**, 529 (1980).

247 H. Hartmann, M. Fleissner, G. Gann and H. Sillescu, J. Magn. Res., **3**, 355 (1965).

248 A. F. Schreiner and T. B. Brill, Inorg. Nucl. Chem. Lett., **6**, 355 (1970).

249 A. Kalman and D. W. J. Cruickchank, Acta Crystallogr., **B26**, 1782 (1970).

250 J. C. Morrow, Acta Crystallogr., **13**, 443 (1960).

251 M. T. Rogers and K. V. S. Rama Rao, J. Chem. Phys., **49**, 1229 (1968).

252 P. K. Burkert and F. M. Hutter, Z. Naturforsch., **32b**, 15 (1977).

253 S. Okrasinski and G. Mitra, J. Inorg. Nucl. Chem., **36**, 1908 (1974).

254 J. D. MacCullough, Acta Crystallogr., **17**, 1067 (1964).

255 A. A. Boguslavskii and S. K. Sherbakova, Izv. Akad. Nauk SSSR, Ser. fiz., **42**, 2142 (1978).

256 M. T. Rogers and K. V. S. Rama Rao, J. Chem. Phys., **58**, 3233 (1973).

257 P. K. Burkert, F. M. Hutter and D. Koth, Z. Naturforsch., **30b**, 198 (1975).

258 P. K. Burkert, J. Mol. Struct., 83, 307 (1982).

259 R. A. Johnson and M. T. Rogers, Adv. Nucl. Quadr. Res., 1, 297 (1974).

260 P. K. Burkert and M. F. Eckel, Z. Naturforsch., 28b, 5 (1973).

261 P. K. Burkert and M. F. Eckel, Z. Naturforsch., 28b, 379 (1973).

262 M. Maćkowiak, J. Stankowski, B. Zeks and R. Blinc, Acta Phys. Polon. A57, 575 (1980).

263 W. Belzhold and E. W. Uchling, Phys. Rev., 175, 624 (1968).

264 F. Milia, Ferroelectrics, 20, 229 (1978).

265 A. P. Zhukov, I. S. Res, V. I. Pakhomov and G. K. Semin, Phys. Stat. Solidi, 27, K 129 (1968).

266 M. Maćkowiak, J. Stankowski, E. Lipinski, M. Zdanowska-Fraczek and F. Milia, Solid State Commun., 38, 337 (1981).

267 M. Maćkowiak, J. Stankowski and E. Lipinski, Physica, 106B, 421 (1981).

268 B. Biedenkapp and A. Weiss, Z. Naturforsch., 19a, 1518 (1964).

269 M. T. Rogers and J. Ryan, J. Phys. Chem., 72, 1340 (1968).

270 Yu. K. Maksyutin, E. N. Guryanova and G. K. Semin, Uspekhi khim., XXXIX, 727 (1970).

271 A. Weiss, Adv. Nucl. Quadr. Res. (J. Smith, ed.), 1, p. 1; Heyden and Son, London, 1974.

272 J. Rupp-Bensadon and E. A. C. Lucken, J. Chem. Soc., Dalton Trans., 495 (1983).

273 J. Rupp-Bensadon and E. A. C. Lucken, J. Chem. Soc., Dalton Trans., 19 (1983).

274 L. Guibe and G. Jugie, Molecular Interactions, 2, 343 (1980).

275 H. G. Dehmelt, J. Chem. Phys., 21, 380 (1953).

276 T. Deeg and A. Weiss, Ber. Bunsenges. Phys. Chem., 80, 2 (1976).

277 A. Andreeva, I. Kuramshin, A. Muratova, D. Osokin, A. Pudovik and I. Safin, Izv. Akad. Nauk SSSR, Ser. fiz., 39, 2590 (1975).

278 P. G. Huggett, R. J. Lynch, T. C. Waddington and K. Wade, J. Chem. Soc., Dalton Trans., 1164 (1980).

279 Yu. K. Maksyutin, E. N. Guryanova, E. A. Kravchenko and G. K. Semin, J. Chem. Soc. D, 13, 429 (1973).

280 M. Webster and H. G. Blayden, J. Chem. Soc. A, 2443 (1969).

281 Y. Hermodsson, Acta Crystallogr., 13, 656 (1960).

282 C.-I. Bränden, Acta Chem. Scand., 17, 759 (1963).

283 I. A. Safin, I. Ya. Kuramshin, A. A. Muratova, A. N. Pudovik and V. P. Plekhov, Zh. obshch. khim., 45, 2400 (1975).

284 A. I. Andreeva, I. Ya. Kuramshin, A. A. Muratova, D. Ya. Osokin, A. N. Pudovik and I. A. Safin, Koord. khim., 2, 683 (1976).

285 D. U. Zakirov, I. Ya. Kuramshin, I. A. Safin, A. N. Pudovik and L. A. Zhelonkina, Zh. obshch. khim., 47, 1522 (1977).

286 A. I. Andreeva, I. Ya. Kuramshin, D. Ya. Osokin, I. A. Safin, A. N. Pudovik and A. S. Khramov, Koord. khim., 3, 1194 (1977).

287 H. Terao, T. Okuda and H. Negita, Bull. Chem. Soc. Jap., 51, 710 (1978).

288 T. Okuda, H. Ishihara, K. Yamada and H. Negita, Bull. Chem. Soc. Jap., 52, 307 (1979).

289   M. Kaplansky and M. A. Whitehead, Can. J. Chem., 48, 697 (1970).
290   S. Ardjomande and E. A. C. Lucken, Helv. Chim. Acta, 54, 176 (1971).
291   S. Ardjomande and E. A. C. Lucken, J. Chem. Soc., Perkin Trans., 11, 790 (1975).
292   J. A. S. Smith and D. A. Tong, J. Chem. Soc. A, 173 (1971).
293   D. F. R. Gilson and R. M. Hart, Can. J. Chem., 48, 1976 (1970).
294   T. Chiba, J. Phys. Soc. Jap., 13, 860 (1958).
295   T. Okuda, H. Ishihara, K. Yamada and H. Negita, Bull. Chem. Soc. Jap., 50, 1007 (1977).
296   E. N. Guryanova, V. V. Puchkova and A. F. Volkov, Zh. strukt. khim., 15, 439 (1974).
297   T. Okuda, H. Ohta, H. Ishihara, K. Yamada and H. Negita, Bull. Chem. Soc. Jap,. 53, 2721 (1980).
298   J. C. Carter and G. Jugie, IV. Internat. Sympos. NQR Spectr., p. 34, Osaka, 1977.
299   T. Okuda, Y. Furukawa and H. Negita, Bull. Chem. Soc. Jap., 45, 2245 (1972).
300   A. F. Volkov, I. P. Romm, E. N. Guryanova and K. A. Kocheshkov, Izv. Akad. Nauk SSSR, Ser. khim., 1365 (1976).
301   M. Z. Yusupov, V. S. Grechishkin, A. T. Kosulin, V. P. Anferov and V. S. Versilov, Org. Magn. Res., 3, 515 (1971).
302   S. C. Wallwork and I. J. Worrall, J. Chem. Soc., 1816 (1965).
303   J. D. Forrester, A. Zalkin and D. H. Templeton, Inorg. Chem., 3, 63 (1964).
304   P. A. Renes and C. N. McGillavry, Rec. Trav. Chim. Pays-Bas, 63, 283 (1944); 64, 275 (1945).
305   V. S. Grechishkin and M. Z. Yusupov, Zh. fiz. khim., 44, 2933 (1970).
306   V. S. Grechishkin and M. Z. Yusupov, Zh. strukt. khim., 14, 1028 (1973).
307   A. D. Gordeev, V. S. Grechishkin, M. Z. Yusupov, Zh. strukt. khim., 12, 725 (1971).
308   V. S. Grechishkin and I. A. Kyuntzel, Zh. strukt. khim., 5, 53 (1964).
309   V. S. Grechishkin and I. A. Kyuntzel, Opt. spektrosk., 16, 161 (1964).
310   M. F. Shostakovskii, O. Kh. Poleshuk, Yu. K. Maksyutin and I. G. Orlov, Izv. Akad. Nauk SSSR, Ser. khim., 15 (1973).
311   O. Kh. Poleshuk, D. M. Kizhner and Yu. K. Maksyutin, Zh. fiz. khim., 53, 178 (1979).
312   I. A. Kyuntzel, A. D. Gordeev and S. I. Zimmerman, Koord. khim., 3, 1035 (1977).
313   T. Okuda, J. Sci. Hiroshima Univ., A 35, 213 (1971).
314   T. Okuda, Y. Furukawa and H. Negita, Bull. Chem. Soc. Jap., 45, 2940 (1972); 45, 2245 (1972).
315   A. D. Gordeev and I. A. Kyuntzel, Zh. strukt. khim., 15, 935 (1974).
316   T. B. Brill, J. Magn. Res., 15, 395 (1974).
317   I. A. Kyuntzel and Yu. I. Rosenberg, Teor. eksp. khim., 7, 565 (1971).
318   J. C. Carter, P. Haran and G. Jugie, C. R. Acad. Sci. (Paris), 282 C, 623 (1976).
319   L. A. Lobanova, E. N. Guryanova and A. F. Volkov, Izv. Akad. Nauk SSSR, Ser. fiz., 39, 2574 (1975).
320   L. A. Popkova, E. N. Guryanova and A. F. Volkov, J. Mol. Struct., 83, 341 (1982).

321 L. A. Lobanova, E. N. Guryanova and A. F. Volkov, Teor. eksp. khim., 14, 85 (1977).

322 A. Schmitt and W. Zeil, Z. Naturforsch., 18a, 428 (1963).

323 A. L. Edwards, J. Chem. Soc., 3714 (1964).

324 T. Okuda, K. Yamada and H. Negita, Bull. Chem. Soc. Jap., 53, 2659 (1980).

325 I. P. Gol'dshtein, E. N. Guryanova, A. F. Volkov and M. E. Peisakhova, Zh. obshch. khim., 18, 1669 (1973).

326 E. A. Kravchenko, T. L. Novoderezhkina, O. N. Gilyarov, B. N. Kulikovskii and V. G. Lebedev, Zh. neorg. khim., 6, 1720 (1980).

327 B. Buss and B. Krebs, Inorg. Chem., 10, 2795 (1971).

328 I. A. Kuz'min and S. I. Kuznetzov, Koord. khim., 8, 159 (1982).

329 Y. Morino and H. Uehara, J. Chem. Phys., 45, 4543 (1966).

330 C.-I. Branden and I. Lindquist, Acta Chem. Scand., 14, 726 (1960).

331 Comprehensive Inorganic Chemistry. Vol. 3, Pergamon Press, Oxford 1973, p. 416.

332 C.-I. Branden, Acta Chem. Scand., 16, 1806 (1962).

333 S. M. Chizhikova, G. N. Zviadadze, G. M. Denisova, B. E. Dzevitzkii and A. I. Kuz'min, Izv. Akad. Nauk SSSR, Ser. met., 86 (1980).

334 A. I. Kuz'min and G. N. Zviadadze, Koord. khim., 6, 1677 (1980).

335 A. I. Kuz'min, S. I. Kuznetzov, S. M. Chizhikova, G. M. Denisova, G. N. Zviadadze and B. E. Dzevitzkii, Zh. fiz. khim., 53, 155 (1979).

336 A. I. Kuz'min, S. M. Chizhikova, G. M. Denisova, G. N. Zviadadze, B. E. Dzevitzkii and S. I. Kuznetzov, Zh. fiz. khim., 53, 150 (1979).

337 C.-I. Branden and I. Lindquist, Acta Chem. Scand., 17, 353 (1963).

338 M. Burgard, J. MacCordick and E. A. C. Lucken, Inorg. Nucl. Chem. Lett., 8, 185 (1972).

339 a) L. A. Zemnukhova and R. L. Davidovich, Izv. Akad. Nauk SSSR, Ser. fiz., 45, 1764 (1981);
b) L. A. Zemnukhova, R. L. Davidovich and T. L. Semenova, Zh. fiz. khim., 53, 48 (1979).

340 E. A. Kravchenko, R. L. Davidovich, L. A. Zemnukhova and Yu. A. Buslaev, Dokl. Akad. Nauk SSSR, 214, 611 (1974).

341 T. B. Brill, P. E. Carrou and G. G. Long, J. Inorg. Nucl. Chem., 33, 3285 (1971).

342 B. Chabot and E. Parther, Acta Crystallogr., B34, 645 (1978).

343 E. Lazarini, Acta Crystallogr., B33, 2686 (1977).

344 T. Okuda, M. Terao, O. Ege and H. Negita, J. Chem. Phys., 52, 5489 (1970).

345 N. Weiden and A. Weiss, J. Magn. Res., 20, 334 (1975).

346 G. E. Peterson and P. M. Bridenbaugh, J. Chem. Phys., 51, 238 (1969).

347 E. A. Pisarev, G. K. Semin, D. V. Drobot, S. I. Kuznetzov and E. V. Bryukhova, Zh. neorg. khim., 23, 1171 (1978).

348 Y. Kume and D. Nakamura, Bull. Chem. Soc. Jap., 55, 309 (1982).

349 A. Reddoch, J. Chem. Phys., 35, 1085 (1961).

350 H. Negita, M. Hiura, K. Yamada and T. Okuda, J. Mol. Struct., 58, 205 (1980).

351 A. Zalkin and D. E. Sands, Acta Crystallogr., 11, 615 (1958).

352 K. Mucker, G. S. Gordon and O. Johnson, Acta Crystallogr., B24, 874 (1968).

353 D. E. Sands and A. Zalkin, Acta Crystallogr., 12, 723 (1959).

354 J. L. Templeton and R. E. McCarley, Inorg. Chem., 17, 2293 (1978).

355 D. E. Sands, A. Zalkin and R. E. Elson, Acta Crystallogr., 79, 497 (1975).

356 R. G. Barnes, S. L. Segel, P. J. Bray and P. A. Casabella, J. Chem. Phys., 26, 1345 (1957).

357 R. G. Barnes and S. L. Segel, J. Chem. Phys., 25, 578 (1956).

358 G. Ludwig, J. Chem. Phys., 25, 159 (1956).

359 P. J. Bray, J. Chem. Phys., 23, 703 (1955).

360 H. Chihara, N. Nakamura, H. Okuma and S. Seki, J. Phys. Soc. Jap., 24, 306 (1968).

361 S. Hagiwara, K. Kato, Y. Abe and M. Minematsu, J. Phys. Soc. Jap., 12, 1166 (1957).

362 N. Okubo, J. Phys. Soc. Jap., 51, 524 (1982).

363 R. S. Yamasaki and C. D. Cornwell, J. Phys. Soc. Jap., 30, 1265 (1959).

364 K. Boswijk and E. Wiebenga, Acta Crystallogr., 7, 417 (1954).

365 I. A. Safin, Zh. strukt. khim., 4, 267 (1963).

366 E. Bryukhova, V. Egorov, I. Alimov and G. Semin, Izv. Akad. Nauk SSSR, Ser. khim., 8, 1919 (1974).

367 S. H. Mastin and R. R. Ryan, Inorg. Chem., 10, 1757 (1971).

368 R. R. Ryan, S. H. Mastin and A. C. Larson, Inorg. Chem., 10, 2793 (1971).

369 N. Habibi, B. Ducourant, R. Fourcade and G. Mascherpa, Bull. Soc. Chim. Fr., 11, 2320 (1974).

370 A. Byström, S. Backlund and K.-A. Wilhelmi, Arkiv Kemi, 4, 175 (1951).

371 a) B. Ducourant, R. Fourcade, E. Philippot and G. Mascherpa, Rev. Chim. Miner., 12, 485 (1975);
b) A. A. Udovenko, R. L. Davidovich, L. V. Samaretz and L. A. Zemnukhova, Koord. khim., 1, 1419 (1975).

372 T. Okuda, N. Yoshida, M. Hiura, H. Ishihara, K. Yamada and H. Negita, J. Mol. Struct., 96, 169 (1982).

373 R. Brüggemann, F. Reiter and L. Voitländer, Z. Naturforsch., 27a, 1525 (1972).

374 W. van Bronswyk and R. Nyholm, J. Chem. Soc., A, 2084 (1968).

375 T. J. Bastow and H. J. Whitfield, J. Mol. Struct., 58, 305 (1980).

376 S. I. Kuznetzov, S. I. Troyanov, E. V. Bryukhova, H. S. Lyopis and S. K. Sherbakova, Zh. fiz. khim., 53, 15 (1979).

377 J. C. Carter and J. A. S. Smith, Chem. Commun., 835 (1974).

378 J. C. Carter and J. A. S. Smith, III. Internat. Sympos. NQR Spectr., p. 84 (1975).

379 V. E. Ovchinnikov, A. A. Udovenko, L. P. Solovyeva, L. M. Volkova and R. L. Davidovich, Koord. khim., 8, 1539 (1982).

380 A. A. Udovenko, L. M. Volkova, R. L. Davidovich and L. A. Zemnukhova, Koord. khim., 3, 259 (1977).

381 T. J. Bastow and H. J. Whitfield, J. Magn. Res., 37, 269 (1980).

382 T. Babushkina, O. Poleshuk, Yu. Maksyutin, I. Alimov, S. Sokolov and E. Mikhailovskaya, Koord. khim., 1, 1266 (1975).

383 Z. Trontelj and J. Pirnat, Proc. II. Internat. Sympos. NQR Spectr., p. 191, Vallerini Publishers, Pisa, 1975.

384 T. J. Bastow and H. J. Whitfield, Austr. J. Chem., 27, 1397 (1974).

385 B. Krebs, Angew. Chim. Internat. Edit., 8, 146 (1969).

386 B. Krebs, G. Henkel and M. Dartmann, Acta Crystallogr., B35, 274 (1979).

387 B. Krebs and D. Sinram, J. Less-Common Metals, **76**, 7 (1980).

388 L. Niqvist and G. Johansson, Acta Chem. Scand., **25**, 1615 (1971).

389 I. G. White, Acta Crystallogr., **16**, 397 (1963).

390 B. Brehler, Fortschr. Mineral., **38**, 198 (1960).

391 H. R. Oswald and H. Jaggi, Helv. Chim. Acta, **43**, 72 (1960).

392 H. R. Oswald, Helv. Chim. Acta, **43**, 77 (1960).

393 J. M. van der Berg, Acta Crystallogr., **14**, 1002 (1961).

394 S. Ščavničar, Z. Kristallogr., **114**, 85 (1960).

395 P. Bayliss and W. Nowacki, Z. Kristallogr., **135**, 308 (1972).

396 N. Tideswell, F. Kruse and J. McCullough, Acta Crystallogr., **10**, 99 (1957).

397 V. Cupcik and L. Vesela, Referate Diskussionstagung. Sekt. Kristallkunde in der Deutschen Mineralogie, Marburg, 1965.

398 N. Morimoto, Mineral Jap. (Sapporo), **1**, 160 (1954).

399 A. A. Vaipolin, Kristallografiya, **10**, 509 (1966).

400 A. L. Renninger and B. L. Averbach, Acta Crystallogr., **B29**, 1583 (1973).

401 G. Carron, Acta Crystallogr., **16**, 338 (1963).

402 R. J. Gillespie, Can. J. Chem. **39**, 318 (1961).

403 I. A. Safin and I. N. Pen'kov, Dokl. Akad. Nauk SSSR, **147**, 410 (1962).

404 E. A. Kravchenko and G. K. Semin, Izv. Akad. Nauk SSSR, Zh. neorg. mater., **5**, 1161 (1969).

405 I. N. Pen'kov and I. A. Safin, Dokl. Akad. Nauk SSSR, **156**, 139 (1964).

406 M. Rubinshtein and P. C. Taylor, Phys. Rev., **B9**, 4258 (1974).

407 E. A. Kravchenko, S. A. Dembovskii, A. P. Chernov and G. K. Semin, Phys. Stat. Solidi, **31**, K19 (1969).

408 N. Abrikosov, V. Bankina, L. Poretzkaya, E. Skudnova and L. Shelimova, Poluprovodnikovye soedineniya, ikh poluchenie i svoistva, Nauka, Moskva, 1967.

409 I. N. Pen'kov and I. A. Safin, Fiz. tverd. tela, **6**, 2467 (1964).

410 T. J. Bastow and H. J. Whitfield, J. Solid State Chem., **40**, 203 (1981).

411 E. A. Kravchenko, S. A. Dembovskii, A. P. Chernov and G. K. Semin, Izv. Akad. Nauk SSSR, Ser. fiz., **33**, 279 (1969).

412 I. N. Pen'kov, I. A. Safin and S. N. Nenasheva, Dokl. Akad. Nauk SSSR, **183**, 689 (1968).

413 R. S. Abdullin, I. N. Pen'kov, I. A. Safin and M. Sh. Yagfarov, Dokl. Akad. Nauk SSSR, **218**, 859 (1974).

414 I. N. Pen'kov, R. S. Abdullin and S. N. Nenasheva, Dokl. Akad. Nauk SSSR, **219**, 437 (1974).

415 E. A. Kravchenko, S. A. Dembovskii and G. K. Semin, III. All-Union Symposium on Complex Composition Semiconductors (Russ.), Uzhgorod, 1969, Proc., p. 56, Moscow, 1969.

416 I. N. Pen'kov, R. S. Abdullin, N. B. Yunusov and N. V. Togulev, Izv. Akad. Nauk SSSR, Ser. fiz., **42**, 2104 (1978).

417 S. N. Nenasheva, I. N. Pen'kov and I. A. Safin, Dokl. Akad. Nauk SSSR, **183**, 90 (1968).

418 Yu. A. Buslaev, E. A. Kravchenko and V. B. Lazarev, Proc. XV. ICCC, p. 122, Moscow, 1973.

419 Yu. A. Buslaev, E. A. Kravchenko, I. A. Kuz'min, V. B. Lazarev and A. V. Salov, Zh. neorg. khim., **16**, 3367 (1971).

420 I. A. Pen'kov and I. A. Safin, Dokl. Akad. Nauk SSSR, **168**, 1148 (1966).

421 H. E. Doorenbos, J. C. Evans and R. O. Kogel, J. Phys. Chem., **74**, 3385 (1970).

422 P. K. Burkert and F. M. Hutter, Z. Naturforsch., **31b**, 145 (1976).

423 a) S. Kojima, K. Tsukada, S. Ogawa and A. Schimauchi, J. Chem. Phys., **21**, 1415 (1953);
b) H. G. Robinson, H. G. Dehmelt and W. Gordy, J. Chem. Phys., **22**, 511 (1954).

424 M. Mishima, J. Sci. Hiroshima Univ., A **46**, 41 (1982).

425 J. Brunette, M. Burgard, M. J. Leroy and E. A. C. Lucken, J. Mol. Struct., **36**, 269 (1977).

426 L. Donald, Dissertation Abstr., **30B**, N 5, 2112 (1969).

427 M. Buyle-Bodin and A. Monfils, Compt. Rend., **236**, 1157 (1953).

428 K. L. Brown and D. Hall, J. Chem. Soc., Dalton Trans., 1843 (1973).

429 L. Atkinson and P. Day, J. Chem. Soc. A, 2423 (1969).

430 F. Milia, R. Kind and J. Slack, Phys. Rev. B**27**, 6662 (1983).

431 E. Hellner and H. Burzlaff, Naturwiss., **51**, 35 (1964).

432 A. Zemann and J. Zemann, Acta Crystallogr., **12**, 1002 (1959).

433 C. Knowles, Acta Crystallogr., **17**, 847 (1964).

434 N. Hofmann, Z. Kristallogr., **84**, 177 (1933).

435 E. A. Kravchenko, Thesis, Moscow, 1973.

436 P. A. Dyachkov, E. A. Kravchenko, V. B. Lazarev and A. A. Levin, Sb. Yadernyi kvadrupol'nyi rezonans, Vol. 2, p. 59, Kaliningrad, 1977.

437 E. Clementi, J. Chem. Phys., **46**, 4737 (1967).

438 N. Ret, J. C. Jumas, J. Oliver-Fourcade and E. Philippot, Acta Crystallogr., C**39**, 971 (1983).

439 A. Kanisheva and V. Kuznetzov, I. All-Union Symposium on Inorganic Crystal Chemistry (Russ.), Zvenigorod, 1977, Proc., p. 89, Moscow, 1977.

440 H. Graf and H. Schäfer, Z. anorg. allg. Chem., **414**, 211 (1975).

441 A. Kanisheva, V. Kuznetzov, V. Lazarev and T. Tarasova, Zh. strukt. khim., **18**, 1069 (1977).

442 A. F. Wells, Structural Inorganic Chemistry, 3 rd. ed. Clarendon Press, Oxford, 1962.

443 a) J. D. Graybeal and R. J. McKown, J. Phys. Chem., **73**, 3156 (1969);
b) J. D. Graybeal, M. Pathania and S. D. Ing, J. Magn. Res., **9**, 27 (1973).

444 A. F. Volkov and N. I. Smirnov, Dokl. Akad. Nauk SSSR, **211**, 1377 (1973).

445 J. W. McGrath and A. A. Silvidi, J. Chem. Phys., **36**, 1496 (1962).

446 A. F. Volkov, J. Magn. Res., **11**, 73 (1973).

447 R. G. Barnes, S. L. Segel and W. H. Jones, J. Appl. Phys., **33**, Suppl. 1, 296 (1962).

448 A. F. Volkov and G. K. Semin, Izv. Akad. Nauk SSSR, Ser. khim., 1634 (1970).

449 N. I. Smirnov and A. F. Volkov, Teor. i eksperim. khim., **14**, 88 (1977).

450 E. Bang, Mat.-Fys. Medd. Kon, Dan. Vid. Selsk., **33**, 1 (1961).

451 J. G. Smeggil and H. A. Eick, Inorg. Chem., **10**, 1458 (1971).

452 M. Dyke and R. L. Sass, J. Chem. Phys., **68**, 3259 (1964).

453 A. Narath, J. Chem. Phys., **40**, 1169 (1964).

454 P. A. Edwards and R. G. Barnes, J. Chem. Phys., **55**, 4664 (1971).

455 a) R. G. Barnes and P. J. Bray, J. Chem. Phys., 23, 1177 (1955);
     b) R. G. Barnes and P. J. Bray, J. Chem. Phys., 23, 1182 (1955).
456 a) E. H. Carlson and H. S. Adams, J. Chem. Phys., 51, 388 (1969);
     b) E. H. Carlson, Phys. Lett., 29A, 696 (1969).
457 S. I. Parks and W. G. Moulton, Phys. Lett., 26A, 63 (1967).
458 R. G. Barnes and H. Hultsch, Phys. Rev. Lett., 1, 227 (1958).
459 R. Bersohn and R. G. Shulman, J. Chem. Phys., 43, 2298 (1966).
460 D. L. Lyfar, V. E. Goncharuk and S. M. Ryabchenko, Phys. Stat. Sol. (b), 76, 183 (1976).
461 B. E. Vugmeister, M. D. Glinchuk, I. M. Zaritskii, A. A. Konchits, D. L. Lyfar and S. M. Ryabchenko, Zh. eksper. teor. fiz., 69, 1756 (1975).
462 A. V. Bondar, A. Ya. Gordon, D. L. Lyfar, D. F. Baisa and S. M. Ryabchenko, Fiz. tverd. tela, 18, 1235 (1976).
463 W. E. Hughes, C. G. Montgomery, W. G. Moulton and E. H. Carlson, J. Chem. Phys., 41, 3470 (1964).
464 E. H. Carlson, Bull. Amer. Phys. Soc., 11, 377 (1966).
465 D. H. Current, C. L. Foiles and E. H. Carlson, Phys. Rev. B6, 737 (1972).
466 B. W. Mangum and D. B. Utton, Bull. Amer. Phys. Soc., 12, 1043 (1967).
467 R. G. Barnes, R. Lecander and S. L. Segel, Bull. Amer. Phys. Soc., Ser. II, 8, 260 (1963).
468 A. Narath, Phys. Rev., 140, A 552 (1965).
469 R. T. Schumacher and R. L. Hartman, Bull. Amer. Phys. Soc., 10, 316 (1964).
470 R. G. Barnes and S. L. Segel, J. Chem. Phys., 37, 1895 (1962).
471 T. J. Bastow and H. J. Whitfield, J. Magn. Res., 26, 461 (1977).
472 E. A. Kravchenko, V. G. Morgunov, B. Z. Nurgaliev and B. A. Popovkin, VII. Internat. Sympos. NQR Spectr., Abstr., p. BPO4, Kingston, Canada, 1983.
473 E. A. Kravchenko, V. G. Morgunov, L. D. Demina and V. A. Dolgikh, Zh. neorgan. khim., 24, 2337 (1979).
474 A. I. Kuz'min, A. L. Shvartz, G. N. Zviadadze, B. E. Dzevitzkii and V. N. Margulis, Zh. fiz. khim. 53, 51 (1979).
475 G. K. Semin, A. K. Moskalev, V. I. Popolitov, V. A. Egorov and V. F. Peskin, Fiz. tverd. tela, 15, 2217 (1973).
476 A. F. Volkov, L. A. Ivanova and Yu. N. Venevtsev, Izv. Akad. Nauk SSSR, Ser. neorg. mat., 14, 782 (1978).
477 A. F. Volkov, L. A. Ivanova, Yu. N. Venevtsev and L. L. Rappoport, Zh. fiz. khim., 56, 1002 (1982).
478 A. P. Zhukov, L. V. Soboleva, L. M. Belyaev and A. F. Volkov, Ferroelectrics, 21, 601 (1978).
479 E. A. Kravchenko, A. M. Klimakov and B. A. Popovkin, Koord. khim., 4, 708 (1978).
480 J. Olivier-Fourcade, E. Philippot and M. Maurin, Z. anorg. allg. Chem., 446, 159 (1978).
481 S. Särnstraud, Acta Crystallogr., B34, 2402 (1978).
482 a) V. Krömer, Acta Crystallogr., B34, 2695 (1978);
     b) V. Krömer, Acta Crystallogr., B31, 234 (1975).
483 B. Z. Nurgaliev, B. A. Popovkin, S. Yu. Stefanovich, Zh. neorg. khim., 28, 2207 (1983).

484 D. Rogers and A. C. Skapski, Proc. Chem. Soc., 400 (1964).

485 a) P. S. Gopalakrishnan and H. Manohar, Cryst. Struct. Commun., 4, 203 (1975);
   b) G. Thornton, Acta Crystallogr., B33, 1271 (1977).

486 A. J. Hegedüs, G. Baksy and L. Chudik-Major, Acta Chim. cad. Sci. Hung., 77, 227 (1973).

487 A. C. Skapski and D. Rogers, Chem. Commun., 611 (1965).

488 K. Dihlström, Z. anorg. Chem., 239, 57 (1938).

489 B. Kinberger, Acta Chem. Scand., 24, 320 (1970).

490 a) M. M. Quarashi and W. H. Barnes, Amer. Mineralogist, 37, 423 (1952);
   b) M. M. Quarashi and W. H. Barnes, Amer. Mineralogist, 38, 489 (1953).

491 M. Tanaka, R. Saito and D. Watanabe, Acta Crystallogr., A36, 350 (1980).

492 Yu. N. Venevtzev, L. A. Ivanova, V. I. Popolitov, V. I. Ponomarev, N. V. Rannev, A. N. Lobachev and L. O. Atovmyan, Ferroelectrics, 21, 417 (1978).

493 A. F. Volkov, Kristallografia, 19, 781 (1974).

494 A. F. Volkov, V. I. Svergun, Yu. N. Venevtzev and G. K. Semin, Izv. Akad. Nauk SSSR, Ser. fiz., 33, 266 (1969).

495 V. M. Buznik and A. K. Moskalev, Zh. fiz. khim., 53, 77 (1979).

496 a) R. Kind, H. Graniher, B. Derighetti, W. Faldner and E. Brun, Solid State Commun., 6, 439 (1968);
   b) G. E. Peterson and P. Bridenbaugh, J. Chem. Phys., 48, 3402 (1968).

497 E. Schempp, G. E. Peterson and J. R. Carruthers, J. Chem. Phys., 53, 306 (1970).

498 F. Wolf, D. Kline and H. Story, J. Chem. Phys., 53, 3538 (1970).

499 a) R. M. Cotts and W. D. Knight, Phys. Rev., 96, 1285 (1954);
   b) R. R. Hewitt, Phys. Rev., 121, 45 (1961).

500 Yu. A. Buslaev, E. A. Kravchenko, V. I. Pakhomov, V. M. Skorikov and G. K. Semin, Chem. Phys. Lett., 3, 455 (1969).

501 K. V. Gopalakrishnan, L. C. Gupta and R. Vijayaragharan, Pramana, 6, 343 (1976).

502 S. C. Abrahams, P. B. Jamieson and J. L. Bernstein, J. Chem. Phys., 47, 4034 (1967).

503 N. V. Togulev, V. I. Kal'chev and I. N. Pen'kov, Izv. Akad. Nauk SSSR, Ser. fiz., 45, 1784 (1981).

504 M. D. Glinchuk, A. Y. Kudzin, S. M. Ryabchenko and A. D. Skorbun, J. Mol. Struct., 83, 105 (1982).

505 B. Aurivillius, Arkiv kemi 1, 499 (1950).

506 B. Aurivillius, C.-I. Lindblom and P. Stenson, Acta Chem. Scand., 18, 1555 (1964).

507 A. Watanabe and M. Goto, J. Less Common Metals, 61, 265 (1978).

508 J. Grigas, Ferroelectrics, 20, 173 (1978).

509 L. Ayo and V. Kokorina, Optiko-mekh. promishlennost, 4, 39 (1961).

510 L. Guseva, I. Ganeev, A. Dronov and I. Rez, Optika i spektroskopia, 24, 298 (1968).

511 a) N. I. Butzko, E. G. Moroz and I. Osipshin, Ukr. Fiz. zh., 12, 12 (1967);
   b) N. I. Butzko, E. G. Moroz, I. Osipshin, V. Pryamukhin and I. Zhezhnich, Ukr. Fiz. zh., 15, 507 (1970).

512 I. S. Rez, Uspekhi fiz. nauk, 93, 633 (1967).

513 N. D. Gavrilova, V. A. Koptzik, V. K. Novik and T. V. Popova, Ferroelectrics, 20, 199 (1978).

514 D. F. Baisa and S. V. Mal'tsev, J. Mol. Struct., 83, 387 (1982).

515 A. V. Bondar and S. M. Ryabchenko, J. Mol. Struct., 83, 85 (1982).

516 I. N. Pen'kov, Thesis, Moscow, 1970.

517 A. Novoselova, B. Popovkin, G. Gospodinov, I. Odin and E. Kravchenko, Problemi kristallologii, MGU, Moskva, 1971, p. 190.

518 G. K. Semin, I. M. Alimov and T. L. Khotzyanova, Izv. Akad. Nauk SSSR, Ser. fiz., 42, 2055 (1978).

519 I. N. Pen'kov, R. S. Abdullin and V. P. Kal'tchev, Zh. fiz. khim., 53, p. 38 (1979).

520 a) M. Rubinstein and P. C. Taylor, Phys. Rev. Lett., 29, 119 (1972);
     b) M. Rubinstein and P. C. Taylor, Phys. Rev., 9, 4258 (1974).

521 P. C. Taylor and M. Rubinstein, Adv. Nucl. Quadr. Res., 2, 325 (1975).

522 P. C. Taylor, M. Rubinstein, Tr. VI. Mezhdunar. konf. amorphnym zhidk. poluprovodn. Nauka, Leningrad, 1976, p. 118.

523 E. A. Kravchenko, V. G. Morgunov, B. N. Kulikovskii, T. L. Novoderezkina and M. Meisel, J. Chem., 23, 143 (1983).

524 H. van Bueren, Defecti v Kristallakh, IL Moskva, 1962, p. 271.

525 E. A. Kravchenko, N. V. Timofeeva and G. Z. Vinogradova, J. Mol. Struct., 58, 253 (1980).

526 I. N. Pen'kov and I. A. Safin, Fiz. tverd. tela, 7, 190 (1965).

527 S. I. Berul', V. B. Lazarev and A. V. Salov, Zh. neorg. khim., 16, 2012 (1971).

528 V. G. Kuznetzov, A. S. Kanisheva and A. V. Salov, Zh. neorg. khim., 17, 247 (1972).

529 Yu. I. Malov, N. N. Vershinin and O. N. Breusov, Izv. Akad. Nauk SSSR, Ser. khim., 1638 (1977).

530 Yu. A. Buslaev, E. A. Kravchenko, V. B. Lazarev and S. F. Marenkin, Phys. Stat. Solidi (b) 47, K 125 (1971).

531 N. N. Vershinin, Yu. I. Malov, O. N. Breusov, A. V. Anan'in and L. I. Mironkova, Detonatsiya. Kritich. yavleniya. Fiz.-khim. prevrashcheniya v udarn. volnakh, 1978, c. 137; (Chem. Abstr. 90, 96258 (1979)).

532 I. I. Chernyaev, V. A. Sokolov and V. A. Palkin, Izv. Sekt. Platiny, 28, 142 (1954).

533 Yu. N. Kukushkin and E. S. Postnikov, Zh. prikl. khimii 44, 1406 (1971).

534 E. A. Kravchenko, M. I. Gel'fman, E. F. Shubochkina and Yu. A. Buslaev, Koord. khim., 5, 1237 (1979).

535 E. A. Kravchenko, V. G. Morgunov and M. I. Gel'fman, J. Mol. Struct., 83, 163 (1982).

536 E. A. Kravchenko, V. G. Morgunov, M. I. Gel'fman and T. V. Zhuckshwerdt, Koord. khim., 10, 114 (1984).

537 R. A. Marino, H. R. Wende, J. A. Apps and S. M. Klainer, J. Mol. Struct., 58, 445 (1980).

538 S. N. Popov and N. N. Krainik, Fiz. tverd. tela, 12, 3022 (1970).

539 A. R. Kessel, I. A. Safin and A. M. Gol'dman, Fiz. tverd. tela, 12, 3070 (1970).

540 V. L. Matukhin, I. A. Safin and V. F. Shamray, Dokl. Akad. Nauk SSSR, **238**, 1388 (1978).

541 V. L. Matukhin, I. A. Safin and V. F. Shamray, Izv. Akad. Nauk SSSR, Ser. fiz., **45**, 1768 (1981).

542 V. L. Matukhin, I. A. Safin and V. F. Shamray, J. Mol. Struct., **83**, 425 (1982).

543 A. M. Petrosyan, Thesis, Moskva, 1980.

544 S. Kojima, T. Tsukada, S. Ogawa and A. Shimauchi, J. Chem. Phys., **23**, 1963 (1955).

545 G. K. Semin, A. K. Moskalev, V. I. Pakhomov, E. M. Mikhailova, E. E. Vinogradov and L. A. Azarova, Dokl. Akad. Nauk SSSR, **211**, 148 (1973).

546 E. Selte and A. Kjekshus, Acta Chem. Scand., **24**, 1912 (1970).

547 A. M. Petrosyan, A. F. Volkov, Yu. S. Bogachev and Yu. N. Venevtsev, XIII. Europ. Congr. Mol. Spectr., Wroclaw, Poland, 1977, Abstr., p. 345.

548 T. Okuda, H. Gotou, Y. Nishiyama and A. Shimauchi, Sci. Light (Japan), **26**, 183 (1977).

549 A. M. Petrosyan, R. I. Kukhtin and Yu. N. Venevtsev, Zh. Eksper. Teor. Fiz., **76**, 2138 (1979).

550 a) A. R. Kessel, IV. Mezhdunar. Konf. Segnetoel., Leningrad, 1977. Abstr., p. 245;
b) A. R. Kessel, Ferroelectrics, **22**, 759 (1978).

551 R. L. Armstrong and H. M. van Dreil, Adv. Nucl. Quadr. Res., **2**, 179 (1975).

552 A. E. Geissberger and P. J. Bray, J. Non-Cryst. Solids, **54**, 121 (1983).

553 N. E. Ainbinder and I. G. Shaposhnikov, Adv. Nucl. Quadr. Res., **3**, 67 (1978).

554 H. Chihara and N. Nakamura, Adv. Nucl. Quadr. Res., **4**, 1 (1981).

555 H. Ishihara, J. Sci. Hiroshima Univ., A, **45**, 319 (1981).

556 I. J. F. Poplett, Adv. Nucl. Quadr. Reson., **4**, 115 (1981).